Shear behavior of plane joints under CNL and DNL conditions: Lab testing and numerical simulation

To the Faculty of Geosciences, Geoengineering and Mining
of the Technische Universität Bergakademie Freiberg
approved

THESIS

to attain the academic degree of
Doctor of Engineering
Dr.-Ing.

by Dipl.-Ing. Dang, Wengang
born on the August.08, 1987 in China

Reviewers: Prof. Dr.-Ing. habil. Heinz Konietzky, Freiberg
Prof. Dr.-Ing. habil. Andreas Henk, Darmstadt
Prof. Dr.-Ing. habil. Zilong Zhou, Changsha, China

Date of the award: 21.02.2017

Acknowledgements

The work described within this thesis was conducted at the Chair for Rock Mechanics, Geotechnical Institute (IFGT), TU Bergakademie Freiberg (TUBAF), Germany, from September 2013 to September 2016.

Foremost, I wish to express my sincere gratitude to Prof. Dr. –Ing. habil. Heinz Konietzky, my supervisor, for his constant support and instructive guidance for the development of my dissertation. I would like to thank him for being open to my ideas and for encouraging and helping me to complete my work.

I would also like to thank the National Basic Research Program of China (Grand No. 2015CB060200), the National Natural Science Foundation of China (Grant Nos. 51274254, 51322403) and Chinese Scholarship Council (CSC), for the financial support.

In addition, I would like to thank all my colleagues at the Chair for Rock Mechanics for their constant support. They have provided me with many valuable suggestions and advices during my stay in Freiberg. Specifically, I would like to thank Dr. Thomas Frühwirt, Mr. Tom Weichmann, Mrs. Beatrice Tauch and Mr. Gerd Münzberger from the Rock Mechanical Laboratory for their support during sample preparation and conducting the experiments required for my thesis. I would also like to thank Mrs. Angela Griebsch and Mrs. Haina Chen-Konietzky for helping me throughout my stay in Freiberg. Special thanks to Dr. Martin Herbst for support in respect to numerical simulations required for my research. I would also like to thank Mr. Syed Muntazir Abbas and Mr. Vishal Vilas Yadav for helping me improve the English in my thesis report.

I would also like to thank Prof. Xibing Li, Prof. Zilong Zhou and Prof. Zhixiang Liu in Central South University, China. They have provided me with additional guidance and financial support for my research.

I would like to express my heart felt gratitude to all my friends at TU Freiberg for sharing their valuable experiences with me throughout my stay in Germany. Thank you all for your valuable comments and suggestions, which have contributed to improve my understanding in different fields.

Finally, I would like to thank my parents for their understanding and support.

Abstract

The aim of this research work is to deepen the understanding of joint shear behavior under different boundary conditions. For this purpose, joint closure tests under quasi-static and dynamic conditions, direct shear and cyclic shear tests under CNL and DNL boundary conditions of plane joints are performed using GS-1000 big shear box device. The dissertation also presents the procedure to simulate the shear box device and simulating the behavior of plane joints at the micro-scale using FLAC^{3D}. Special attention has been given to understand the influencing factors of the normal stress level, direct shear rate, horizontal cyclic shear frequency, normal impact frequency, horizontal cyclic shear displacement amplitude and vertical impact force amplitude.

Lab test and numerical simulation results show that the quasi-static joint stiffness increases with increasing normal force. Dynamic joint stiffness decreases with increasing superimposed normal force amplitudes. Normal impact frequencies have little influence on the joint stiffness. Rotations and stress changes at the plane joint during shearing are proven. Rotations and development of stress gradients can be decreased significantly by increasing the size of the bottom specimen and applying a shear velocity at the upper shear box and normal loading piston. Furthermore, peak shear force increases with increasing normal force. Friction angle of cyclic shear tests is smaller than that of direct shear tests. Moreover, significant time shifts between normal and shear force (shear force delay), normal force and friction coefficient (friction coefficient delay) during direct shear tests under DNL boundary conditions are observed and the reference quantity 'shear-velocity-normal-impact-frequency' (SV-NIF) to describe the behavior under DNL boundary conditions is defined. Peak shear force and minimum friction coefficient increase with increasing SV-NIF. Relative time shift between normal force and shear force decreases with increase of SV-NIF. The mechanical behavior of the GS-1000 big shear box device is simulated and the loss of normal force caused by the tilting of the loading plate is quantified.

Finally, the novel direct and cyclic shear strength criterions under DNL conditions are put forward. The shear strength criterions are in close agreement with the measured

values, which indicates that the novel shear strength criterions are able to predict the shear strength under DNL conditions.

Table of Contents

List of Figures

List of Tables

Abbreviations

CCNL	cyclic shear test under constant normal load conditions
CDNL	cyclic shear test under dynamic normal load conditions
CNL	constant normal load
CNS	constant normal stiffness
DCNL	direct shear test under constant normal load conditions
DDNL	direct shear test under dynamic normal load conditions
DNL	dynamic normal load
JCS	joint wall compressive strength
JRC	joint roughness coefficient
SV-NIF	shear velocity to normal impact frequency

1 Introduction

1.1 Problem statement

Rocks encountered in civil engineering, energy engineering, water conservation and hydropower engineering, mining engineering, nuclear waste storage engineering, railway bridge engineering and defense engineering are in general jointed and anisotropic in nature. Their strength under complicated stress conditions have to be analyzed to study stability problems related to tunnels, foundations and underground excavations. Moreover, the shear behavior of jointed rock masses is very important for the design of engineering projects, e.g. for surface and underground excavations, slopes, dam foundations or geothermal reservoirs and for geological hazard evaluations (e.g. Hoek and Brown, 1980; Hoek and Bray, 1981; Babanouri et al., 2011). The shear strength of jointed rock, as a whole, depends on the strength of intact rock, joint strength, orientation, geometry, characteristics and the stress field. Field investigations and laboratory tests are the two most important procedures to understand and quantify the mechanical behavior of joints. Both, direct and cyclic shear tests are used to study the frictional behavior of joints because normal and shear displacements under certain load conditions can be measured easily during the shearing process (see for instance: Barton and Choubey, 1977; Bahaaddini et al., 2013, 2014, 2015 and 2016; Lee et al., 2014; Nguyen et al., 2013 and 2014; Crawford and Curran, 1981; Kana et al., 1996; Lee et al., 2001; Jafari et al., 2003; Bagde and Pertros, 2005; Belem et al., 2000, 2004 and 2007; Guo et al., 2011; Liu et al., 2011, 2012; Konietzky et al., 2012; Cabalar et al., 2013 ; Sneed et al., 2015; Zhou et al., 2015; Dandrea and Tozzo, 2016; Dang et al, 2016; Li et al., 2016; Mohapatra et al., 2016; Nabassé et al., 2016; Suhr and Six, 2016).

1.2 Objective of this work

The aim of this research work is to deepen the understanding of joint shear behavior under different boundary conditions. Lab tests and numerical simulations are presented in this thesis. Firstly, joint closure tests under quasi-static and dynamic conditions are conducted. Then, dynamic laboratory shear tests are performed under

different stress boundary conditions (Figure 1). Effects of various parameters such as the normal load level, vertical and horizontal impact frequencies, vertical impact amplitudes, horizontal shear displacement amplitudes and shear velocities on the shear behavior of rock joints are investigated. In parallel with the lab experiments, numerical simulations are carried out to model the shear box device and study the shear behavior of plane joints in detail. Finally, results obtained from numerical simulations are analysed and compared with the results obtained from lab tests. Thus, a much more detailed insight into the plane joint behavior under different boundary conditions is obtained.

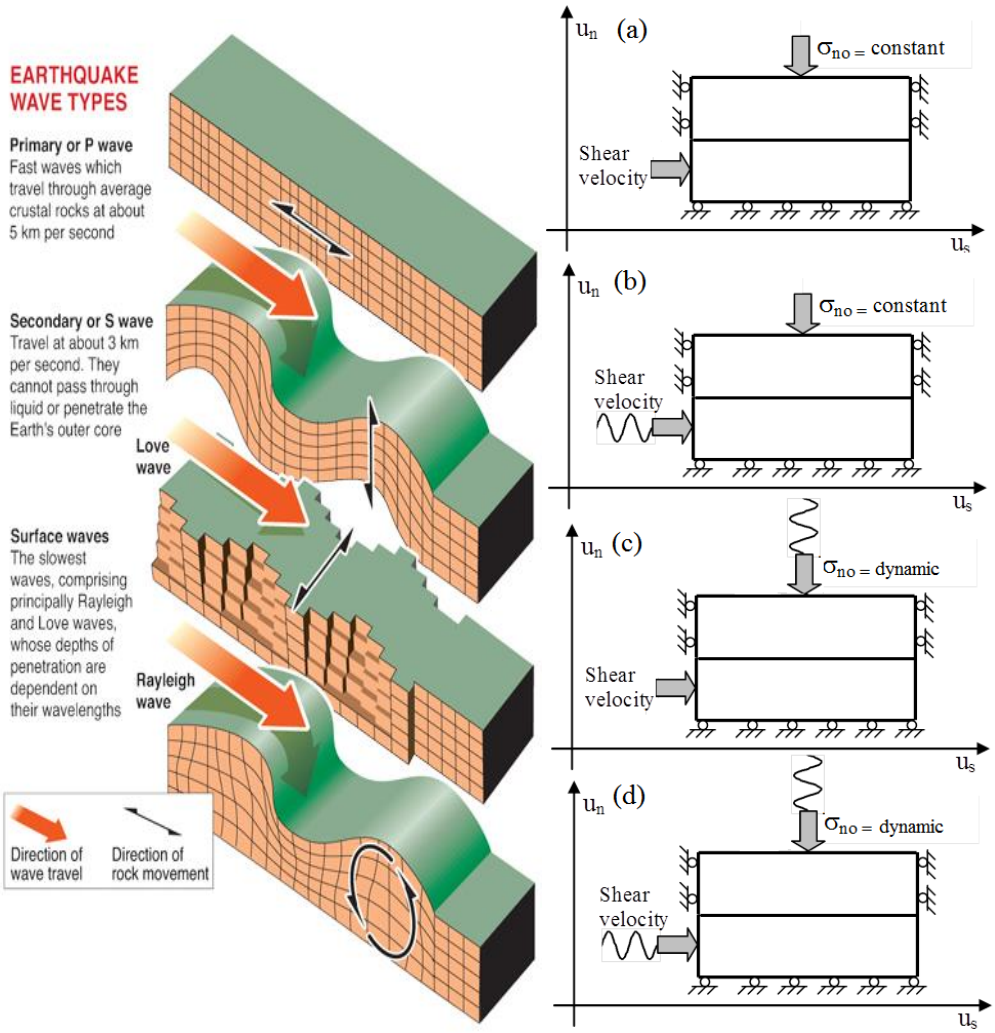

Figure 1. Typical earthquake wave types and simplified lab shear test models: (a) direct shear test under CNL conditions, (b) cyclic shear test under CNL conditions, (c) direct shear test under DNL conditions and (d) cyclic shear test under DNL conditions. (http://images.google.de/imgres?imgurl=http%3A%2F%2Fblog.thomsonreuters.com) 11/10/2016

1.3 Structure of the dissertation

The dissertation has been subdivided into six chapters as follows:

The first chapter (current chapter) introduces the topic, outlines the objectives of the work and provides an overview.

The second chapter introduces the theoretical background of shear strength of joints. It provides a literature review about the shear strength of joints under different boundary conditions such as constant normal load, constant normal stiffness and dynamic conditions. Besides, limitations of the previous work are discussed.

The third chapter describes the new developed shear box tests apparatus GS-1000, sample preparation and sample installation.

The fourth chapter describes joint stiffness determination based on joint closure tests under quasi-static and dynamic conditions.

The fifth chapter presents the four types of laboratory experiments: direct shear tests under CNL boundary conditions, cyclic shear tests under CNL boundary conditions, direct shear tests under DNL boundary conditions and cyclic shear tests under DNL boundary conditions including discuss of the results.

The sixth chapter deals with numerical simulations of the shear box device GS-1000 and the shear tests. The simulation results are compared with the experimental results. Special attention is paid to the stress behavior at the interface and the rotational behavior of top specimen and loading plate. Finally, the novel ideas for modified set-up of direct shear apparatus are presented, which can reduce inclination of the top specimen and homogenize stresses at the interface.

The seventh chapter summarizes work presented in the chapters before. Conclusions are drawn, achievements and new finding are summarized and recommendations for future research work are given.

1.4 Major contributions of the thesis

This thesis focuses on experimental studies of using the new developed big shear box device GS-1000 for direct and cyclic shear tests on plane joints under CNL and DNL conditions. Numerical simulations are used to interpret results. The main findings are:

- The quasi-static joint stiffness increases with increasing normal force. Dynamic joint stiffness decreases with increasing superimposed normal force amplitudes. Normal impact frequencies have little influence on the joint stiffness.
- A 3-dimensional numerical model of the GS-1000 shear box device is developed. The mechanical behavior of the shear box device is simulated and the loss of normal force caused by the tilting of the loading plate is quantified.
- Rotations and stress changes at the joint during shearing are proven. Rotations and development of stress gradients can be decreased significantly by increasing the size of the bottom specimen and applying a shear velocity at the upper shear box and normal loading piston.
- Peak shear force increases with increasing normal force. Friction angle of cyclic shear tests is smaller than that of direct shear tests.
- Significant time shift between normal and shear force (shear force delay), normal force and friction coefficient (friction coefficient delay) during direct shear tests under DNL boundary conditions are observed.
- The reference quantity 'shear-velocity-normal-impact-frequency' (SV-NIF) to describe the behavior under DNL boundary conditions is defined. Peak shear force and minimum friction coefficient increase with increasing SV-NIF. Relative time shift between normal force and shear force decreases with increase of SV-NIF.
- A criterion to calculate the shear strength of joints under constant shear velocity and sinusoidal normal loading is proposed as follows:

$$\tau = \{c_1 + c_2 \cdot \sin[2\pi f(t + \frac{\pi}{f})]\} \cdot \frac{F_s + F_d \ \sin(2\pi f t)}{S}$$

where c_1 and c_2 are material constants; c_1 decreases and c_2 increases with increasing impact amplitudes.

- A criterion to calculate the shear strength of joints under cyclic shear velocity and sinusoidal normal loading is proposed as follows:

$$\tau = ABS(k\sum_{n=0}^{n\max}(\frac{1}{2n+1}\sin((2n+1)t))) \cdot \frac{F_s + F_d \sin(2\pi ft)}{S} \text{.....} (n \in (0,1,2,3\ldots))$$

- Adaption of numerical calculation schemes to simulate cyclic and direct shear tests under CNL and DNL boundary conditions at the micro-scale.

2 State of the art

In this chapter, structural and engineering geological features of joints are introduced. A brief review of state-of-the-art in respect to joint behavior is given. Showing shortcomings and limitations of previous research lead to the definition of the objectives for this thesis.

2.1 Structural and engineering geological features of joints

Figure 2. Columnar joints.
(Http://Geologyfieldcamp.Sdsmt.Edu/Photogallery%202007.Htm) 11/10/2016

After a long geological process, quite a lot of intact rocks are divided into a large number of joints, fissures and faults (e.g., Figure 2). Joints are discrete brittle fractures in a rock along which there has been little or no movement parallel to the plane of fracture, but slight movement normal to it (Allaby, 2008). Joints, bedding plane, faults, and other recurrent planar fractures radically alter the mechanical behavior of rocks and rock masses. As joints are often showing preferred orientations, their effect is to create pronounced anisotropy in the properties of the rock mass, in particular, anisotropy of strength. For instance, the strength of a foundation loaded obliquely to the orientation of bedding planes may have less than one half of the strength in case the load is applied perpendicular or parallel to the bedding planes. Moreover,

anisotropy commonly exists in many rocks that have continuous structure, because of preferred orientations of mineral grains or directional stress history. Thus, rock masses are in general anisotropic in terms of different properties which affect the mechanical and hydro-mechanical coupled behavior. In particular, discontinuities line planar planes of weakness make the rock mass weaker, more deformable and lead to larger anisotropy in strength. Joints also affect hydraulic behavior; for example, they result in higher permeability in directions parallel to discontinuities. The gombination of these factors is a great challenge for the geotechnical design.

Foundations on jointed rocks may settle significantly due to joint closer under normal load (especially for the mismatched joints) even if the rock itself is very stiff. Dams underlain by discontinuous rock are subjected to damage if rock blocks slip along one or more weak surfaces (Figure 3). More than one dam failure has been attributed to this failure mechanism. Movement of blocks along single or multiple planes of weakness also causes failure of slopes (Figure 4).

Figure 3. The ruins of the dam of the Malpasset arch after its failure in 1959. The movement of a wedge delimited by discontinuities in the rock caused the rupture of the concrete arch. More than 500 people died in the valley below. (https://en.wikipedia.org/wiki/Malpasset_Dam) 11/10/2016

Figure 4. Landslide in Zhejiang Yongtai.
(http://www.jiaodong.net/2004/12/199510.htm) 26/02/2017

Shear strength of rock joints is produced by surface frictional resistance to sliding, interlocking effects between the individual rock grains and natural apparent cohesion. It is important to distinguish between closed joints, open joints and filled joints (Figure 5). Filled joints, ranging from those that contain soft plastic materials such as clay at a microscopic level, to faults that contain gouge or breccia at a macroscopic level, constitute a rather special set of problems and their shear strength principally depends on the physical and mineralogical properties of the material separating the joint walls. In contrast, the shear strength behavior of closed joints depends on, apart from the level of effective normal stress acting on the plane of sliding, the properties of the rock walls including rock type, degree of roughness, size of the joint (scale effect), degree of weathering, presence of moisture, and water pressure. Moreover, Zhao (1997a) and Zhao and Zhou (1992) have suggested a new parameter - the joint matching coefficient – JMC (Figure 6). This roughness index is based on the percentage of joint surface in contact. When the two surfaces completely fit together, the joint is totally matched. The degree of matching is therefore represented by the degree of fitness of the joint surfaces.

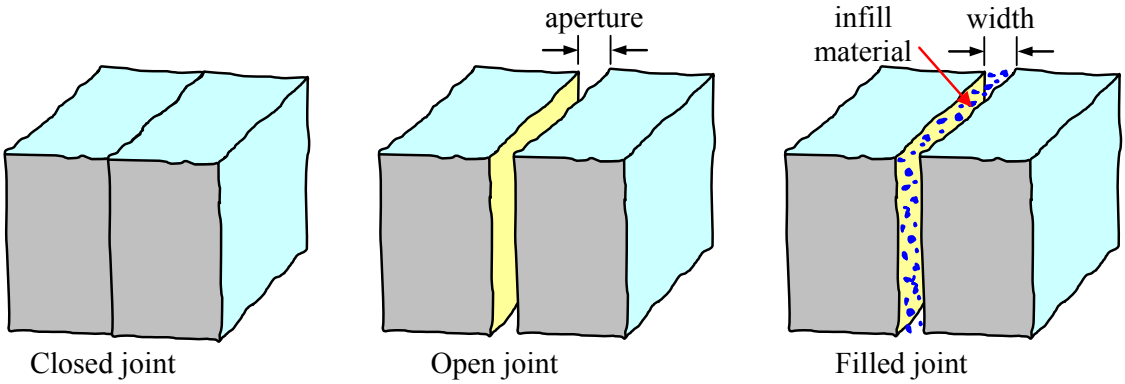

Figure 5. Illustration of joint aperture and joint filling.

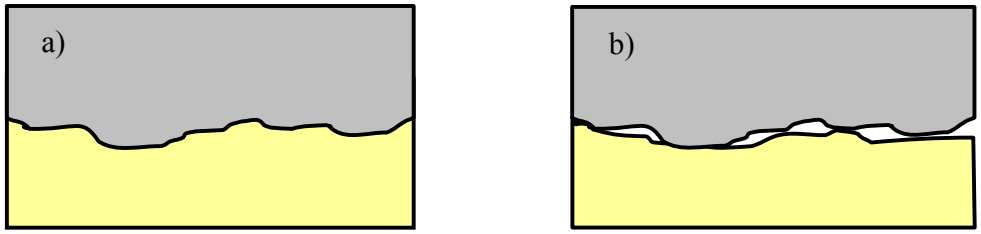

Figure 6. Definition of joint matching: (a) matched joint; (b) mismatched joint.

2.2 Classical investigation techniques for joints

Joint closure tests and shear box tests are the most popular techniques to investigate the behavior of joints in the laboratory. Static shear box tests are a standard method to get basic mechanical properties like friction angle and cohesion. In order to simulate realistic in-situ quasi-static boundary conditions, direct shear tests under CNL and CNS conditions are performed in the past decades (Figure 7) (e.g. Oda and Konishi, 1974; Barton and Choubey, 1977; Bahaaddini et al., 2013, 2014, 2015 and 2016; Lee et al., 2014; Nguyen et al., 2013 and 2014; Oh et al., 2015; Kang et al, 2015; Dindarloo and Siami-Irdemoosa, 2016; Johansson, 2016). Moreover, in situ the deformation and stability of jointed rock masses may be influenced by dynamic loadings due to blasting or earthquake excitation. That means, rock masses suffer dynamic loads in addition to static loads. Recently, also dynamic effects on rock joints are investigated (e.g. Bagde and Pertros, 2005; Belem et al., 2007; Guo et al., 2011; Liu et al., 2011, 2012; Konietzky et al., 2012; Cabalar et al., 2013 ; Zhou et al., 2015; Nguyen et al., 2013 and 2014). Furthermore, with increasing computational power and software development, the used of numerical simulations are becoming more and more popular to investigate joint behavior (e.g., Potts et al., 1987; Dounias

and Potts, 1993; Dounias and Potts, 1995; Oda and Iwashita, 2000; Tejchman and Bauer, 2005; Yan and Ji, 2010; Duriez et al., 2011; Bahaaddini et al., 2013, 2014, 2015 and 2016; Wijewickreme et al., 2013; Nguyen et al., 2013 and 2014; Dabeet, 2014; Lin et al., 2014; Dabeet et al., 2015; Hazeghian and Soroush, 2015; Asadzadeh and Soroush, 2016; Liu, 2016).

2.2.1 Laboratory tests

2.2.1.1 Quasi-static lab tests

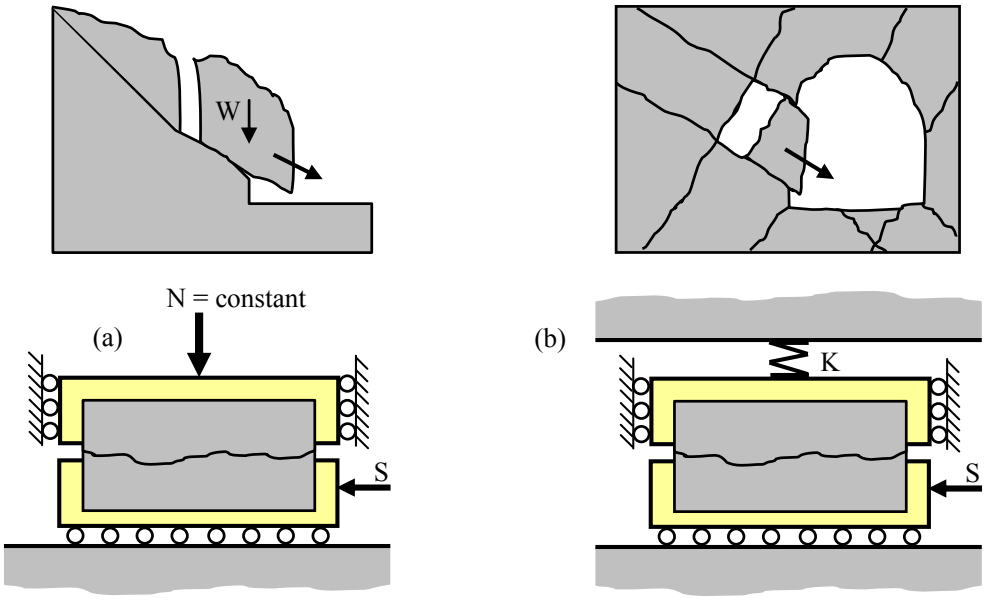

Figure 7. Simulation of in-situ boundary conditions for direct shear tests under quasi static conditions (Brady and Brown, 2005).

The typical behavior of a planar joint under direct shear is illustrated in Figure 8. The shear stress increases until the peak shear stress is reached. Then the shear stress decreases to some residual value that remains constant even for large shear displacement. The peak and residual shear stresses under different normal stresses are given by two linear relations as illustrated in Figure 8. The relation for the peak shear stress has a slope angle of ϕ_p (peal friction angle) and an intercept of c (cohesion) on the shear stress axis. The residual stress line has a slope angle of ϕ_r (residual friction angle). The peak shear strength is the highest stress sustainable just prior to complete failure of sample under shear load; after this, stress cannot be maintained and major

strains usually occur by displacement along failure surfaces (Allaby, 2008). The peak shear strength of a rock joint undergoing shear displacement is dependent on the normal load applied across the interface, surface characteristics such as roughness and joint wall strength, and the boundary conditions. The residual shear strength (Allaby, 2008) is the ultimate strength along a surface or parting in rock after shearing has occurred.

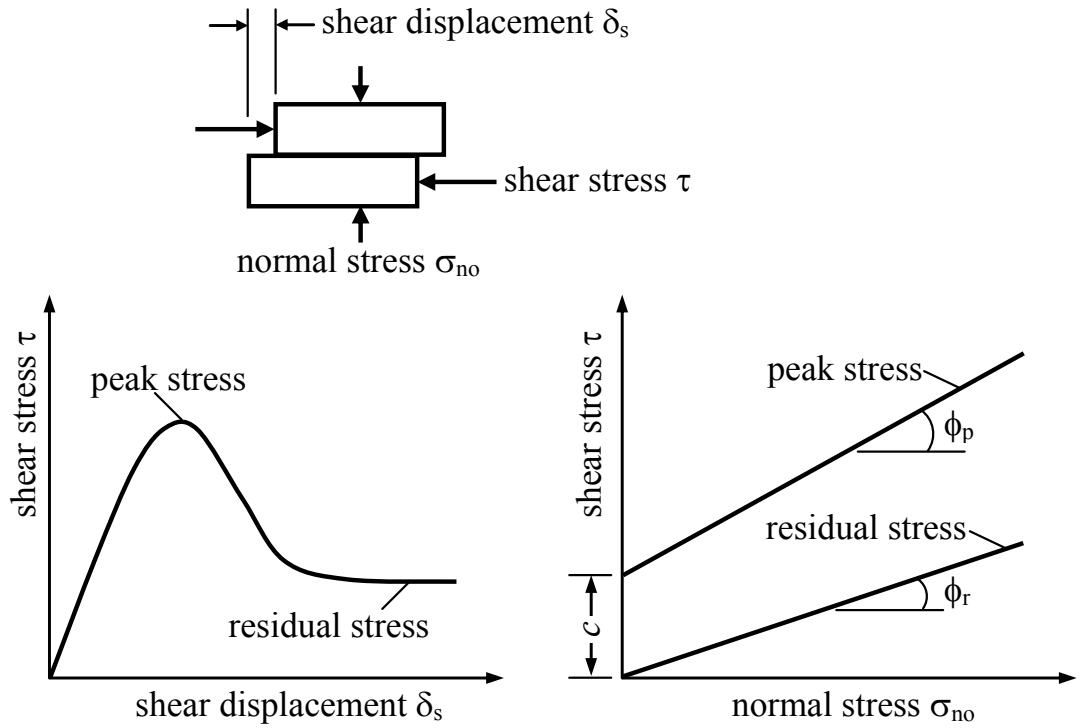

Figure 8. Shear behavior of planar joint surfaces (Allaby, 2008).

The relationship between peak shear stress and initial normal stress for rock joints can be represented by the Mohr-Coulomb failure equation:

$$\tau_p = \sigma_{no} \tan(\phi_p) + c \tag{1}$$

where τ_p is the peak shear stress of the joint,

ϕ_p is the peak internal friction angle of the joint,

c is the cohesion of the joint.

The cohesion for the residual shear stress has dropped to zero, therefore, the relationship between residual shear stress and initial normal stress can be represented by following equation:

$$\tau_r = \sigma_{no} \tan(\phi_r) \tag{2}$$

where τ_r is the residual shear stress of the joint,

ϕ_r is the residual internal friction angle of the joint.

Patton (1966) carried out shear tests on 'saw-tooth' specimens such as the one illustrated in Figure 9. Shear displacement in these specimens are connected with vertical displacement components causing dilation (increase in volume). The shear strength of Patton's saw-tooth specimens can be represented by:

$$\tau_p = \sigma_{no} \tan(\phi_b + i_1) \tag{3}$$

where i_1 is the dilation angle,

ϕ_b is the basic friction angle ($\phi_b \approx \phi_r$).

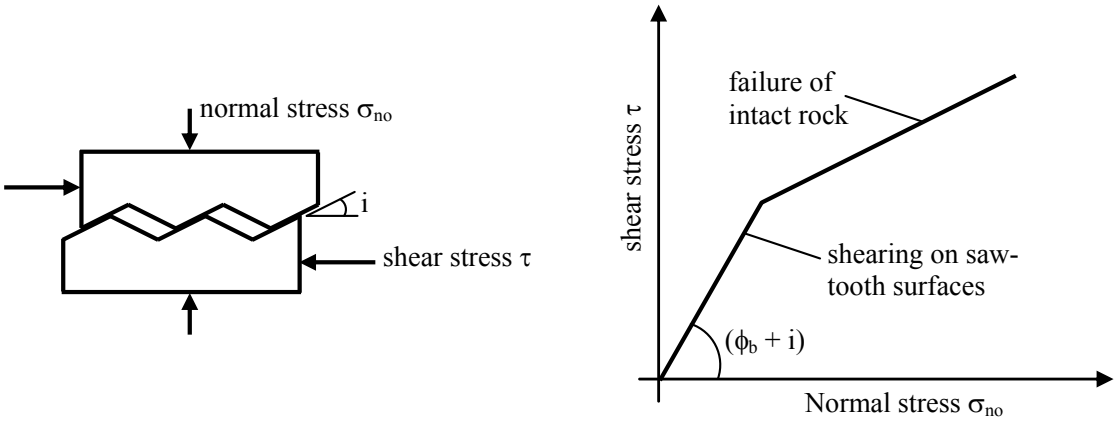

Figure 9. Patton's experiment on the shear strength of saw-tooth specimens.

The surface roughness of natural rock joints is an extremely important parameter, which has influence on the shear strength of joints, especially in case of unfilled joints. Generally, the shear strength of the joint surface increases with increasing surface roughness. Barton (1976) has proposed a joint roughness coefficient (JRC), which is part of the Q – rockmass classification system. Figure 10 shows typical roughness profiles for the entire JRC range. Based upon the results of experimental investigation, Barton (1973, 1976) suggested a relationship between shear strength of rough rock joints and JRC as follows:

$$\tau = \sigma_{no} \tan\left(\phi_b + JRC \log_{10}\left(\frac{JCS}{\sigma_{no}} \right) \right) \tag{4}$$

where *JRC* is the joint roughness coefficient,

JCS is the joint wall compressive strength.

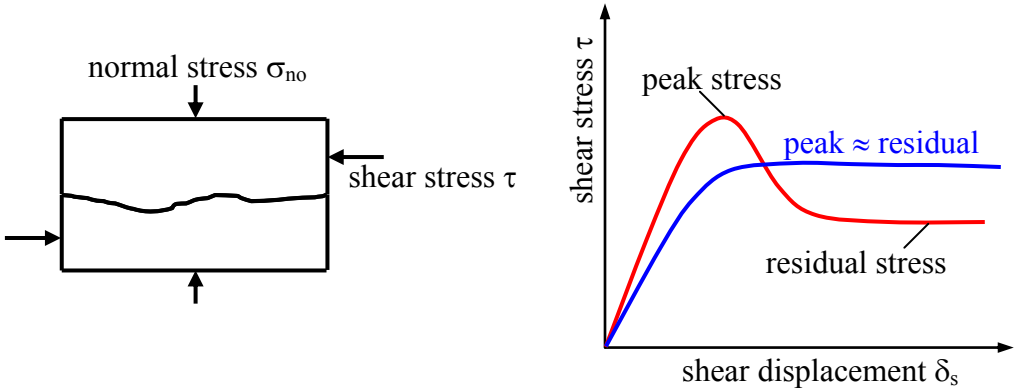

Figure 10. Shear behavior of rough rock joints (Barton, 1973 and 1976).

Depending on joint characteristics peak and residual shear stresses can be different. The red curve in Figure 10 indicates that the residual shear stress is significantly smaller than peak shear stress (typical for rough and brittle joints). However, the blue curve shows that the residual shear stress is only slightly lower than the peak shear stress. This is a typical behavior of ductile rock joints (Grasselli, 2001, 2002).

Grasselli et al. (2001, 2006) had investigated the size and distribution of contact areas of rough surfaces in a 3-dimensional manner during shearing and concluded that damaged area increases with increasing stress and displacement. Based on the results of more than 50 constant normal load direct shear tests, Grasselli and Egger (2003) developed a new constitutive criterion for peak shear strength of rock joints under constant normal load conditions:

$$\tau_p = \sigma_{no} \tan\left[\phi_b + \left(\frac{\theta^*_{\max}}{C} \right)^{1.18\cos\alpha} \right] \left[1 + e^{-\left(\frac{\theta^*_{\max}}{9 A_0 C} \right)\left(\frac{\sigma_{no}}{\sigma_t} \right)} \right] \tag{5}$$

where θ^*_{max} is the maximum apparent dip angle of the surface with respect to

the shear direction,

C is the roughness parameter,

α is the angle between the schistosity plane and the normal to the joint, if the rock does not exhibit schistosity, α is assumed to be zero,

A_0 is the maximum possible contact area in the shear direction,

σ_t is the tensile strength of the intact rock.

Belem et al. (2004) suggested a new peak shear strength criterion taking into account anisotropy of surface morphology to predict the shear behavior of irregular and regular joint surfaces under constant normal load and constant normal stiffness:

$$\tau_p = \sigma_{no} \tan(\phi_b + i_d) + K_n \left[u_s^o \tan(i_p)\right] \tan(\phi_b + i_d) \tag{6}$$

where K_n is the normal stiffness,

i_p is the peak dilation angle,

i_d is dilatancy-degradation angle and can be expressed as

$$i_d = 2\theta_s^o \exp\left[-\frac{\sigma_{no}}{\sigma_c}\frac{u_s^o}{a_o}\left(\frac{u_s^o}{u_s^{\max}} + \frac{2}{3}\frac{(k_a)^2}{DR_r^o}\right)\right] \tag{7}$$

where θ^0_s is the initial surface angularity,

σ_c is the compressive strength of rock,

u_s^o is the shear displacement in 1st quadrant of cyclic shear curve,

a_o is the maximum amplitude of surface,

u_s^{max} is the cumulated maximum shear displacement in 1st quadrant for n cycles of shearing,

k_a is the degree of surface apparent anisotropy,

DR^0_r is the initial degree of surface roughness.

Jiang et al. (2006) carried out direct shear tests on rock joints under low initial normal stress and measured the surface roughness of rock joints before and after shearing by using a 3D laser scanning profilometer system. They found that the residual shear strength under constant normal stiffness boundary condition is higher than residual

shear strength under constant normal load boundary condition. They also suggested a relation between shear stress and 3D fractal dimensions as follows:

$$\tau = \sigma_{no} \tan\left(500(D_s - 2)\log\left(\frac{JCS}{\sigma_{no}} \right) + \phi_b \right) \quad (8)$$

where D_s is the real fractal dimension of a rough surface.

Tatone and Grasselli (2012) investigated joint roughness scale dependency using a high-resolution surface measurement tool. Large scale (2 m x 6 m) fracture surfaces in-situ and small scale (100 mm x 100 mm) samples in the laboratory were digitized. The experimental results indicate that roughness of joint surface increases with increasing the sampling window size. However, the resolution of surface measurements has greater influence on roughness determination than sampling window size. Therefore, the observation suggests that the decrease of roughness of joint surface with increasing sample size may be attributed to inconsistent measurement resolution.

2.2.1.2 Dynamic lab tests (shear velocity dependency)

Shear velocity dependent behavior of joints is important for many geotechnical applications, like studies of earthquake mechanisms (creep and rate studies) or engineering problems in which the loading may either occur over long time periods (e.g. creep of rock slopes), or over short time periods (blast and seismic loads) or periodic (machinery vibrations). Lot of researchers have investigated the shear velocity dependent behavior, like Schneider, 1977; Crawford and Curran, 1981; Gillette et al., 1983; Jafari et al., 2003; Li and Zhu, 2012; Atapour and Moosavi, 2013; Nguyen et al., 2013 and 2014).

Schneider (1977) performed direct shear tests on shale to determine the shear velocity effects on shear behavior of rock joints made by a diamond saw cut parallel to the bedding. The frictional resistance was measured at six different shear velocities (i.e., 200, 100, 10, 1.0, 0.1 and 0.01 mm/min). It was shown that with the same normal stress,

the frictional resistance is greater at higher shear velocity. It was concluded that the frictional resistance depends on the normal stress and shear velocity.

Crawford and Curran (1981) conducted tests on many rock types such as syenite, dolomite, sandstone and granite. The tests were performed at constant rates of shear displacement varying from 0.05 to 200 mm/sec at normal loads of up to 100 kN. The results indicate that the shear strength of rock joints is dependent on the shear velocity. In general, for harder rocks, the shear strength was found to decrease with increasing shear velocity. Conversely, the shear strength of softer rock joints increased with increasing shear velocity.

Gillette et al. (1983) conducted direct shear experiments on artificial rock joints. They found a general trend indicating increasing shear strength with increasing shear velocity for their tests. They stated that velocity effects were observed for most of the tested rock samples.

Barla et al. (1990) have also conducted direct shear tests on single joints under dynamic loading. The tests were performed on saw-cut surfaces of dry sandstone. Dynamic tests were conducted at loading velocities from 1.0 to 10.0 MPa/sec and normal stresses of 0.5, 1.0 and 1.5 MPa. The experimental results indicate that the dynamic shear strength is greater than the corresponding static one and increases with increasing shear stress rate. The normal stress decreases with increasing shear loading rate.

Jafari et al. (2003) performed some tests on artificial joints and observed that shear strength reduced with increasing shear velocity under constant normal load boundary conditions.

Li and Zhu (2012) used new RGB (red, green and blue) colour model to research P wave velocity and joint surfaces damaging behavior. The results showed that the velocity of P waves across joints decreases with the increase of joint surface roughness.

Atapour and Moosavi (2013) investigated the effect of shear velocity on the shearing behavior of artificial joints at different normal stress levels. Artificial joints with planar and rough surfaces produced from plaster (simulating soft rock joints) and concrete (simulating medium to hard rock joints). The rough joints had triangular shaped asperities with 10°and 20° inclination angles. Direct shear tests were performed on these joints under various shear velocities in the range of 0.3 to 30 mm/min. The planar plaster–plaster and planer concrete–concrete joints were sheared at three levels of normal stress under constant normal load boundary conditions. The results of the shear tests show that shear strength of planar and rough plaster–plaster joints is decreased when the shear velocity was increased. Shear strength of concrete joints increased with increasing shear velocity. Regardless of the normal stress level, shear stiffness of both planar plaster–plaster and concrete–concrete joints is decreased when the shear velocity is increased.

Nguyen et al., (2013 and 2014) examined the effect of shear velocity on peak shear stress value. CNL tests were performed at normal stress of 2.5 MPa and shear velocity of 1 mm/min, 10 mm/min and 50 mm/min. With increasing shear velocity an increase in peak shear stress was observed. The peak shear stress increases about 8.3% and 12.5% when shear velocity increases from 1 to 10 mm/min and 1 to 50 mm/min, respectively. Based on their own experimental results and Barton's (1976) suggestion, a mathematical model was parameterized to evaluate the peak shear strength of the rock joints at different shear velocities:

$$\tau_p = \left(\frac{v_1}{v_2}\right)^n \sigma_{no} \tan\left(\phi_b + JRC \log_{10}\left(\frac{JCS}{\sigma_{no}}\right)\right) \tag{9}$$

where v_1 and v_2 are the shear velocities,

σ_{no} is the normal stress,

ϕ_b is the basic friction angle of the surface,

JRC is the joint roughness coefficient,

JCS is the joint wall compressive strength,

n is the coefficient, which is determined by performing regression analysis using own experimental results (n = 0.02944).

Wang et al. (2016) performed direct shear tests under CNL conditions. Shear rate and joint roughness coefficient (JRC) were taken into consideration. Test results indicate that the peak shear strength is controlled by shear rate and joint roughness. Shear rate has a nonlinear relationship with the peak shear strength, whereas joint roughness exhibits good linearity with a high correlation coefficient. Furthermore, shear rate affects the damage incurred by the rock joints.

2.2.1.3 Dynamic lab tests (cyclic tests)

Dynamic cyclic shear experiments were conducted on fresh artificial rock joints under drained and undrained conditions by Gillette et al. (1983). The tests were carried out at frequencies from 0 to 10 Hz and normal loads from 69 to 3448 kPa. They found that the shear strength of dry rock joints is velocity dependent and shear strength of rock joints increase with increasing shear velocity. Dynamic tests on undrained rock joints revealed that the interstitial water pressure in a joint subjected to dynamic shear displacements stabilizes early in the process and does not continue to increase with increasing number of cycles. They also found that the shear strength of the joint closely follows the effective stress law even during the highly fluctuating water pressures.

Huang et al. (1993) and Qui et al. (1993) conducted cyclic shear tests on artificial and natural joints with normal stress ranging from 0.5 to 6.0 MPa. Experimental results show that under low normal stresses, surface damage was primarily caused by wear which was a gradual process of asperity degradation. Under high normal stresses, damage occurred more rapid and catastrophic (asperities were sheared). Under moderate normal stresses, the mode of damage was wear. They also developed a quantitative theory for joint behavior under cyclic loading.

Ahola et al. (1996) have studied the dynamic behavior of natural and artificial rock joints. The dynamic lab tests were performed under both harmonic and earthquake loading conditions with frequencies ranging from 1.4 to 3.5 Hz. They observed that the shear resistance could be quite different for the forward and backward shear directions depending on the joint roughness and interlocking nature of the joint

surfaces. The joint dilation response during dynamic tests showed very little hysteresis between the forward and reverse shear directions.

Divoux et al. (1997) introduced a mechanical constitutive model based on experimental results of cyclic shear tests.

Fox et al. (1998) investigated the influence of interface roughness on dynamic shear behavior in jointed rock. An interlock/friction model was developed and used to predict the behavior of natural jointed rock specimens subjected to dynamic shear load.

Lee et al. (2001) investigated the asperity degradation of rough rock joints under cyclic shear loading. Cyclic shear lab tests were conducted for two joint types of Hwangdeung granite and Yeosan marble: saw-cut and split tensile joints. They recognized high peak shear strength and non-linear dilation in the first loading cycle, different frictional resistance for the reverse shear loading direction, anisotropic shear behavior and its dependence on the normal stress level.

Jafari et al. (2003) studied the influence of cyclic shear tests on the degradation of an undulated artificial joint of mortar and found that during cyclic shear displacement degradation will occur, depending on the cyclic displacement magnitude and normal stress applied. During small earthquakes and low amplitude dynamic loadings, asperities will be slightly affected, but during strong earthquakes and under high amplitude dynamic loadings, asperities may be totally damaged. The shear strength of joint replicas is decreasing during small repetitive cyclic loadings. The number of load cycles and stress amplitude are two main parameters controlling the shear behavior of rock joints during cyclic loading. Dilation angle, degradation of asperities and wear are three main factors which affect the shear strength of rock joints during large cyclic displacements. The shear behavior of rock joints during sliding is in direct relation to the normal stress level and may change from sliding to breaking during cyclic displacements. Based on the experimental results, mathematical models were developed to evaluate the shear strength of the rock joints under cyclic shear loading. In case of low amplitude cyclic loading (shear velocity from 0.05 to 0.4 mm/sec and maximum shear displacement of 0.1 mm), the following relation is proposed:

$$\frac{\tau}{\sigma_{no}} = \frac{a\left(NC_s\right)^m \left(\omega_n A_n\right)^n}{1 + a\left(NC_s\right)^m \left(\omega_n A_n\right)^n} \tag{10}$$

where NC_s is the number of stress cycles,

ω_n is the normalized shear velocity,

A_n is the normalized stress amplitude,

a = 0.3; m = -0.045; n = -0.17.

In case of large cyclic shear displacements (maximum shear displacement of 15 mm), the following relation is proposed:

$$\frac{\tau}{\sigma_{no}} = \frac{b\left(NC_d\right)^p \left(i_n\right)^q + c}{1 + b\left(NC_d\right)^p \left(D_n\right)^q} \tag{11}$$

where NC_d is the number of displacement cycles,

i_n is the normalized dilation angle,

D_n is the normalized degradation (normalized by maximum value of asperity amplitude),

B = -0.33; c = 1.44; p = 0.12; q = 0.3.

Belem et al. (2007) conducted tests on three different specimens with different shapes (hammered, corrugated and rough) under monotonic and cyclic shear test conditions. Surface topographical data were measured before and after each shear test using a laser sensor profilometer. Based on the experimental results and previously proposed surface roughness description parameters, they have proposed two rock joint surface roughness degradation models to predict the variation of joint surface degradation during monotonic and cyclic shearing.

Ferrero et al. (2010) have developed a new apparatus for monotonic cyclic shear tests. The lab cyclic tests were performed with frequencies ranging from 0.013 to 3.9 Hz and maximum displacements between 1.0 and 4.0 mm. The experimental results show that the strength decrease is strongly controlled by the amplitude since, for equal global displacement, smaller amplitudes determine the damage of asperities in a

smaller range with a consequent lower global degradation when compared with cycles of larger size.

Konietzky et al. (2012) conducted dynamic tests on shalestone samples with dynamic normal load (earthquake signal) of about 550 kN and a shear load of about 300 kN. They found that shear strength decreases with ongoing shear displacement and the dynamic input also leads to further settlement (joint closure).

Thevenet et al. (2013) investigated the behavior of adhesively bonded joints under cyclic shear loading with different impact amplitudes. They underlined, that the evolution of viscous deformations and damage depends on the loading type.

Mirzaghorbanali et al. (2014) performed cyclic shear tests in the lab on artificial rock joints with different shear rates and initial normal stresses under CNS conditions and found that shear strength decreases with increase in the number of loading cycles and shear rate. When the normal force was increased, the effect of shear rate became less pronounced.

Nguyen et al. (2014) conducted cyclic shear tests on Mayen-Koblenz slate and found, that peak shear stress of the jointed rock under dynamic loading shows tendency to increase with time. Depending on the joint orientation the peak shear stresses are higher or lower in the positive or negative shear direction, respectively. The peak shear stress under dynamic loading is approximately 30% higher than that under static loading. The normal stress was nearly constant during cyclic shearing.

Furthermore, the cyclic loading applied in the normal direction was also investigated by other researchers (Bagde and Petros, 2005; Guo et al., 2011; Liu et al., 2011, 2012; Ling et al., 2015; Zhou et al., 2015). Bagde and Petros (2005) studied the fatigue properties of intact sandstone under different waveforms, amplitudes and frequencies. They concluded that all these three factors have great effect on the fatigue properties. The most critical damage was observed applying square waves with low frequency and low amplitude. Guo et al. (2011) investigated the fatigue damage and irreversible deformation of salt rock under uniaxial cyclic loading. They found that fatigue life

time of rocks is mainly influenced by its structure as well as applied stress amplitude. Liu et al. (2011, 2012) carried out axial cyclic loading tests on sandstone samples. They recognized that under large confining pressure the samples failed after fewer cycles. They also found, that axial strain and number of cycles up to failure increase with increasing frequency. Ling et al. (2015) performed cryogenic cyclic triaxial tests on frozen compacted sand from Nehe, Heilongjiang Province in China. The results indicate that the freeze–thaw process has significant effect on the dynamic shear modulus and damping ratio, which slightly change after one freeze–thaw cycle. Dynamic shear modulus increases with increasing initial water content, temperature, loading frequency and confining pressure. Damping ratio increases with increasing initial water content, while decreases with increasing temperature and loading frequency. Furthermore, empirical expressions were formulated to estimate dynamic shear modulus and damping ratio of the frozen compacted sand.

2.2.2 Numerical simulations

Numerical simulations can provide additional information which cannot be obtained from lab tests. In the last ten years, several researchers have used numerical simulations (FDM, FEM, DEM) to investigate the mechanical behavior of joints (Duriez et al., 2011; Bahaaddini et al., 2013, 2014, 2015 and 2016; Wijewickreme et al., 2013; Nguyen et al., 2013 and 2014; Wang et al., 2015; Zou et al., 2015; Liu, 2016).

Douglas et al (2007) simulated a laminar-type simple shear apparatus by 3D DEM. Nguyen et al. (2013, 2014) introduced an approach to reproduce the roughness of the joint by grid manipulation. Duriez et al. (2011) simulated the shear process for different loading paths by DEM and formulated an incrementally nonlinear constitutive relation to describe the mechanical behavior of infilled rock joints. Bahaaddini et al (2013, 2014, 2015 and 2016) investigated the effect of joint length on the shear behavior of rough rock joints using a particle bases approach and found that with increasing joint length, the peak shear strength, the peak dilation rate and the shear stiffness decrease while the peak shear displacement increases. Wang et al (2015) analyzed direct shear tests on ballast by DEM under different normal stresses.

With clumped particles, the interlocking of ballast stones in the direct shear test was investigated. The results demonstrate that shear resistance increases with normal stress application, indicating that the lateral confinement of ballast leads to less vertical settlement and more track stability.

2.3 Limitations and shortcomings of previous studies

Figure 11. Landslide caused by earthquakes.
(http://baike.baidu.com/link?url=tm9ezcGeqWpkbQM3TJygs1JJKnBWPSaTuQRYJQgfXf2TQlH5PZm5PSc0EvfQA28WFvBc2hq8KUYnb6vV5iBHZ)21/08/2016

The above mentioned dynamic research works can be divided into two groups: studies of the cyclic or dynamic impact normal to the joint plane (Bagde and Pertros, 2005; Belem et al., 2007; Guo et al., 2011; Liu et al., 2011, 2012; Zhou et al., 2015) and studies, which consider cyclic shearing parallel to the joint plane (Crawford and Curran, 1981; Kana et al., 1996; Lee et al., 2001; Jafari et al., 2003; Konietzky et al., 2012; Cabalar et al., 2013 ; Nguyen et al., 2014). However, due to the limitations of the used shear box devices, there is little research on direct/cyclic shear tests under DNL conditions. During an earthquake, movements along rock discontinuities in foundations, dams, tunnels, slopes etc. occur under very complex loading conditions (Figure 11). Stein (1999) had already proved that an earthquake alters the shear and normal stresses on surrounding faults in a complex dynamic manner. Therefore, it is

imperative to understand the variation of shear strength of rock joints under complex dynamic force and/or stiffness conditions (e.g., direct shear tests under CNL/DNL conditions and cyclic shear tests under CNL/DNL conditions). Furthermore, joint closure tests and complex analysis of shear box tests with explicit consideration of interaction between test device and sample leads to deeper understanding and enhanced data interpretation. According to the available literature, limitations and shortcomings of the traditional tests of joints can be summarized as follows:

- Joint stiffness tests are quite seldom performed, because they need very high measurement accuracy.
- The prior aim of lab testing is the determination of rock parameters. However, the lab measurements do not only reflect the rock properties, but also contain, at least to some extent, the influence of the test equipment. Even if measurements are designed to minimize the influence of the test equipment often some measurement values are effected by the measurement equipment. Therefore, it is necessary to evaluate the measured values under consideration of the complete test equipment, which is not done so far in most cases.
- ISRM suggested methods for lab shear tests recommended the use of three to four transducers to measure vertical displacement (Muralha, et al., 2014). However, most previous studies have considered only the average normal displacements to evaluate the dilation of jointed specimens during direct shearing (Li, et al., 2006; Crawford and Curran, 1981; Mirzaghorbanali, et al., 2013; Hossaini, et al., 2014; Liu, et al., 2014; Indraratna and Haque, 1997; Manda, et al., 2005; Moradian et al., 2010).
- Non-uniform deformations and stresses in the specimen during the direct shear tests were revealed in soil mechanical tests, but evaluation of direct shear tests of rock or rock like materials with plane joints considers only the average shear stress to evaluate the shear strength at the contact surface.
- Earthquakes and rock bursts are very complex dynamic events, where shearing under DNL conditions is a common phenomenon. However, because of the limitations of the shear box device, there is very little research on shear tests under DNL conditions. The understanding of the shear behavior under DNL conditions is almost unknown.

Therefore, the aim of this study is to investigate the shear behavior of artificial jointed specimens having a smooth plane joint surface under CNL/DNL boundary conditions. Special attention is paid to the influencing factors like normal stress, direct shear rate, horizontal cyclic shear frequency, normal impact frequency, horizontal cyclic shear displacement amplitude and vertical impact force amplitude.

3 Shear box device GS1000 and specimen preparation

In this chapter, big shear box apparatus GS-1000 is introduced. Furthermore, specimen preparation and installation process are described. GS-1000 shear box device can perform quasi-static and dynamic shear tests under different boundary conditions.

3.1 Shear box test apparatus GS-1000

Big shear box test apparatus GS-1000 (Figure 12) was developed by a team at the Chair for Rock Mechanics at TU Bergakademie Freiberg and belongs to the rock mechanical laboratory at the Geotechnical Institute of the TU Bergakademie Freiberg ((Luge, 2011; Konietzky, et al., 2012). It can perform direct shear tests under static, dynamic (in both vertical and horizontal directions) and hydro-mechanical coupled conditions with extreme high loads (up to 1000 kN), big sample dimensions (up to 400 x 200 mm^2) and superimposed dynamic loads up to 40 Hz with force amplitudes of up to ± 500 kN in both normal and shear directions.

Table 1. Technical data of GS-1000 shear box device.

Item	Value
Normal force	from 0 kN to +1000 kN
Shear force	from -300 kN up to +800 kN
Maximum shear displacement	50 mm
Shear velocity	from <1e-7 mm/s up to 70 mm/s
Frequency	from 0 Hz to 40Hz
Dynamic loading	-500 kN up to +500 kN superimposed on static force level

The main technical data of GS-1000 is shown in Table 1. 16-bit signal resolution is applied for all measurements. LVDT's are used to measure vertical and horizontal displacements and load cells are used to measure forces in normal and shear directions. According to ISRM suggested methods (Muralha et al., 2014), GS-1000 shear box device uses four vertical LVDT's with high accuracy (+/- 0.001 mm) to measure vertical displacement. These LVDT's are positioned at the four corners of the upper part of the shear box (Figure 13). The GS-1000 apparatus consists of two

parts: a hydraulic and a mechanical part including loading system, shear box, water cooling system and loading aggregate and a control and measurement part including measuring system, control unit and data acquisition system (see also Figure 12).

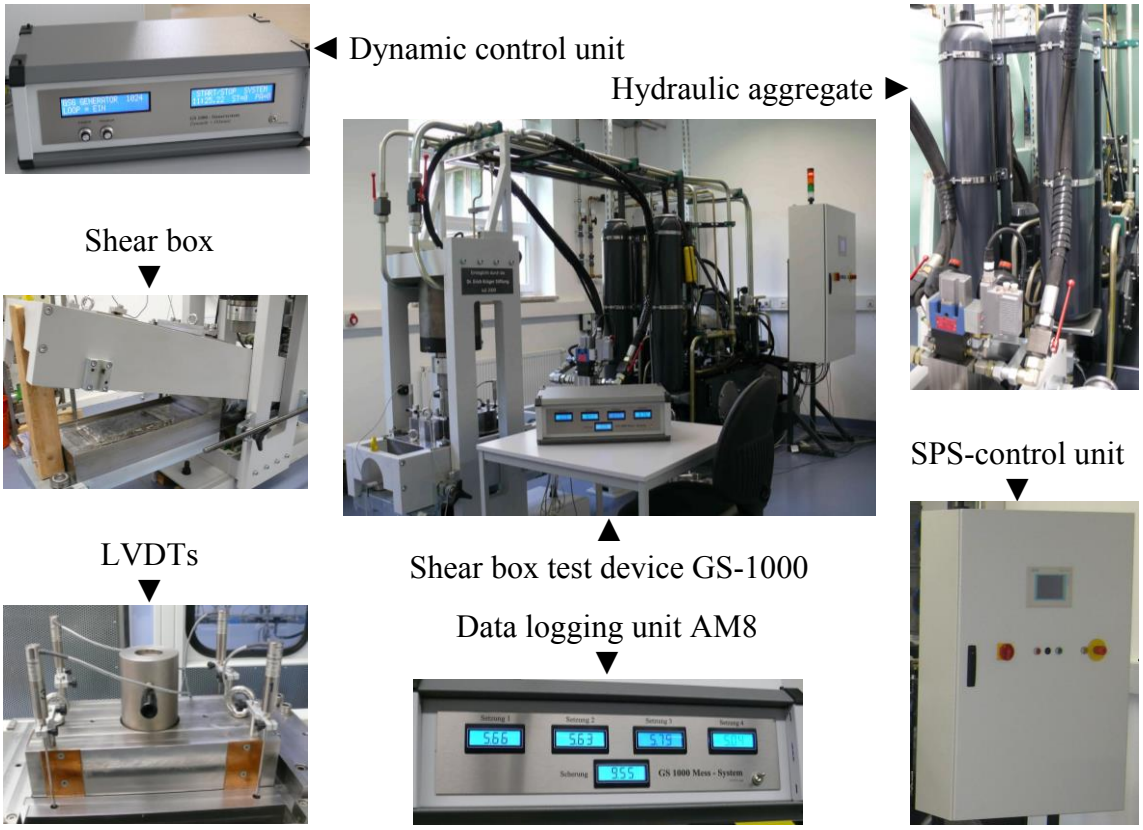

Figure 12. Overview of direct shear test apparatus GS-1000 (Luge, 2011; Konietzky, et al., 2012).

For the dynamic tests up to 40 Hz under full load or for tests with higher frequencies at reduced loads, a special designed generator (GSG) on the basis of two coupled dual-boards NET16LU was developed. The NET16LU unit comes with 2 TCP/IP interfaces for fast communication with GBSS software. The GSG works on the basis of a 16 bit digital signal synthesis with synchronous and separate gate for normal and shear force. Standard signals (sinus, rectangle, ramps etc.) as wells as arbitrary signals, e.g. from earthquake recordings, can be used. A sampling rate between 1 and 10.000 Hz can be chosen. Dilatancy controlled testing can be performed independently from the PC with 16 bit accuracy using the dual board NET16LU unit.

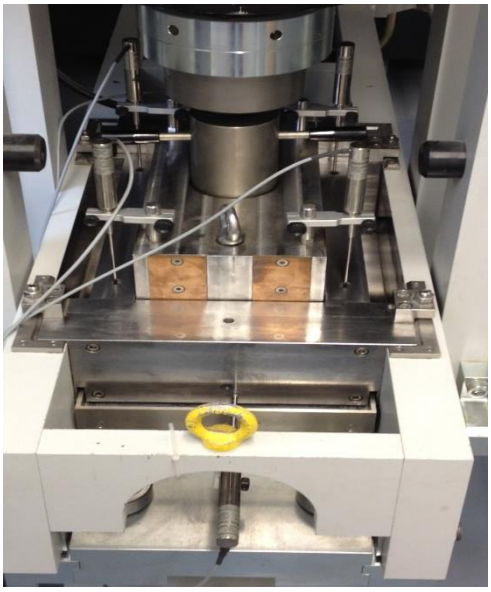

Figure 13. LVDT's for the normal and shear displacement measurement.

3.2 Plane joint specimen preparation and installation

In order to have several samples with nearly identical properties available, laboratory specimens were made of artificial material. In this study, concrete replicas of jointed rock were used. The fact that replicas made from the same cast have nearly identical surface characteristics permits one to perform parameter studies to investigate the influence of different static and dynamic boundary condition on the joint behavior.

Sample preparation and direct shear tests were conducted according to the recommendation of the International Society for Rock Mechanics (ISRM, 1974 and 1978) and the American Society for Testing and Materials (ASTM, 2002). The specimen size is 300 mm x 160 mm x 150 mm (length/width/height). Each specimen contains a smooth plane joint which separates the specimen into two equal halves 75.0 mm high. The inherent roughness of this shear plane is determined by the wooden formwork used for manufacturing and varies less than 1.0 mm deviation from a perfect plane. The specimens were made of CEM I 32.5 R cement and Hohenpockaer glass sand with a mass ratio of 1:3. Specimens were cured at room temperature for 28 days. Testing of these samples gave following results: tensile strength 2.5 MPa, uniaxial compression strength 19.1 MPa, Young's

modulus 30 GPa, Poisson's ratio 0.2, cohesion 7.2 MPa, internal friction angle 40° , dilation angle 10° and density 2.5 g/cm^3.

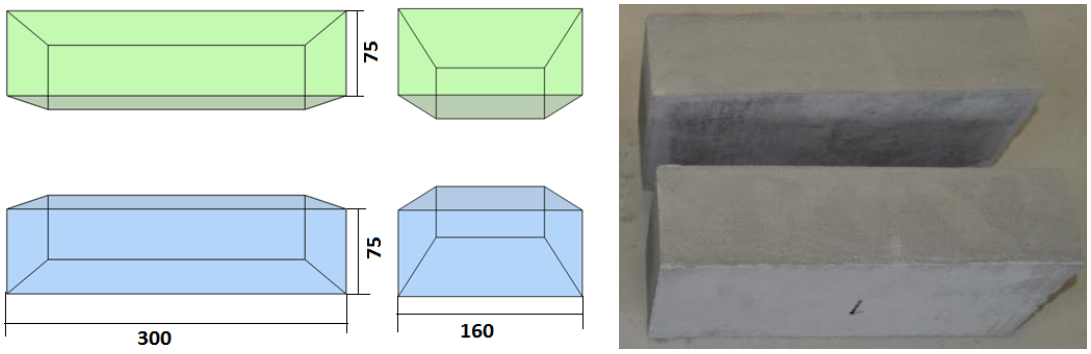

(a) **(b)**

Figure 14. Lower and upper part of the sample: (a) geometry and size in mm, and (b) sample photo.

Geometry of specimens is shown in Figure 14. The samples are fixed inside the lower and upper shear boxes by grouting. The grout is produced by a mixture of sand, special cement (fast hydration) and water. The strength of the grout is significantly larger than that of intact sample material. The sample is then left for at least 48 hours to allow the grout to dry. Figure 15 shows the procedure of the sample installation. The installation procedure is described as follows.

- **Step 1:** Grease is smeared evenly on the inner surface of the shear box, and a plastic film is placed inside the shear box.
- **Step 2:** Some grout is filled and leveled at the bottom part of the shear box. Then, the bottom part of the specimen is placed in the shear box (making sure that the sample is in the central part of the shear box, and that the upper surface of the sample and the shear surface of the GS-1000 are at the same horizontal level).
- **Step 3:** The space between the bottom part of the specimen and the shear box is filled with grout, and the plastic film is installed around the specimen. The specimen, plastic film and the shear surface of the GS1000 device are kept at the same horizontal level.
- **Step 4:** The upper part of the specimen is put inside the box and the plastic film is installed as explained in step 3. The unoccupied space in the shear box

is filled completely with grout. A flat metal plate is used to make the upper grout surface flat.

- **Step 5:** 40 minutes later, the loading plate is added. After 3 days, it is possible to perform the shear test.
- **Step 6:** The shear box is placed under the vertical loading piston and at the same time, the horizontal frame of the GS-1000 is fixed. The five Linear Variable Differential Transformer **(**LVDT's) sensors for the horizontal and vertical displacement measurement are installed.

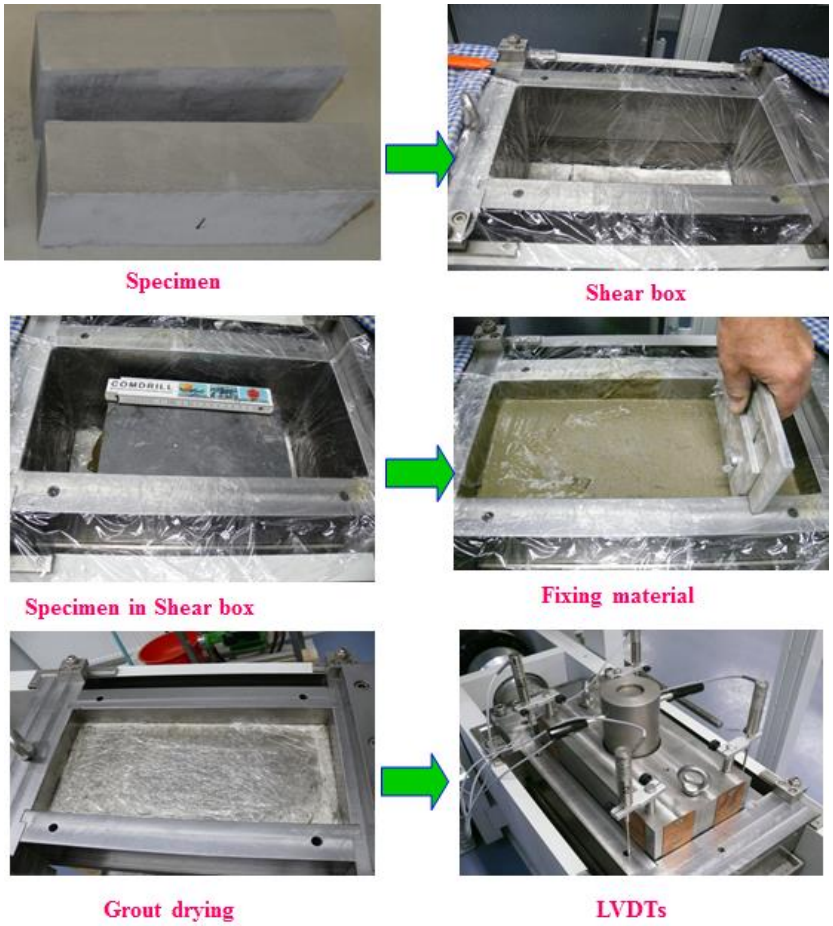

Figure 15. Specimen installation.

4 Joint stiffness determination

In this chapter, joint closure tests performed under quasi-static and dynamic conditions are explained. Based on these lab test results, joint normal stiffness is determined.

4.1 Test set-up

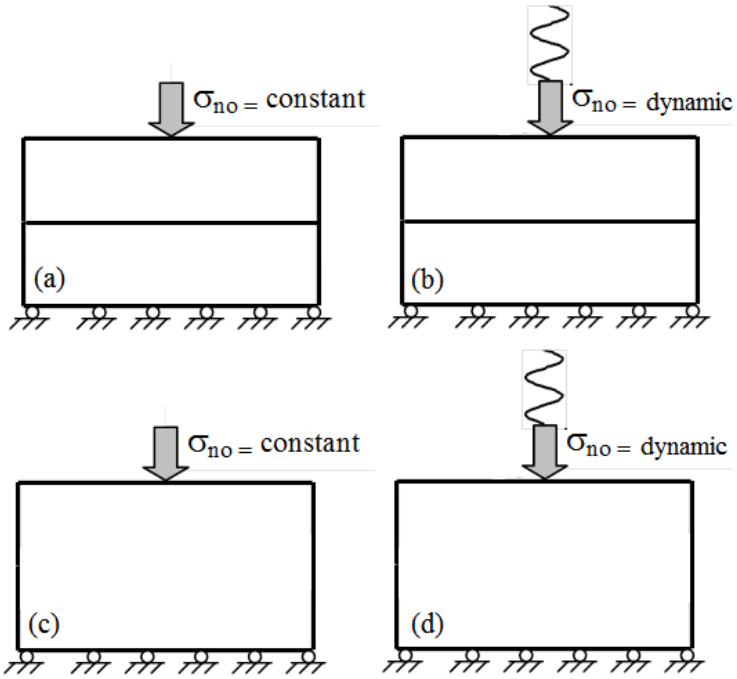

Figure 16. Set-up of joint closure test: (a) quasi-static test for jointed specimen, (b) dynamic test for jointed specimen, (c) quasi-static test for intact specimen and (d) dynamic test for intact specimen.

In order to obtain the joint stiffness, joint closure tests were performed in the laboratory. Test set-up for the joint closure tests under quasi-static and dynamic boundary conditions are illustrated in Figure 16. For the quasi-static tests, the normal force started at 0 up to 180 kN with a loading rate of 10 kN/min followed by unloading to 10 kN with a unloading rate of 10 kN/min. Then, the normal force increased to 90 kN with a loading rate of 10 kN/min. For the dynamic tests, the static normal force F_s was fixed at 90 kN superimposed by a dynamic vertical force of

± 10 kN to ± 60 kN with frequencies from 0.25 Hz to 4.0 Hz, The vertical dynamic sinusoidal excitation is applied as a superimposed forced as follows:

$$F_{sd} = F_d \sin(2\pi f t) \tag{12}$$

where F_{sd} is the dynamic normal force,

F_d is the amplitude of dynamic normal force,

f is the frequency,

t is the time.

The tests were conducted for both the intact specimen and jointed specimen. The displacement system is shown in Figure 17. The test parameters are summarized in Table 2.

Table 2. Test parameters for joint closure test.

Sample	Stage	F_s	f	F_d	*cycle*
		(kN)	(Hz)	(kN)	(-)
1	1	180	0	0	0
	2	30	0	0	0
	3	180	0	0	0
	4	90	0	0	0
2	1	90	0.5	±10	10
	2	90	0.5	±20	10
	3	90	0.5	±30	10
	4	90	0.5	±45	10
	5	90	0.5	±60	10
3	1	90	0.25	±45	10
	2	90	0.5	±45	10
	3	90	1	±45	10
	4	90	2	±45	10
	5	90	3	±45	10
	6	90	4	±45	10

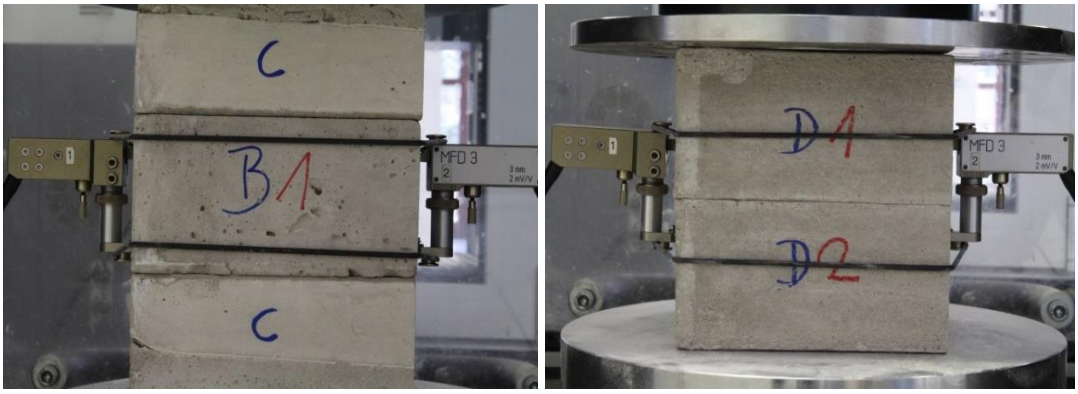

Figure 17. Displacement measuring device.

As Figure 17 shows, the applied displacement measuring system can measure the displacement of the matrix or the joint directly and avoids errors caused by the interfaces between specimen and loading plates in case of using external displacement measuring. The joint displacement and joint stiffness can be calculated by the following formula:

$$l_{Joint} = l_{D1D2} - l_{B1} \tag{13}$$

where l_{Joint} is the displacement of joint,
l_{D1D2} is the displacement of the joint specimen (measured),
l_{B1} is the displacement of the intact specimen (measured).

$$K_{Joint} = F_N / l_{Joint} \tag{14}$$

where K_{Joint} is the joint normal stiffness,
F_N is the normal force.

4.2 Test results

4.2.1 Quasi-static test results

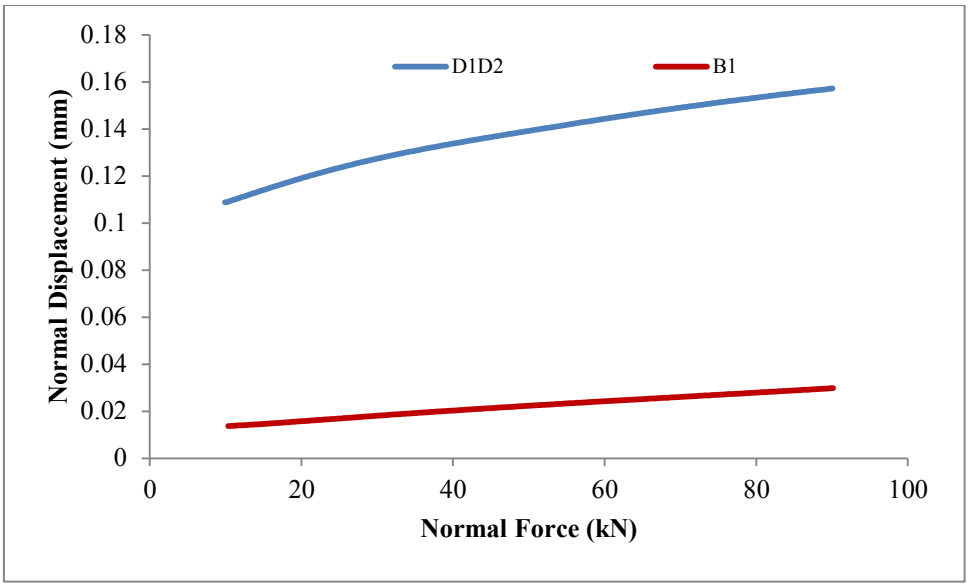

Figure 18. Joint closure test: measured displacements vs. normal force.

Only repeated loading/unloading parts are selected for calculation. As shown in Figure 18 and Figure 19, the measured normal displacements are normalized so that a normal force of 0 kN corresponds to a normal displacement of 0 mm.

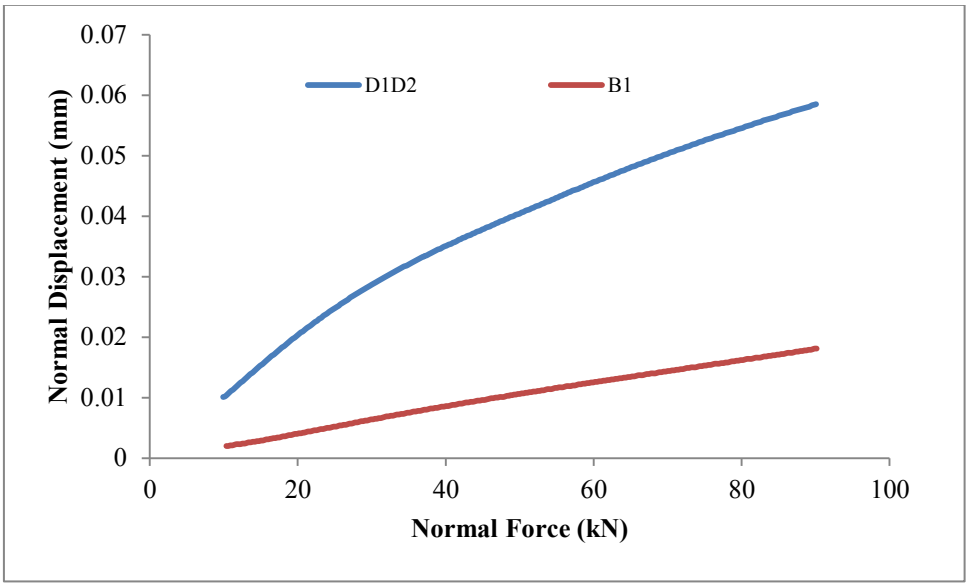

Figure 19. Joint closure test: normalized displacements vs. normal force.

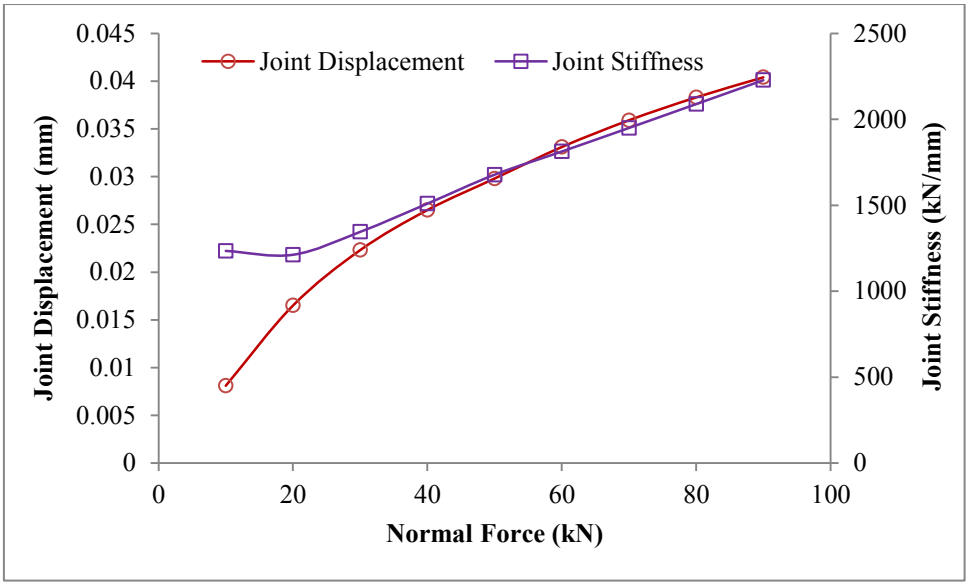

Figure 20. Joint closure test: joint stiffness and joint displacement vs. normal force.

4.2.2 Dynamic test results

The normal displacement of joint increases with increasing normal loads or superimposed normal force amplitudes, as documented in Figure 21, Figure 22 and Figure 23, and this holds for both, quasi-static and dynamic conditions. However, quasi-static stiffness increases with increasing normal force (this behavior is similar to the well-known phenomenon of 'small strain stiffness' in soil mechanics), but dynamic stiffness decreases with increasing superimposed normal force amplitudes. Normal impact frequencies have no significant influence on the stiffness. It has to be said, that the last conclusion has been drawn from tests at a very restricted frequency range and general validation and is therefore not given.

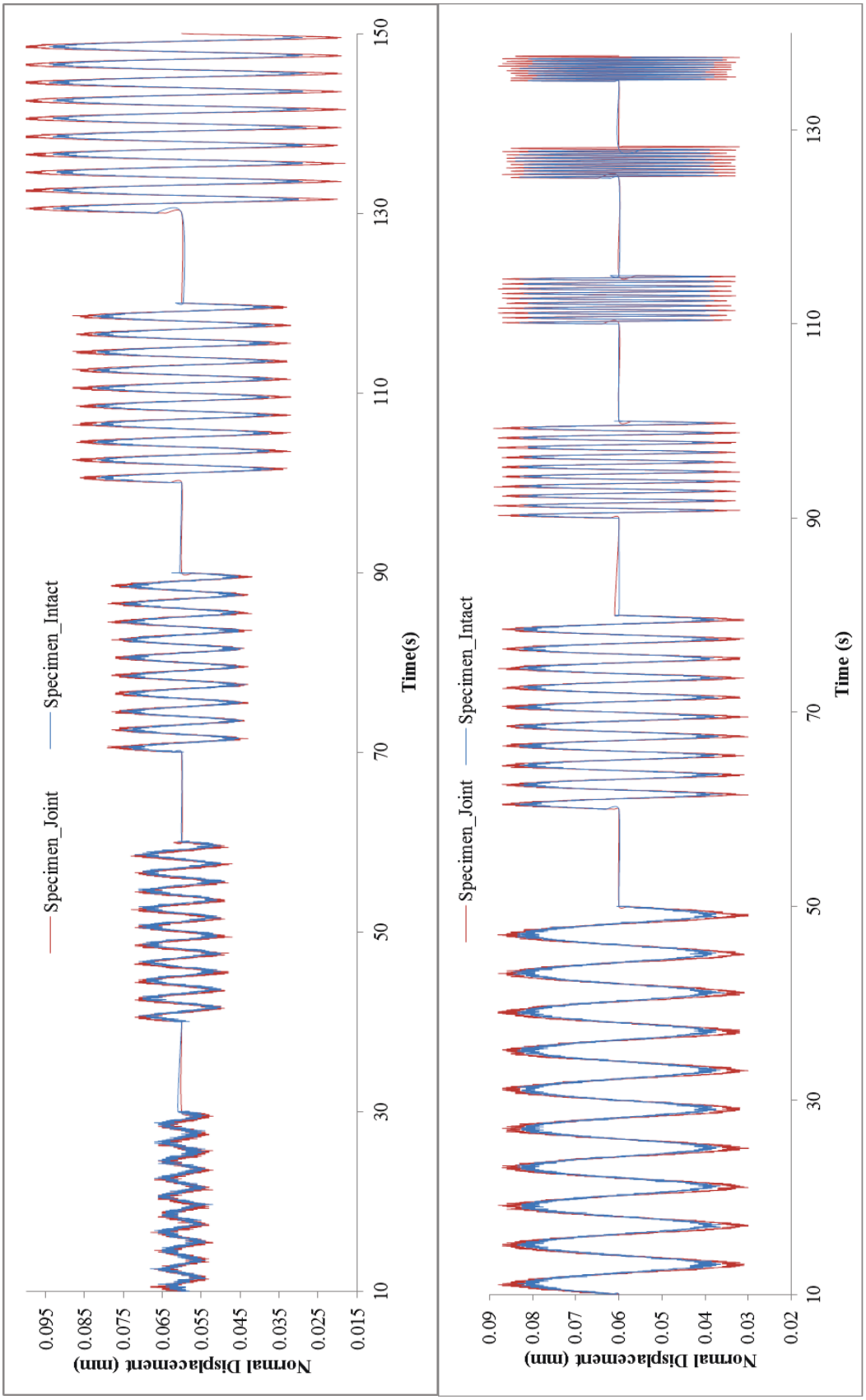

Figure 21. Dynamic joint closure test: normal displacement vs. time.

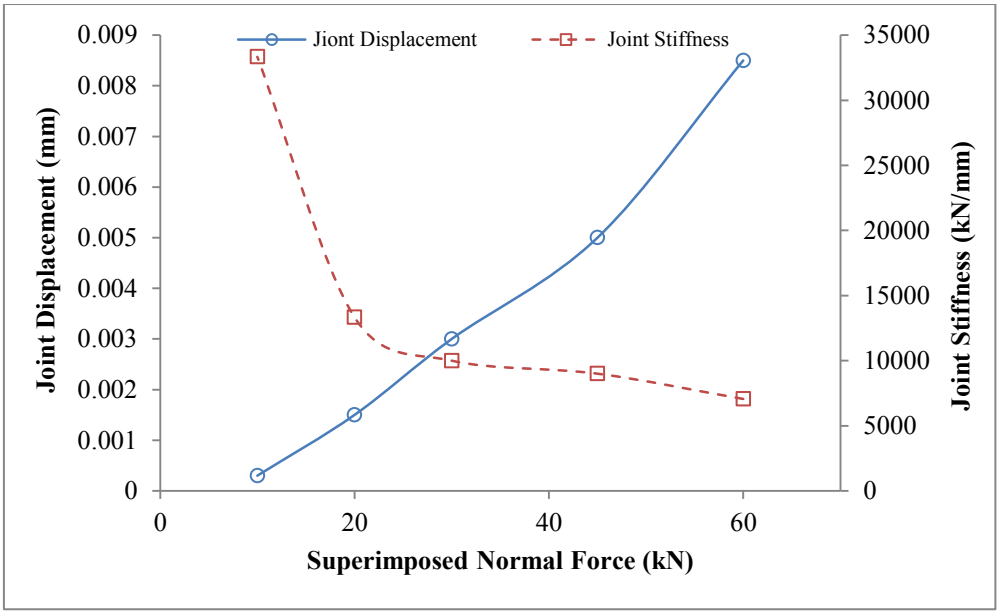

Figure 22. Dynamic joint closure test: joint normal displacement and joint normal stiffness vs. different superimposed normal forces.

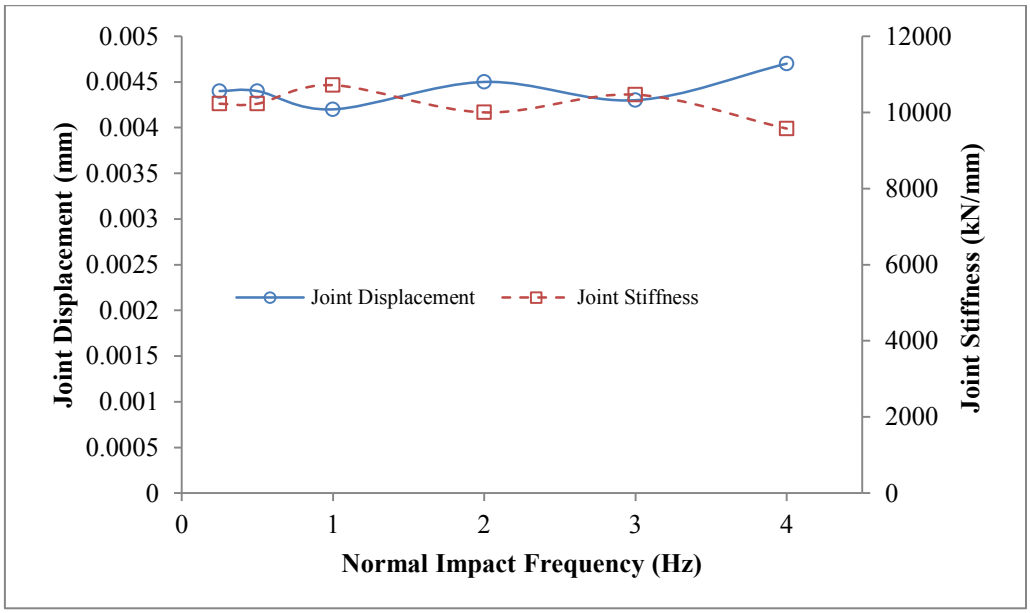

Figure 23. Dynamic joint closure test: joint normal displacement and joint normal stiffness vs. different normal impact frequencies.

5 Laboratory shear tests

In this chapter, four kinds of lab shear tests are presented: Quasi-static direct shear tests under CNL conditions, cyclic shear tests under CNL conditions, direct shear tests under DNL conditions and cyclic shear tests under DNL conditions. The target of these investigations is to get a deeper understanding of the shear behavior under consideration of different normal load levels, vertical and horizontal impact frequencies, vertical impact amplitudes, and horizontal shear displacement amplitudes. Especially development of normal force, shear force, friction coefficient, time shift and dilation are investigated.

5.1 Shear tests under CNL conditions

5.1.1 Direct shear tests under CNL conditions

5.1.1.1 Test set-up

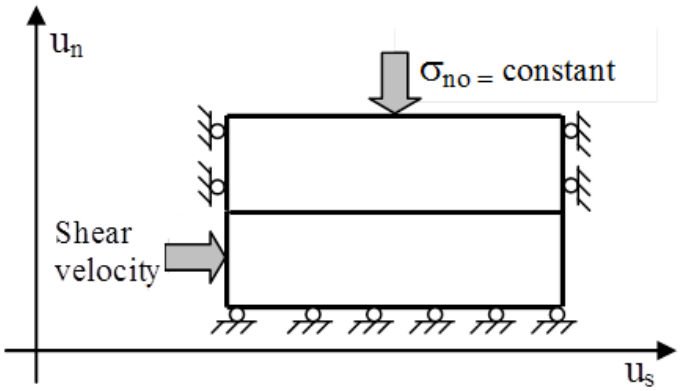

Figure 24. Set-up of direct shear test (CNL-test).

Set-up of direct shear tests under CNL boundary conditions is illustrated in Figure 24. For the first two samples (DCNL_1 and DCNL_2), the constant normal forces were 30 kN, 60 kN, 90 kN, 180 kN and 360 kN, respectively. The shear velocity was 3.0 mm per minute with maximum shear displacement of 2.0 cm. For the samples DCNL_3, DCNL_4 and DCNL_5, the joint behavior influenced by velocity was tested. Different shear velocities were chosen: 100 mm/minute, 10 mm/minute, 1.0 mm/minute and 0.1 mm/minute, respectively, under constant normal load of 60 kN, 90 kN and 180 kN. Test parameters are summarized in Table 3.

Table 3. Test parameters for direct shear test under CNL conditions (multi-stage tests).

Sample	Stage	Input Parameters			Sample	Stage	Input Parameters		
		F_s	v	u_{s_max}			F_s	v	u_{s_max}
		(kN)	(mm/min)	(mm)			(kN)	(mm/min)	(mm)
DCNL_1	1	30	3	20	DCNL_4	1	90	100	25
	2	60	-3	20		2	90	-10	25
	3	90	3	20		3	90	10	20
	4	90	-3	20		4	90	-1	20
	5	60	3	20		5	90	1	20
	6	30	-3	20		6	90	-0.1	20
DCNL_2	1	90	3	20	DCNL_5	1	180	100	25
	2	180	-3	20		2	180	-10	25
	3	360	3	20		3	180	10	20
	4	360	-3	20		4	180	-1	20
	5	180	3	20		5	180	1	20
	6	90	-3	20		6	180	-0.1	20
DCNL_3	1	60	100	25	Note: velocity above 0 means forward shearing (push); velocity below 0 means backward shearing (pull).				
	2	60	-10	25					
	3	60	10	20					
	4	60	-1	20					
	5	60	1	20					
	6	60	-0.1	20					

5.1.1.2 Test results

An example of the relationship between shear force and shear displacement is shown in Figure 25. Shear forces increase with increasing normal forces. During each direct shear stage, shear forces increase linearly with increasing shear displacement until the peak shear forces are reached. After reaching the peak shear force, frictional sliding is observed at a residual shear stress level nearly identical to the peak value. Shear force versus shear displacement plots show three stages of deformation described as:

Stage 1: This stage is characterized by compaction and initial non regular relationship between shear force and shear displacement. In this stage, specimen and shear boxes are adjusted to each other, so that a shape- and force-fit contact is created.

Stage 2: The second stage comprises linear elastic deformations with increasing shear force until peak shear force is reached. Unloading of shear stress may recover the shear displacement elastically.

Stage 3: The third stage is characterized by friction sliding. In this stage, the shear force remains stable with a little fluctuation due to joint roughness and damage.

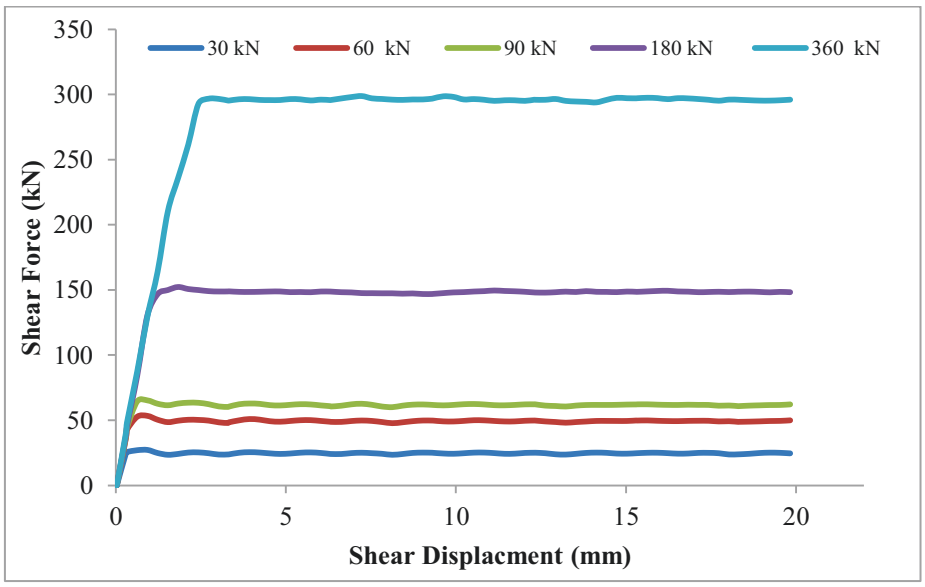

Figure 25. Shear force vs. shear displacement under different normal force at shear velocity of 3.0 mm/min.

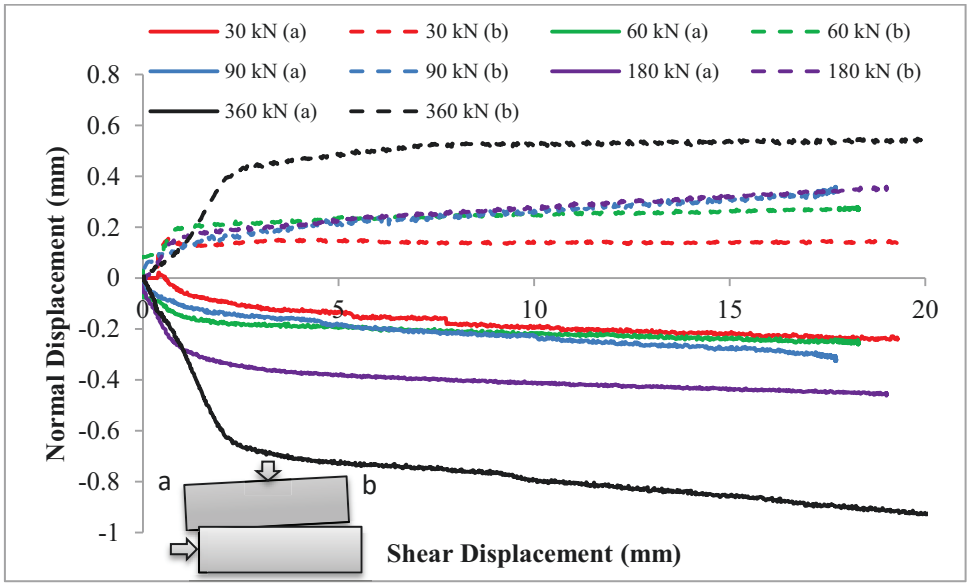

Figure 26. Shear displacement vs. normal displacement at shear velocity of 3.0 mm/min (a: left side of sample, b: right side of sample).

Rotation of the upper part of the specimen is calculated using the formula:

$$\alpha = \arctan\left(\frac{|u_{n(a)}| + |u_{n(b)}|}{a}\right) \tag{15}$$

where $u_{n(a)}$ is normal displacement of left side,

$u_{n(b)}$ is normal displacement of right side,

a is total length of specimen (= 300 mm).

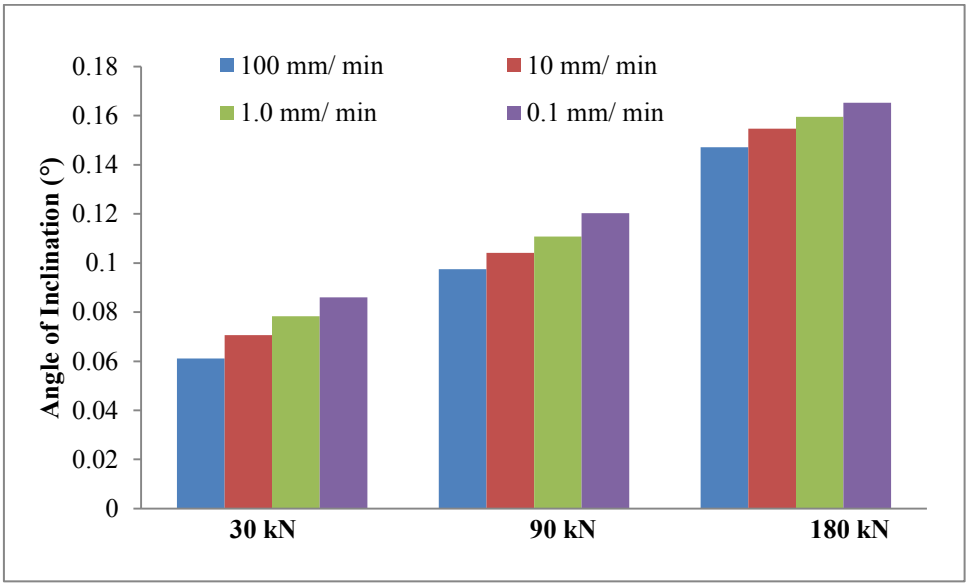

Figure 27. Peak angle of inclination influenced by shear velocities and normal forces.

Figure 26 shows a bi-linear inclination (rotation) behavior of the sample during shearing. Positive and negative displacement rates, respectively, are high up to about 2.5 mm shear displacement and become much smaller afterwards. Figure 27 shows that sample rotation (inclination) decreases with increasing shear velocity. Under normal loadings of 30 kN, 90 kN and 180 kN, with the decrease of shear velocities, the peak angle of inclination has the similar increasing trend. At the same shear velocity, the peak angle of inclination increases with increasing normal force.

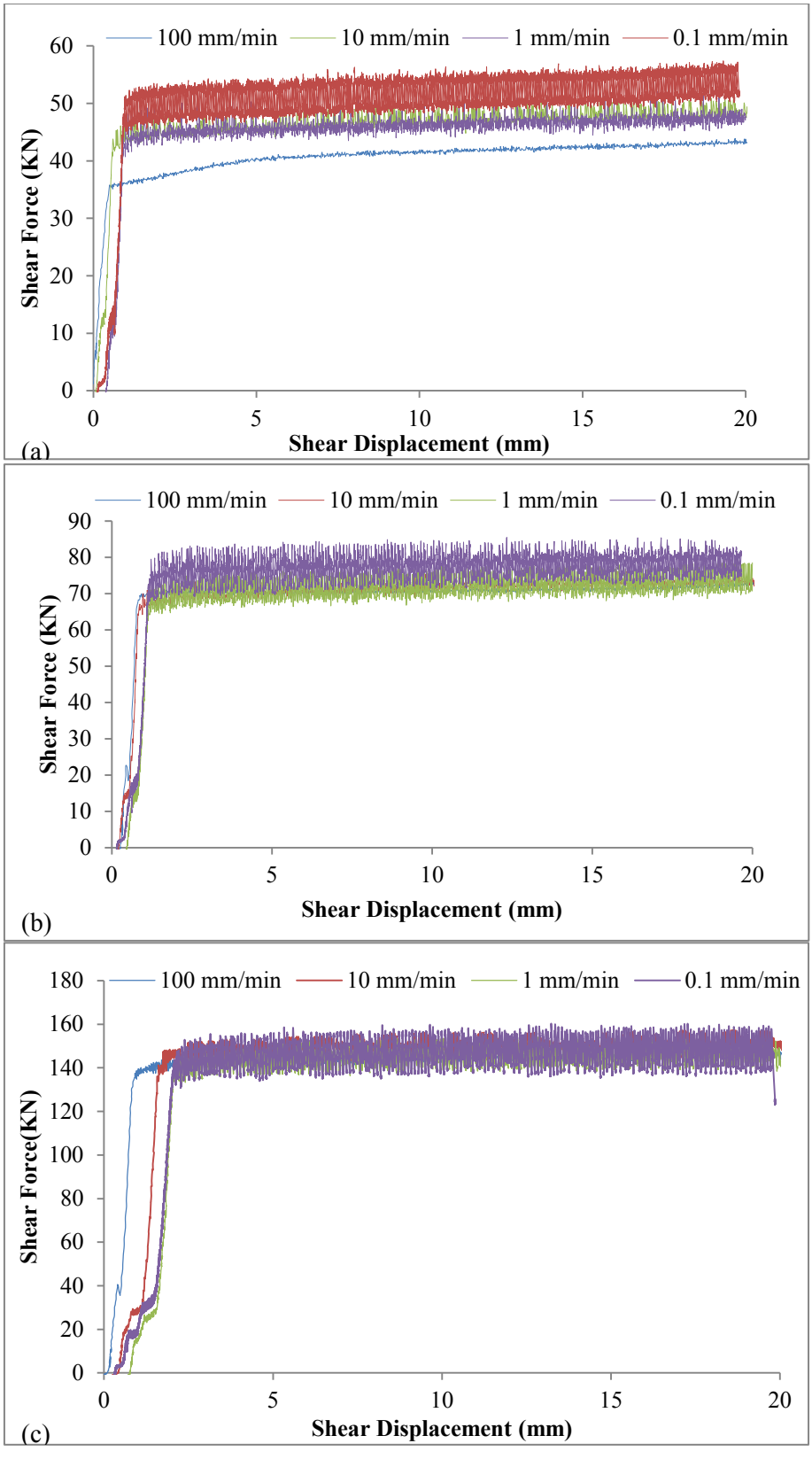

Figure 28. Shear force vs. shear displacement at shear velocities of 100 mm/minute, 10 mm/minute, 1.0 mm/minute and 0.1 mm/minute: (a) normal force 60 kN, (b) normal force 90 kN and (c) normal force 180 kN.

Figure 28 shows the relationship between shear displacement and shear force under different normal forces and shear velocities. It is obvious that shear force increases with increase of normal force and decreases with increase of shear speed. The shear force fluctuations inside the frictional sliding stage are bigger at smaller shear velocities.

Friction angle and cohesion of the interface are calculated according to the Mohr-Coulomb theory as shown by Eq. 16, whereby cohesion is zero (Figure 29). The friction coefficient of 0.824 corresponds to a friction angle of 39.5°.

$$\tau = 0.824\,\sigma_n \tag{16}$$

where σ_n is normal stress,

τ is shear stress.

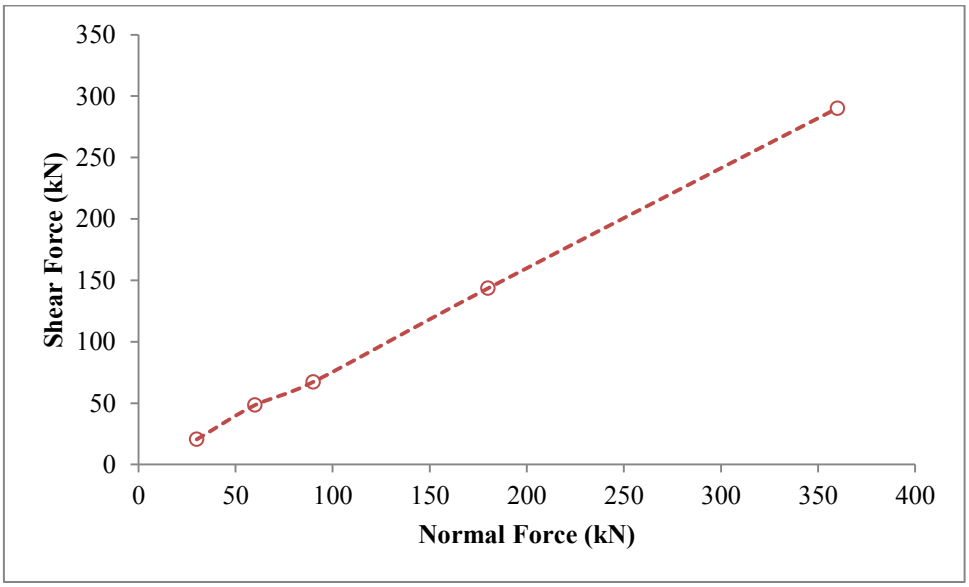

Figure 29. Normal force vs. peak shear force.

5.1.2 Cyclic shear tests under CNL conditions

5.1.2.1 Test set-up

In this test, the cyclic loading was applied as a dynamic sinusoidal excitation in the horizontal direction and application of constant normal load on top of the specimen (Figure 30).

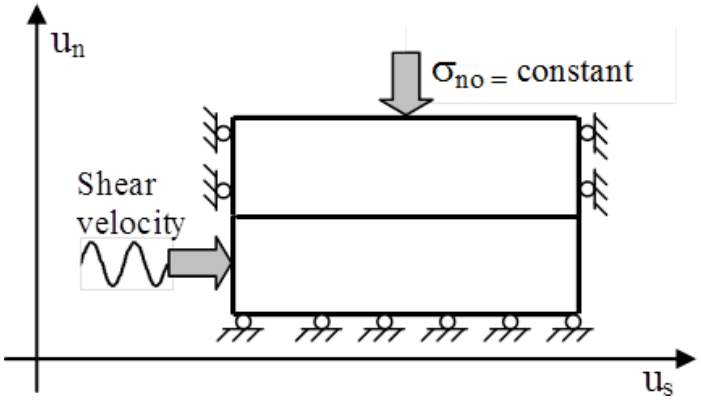

Figure 30. Set-up of cyclic shear test (CNL-test).

The shear displacement controlled sinusoidal excitation was applied horizontally to the bottom part of specimen as follows:

$$u_s = u_{\max} \sin(2\pi f t) \tag{17}$$

where u_s is the shear displacement,
u_{max} is the amplitude of shear displacement,
f is the frequency,
t is the time.

All cyclic tests were performed with 10 shearing-cycles at each normal load level. For sample CCNL_1, the shear amplitude was maintained close to ± 5.0 mm at 1.0 Hz. The constant normal loads applied on top of the specimen are 30 kN, 60 kN, 90 kN, 180 kN, 360 kN and 480 kN, respectively. For samples CCNL_2, CCNL_3, CCNL_4, the shear displacement amplitude was maintained close to ± 0.5 mm, the cyclic shear frequencies were 0.25 Hz, 0.5 Hz, 1.0 Hz, 2.0 Hz, 3.0 Hz, 4.0 Hz, 5.0 Hz, 10.0 Hz and

20.0 Hz, respectively, and the constant normal loads applied on top of the specimen were 30 kN, 90 kN and 180 kN, respectively. For samples CCNL_4, CCNL_5, CCNL_6, keeping the frequency at 1.0 Hz, the shear displacement amplitude was maintained close to ± 0.5 mm, ± 1.0 mm, ± 2.0 mm, ± 4.0 mm and ± 8.0 mm, respectively, and the constant normal loads applied on top of the specimen were 30 kN, 90 kN and 180 kN, respectively. The input dynamic signals are shown in Figure 31. The specific test schemes are shown in Table 4.

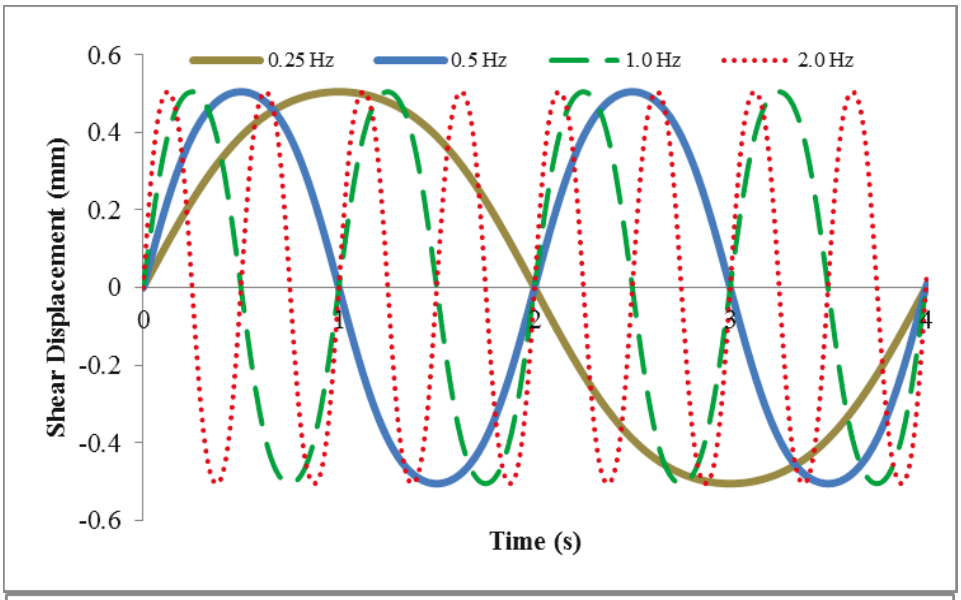

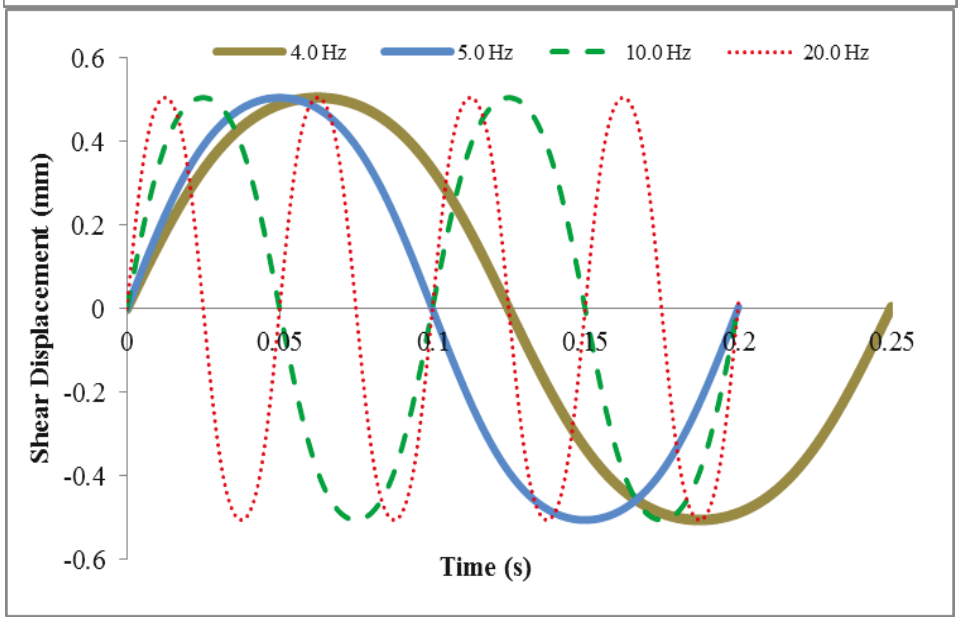

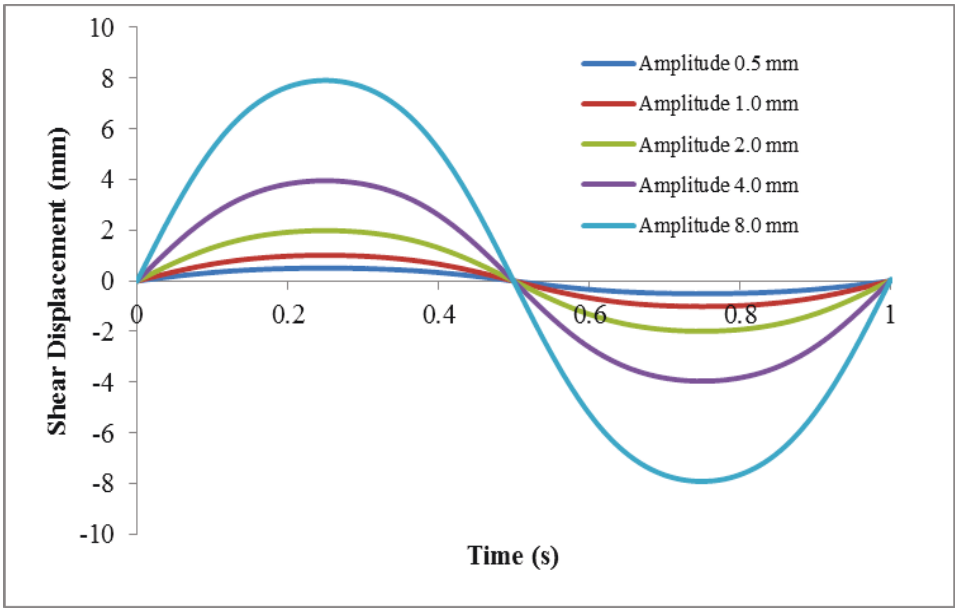

Figure 31. Dynamic input signals.

Table 4. Test parameter for cyclic shear test under CNL conditions.

Sample	Stage	F_n (kN)	f (Hz)	u_{max} (mm)	Sample	Stage	F_n (kN)	f (Hz)	u_{max} (mm)
CCNL_1	1	30	1	5	CCNL_4	1	180	0.25	5
	2	60	1	5		2	180	0.5	5
	3	90	1	5		3	180	1	5
	4	180	1	5		4	180	1.5	5
	5	240	1	5		5	180	2	5
	6	360	1	5		6	180	3	5
	7	480	1	5		7	180	4	5
CCNL_2	1	30	0.25	5		8	180	5	5
	2	30	0.5	5		9	180	10	5
	3	30	1	5		10	180	20	5
	4	30	1.5	5	CCNL_5	1	30	1	0.5
	5	30	2	5		2	30	1	1
	6	30	3	5		3	30	1	2
	7	30	4	5		4	30	1	4
	8	30	5	5		5	30	1	8
	9	30	10	5	CCNL_6	1	90	1	0.5
	10	30	20	5		2	90	1	1
CCNL_3	1	90	0.25	5		3	90	1	2
	2	90	0.5	5		4	90	1	4
	3	90	1	5		5	90	1	8
	4	90	1.5	5	CCNL_7	1	180	1	0.5
	5	90	2	5		2	180	1	1
	6	90	3	5		3	180	1	2
	7	90	4	5		4	180	1	4
	8	90	5	5		5	180	1	8
	9	90	10	5					
	10	90	20	5					

5.1.2.2 Test results

Tests under different normal loads, but same shear displacement amplitudes

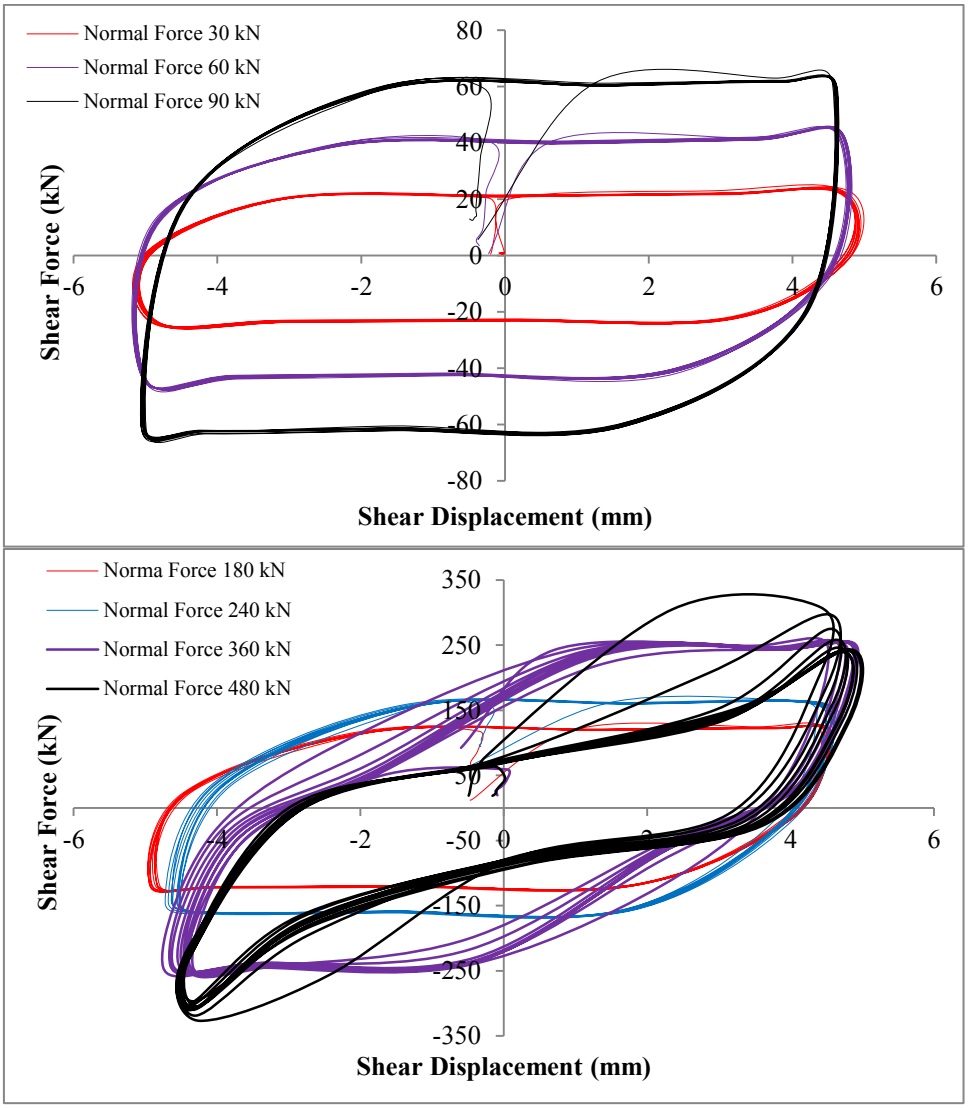

Figure 32. Shear force vs. shear displacement for multi-stage cyclic shear tests under different normal loads.

Figure 32, Figure 33, Figure 35 and Figure 35 show that peak shear forces increase with increasing normal forces. The absolute values of peak shear force in the positive shear direction (push direction) and in the negative shear direction (pull direction) are more or less the same. Under low normal loads (loads below 240 kN), strong shear forces increase with increasing shear displacement is observed: the peak value is reached after short shear displacement and is kept constant afterwards. With

increasing normal loads, larger shear displacements are necessary to reach the peak shear force.

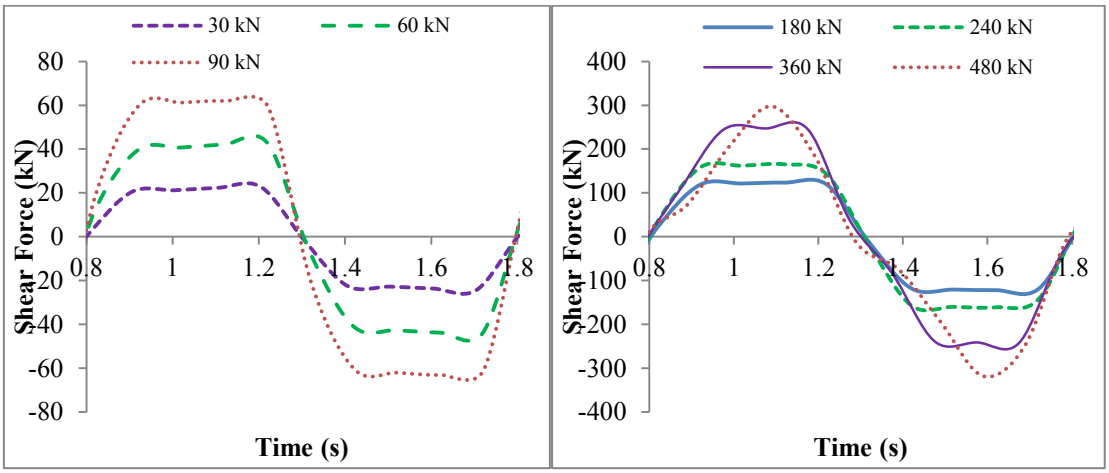

Figure 33. Shear force vs. time for different normal loads (frequency 1.0 Hz), shear displacement amplitude 5.0 mm.

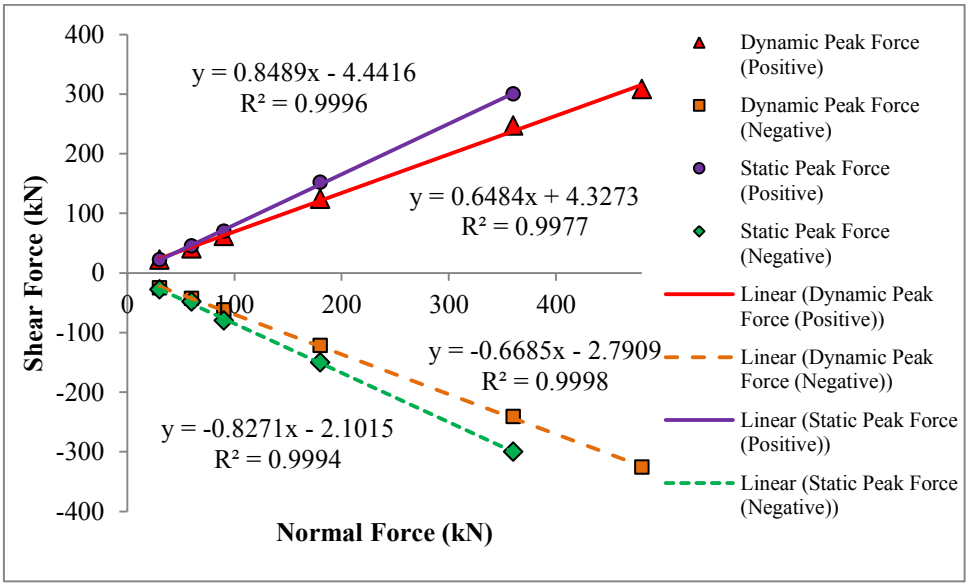

Figure 34. Peak shear forces in positive and negative directions vs. normal forces.

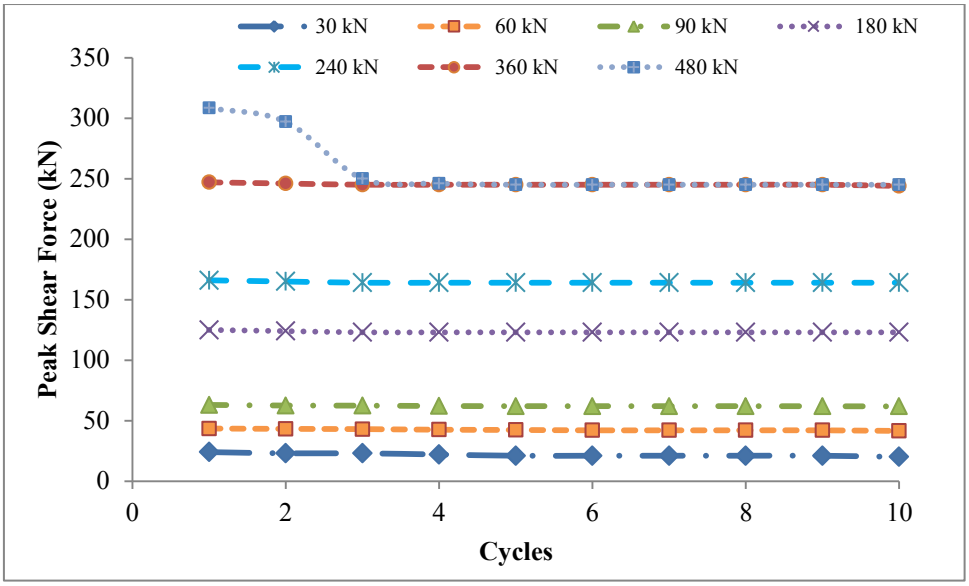

Figure 35. Peak shear forces within cycles in push direction.

Under higher normal loads (loads above 360 kN), the shape of the curve of shear forces versus shear displacements changes. After several cycles, under a normal load of 480 kN and up to shear displacements of about ± 2.0 mm, the induced shear forces are below 100 kN. This is smaller than under the normal load of 180 kN, 240 kN or 360 kN. Consequently, the general conclusion that shear forces increase with increasing normal loads is no longer true. This statement is valid only for low normal loads (in our case below 240 kN). As indicated by the results documented in Figure 33 contact surface is damaged seriously under high normal loads and the friction coefficient of the interface becomes smaller in a certain area. After extended shear displacement, induced shear forces increase and reaches the peak value. Peak shear forces reduce with the increase of cyclic shear cycles and finally reach a constant value (Figure 35).

When considering only the peak state, the relationship between the maximum values of shear forces in push and pull directions, respectively, and normal forces are nearly linear (Figure 34). Compared with the peak values of shear forces under static conditions, the peak shear forces monitored during cyclic tests show lower values, in other words, the friction angle is somewhat smaller in a cyclic shearing process. The inclination (or rotation) of the upper part of the specimen is also measured, and the inclination angle is calculated according to formula Eq.15.

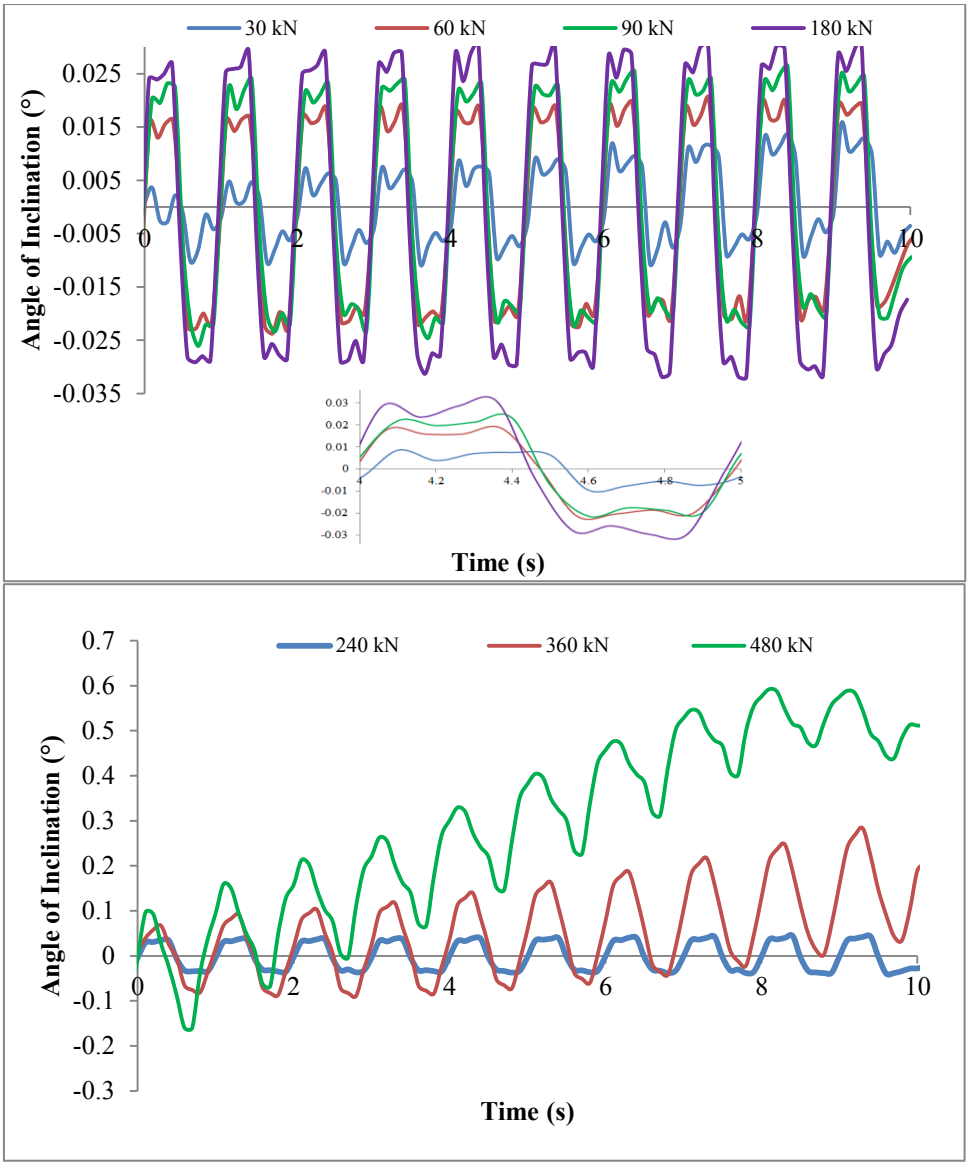

Figure 36. Angle of inclination vs. time under different normal loads.

Figure 36 illustrates the vertical movement of the top specimen during cyclic shearing. Rotation occurs during each cycle. Under low normal load (below 240 kN), normal displacements increase on one side and decrease on the other side of the sample. The corresponding angle of inclination is increasing until a peak value is reached. During this period, the top specimen shows an anti-clockwise rotational trend and finally reaches a plateau level. Afterwards, the normal displacements increase at the left side and reduce at the right side and the corresponding angle of inclination is decreasing. Finally, a peak state with plateau is reached again and movement starts in the opposite direction. During this period, the top specimen shows a clockwise rotation until the peak value is reached. Under the normal force of 30 kN,

the maximum angle of inclination is 0.001 degree, while it reaches to 0.003 degree under a normal force of 180 kN. It indicates that rotation increases with increasing normal load. However, when normal load exceeds 360 kN, the inclination towards the positive side (push direction) is increasing during each cycle. This implies that settlement of the top specimen increases step by step and the purely rotational behavior is superimposed by a translational component. This is mainly caused by wear of the joint surfaces followed by damage of the specimen and is in agreement with curves shown in Figure 32.

The test results shown above indicate that in order to avoid damage of the specimen during the cyclic loading, normal loads should be kept below 240 kN. Therefore, only normal loads of 30 kN, 90 kN and 180 kN are chosen to investigate the cyclic shear behavior influenced by different cyclic shear frequencies and shear displacement amplitudes.

Tests under different cyclic shear frequencies

In each cycle, the shear force development is almost identical. In order to compare the results under different impact frequencies, the test results are condensed and shown in Figure 37, Figure 38 and Figure 39. Under low normal load (30 kN) and dynamic excitation in the horizontal direction below 5.0 Hz, shear force (in the stable state) is about 18 kN. The influence of shear frequencies on shear force is very small. But when the shear frequency is above 10 Hz, shear force increases dramatically. In the positive shear direction, the peak shear force value is up to 29 kN and in the negative shear direction the corresponding value is up to -34 kN. Therefore, it can be concluded that peak shear strength increases with increasing impact frequencies.

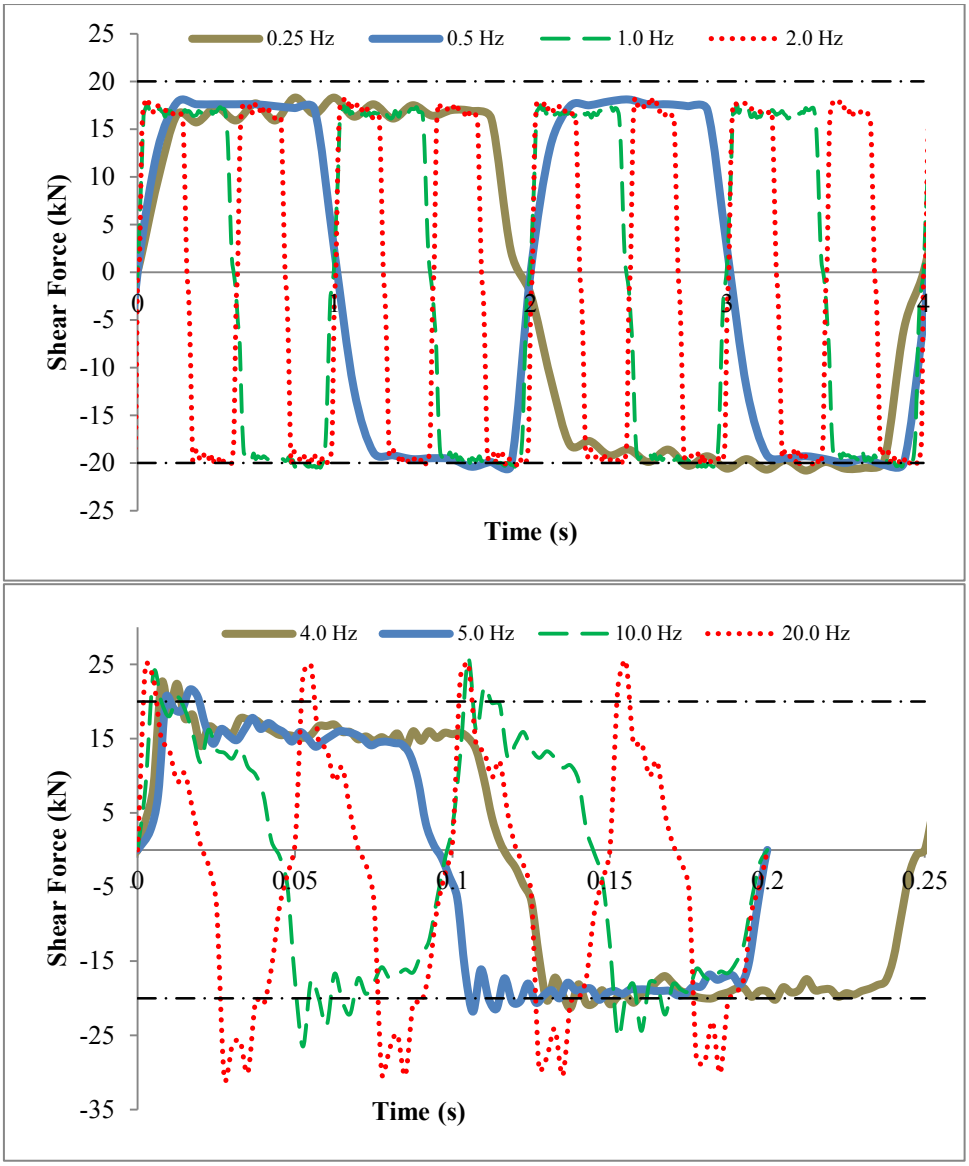

Figure 37. Shear forces vs. time under different horizontal excitation frequencies, shear displacement amplitude of 5.0 mm and normal force of 30 kN.

When normal load increases to 90 kN, peak shear forces are about 60 kN in the forward shear direction and -60 kN in the backward shear direction for all the frequencies, in other words, impact frequencies have little effect on shear forces. Under normal load of 180 kN, when the impact frequencies are 5.0 Hz or smaller, peak shear forces in the positive direction and negative direction are 120 kN and -120 kN, respectively. However, peak shear forces are only about 75 kN in the positive shear direction and -100 kN in the negative shear direction under cyclic shear frequency of 20.0 Hz. That means that peak shear forces decrease with increasing impact frequencies.

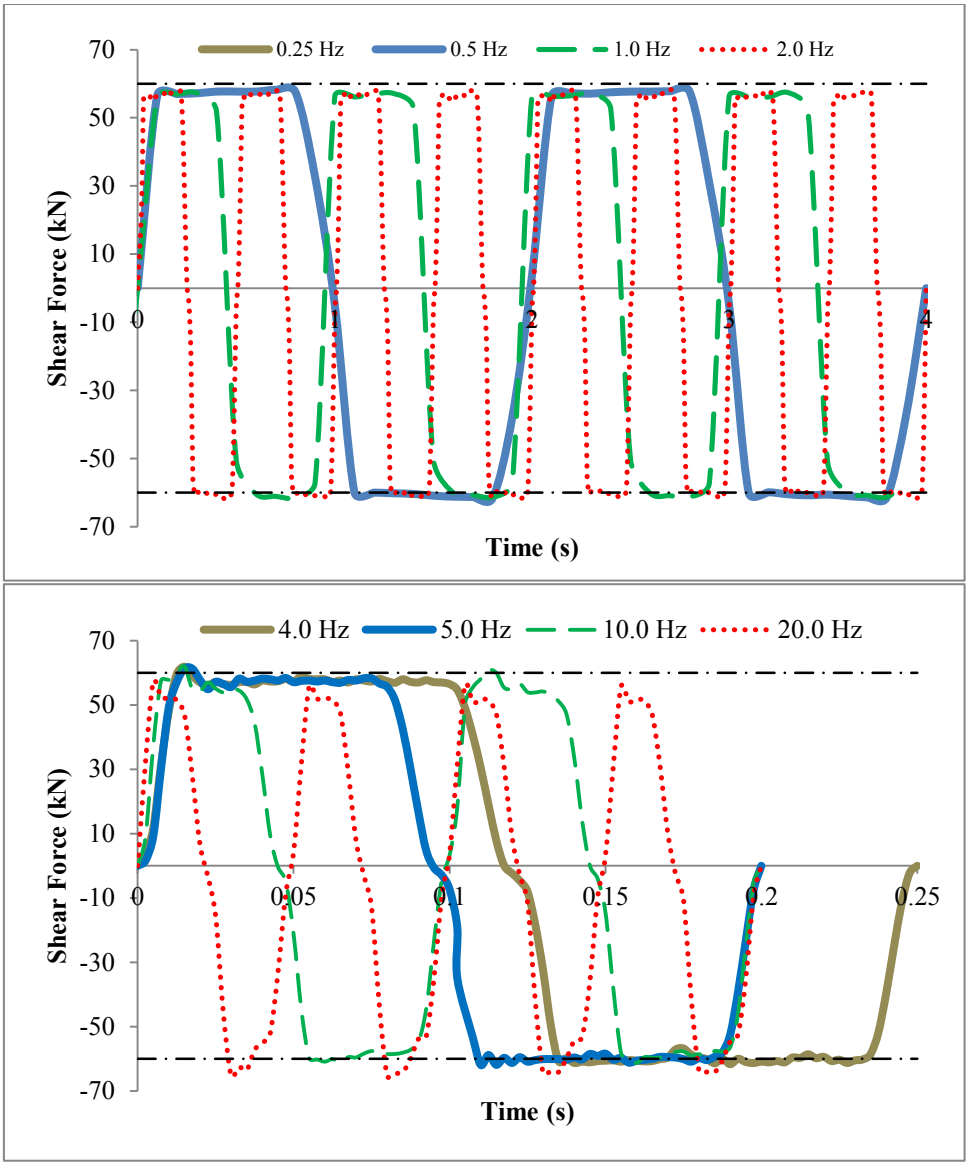

Figure 38. Shear forces vs. time under different horizontal excitation frequencies, shear displacement amplitude of 5.0 mm and normal force of 90 kN.

As presented already in Chapter 2, shear rates have influence on the shear behavior (Schneider, 1977; Crawford and Curran, 1981; Gillette et al., 1983; Jafari et al., 2003; Li and Zhu 2012; Atapour and Moosavi, 2013; Nguyen et al., 2013 and 2014). The tests presented here have constant impact amplitudes while the impact frequencies are changed. That means that shear velocities are also changed (higher impact frequency means higher shear velocities). The horizontal cylinder has to overcome the shear resistance produced by two parts: one is the shear resistance of the joints, and the other is caused by the instantaneous acceleration of the bottom shear box incl. bottom specimen and the horizontal piston. The second one becomes more important at

higher frequencies. Therefore, the shear force increases with increasing impact frequencies under small normal force (30 kN).

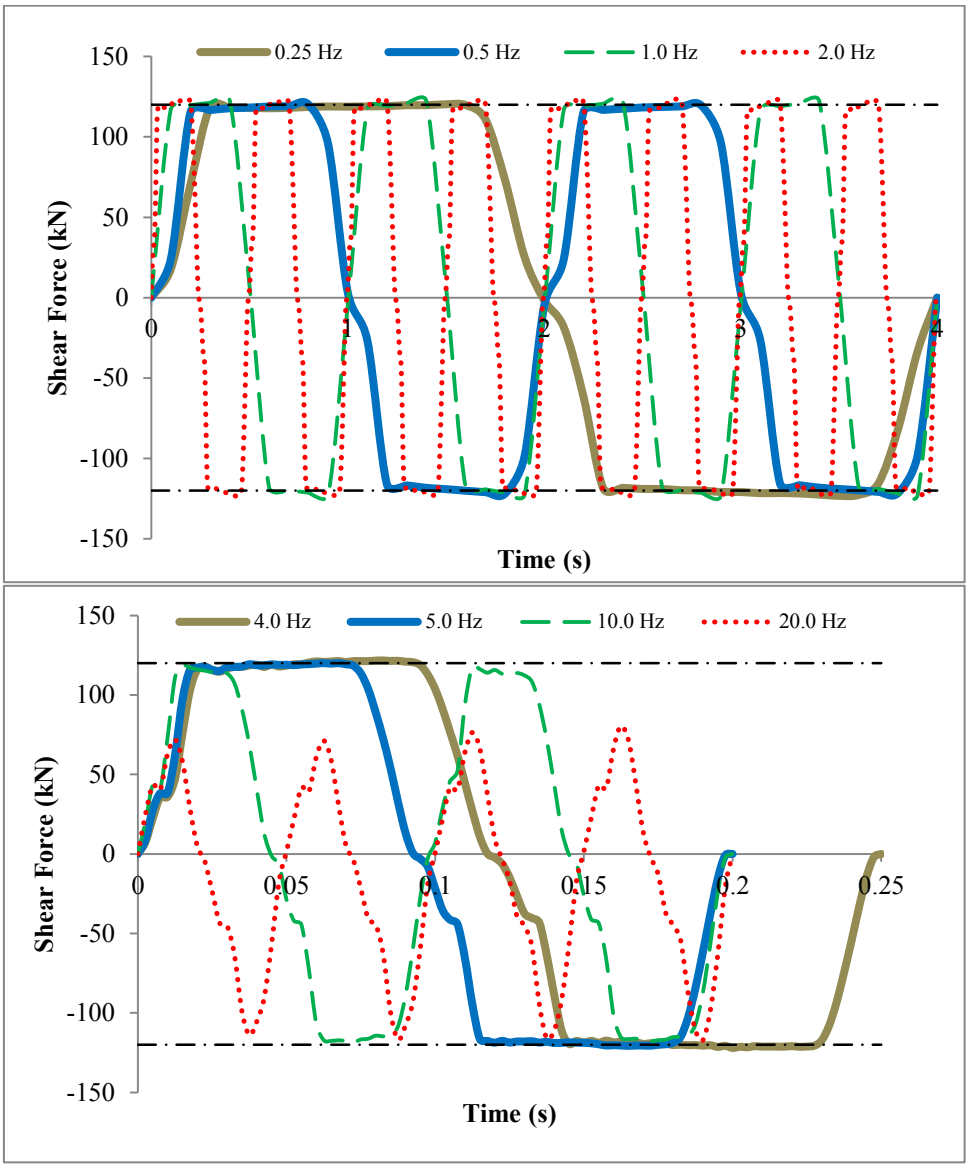

Figure 39. Shear forces vs. time under different horizontal excitation frequencies, shear displacement amplitude of 5.0 mm and normal force of 180 kN.

The development of normal displacement under different frequencies and normal forces are shown in Figure 40 and Figure 41.

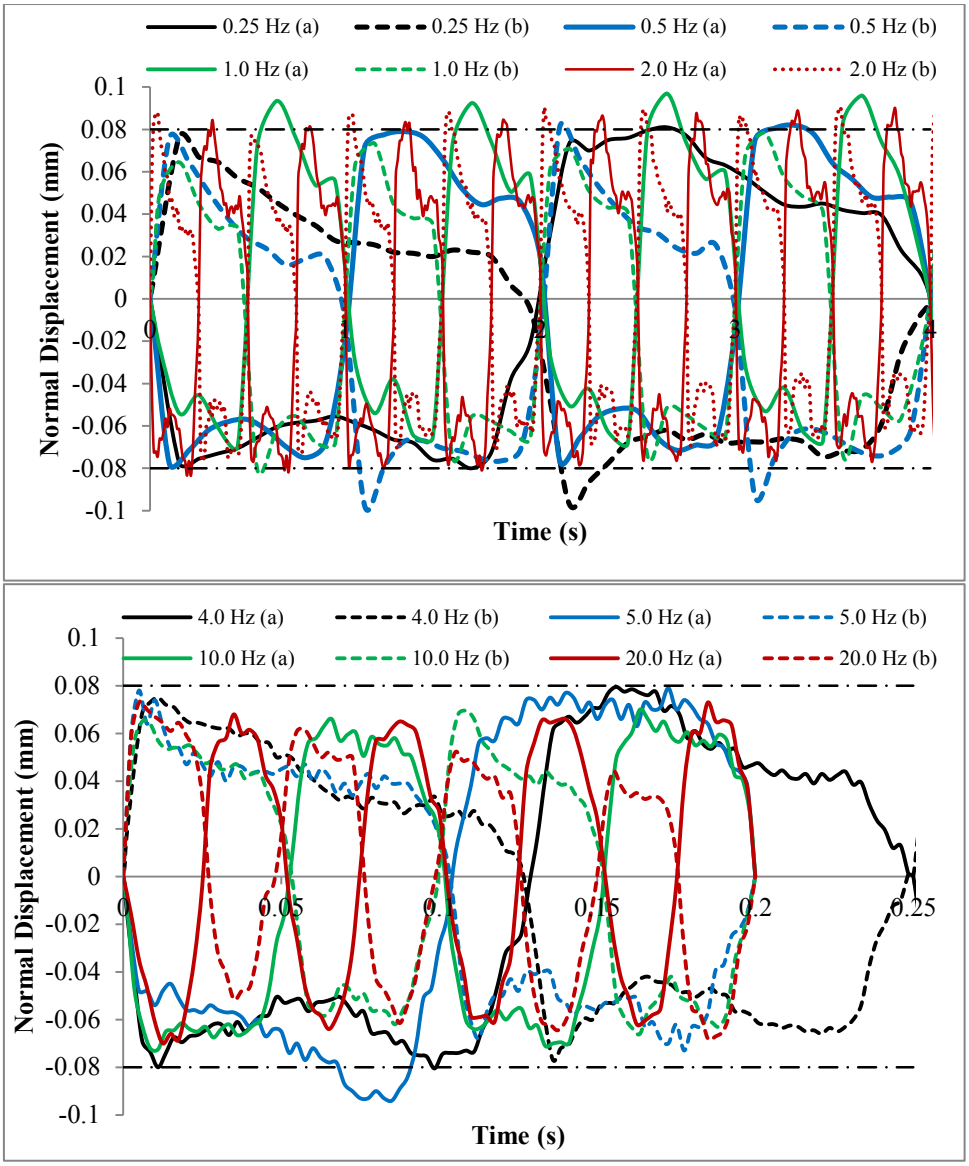

Figure 40. Normal displacement vs. time under different horizontal excitation frequencies, displacement amplitude of 5.0 mm and normal force of 90 kN.

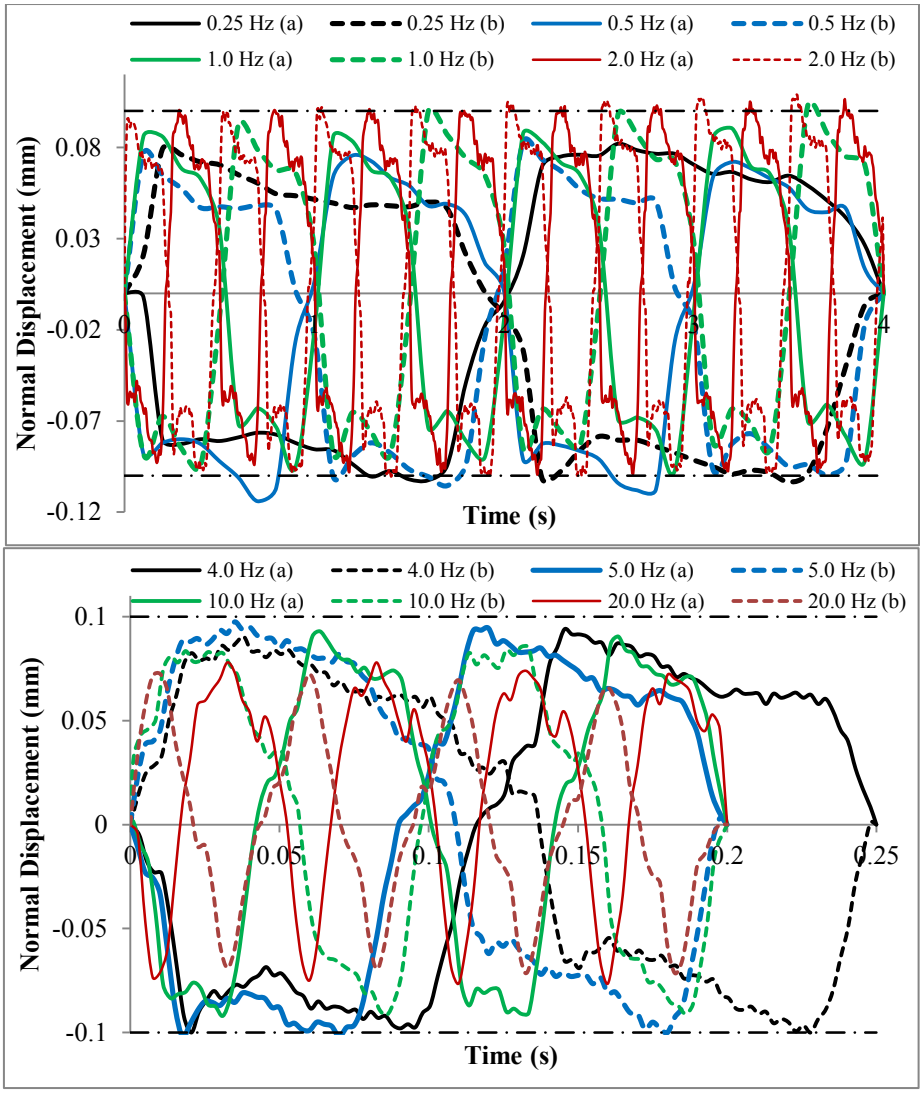

Figure 41. Normal displacement vs. time under different horizontal excitation frequencies, shear displacement amplitude of 5.0 mm and normal force of 180 kN.

Tests under different shear displacement amplitudes

Figure 42, Figure 43 and Figure 44 illustrate how the cyclic shear behavior is influenced by shear displacement magnitudes. Under the same normal load, peak shear forces are nearly independent of the shear displacement amplitudes (Figure 42). This is in contrast to joints having asperities. Figure 43 indicates that shear forces increase with increasing normal loads. Figure 44 shows the sample rotation under different shear displacement amplitudes and normal loads. Considering the same shear displacement amplitude, higher normal loads result in bigger angle of inclination. This is in agreement with results shown in Figure 36: under same normal load, the sample rotation increases with increasing shear displacement.

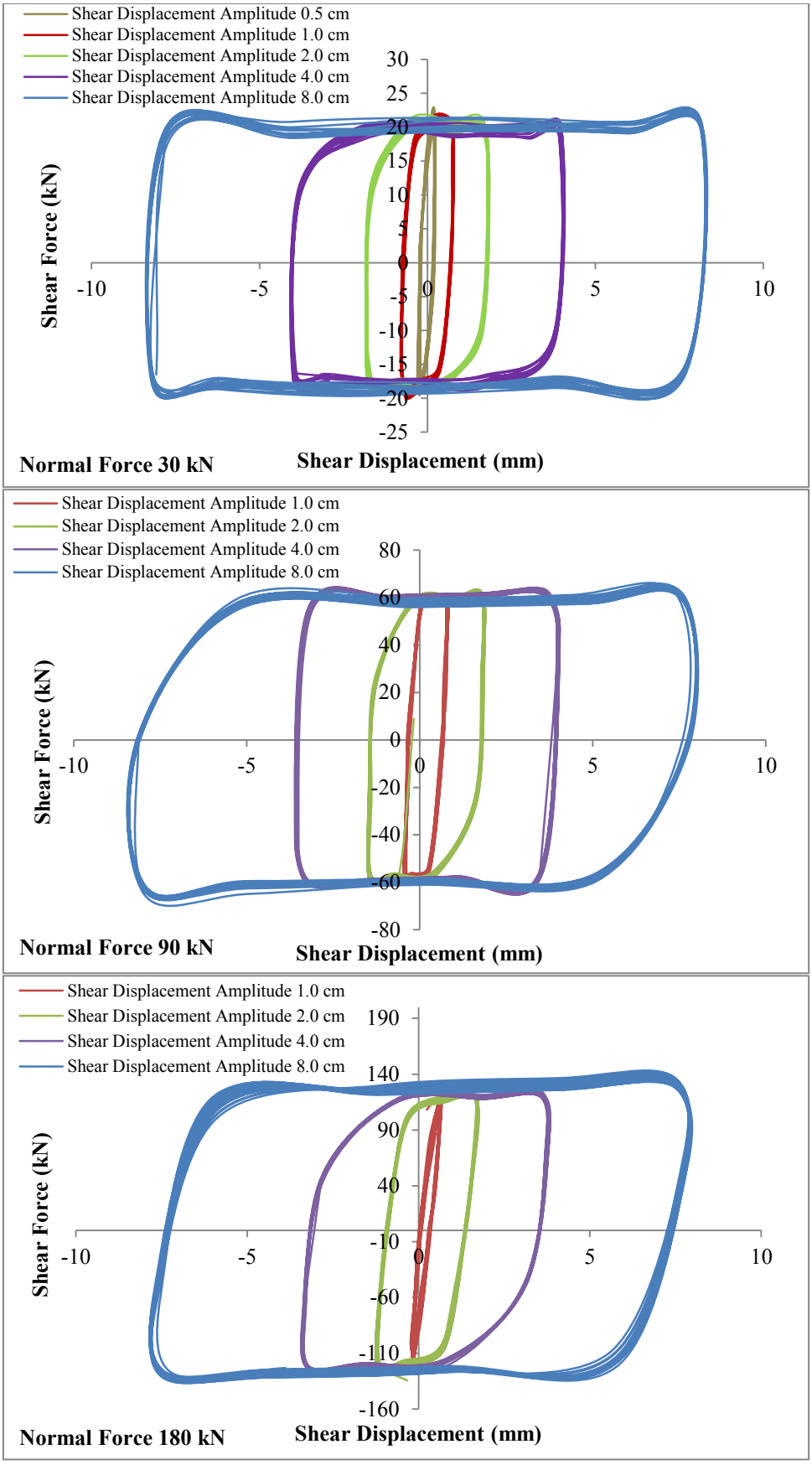

Figure 42. Shear Force vs. shear displacement under different normal forces.

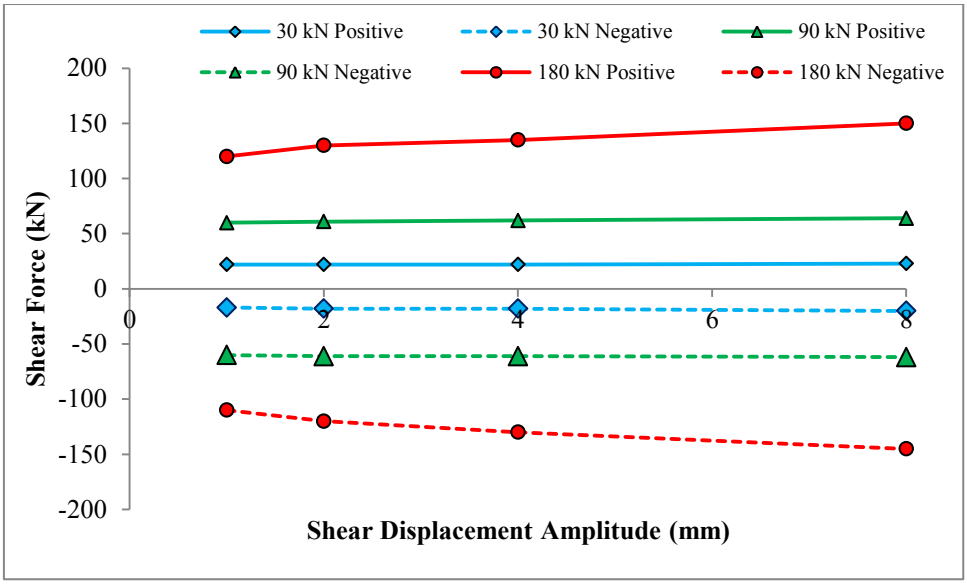

Figure 43. Shear force versus shear displacement amplitude under different normal forces.

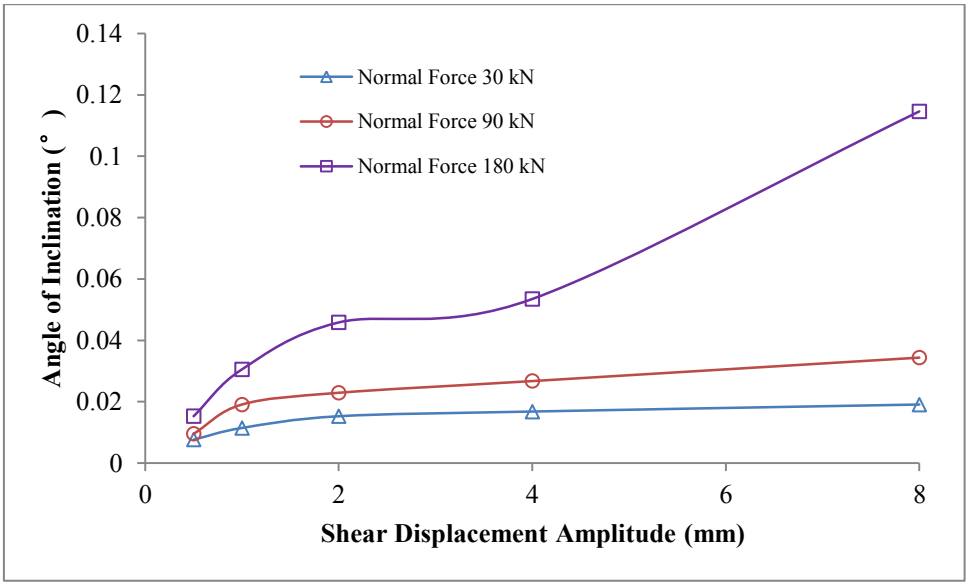

Figure 44. Maximum angle of inclination for different shear displacement amplitudes under different normal forces.

Movement behavior

Nguyen et al. (2014) reported that during the cyclic shear tests, shear movement of one cycle can be subdivided into four phases: Forward advance, forward return, backward advance and backward return. They only considered the average normal displacement at midpoint of the specimen top to evaluate the vertical movement of the

top specimen. Here instead the sample rotation is considered in detail. The normal displacements at the two ends of the specimen are different. The registered frequency of normal displacement at the top of the specimen is approximately twice the input frequency. Shear and normal displacement versus time under normal load of 90 kN, shear displacement frequency of 1.0 Hz and shear amplitude of 5.0 mm are shown in Figure 45 for two cycles.

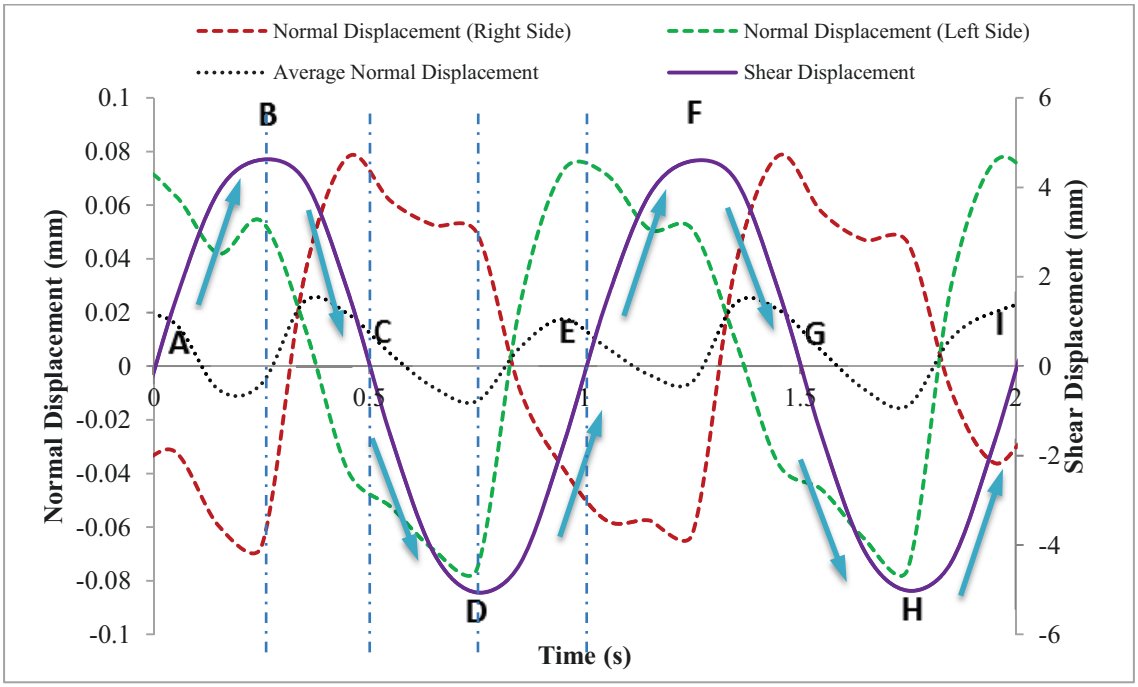

Figure 45. Shear and normal displacement vs. time (horizontal cyclic shear frequency 1.0 Hz, normal load 90 kN). Negative values for normal displacement indicate dilation, positive values indicate compression.

The four phases inside one cycle can be characterized as follows:

Phase I (A to B): Forward advance

The bottom specimen moves in the forward (push) direction. After initial uniform dilation, the left side of the top specimen experience compaction (settlement) while the right side continuously shows dilation (heave). The amplitude of heave and settlement increases with increasing shear displacement. The top part of the specimen experiences uplift.

Phase II (B to C): Forward return

The bottom specimen is moving in the opposite direction. The left side of the top specimen moves upwards and the right side moves downwards. The amplitude of heave and settlement decreases with increasing shear displacement. The average vertical movement is positive (downward direction, joint closure). At point C the sample has reached again the initial position.

Phase III (C to D): Backward advance

Bottom specimen is still moving in the opposite direction. At the left side, upward movement is still observed and at the right side movement direction is changed from compaction to dilation. The amplitude of heave increases with increasing shear displacement. The average vertical movement is negative indicating dilation.

Phase IV (D to E): Backward return

The movement direction of the bottom specimen reverses and has the same direction as in phase I. Normal displacement decreases at the left side and increases at the right side. The amplitude of heave and settlement increases with increasing shear displacement. The specimen experience compaction in this phase.

Time shift

Figure 46 shows the relationship between measured shear force and shear displacement versus time under two different normal loads. This figure reveals a phase shift between the points of reaching maximum shear displacement and maximum shear force. The shear displacement is lagging behind the shear force. This behavior is observed during all experiments. This results are similar to those reported by Ahola et al. (1996) and Nguyen et al. (2013). Ahola et al. (1996) explained the phase shift results on the basis of shear stress buildup to a level required to initiate joint shear. In order to investigate the phase shift during the cyclic shearing in more detail, the influencing factors normal forces and shear displacement amplitudes are taken into account.

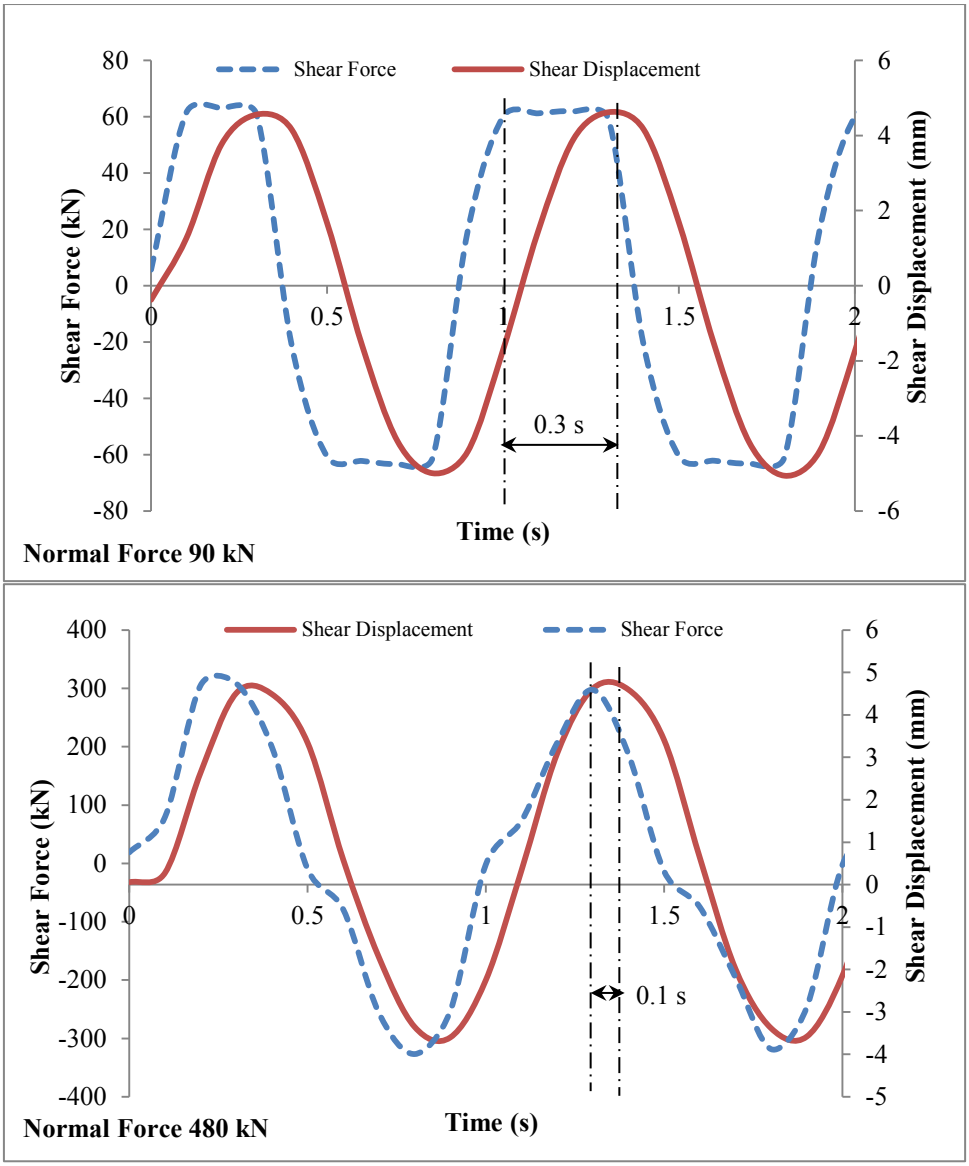

Figure 46. Shear displacement and shear force vs. time (frequency 1.0 Hz, normal load 90 kN and 480 kN, shear displacement amplitude 5.0 mm).

As documented in Figure 47 for the same shear displacement frequency (1.0 Hz) and shear displacement amplitude (5.0 mm), a time shift of 0.225 sec is observed for normal force of 30 kN, whereas a time shift of only 0.05 sec is observed for normal force of 480 kN. This indicates that phase shift decreases with increasing normal forces. In other words: under higher normal loads larger shear displacements are necessary to reach the maximum shear force.

Figure 48 presents the evolution of the time shift between max. shear displacement and max. shear force for different normal loads and different shear displacement

amplitudes. At a frequency of 1.0 Hz, normal loads of 30 kN, 90 kN and 180 kN, respectively, and shear displacement amplitude of 1.0 mm, time shift is 0.26 sec (30 kN), 0.21 sec (90 kN) and 0.1 sec (180 kN), respectively. However, it is 0.41 sec (30 kN), 0.33 sec (90 kN) and 0.27 sec (180 kN) considering a shear displacement amplitude of 8.0 mm. This indicates that phase shift increases with increasing shear displacement amplitude.

A corresponding fitting equation can be deduced for the relation between normal force, shear displacement amplitude and time shift:

$$t = 0.24+5.1e^{-5}F_N-8e^{-6}F_N^2-1.67ln(u)+4.7ln(u)^2-3.7ln(u)^3 \quad (18)$$

where t is the time shift,
F_N is the normal force,
u is the shear displacement amplitude.

It can be concluded, that time shift between shear force and shear displacement is influenced by both, normal load and shear displacement amplitude.

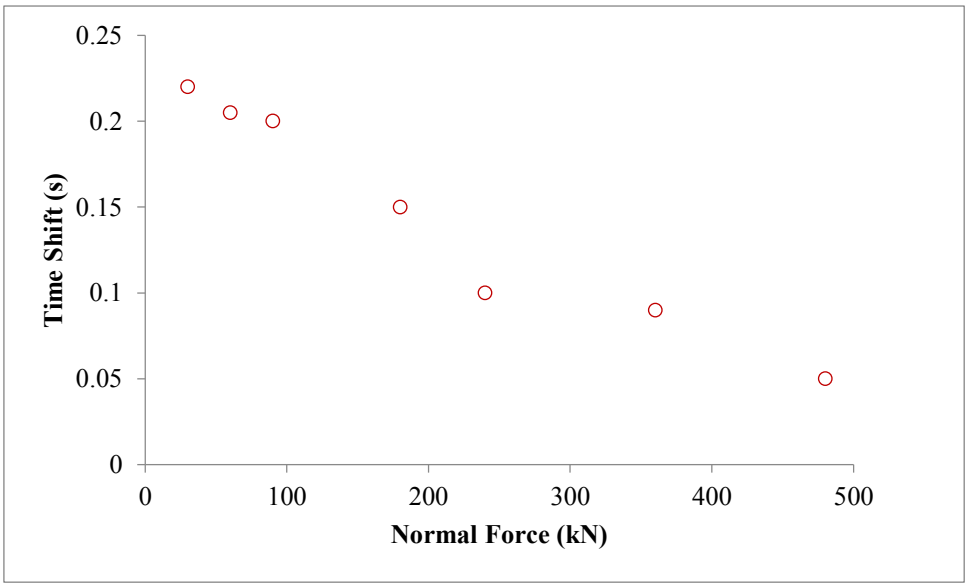

Figure 47. Time shift between max. shear displacement and max. shear force for different normal loads (frequency 1.0 Hz, shear displacement amplitude 5.0 mm).

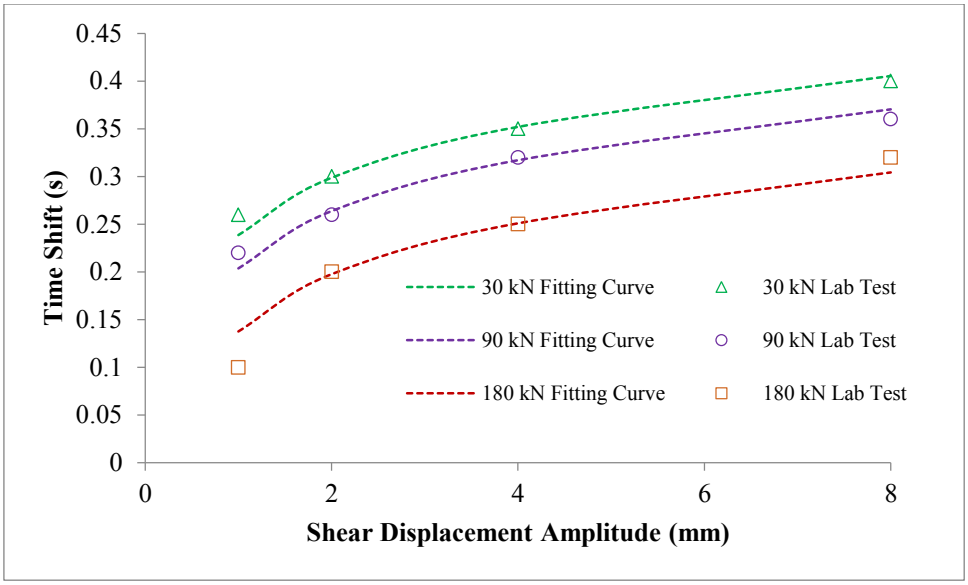

Figure 48. Time shift between max. shear displacement and max. shear force for different normal loads and different shear displacement amplitudes (frequency 1.0 Hz).

5.2 Shear tests under DNL conditions

5.2.1 Direct shear tests under DNL conditions

5.2.1.1 Test set-up

The cyclic loading was applied as a dynamic excitation in the normal direction at the upper shear frame while a constant horizontal shear velocity was simultaneously applied at the lower shear frame (Figure 49). The vertical dynamic sinusoidal excitation is applied as a superimposed force as follows:

$$F_{sd} = F_d \sin(2\pi f t) \tag{19}$$

where F_{sd} is the dynamic normal force,

F_d is the amplitude of dynamic normal force,

f is the frequency,

t is the time.

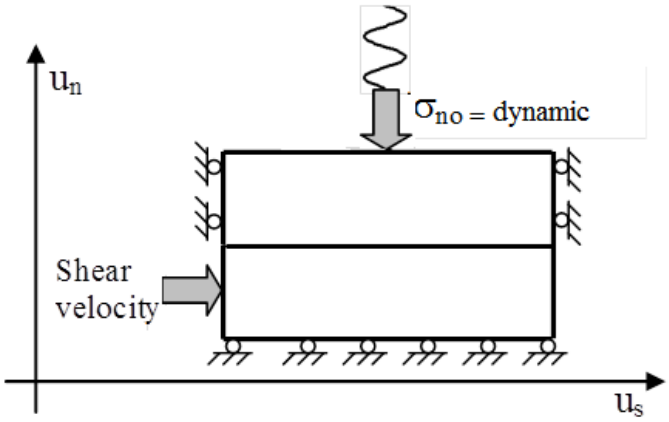

Figure 49. Set-up of direct shear test (DNL-test).

During this test, the constant normal force was step-wise increased from 30 kN to 360 kN (multi-stage test), the superimposed normal force varied from ± 15 kN to ± 180 kN, the vertical impact frequency varied from 0.25 Hz to 5.0 Hz, the maximum shear displacement at each stage was 1.0 cm/2.0 cm, and the constant shear velocity varied from 1.0 mm/min to 100 mm/min. In order to facilitate comparison, for each group only one input parameter was changed. The dynamic tests were conducted according to schemes documented in Table 5. A total of 48 direct shear tests (arranged in 7 groups) under DNL conditions were performed.

5.2.1.2 Test results

Tests under different normal loads, different normal impact frequencies, but same shear velocity

Shear force behavior under different normal loads and superimposed dynamic loads at different frequencies is shown in Figure 50, Figure 51 and Figure 52. In the residual strength stage (shear displacement is over 1.0 mm), maximum and minimum values of shear and normal forces are nearly constant. As Figure 51 indicates, the shear force amplitude does not increase in the same way as the normal force amplitude increases. Increasing frequency at same normal load amplitude leads to a reduction in shear force amplitude.

Table 5. Test parameter for shear test under DNL conditions.

Sample	Stage	F_s (kN)	f (Hz)	F_d (kN)	u_s max (mm)	Shear Velocity (mm/min)
DDNL_1	1	30	1	±15	10	3
	2	60	1	±30	10	3
	3	90	1	±45	10	3
	4	180	1	±90	10	3
	5	240	1	±120	10	3
	6	360	1	±180	10	3
DDNL_2	1	30	0.25	±15	10	3
	2	30	0.5	±15	10	3
	3	30	1	±15	10	3
	4	30	2	±15	10	3
	5	30	3	±15	10	3
	6	30	4	±15	10	3
	7	30	5	±15	10	3
DDNL_3	1	90	0.25	±45	10	3
	2	90	0.5	±45	10	3
	3	90	1	±45	10	3
	4	90	2	±45	10	3
	5	90	3	±45	10	3
	6	90	4	±45	10	3
	7	90	5	±45	10	3
DDNL_4	1	180	0.25	±90	10	3
	2	180	0.5	±90	10	3
	3	180	1	±90	10	3
	4	180	2	±90	10	3
	5	180	3	±90	10	3
	6	180	4	±90	10	3
	7	180	5	±90	10	3
DDNL_5	1	90	1	±10	10	3
	2	90	1	±20	10	3
	3	90	1	±30	10	3
	4	90	1	±45	10	3
	5	90	1	±60	10	3
DDNL_6	1	90	1	±45	10	1
	2	90	1	±45	10	10
	3	90	1	±45	10	25
	4	90	1	±45	20	50
	5	90	1	±45	20	80
	6	90	1	±45	20	100
	7	90	0.5	±45	20	50
	8	90	0.25	±45	10	25
DDNL_7	1	180	1	±90	10	1
	2	180	1	±90	10	10
	3	180	1	±90	10	25
	4	180	1	±90	20	50
	5	180	1	±90	20	80
	6	180	1	±90	20	100
	7	180	0.5	±90	20	50
	8	180	0.25	±90	10	25

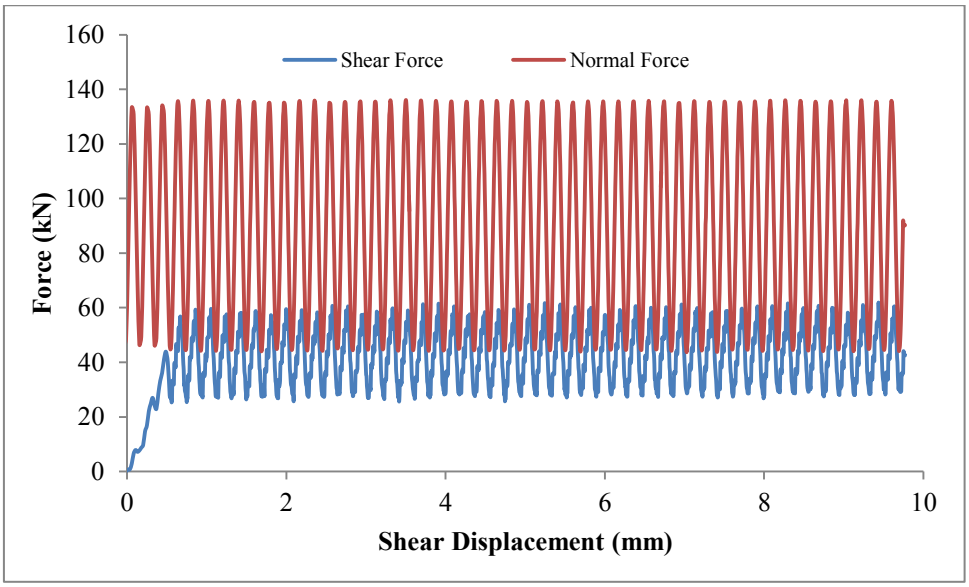

Figure 50. DDNL_3_1: Normal and shear force vs. shear displacement under normal load of 90 kN, superimposed dynamic load of ±45 kN at 0.25 Hz and constant shear velocity of 3.0 mm/min.

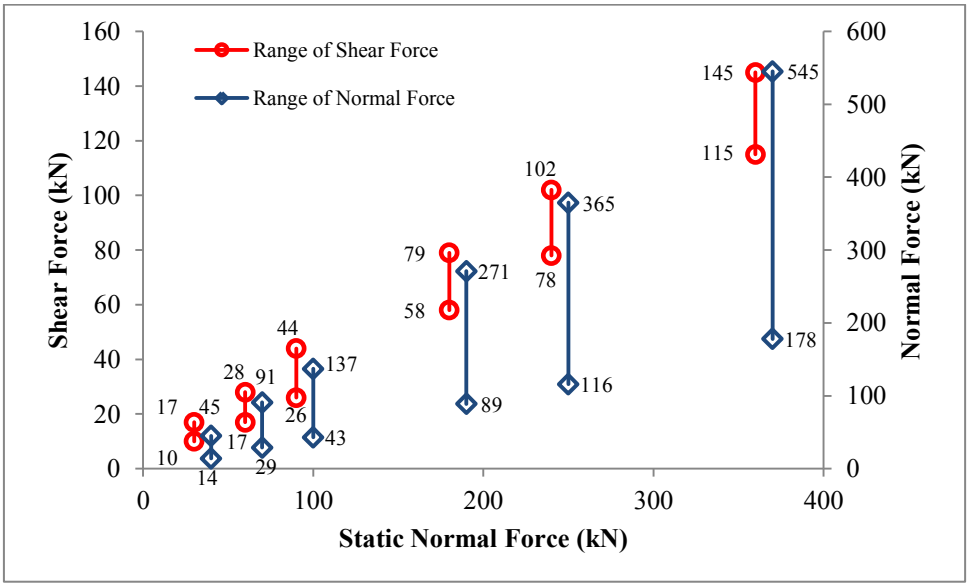

Figure 51. DDNL_1: Range of normal and shear force vs. shear displacement under normal load of 90 kN, superimposed dynamic load of ±45 kN at 0.25 Hz and constant shear velocity of 3.0 mm/min.

Figure 53 shows that similar to the static tests (see Figure 26) a bi-linear inclination relation (rotation) of the sample during shearing under DNL conditions is observed. Heave and settlement rates, respectively, are high up to about 1.0 mm shear

displacement and become much smaller afterwards. As Figure 54 indicates, the angle of inclination deduced from Eq.15 decreases with increase of normal impact frequency.

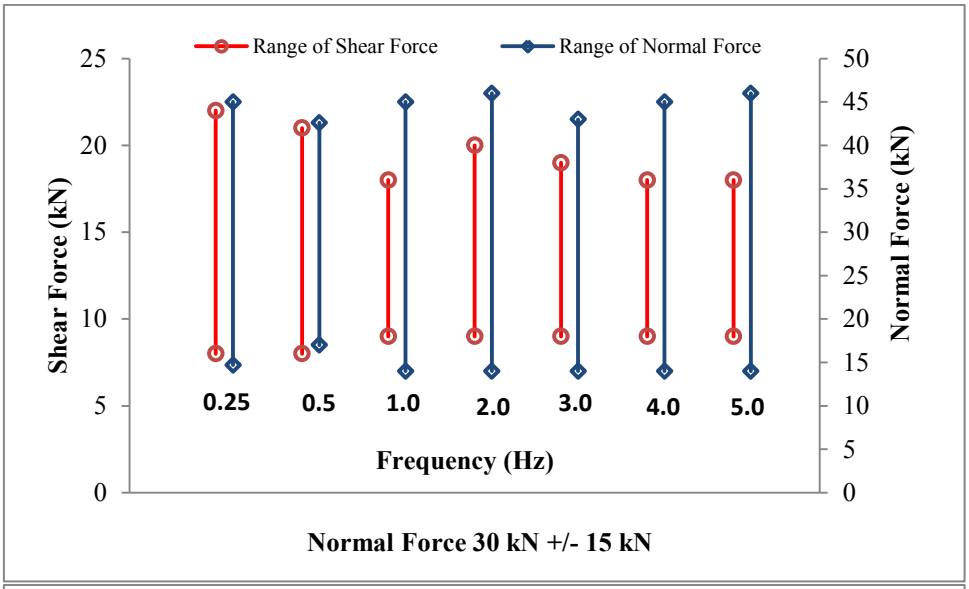

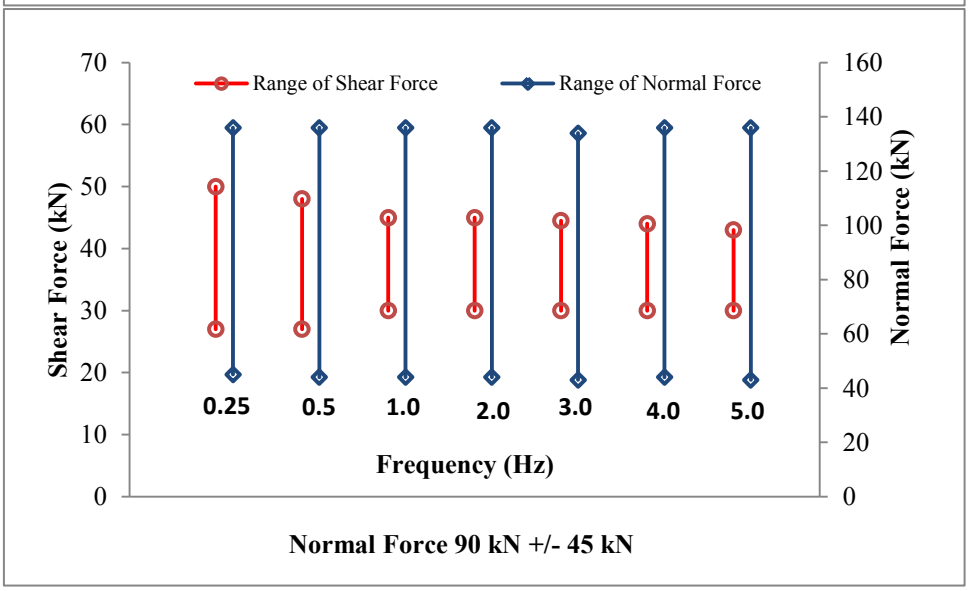

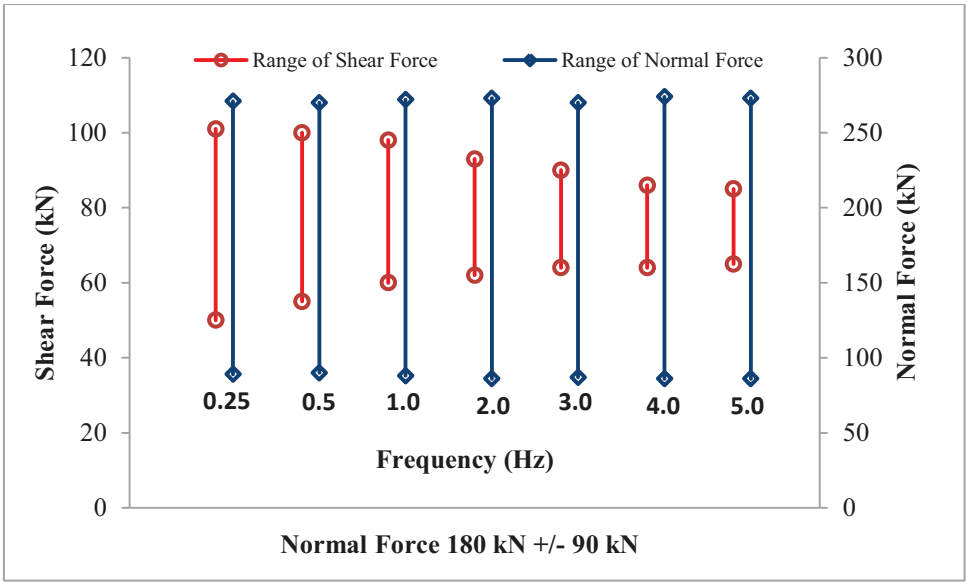

Figure 52. DDNL_2, DDNL_3 and DDNL_4: Range of shear and normal forces under different frequencies and different normal loads at the stable stage.

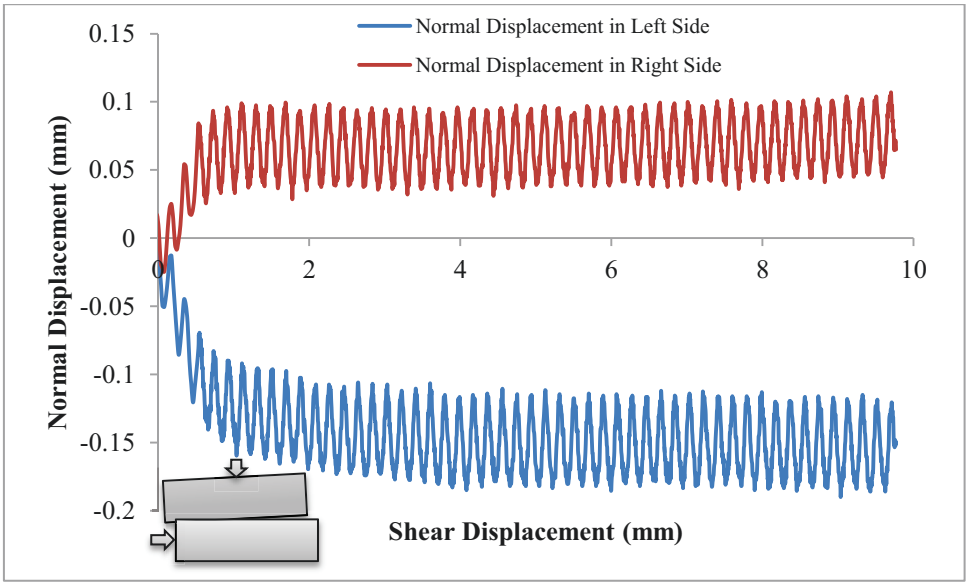

Figure 53. DDNL_3_1: Shear displacement vs. normal displacement (static normal force of 90 kN, superimposed dynamic force of ±45 kN at 0.25 Hz and constant shear velocity of 3.0 mm/min); negative normal displacement indicates settlement.

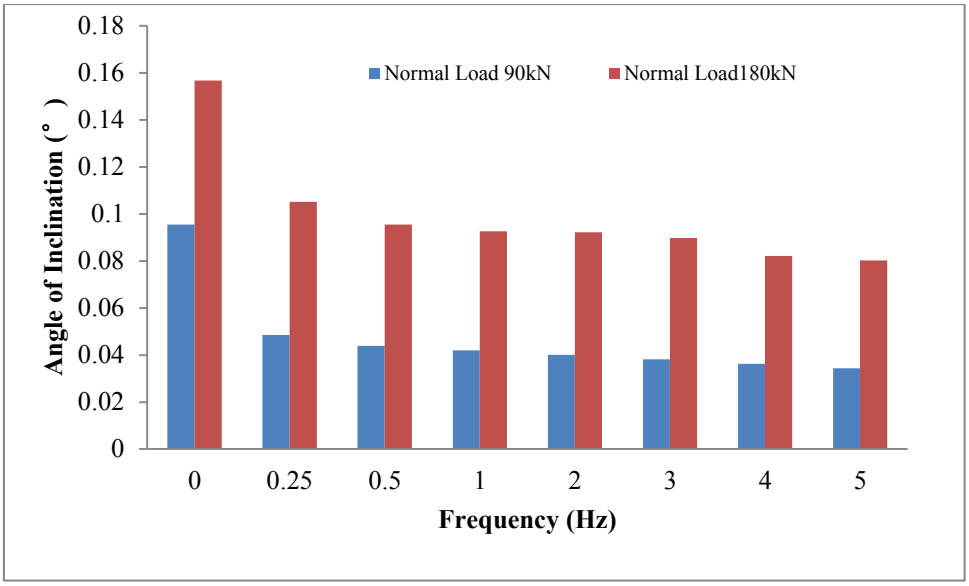

Figure 54. DDNL_3 and DDNL_4: Sample inclination under different normal impact frequencies, different static normal forces and different superimposed dynamic normal forces at constant shear velocity of 3.0 mm/min.

Lab tests results (Table 6, Figure 55, Figure 56 and Figure 57) show that there is a phase shift between normal force and shear force with shear force lagging behind. This phenomenon is observed in all dynamic tests. The relative time shift according to Eq.20 is nearly constant, that means frequency independent. The time shift is caused by the fact that peak shear strength is reached after a certain amount of shear displacement in CNL-Test (see Figure 56). At higher frequencies of superimposed normal load and constant shear velocity, the peak normal force is reached before the maximum shear resistance is activated. Therefore, even within the phase of already decreasing normal force, shear force (resistance) can still increase.

Table 6. Time shift between peak normal force and peak value $\boldsymbol{k}$ ($\boldsymbol{\tau/\sigma}$).

Frequency f (Hz)	30 +/-15	60+/-30	90+/-45	180+/-90	240+/-120	360+/-180	Normal Force F_n (kN)
0.25	2.00	-	1.98	2.00	-	-	Time Shift Δt (s)
0.5	0.98	-	1.00	0.98	-	-	
1	0.48	0.48	0.47	0.49	0.46	0.45	
2	0.28	-	0.28	0.27	-	-	
3	0.18	-	0.17	0.19	-	-	
4	0.14	-	0.14	0.14	-	-	
5	0.11	-	0.11	0.10	-	-	

Friction coefficient $\boldsymbol{k} = \boldsymbol{\tau/\sigma}$ can be calculated. The friction coefficient fluctuates for all normal load levels in a cyclic manner (Figure 55 and Figure 59) but more serrated instead of sinusoidal. The peak friction coefficient is phase lagging behind the peak value of normal force by nearly half cycle in all the tests (Figure 57). A corresponding equation can be deduced for the relation between impact frequency f and time shift Δt:

$$T_{Relative} = \frac{\Delta t}{T_{Period}} \approx 0.5 \quad (T_{period} = 1/f) \tag{20}$$

where $T_{Relative}$ is the relative phase shift,
T_{Period} is the time for one cycle,
f is the frequency,
Δt is the time shift.

Normal displacements are in phase with normal load history. As shown in Figure 56 with increasing normal load level larger shear displacements are needed to reach maximum shear resistance. In case of dynamic loading this effect triggers a decreasing ratio of shear force amplitude to normal force amplitude with increasing static normal load (Figure 58). Under quasi-static CNL-conditions the ratio of peak shear force to peak normal force, defining the coefficient of static friction, is approximately constant for all considered load levels. Consequently, the amplitude ratio between peak dynamic to peak quasi-static shear force is decreasing with increasing normal load, too. A simplified extrapolation of test data measured at low levels of normal load to considerably higher load levels might therefore lead to a marked overestimation of shear strength – even if the low normal load tests were done under DNL-conditions.

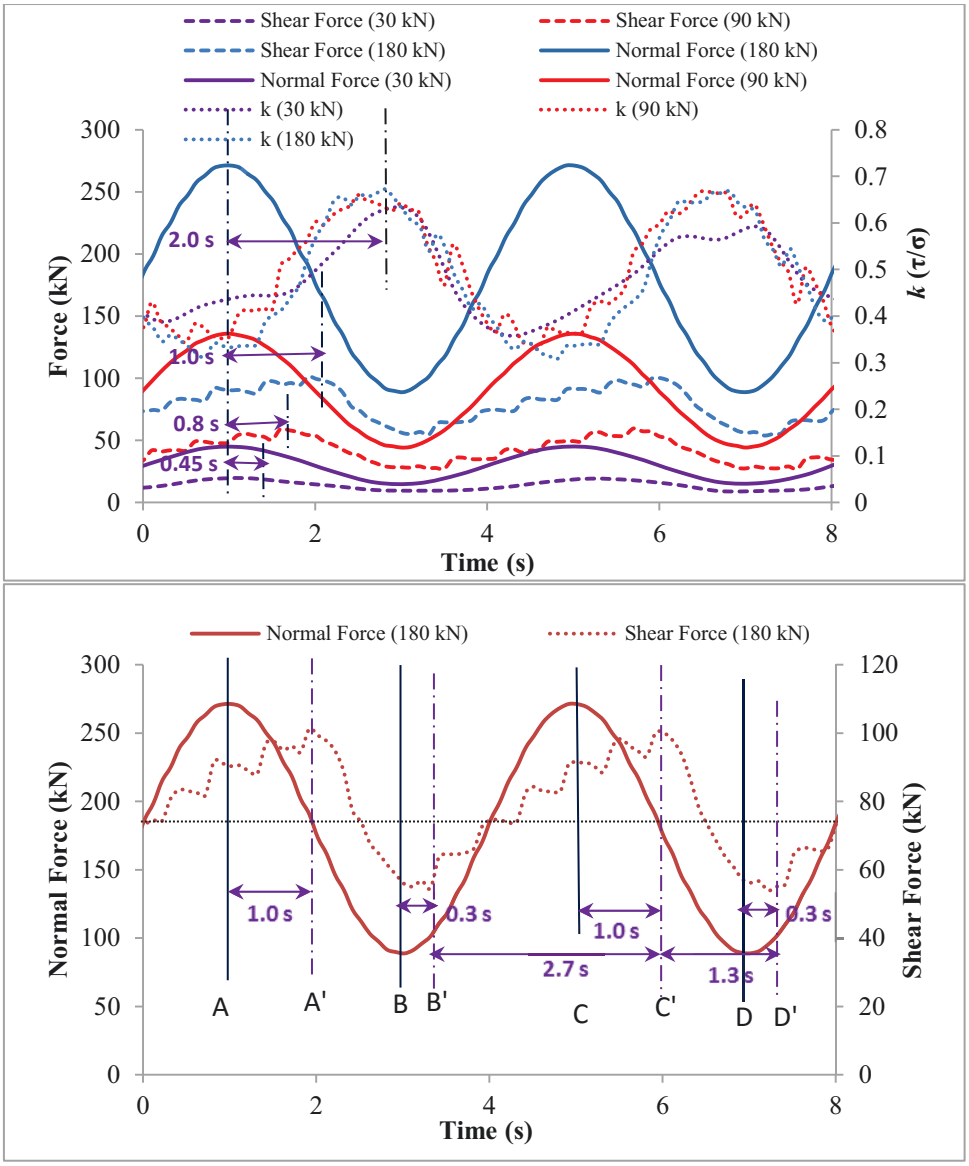

Figure 55. DDNL_2 to DDNL_4: Normal force, shear force and ***τ/σ*** vs. time (frequency 0.25 Hz, static normal loads 30 kN, 90 kN and 180 kN), stable stages were taken and the starting time was shifted to zero.

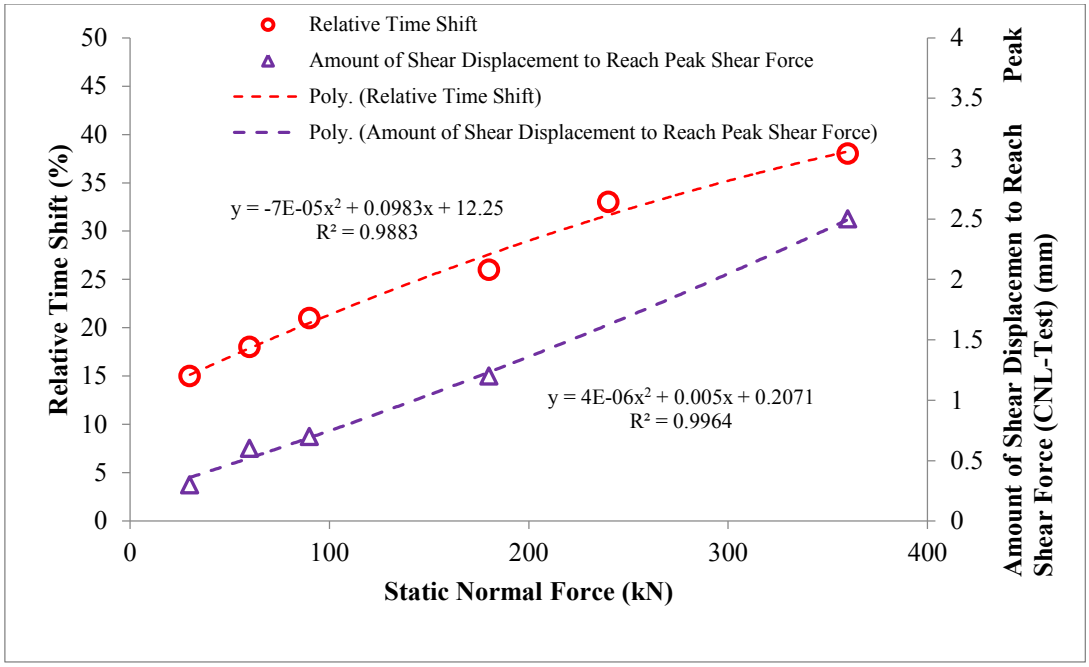

Figure 56. Relative time shift (normal impact frequency 1.0 Hz) between max. normal force and max. shear force and amount of shear displacement to reach peak shear force under different normal forces.

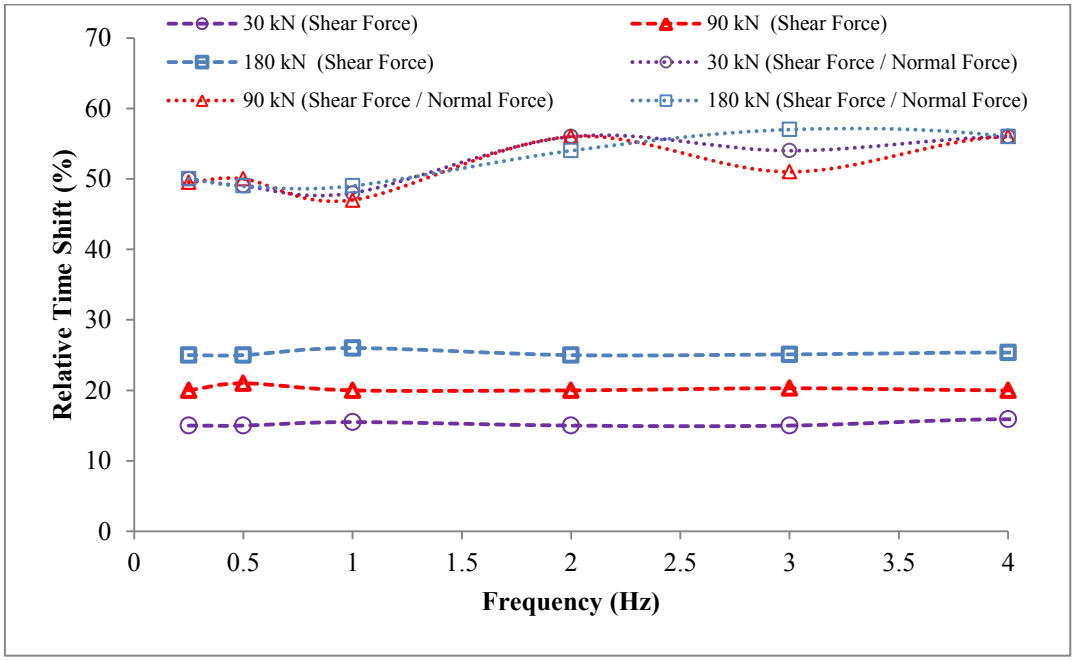

Figure 57. DDNL_2 to DDNL_4: Relative time shift between max. normal forces and max. shear forces as well as max. friction coefficient for different frequencies.

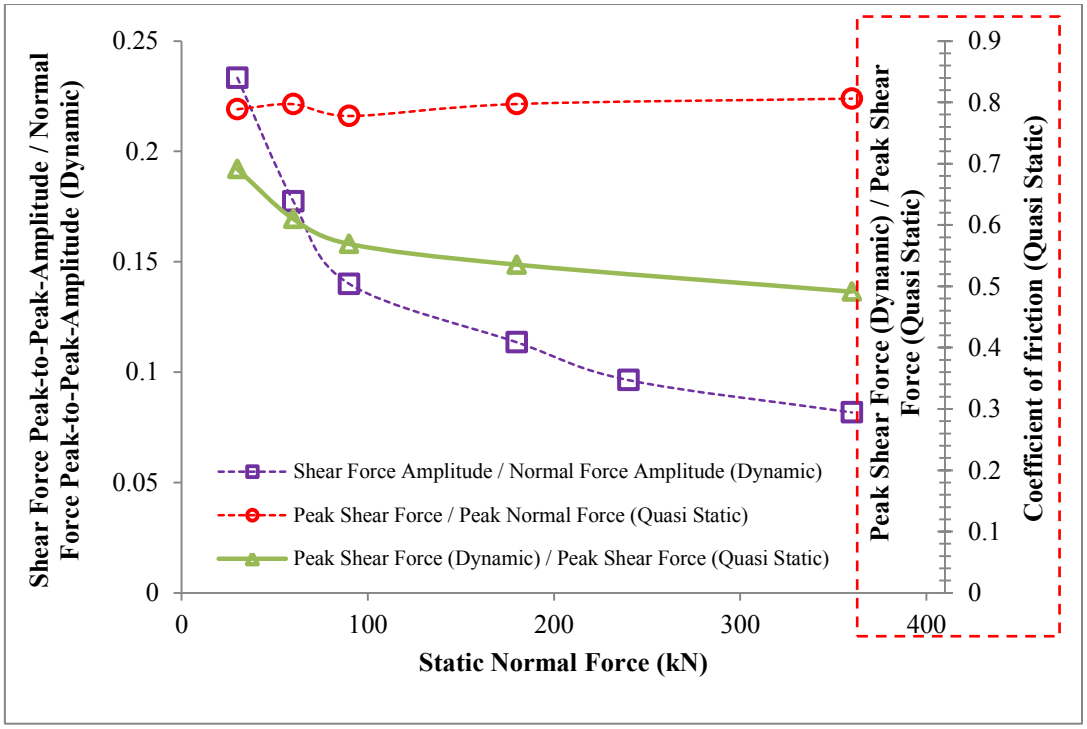

Figure 58. Amplitude ratio of shear force to normal force vs. normal force for quasi static and dynamic (1.0 Hz) conditions.

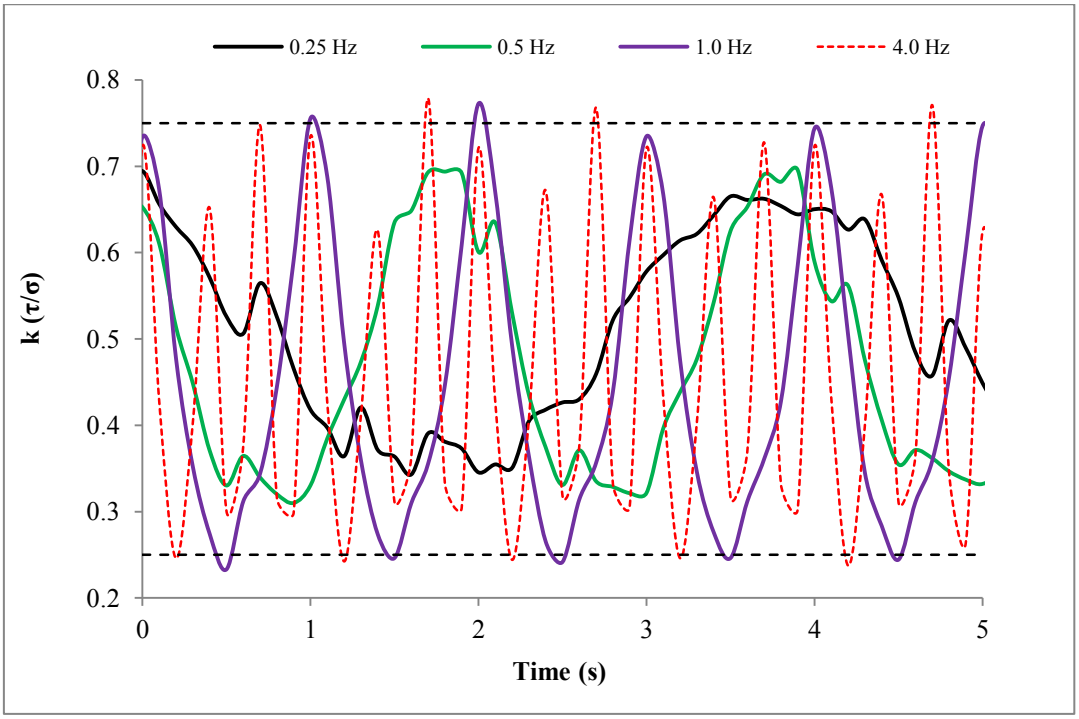

Figure 59. DDNL_3: τ/σ vs. time for different frequencies (quasi-static normal load 90 kN), stable stages were taken and starting time was shifted to zero.

Tests under different normal impact amplitudes, but same shear velocity, same normal impact frequency

Shear forces behavior under different impact amplitudes is shown in Figure 60 and Figure 61. In the residual strength stage, maximum and minimum values of shear and normal forces are nearly constant. As Figure 61 indicates, shear force amplitudes do not increase/decrease in the same way as the normal force amplitudes increase/decrease. Both the peak and minimum shear forces are decreasing with increasing normal force impact amplitudes. Normal displacements are cyclically changing with superimposed dynamic normal forces, and normal displacements increase with increase of normal impact amplitudes.

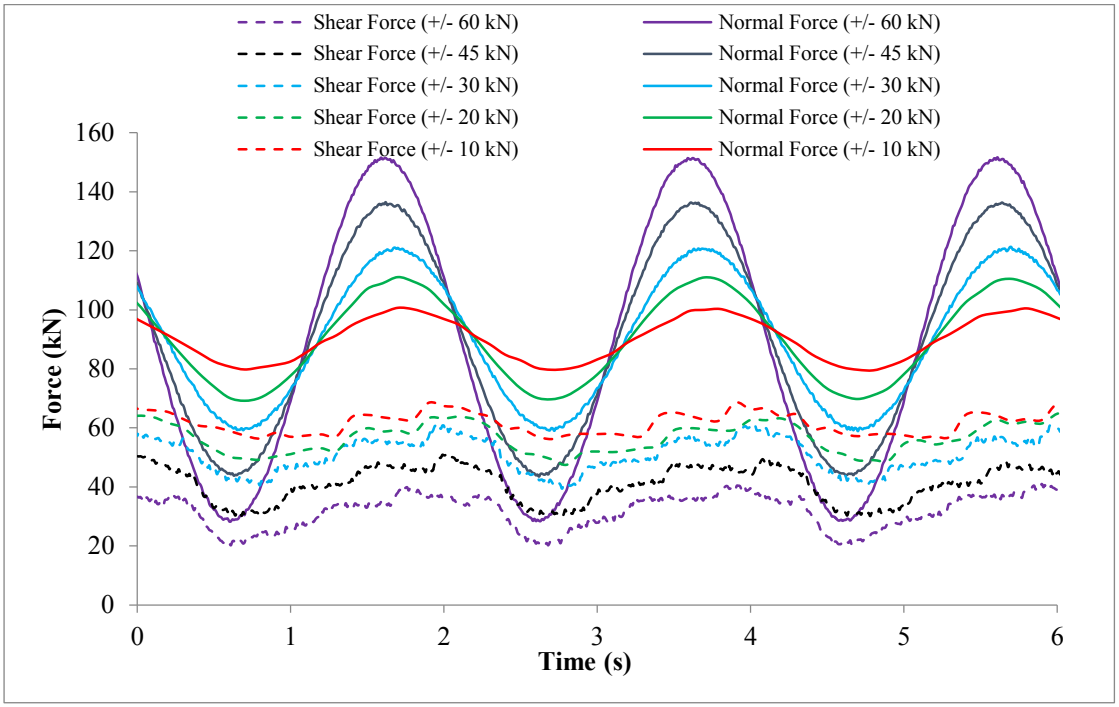

Figure 60. DDNL_5: Shear and normal forces under different superimposed normal loads, stable stages were taken and starting time was shifted to zero.

Figure 62 and Figure 63 show that there is a phase shift between peak normal force and peak shear force with peak shear force lagging, also between normal force and friction coefficient ($k = \tau/\sigma$) with friction coefficient lagging. This phenomenon is observed in all the tests. According to Figure 63, the relative time shift between peak normal force and peak shear force increases with increasing impact amplitude. The relative time shift between peak normal force and peak friction coefficient under

different impact amplitudes is nearly constant (app. half cycle in all the tests). Under superimposed normal load and constant shear velocity, the peak normal force is reached before the maximum shear resistance is activated. Therefore, even within the phase of already decreasing normal force shear force (resistance) can still increase.

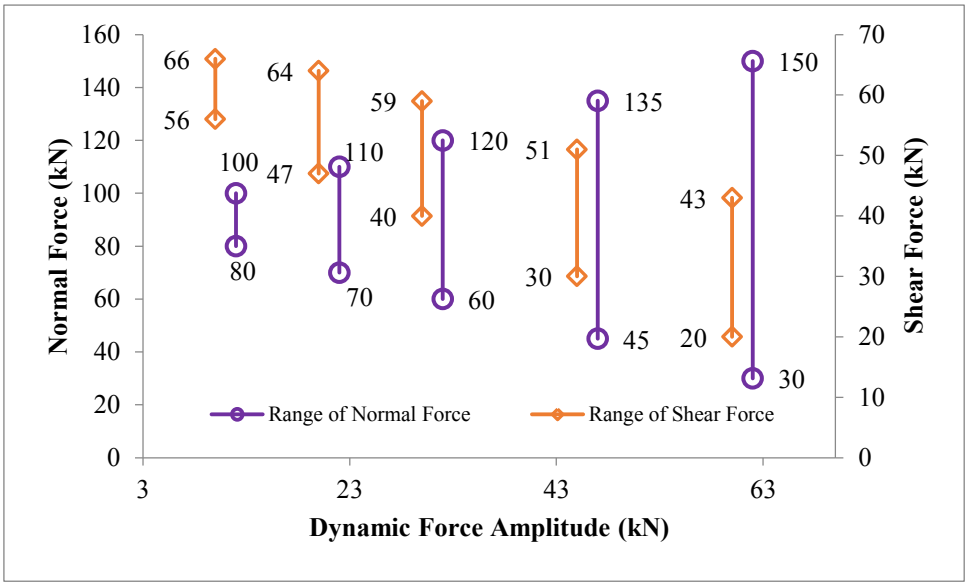

Figure 61. DDNL_5: Range of maximum and minimum shear and normal forces under different superimposed dynamic load, stable stages were taken and starting time was shifted to zero.

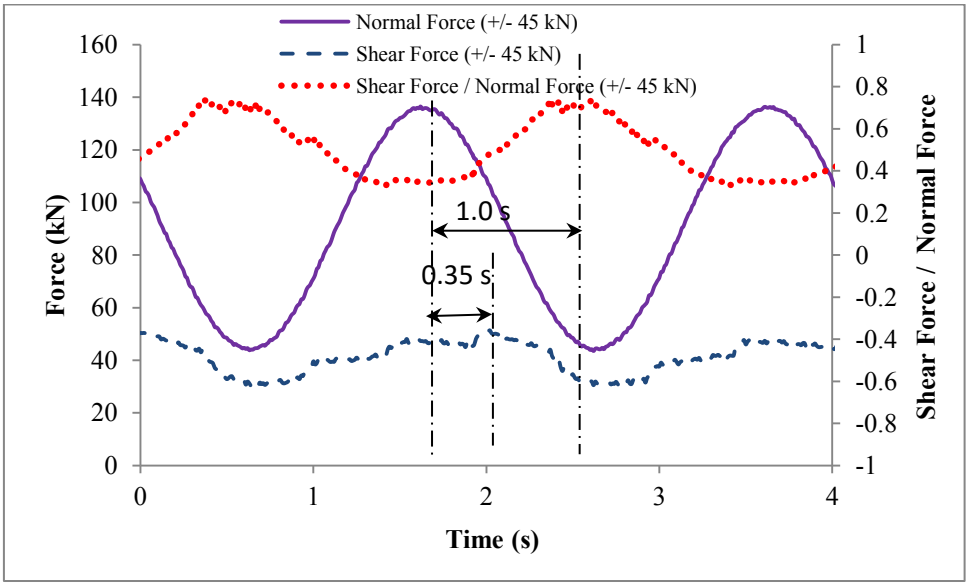

Figure 62. DDNL_5-4: Normal force, shear force and friction coefficient vs. time, stable stages were taken and starting time was shifted to zero.

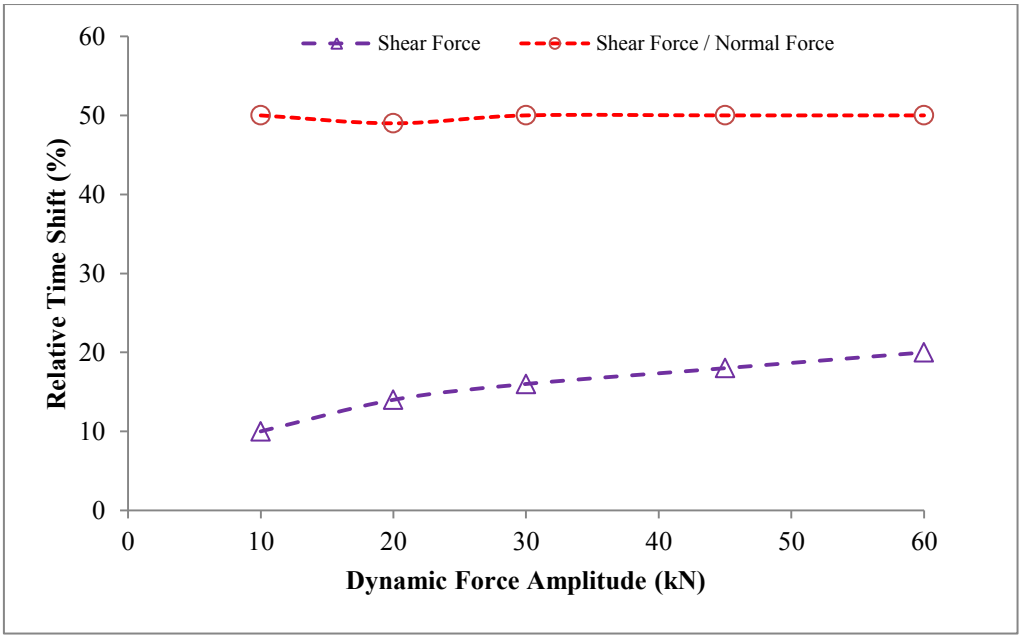

Figure 63. DDNL_5: Relative time shift between max. normal force and max. shear force as well as max. friction coefficient for different dynamic force amplitudes.

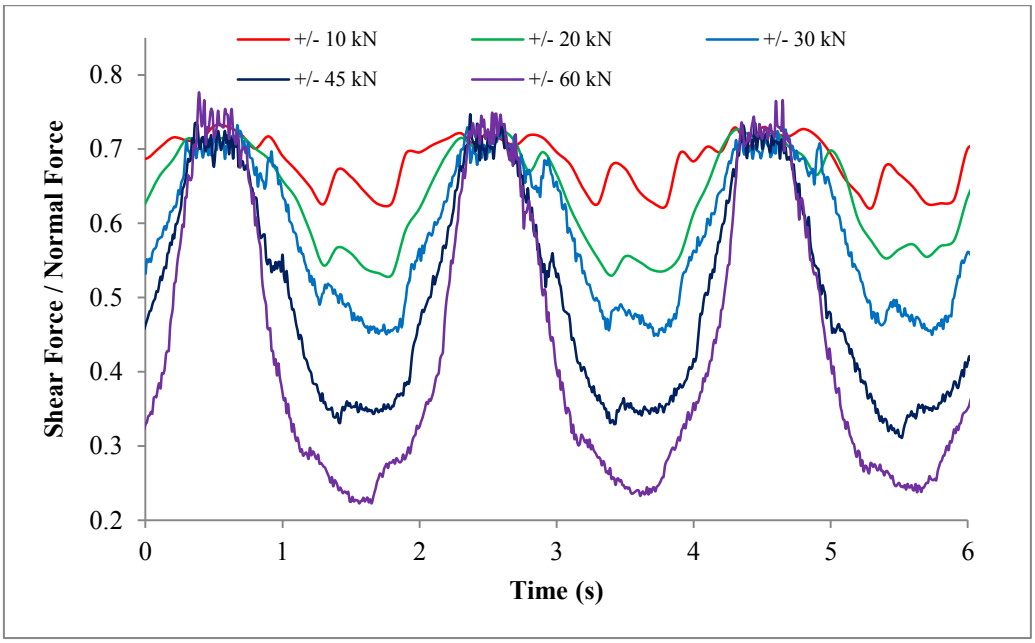

Figure 64. DDNL_5: Friction coefficient vs. time for different impact amplitudes, stable stages were taken and the starting time was shifted to zero.

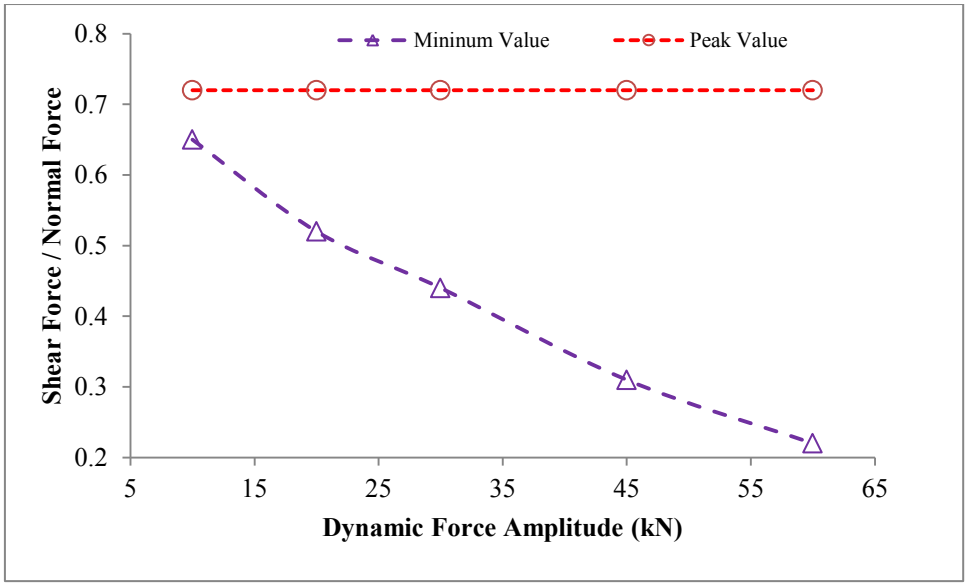

Figure 65. DDNL_5: Peak and minimum values of friction coefficient under different impact amplitudes, stable stages were taken and starting time was shifted to zero.

Figure 64 and Figure 65 show that friction coefficient under different normal impact amplitudes also follows the sinusoidal wave and the amplitude of the sinusoidal wave increases with the increasing of normal impact amplitude. The peak values of the ratio between shear force to normal force are nearly constant, while the minimum values of this ratio decrease with increasing normal impact amplitudes.

Tests under different shear velocities

The nature of the velocity-dependent behavior of joints is important for many geotechnical applications, like the study of earthquake mechanisms or engineering problems in which the loading may occur over long time periods (e.g. creeping rock slopes), short time periods (e.g. blasting or seismic loads) or in a periodic manner (e.g. machinery vibrations).

To examine the effects of the shear velocity on the peak shear stress, shear tests under DNL conditions were performed at normal load levels of 90 kN +/- 45 kN, 180 kN +/- 90 kN; shear velocity varied from 1.0 mm/min to 100 mm/min; normal impact frequencies varied from 0.25 Hz to 1.0 Hz and maximum shear displacement was of 1.0 cm or 2.0 cm. Test results are shown in Figure 66, Figure 67, Figure 68, Figure 69, Figure 70 and Figure 71.

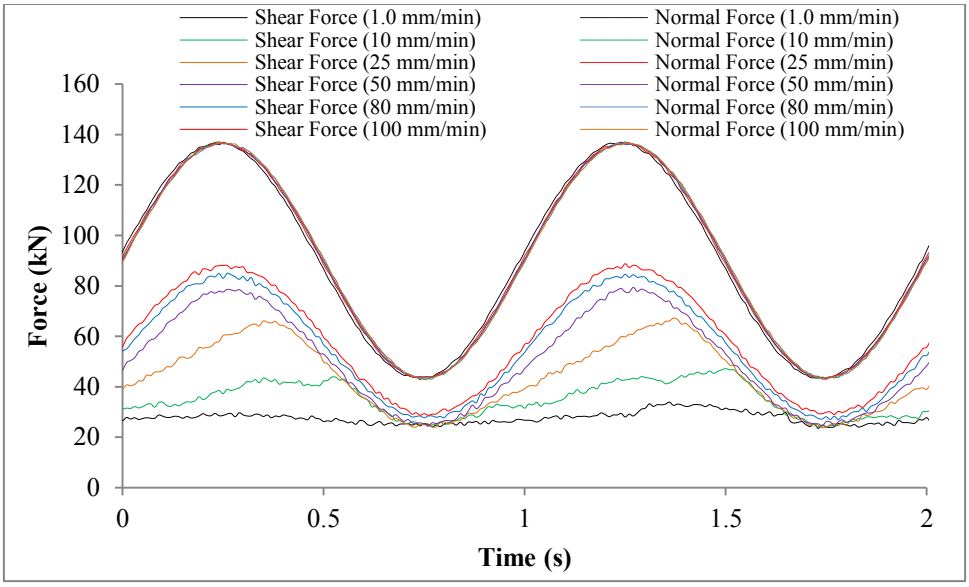

(a) Normal force: 90 kN +/- 45 kN

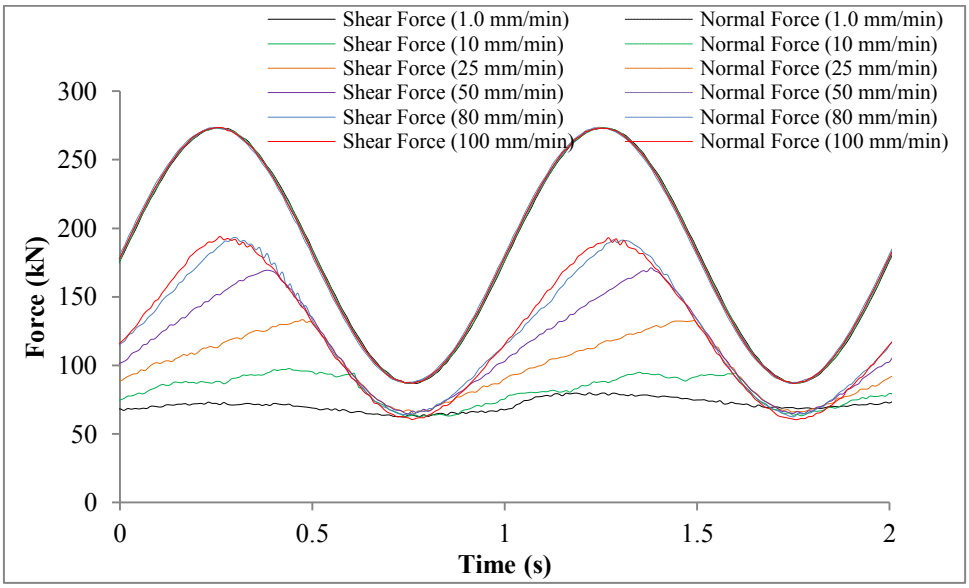

(b) Normal force: 180 kN +/- 90 kN

Figure 66. Forces vs. time under normal impact frequency of 1.0 Hz, stable stages were taken and starting time was shifted to zero.

Figure 66 (a) shows that under the normal force of 90 kN +/- 45 kN and normal impact frequency of 1.0 Hz, at the stable stage the peak shear force is about 90 kN for a shear velocity of 100 mm/min, while the peak shear force is only 30 kN for a shear velocity of 1.0 mm/min. That indicates that, with the same normal impact frequency, peak shear force is increasing with increasing shear velocity under DNL conditions. The minmum shear force is nearly the same value (28 kN~32 kN). This behavior is

also found under normal force of 180 kN +/- 90 kN with normal impact frequency of 1.0 Hz (Figure 66 (b)).

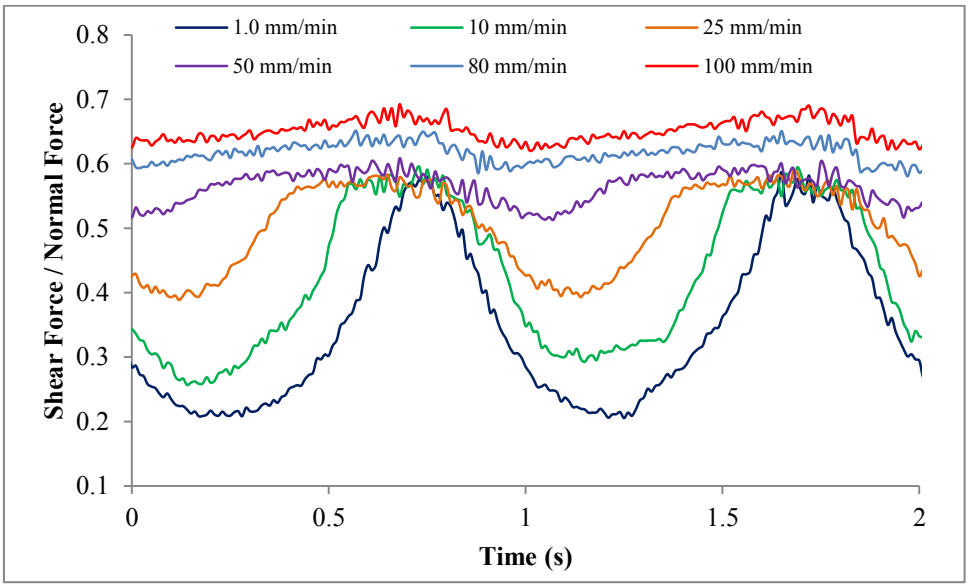

(a) Normal force: 90 kN +/- 45 kN

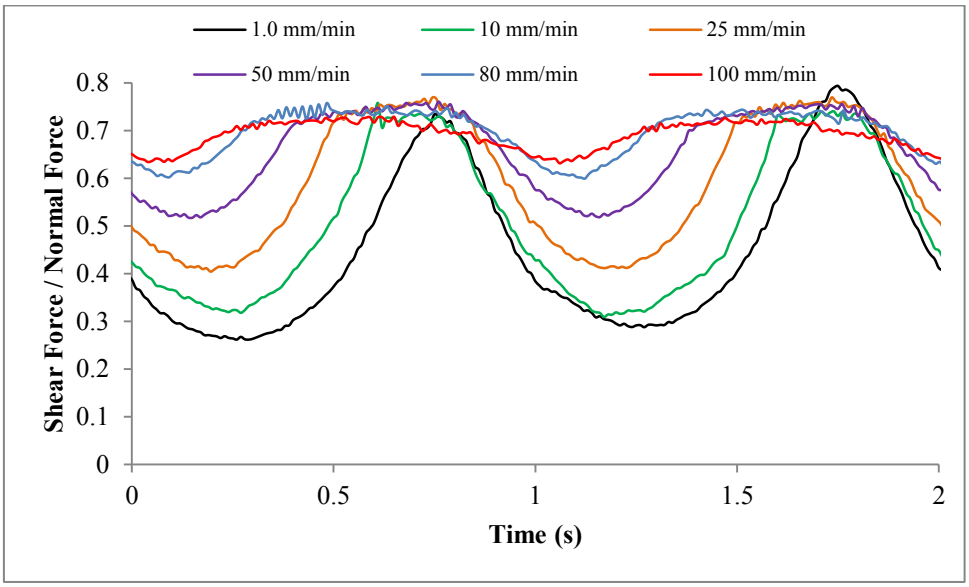

(b) Normal force: 180 kN +/- 90 kN

Figure 67. Friction coefficients vs. time with normal impact frequency of 1.0 Hz, stable stages were taken and starting time was shifted to zero.

The corresponding ratios between shear and normal force are shown in Figure 67. Under the normal force of 90 kN +/- 45 kN with normal impact frequency of 1.0 Hz (Figure 67 (a)), at the stable stage the minimum friction coefficient (shear force/ normal force) is about 0.25 for a shear velocity of 100 mm/min, while the peak

friction coefficient (shear force/ normal force) is about 0.7 for a shear velocity of 1.0 mm/min. It indicates that the minimum friction coefficient increases with decreasing shear velocity under DNL conditions. The peak friction coefficient has nearly the same value (0.68~0.72). Similar relations are obtained from tests with normal force of 180 kN +/- 90 kN (Figure 67 (b)).

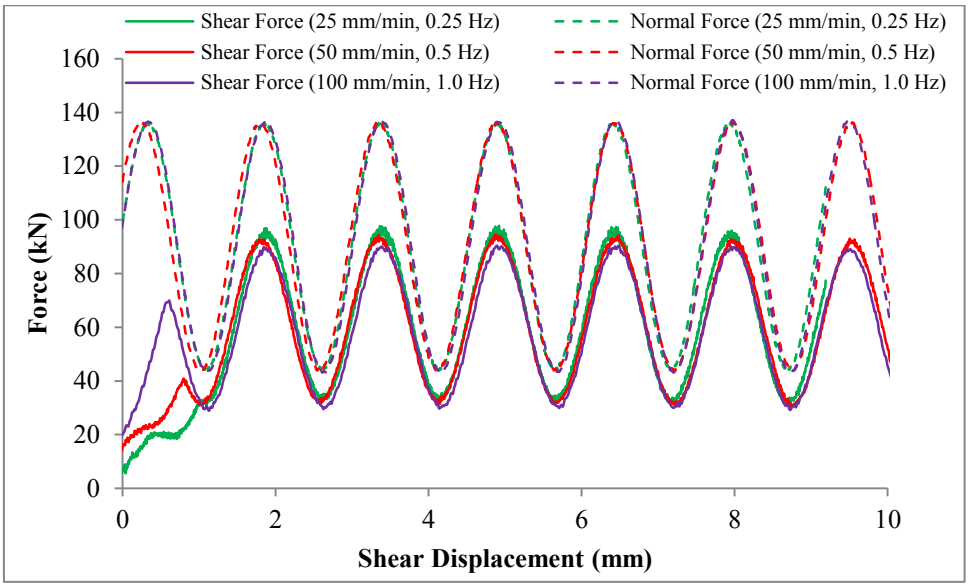

(a) Normal force: 90 kN +/- 45 kN

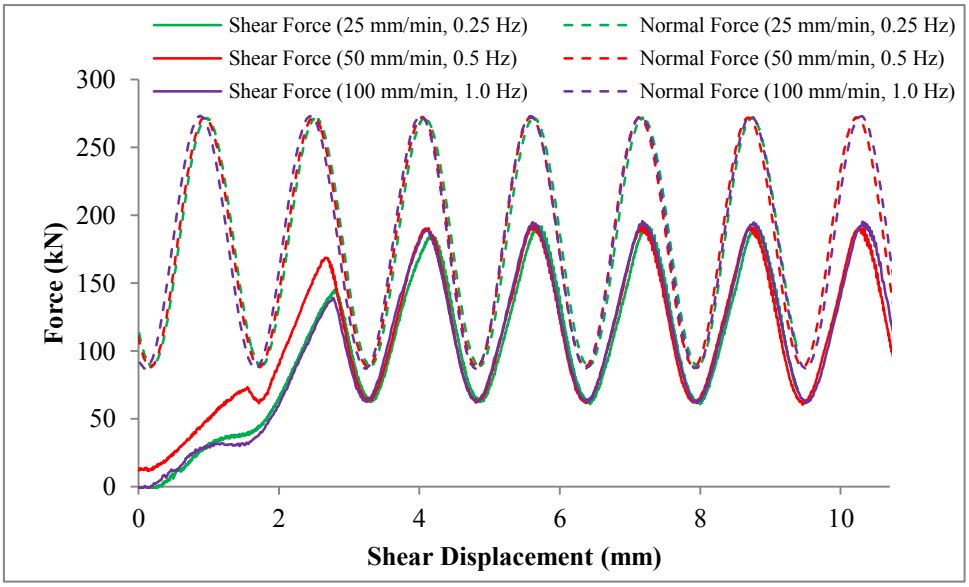

(b) Normal force: 180 kN +/- 90 kN

Figure 68. Forces vs. shear displacement with SV-NIF of 100 mm/min·Hz.

The force vs. shear displacement behavior under different shear velocities and different normal impact frequencies but for same ratios between shear velocity and

normal impact frequency (SV-NIF) is shown in Figure 68. At the stable shearing stage, the peak shear force and minimum shear force have the same value and the obtained curves are nearly identical for the same values of SV-NIF. Thus, the peak shear force and minimum shear force are influenced by both: shear velocity and normal impact frequency, which is represented by the factor SV-NIF.

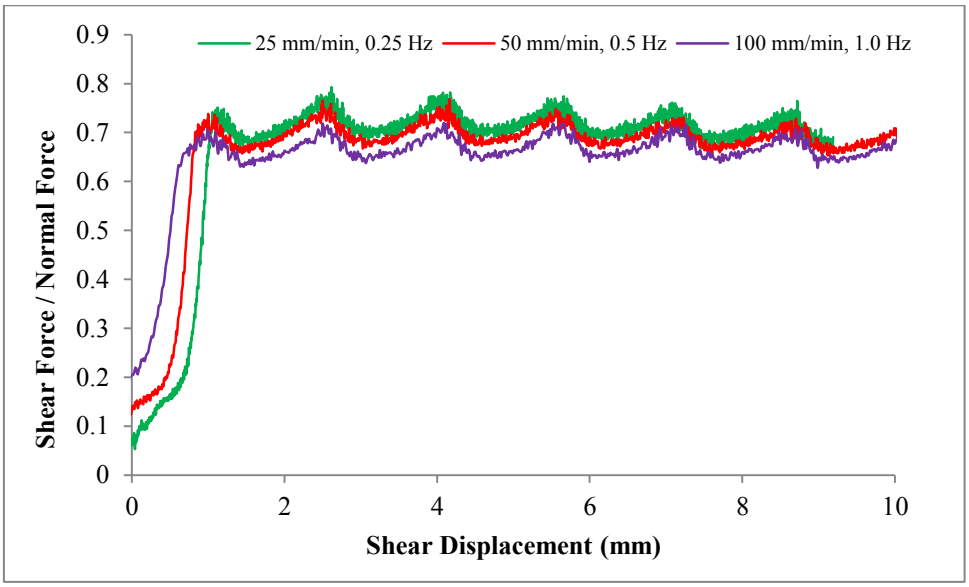

(a) Normal force: 90 kN +/- 45 kN

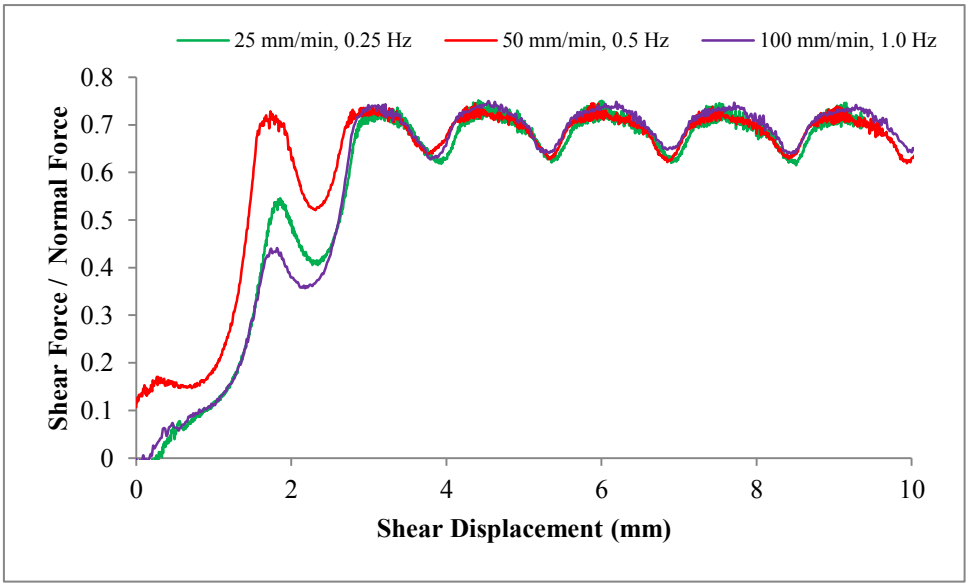

(b) Normal force: 180 kN +/- 90 kN

Figure 69. Friction coefficients vs. shear displacement with SV-NIF of 100 mm/min·Hz.

Moreover, Figure 69 shows that at the stable shear stage, the friction coefficient shows the same trend for the same values of SV-NIF. It can be deduced that under extremely high SV-NIF, the relative time shift will be zero and the friction coefficient will be constant (Figure 70 and Figure 71). That means that the DNL shear behavior is nearly identical to the quasi-static CNL shear behavior.

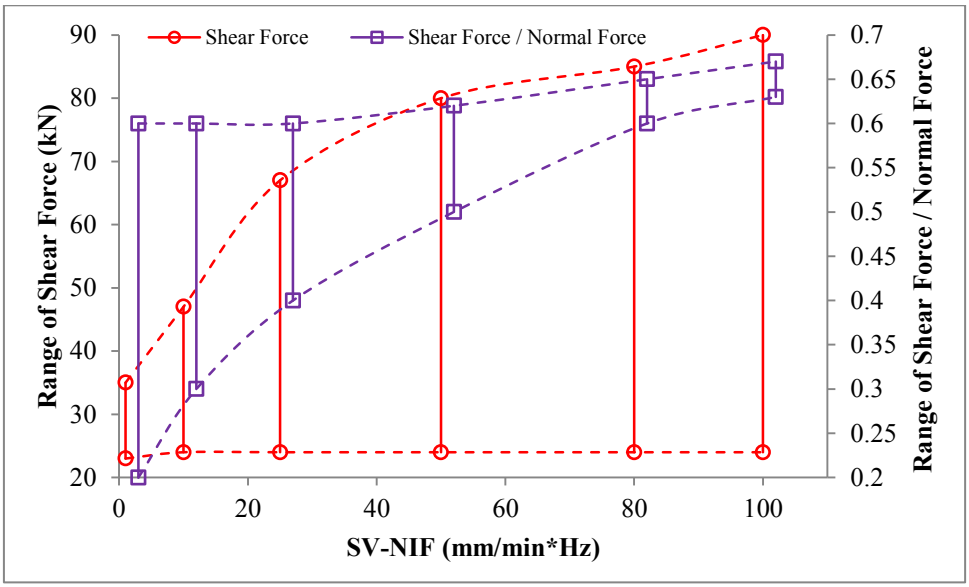

(a) Normal force: 90 kN +/- 45 kN

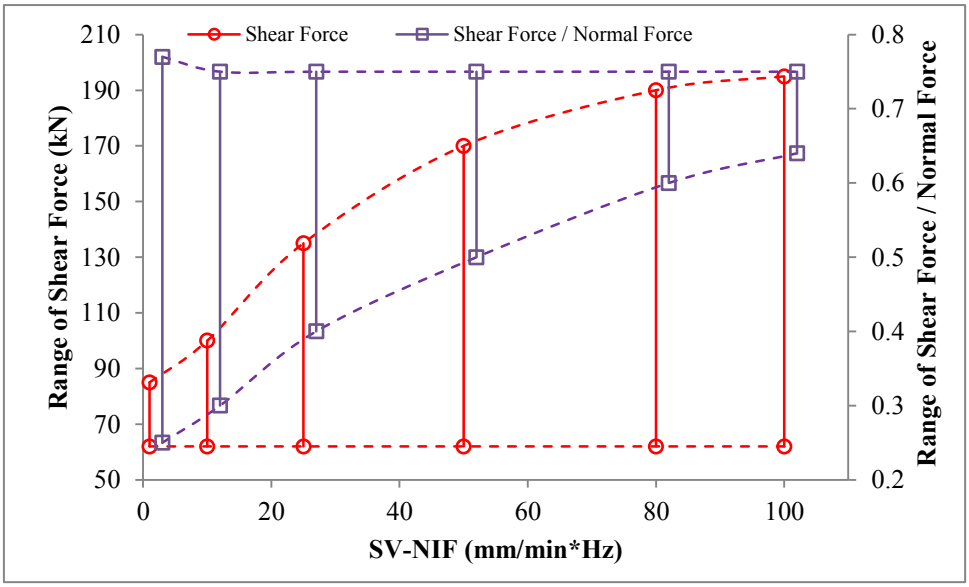

(b) Normal force: 180 kN +/- 90 kN

Figure 70. Range of shear and normal forces as well as friction coefficient vs. SV-NIF.

In the SV-NIF range of 1 mm/min·Hz to 100 mm/min·Hz, the lab test results have shown that the shear behavior of artificial joints is influenced significantly by the ratio

between shear velocity and normal impact frequency (SV-NIF). Shear forces, relations between friction coefficient and shear displacement are nearly identical for same SV-NIF. Minimum friction coefficient increases with increasing SV-NIF, but peak friction coefficient is more or less constant. Peak shear force increases with increasing SV-NIF, whereas minimum shear force is more or less constant. The relative shift between normal force and shear force decreases with increasing SV-NIF, and increases with increasing normal force. Therefore, great care has to be taken in the design of rock mass structures considering dynamic and pseudo-static loading.

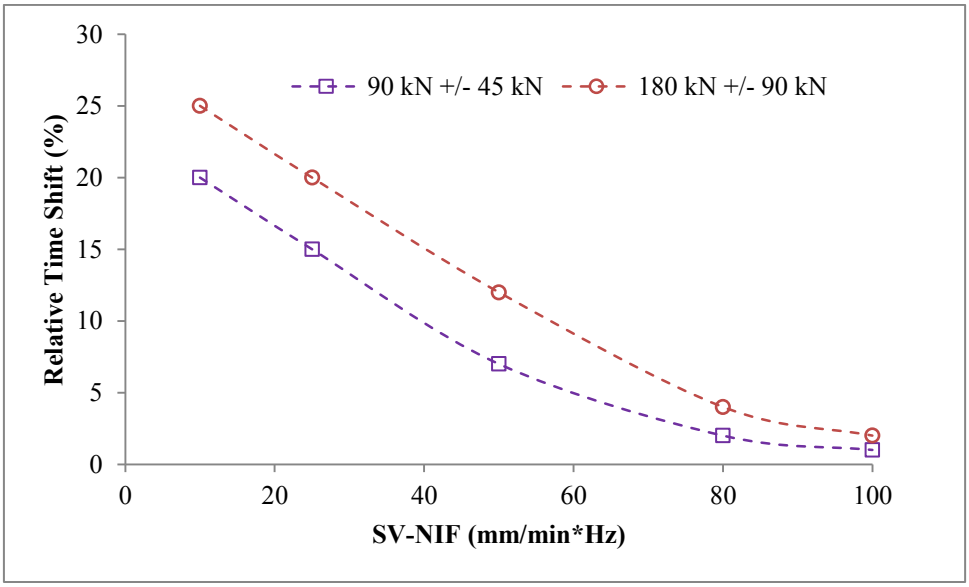

Figure 71. Relative time shift between max. normal force and max. shear force under different SV-NIF.

Shear strength criterion

Figure 59, Figure 62, Figure 64, Figure 67 and Figure 69 illustrate that the friction coefficient shows cyclical (nearly sinusoidal) behavior for all applied impact amplitudes. In respect to time shift the following equation can be deduced:

$$k = c_1 + c_2 \cdot \sin[2\pi f(t + \Delta t)] \tag{21}$$

where k is the friction coefficient,

c_1 is the correction factor 1,

c_2 is the correction factor 2,

f is the normal impact frequency,

Δt is the time shift.

The normal force can be described as:

$$\sigma_n = \frac{F_s + F_d \sin(2\pi f t)}{S} \tag{22}$$

where σ_n is the normal stress,

F_s is the quasi-static normal force,

F_d is the dynamic normal force,

f is the frequency,

t is the time,

S is the joint contact area.

Taking into account the above mentioned considerations and laboratory tests results, the following expression for joint shear strength is proposed for plane joints under sinusoidal DNL conditions:

$$\tau = \{c_1 + c_2 \cdot \sin[2\pi f (t + \frac{\pi}{f})]\} \cdot \frac{F_s + F_d \sin(2\pi f t)}{S} \tag{23}$$

Classically, static shear strength is described by Barton's (1976) criterion:

$$\tau = \sigma_n \tan\left(\phi_b + JRC \log_{10}\left(\frac{JCS}{\sigma_{no}}\right)\right) \tag{24}$$

Assuming, that Barton's criterion might be valid also for dynamic excitation and assuming that for a plane joint JRC can be set to zero, σ_n might be given by Eq.22. Under these assumptions, Barton's criterion might be extended for dynamic loading as follows:

$$\tau = \frac{F_s + F_d \sin(2\pi f t)}{S} \tan \phi_b \qquad (\phi_b = 39.5^\circ) \qquad (25)$$

Figure 72 shows extended classical Barton's criterion (Eq.25) and the new one (Eq.23) together with lab test results. Extended Barton's classical criterion follows the normal force evolution. However, the new criterion considers the time shift between normal and shear forces, which results in considerably lower shear strength values. The new criterion is in close agreement with the measured values (Figure 73, Figure 74 and Figure 75). The application of Barton's or other static criterion for dynamic problems without consideration of the phase shift is not valid. c_1 decreases and c_2 increases with the increase of impact amplitudes.

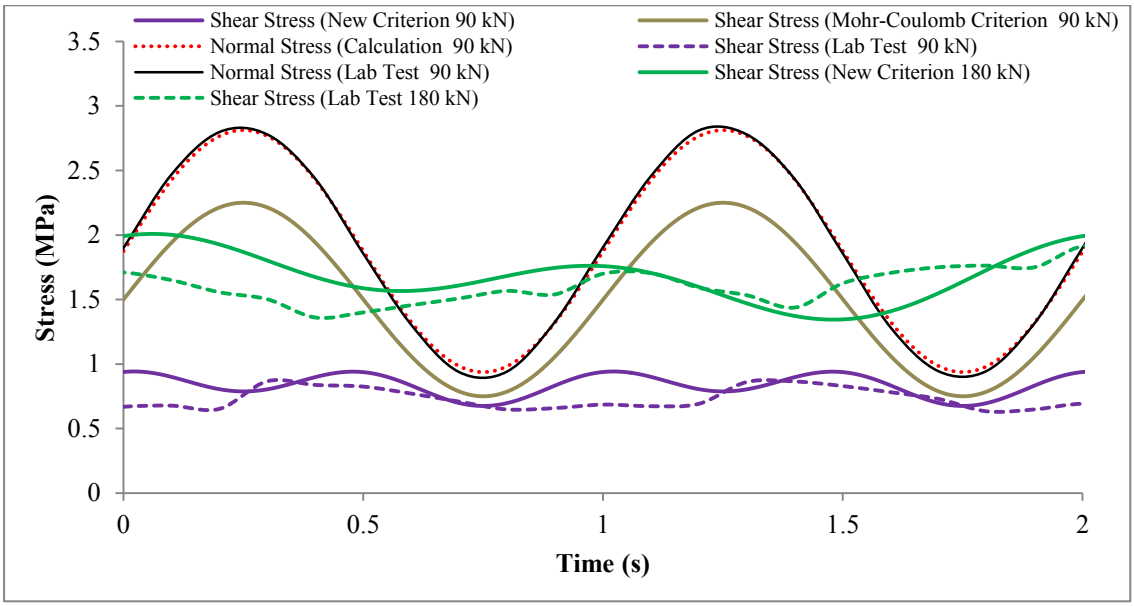

Figure 72. Normal and shear stress vs. time (static normal load 90 kN/180 kN and superimposed dynamic load of ±45 kN/±90 kN, frequency 1.0 Hz and constant shear velocity of 3.0 mm/min), stable stages were taken and starting time was shifted to zero.

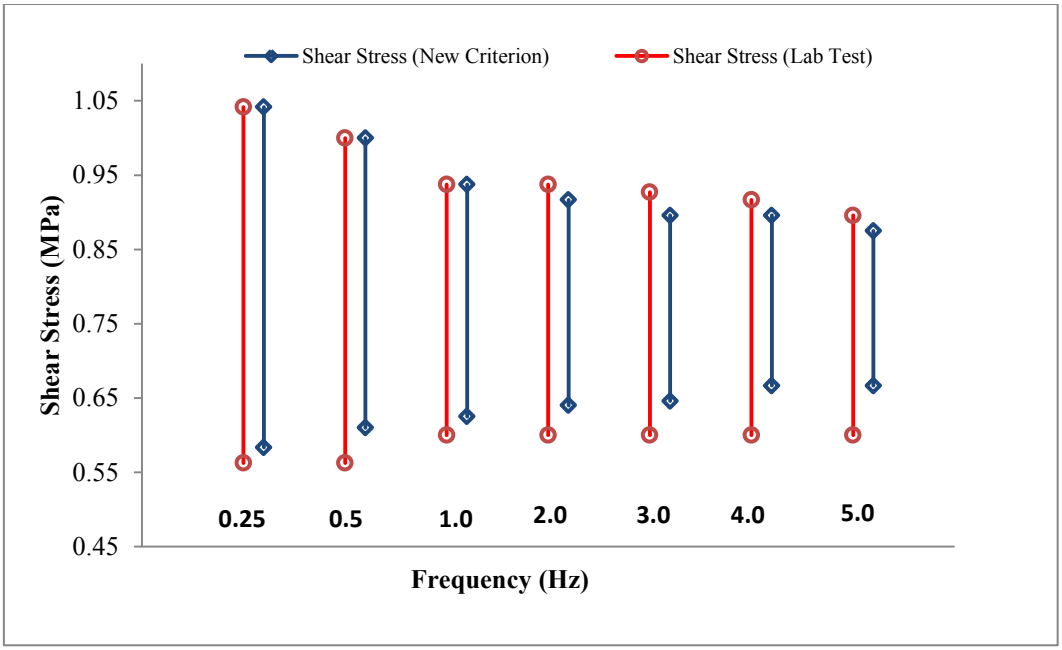

Figure 73. DDNL_3: Range of shear stresses for different frequencies (static normal load 90 kN, superimposed dynamic load of ±45 kN and constant shear velocity of 3.0 mm/min).

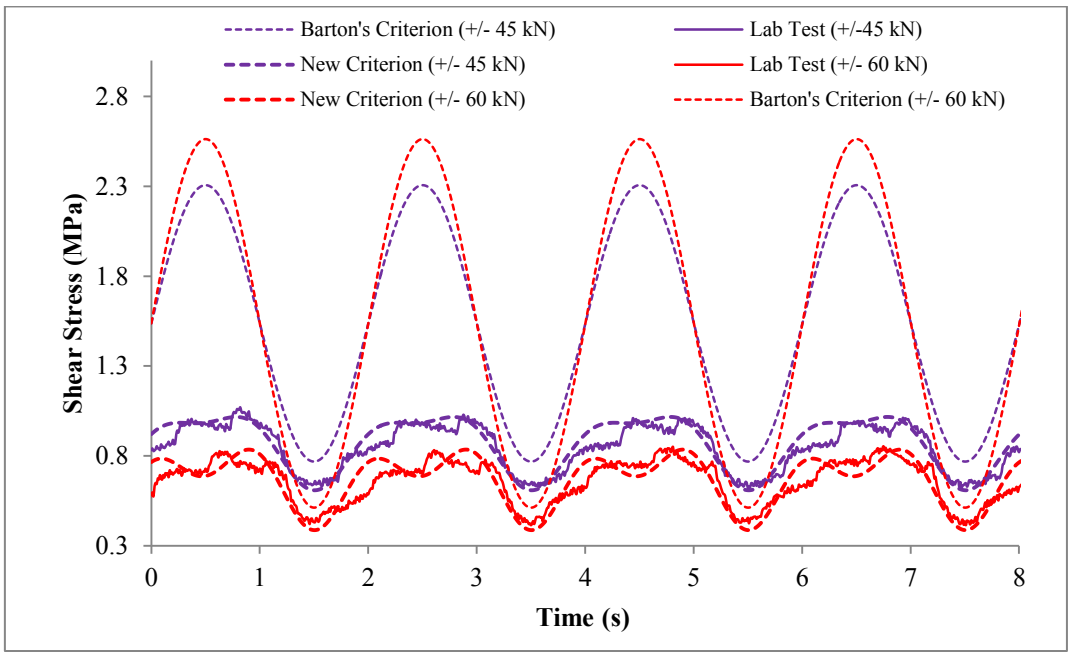

Figure 74. DDNL_5: Shear stress vs. time (static normal load 90 kN, superimposed dynamic load of ±45 kN/±60 kN and constant shear velocity of 3.0 mm/min), stable stages are taken and starting time is shifted to zero.

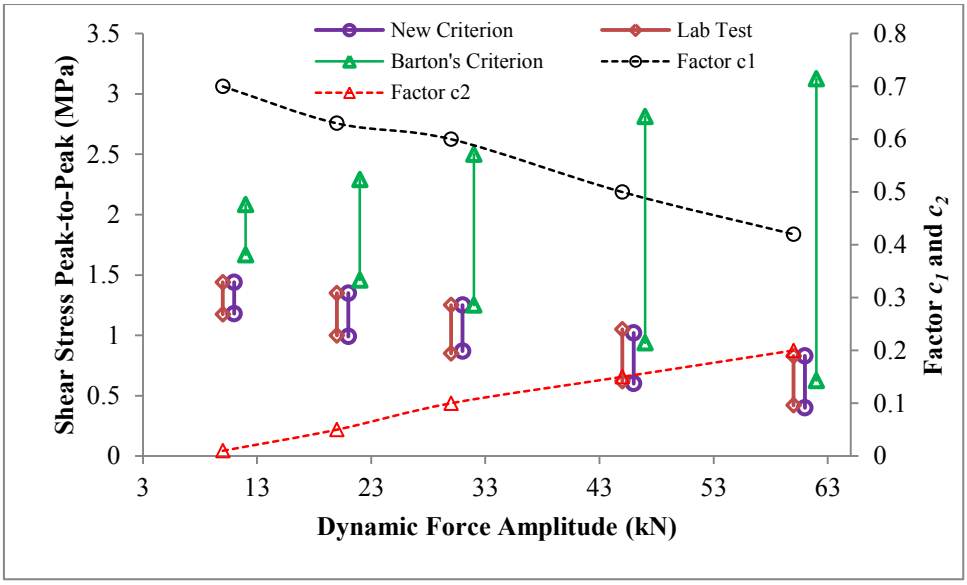

Figure 75. DDNL_5: Shear stress amplitudes and values of factor c_1 and c_2 (Eq.23) under different impact amplitudes and constant shear velocity of 3.0 mm/min.

5.2.2 Cyclic shear tests under DNL conditions

5.2.2.1 Test set-up

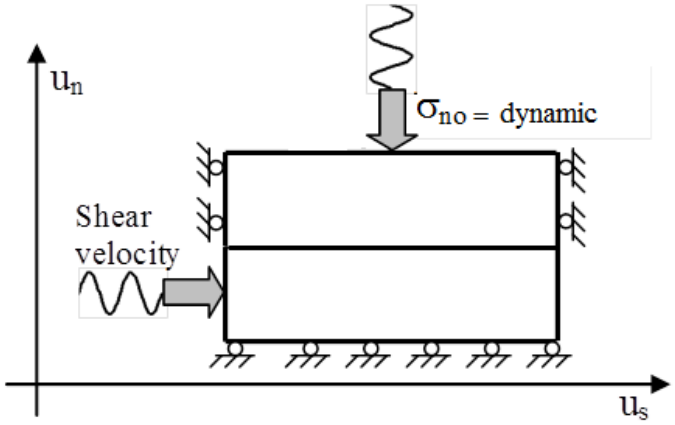

Figure 76. Set-up of cyclic shear test (DNL-test).

Cyclic shear test under DNL conditions are performed like illustrated in Figure 76. The cyclic loading is applied as a dynamic excitation in the normal direction at the upper shear frame. Simultaneously, shear displacement controlled by sinusoidal excitation is applied horizontally to the bottom part of the specimen. The vertical dynamic sinusoidal excitation is applied as a superimposed force as follows:

$$F_{sd} = F_d \sin\left(2\pi f_v t\right) \tag{26}$$

where F_{sd} is the impact normal force,
F_d is the amplitude of normal force,
f_v is the normal impact frequency,
t is the time.

The shear displacement controlled by sinusoidal excitation is given as follows:

$$u_s = u_{\max} \sin\left(2\pi f_h t\right) \tag{27}$$

where u_s is the shear displacement,
u_{max} is the amplitude of shear displacement,
f_h is the horizontal impact frequency,
t is the time.

The cyclic shear behavior was investigated under the influence of different vertical and horizontal impact frequencies, vertical impact amplitudes, horizontal shear displacement amplitudes, and normal load levels. The test scheme was designed as follows: Constant normal loads varied from 30 kN to 360 kN, superimposed normal forces varied from ± 15 kN to ± 180 kN, horizontal shear frequencies varied from 0.25 Hz to 5.0 Hz, vertical impact frequencies varied from 0.25 Hz to 5.0 Hz, horizontal shear displacement amplitudes varied from ± 2.0 mm to ± 8.0 mm and number of test cycles varied from 10 to 50. In order to facilitate comparison for each group, only one input parameter was changed. The dynamic tests were conducted according to schemes documented in Table 7. A total of 57 cyclic shear tests (arranged in 9 groups) were performed.

Table 7. Test parameter for cyclic shear test under DNL conditions.

Sample	Stage	F	f_h	f_v	F_d	u_s	$Cycles_h$	$Cycles_v$
		(kN)	(Hz)	(Hz)	(kN)	(mm)	(-)	(-)
CDNL_1	1	30	0.5	0.5	±15	5	10	10
	2	60	0.5	0.5	±30	5	10	10
	3	90	0.5	0.5	±45	5	10	10
	4	180	0.5	0.5	±90	5	10	10
	5	360	0.5	0.5	±180	5	10	10
CNDL_2	1	90	0.5	0.5	±45	2	10	10
	2	90	0.5	0.5	±45	4	10	10
	3	90	0.5	0.5	±45	8	10	10
	4	180	0.5	0.5	±90	2	10	10
	5	180	0.5	0.5	±90	4	10	10
	6	180	0.5	0.5	±90	8	10	10
CDNL_3	1	90	0.25	1	±45	5	10	40
	2	90	0.5	1	±45	5	10	20
	3	90	1	1	±45	5	10	10
	4	90	2	1	±45	5	20	10
	5	90	3	1	±45	5	30	10
	6	90	4	1	±45	5	40	10
	7	90	5	1	±45	5	50	10
CNDL_4	1	180	0.25	1	±90	5	10	40
	2	180	0.5	1	±90	5	10	20
	3	180	1	1	±90	5	10	10
	4	180	2	1	±90	5	20	10
	5	180	3	1	±90	5	30	10
	6	180	4	1	±90	5	40	10
	7	180	5	1	±90	5	50	10
CNDL_5	1	90	1	0.25	±45	5	40	10
	2	90	1	0.5	±45	5	20	10
	3	90	1	1	±45	5	10	10
	4	90	1	2	±45	5	10	20
	5	90	1	3	±45	5	10	30
	6	90	1	4	±45	5	10	40
	7	90	1	5	±45	5	10	50
CNDL_6	1	180	1	0.25	±90	5	40	10
	2	180	1	0.5	±90	5	20	10
	3	180	1	1	±90	5	10	10
	4	180	1	2	±90	5	10	20
	5	180	1	3	±90	5	10	30
	6	180	1	4	±90	5	10	40
	7	180	1	5	±90	5	10	50

Table continue

Sample	Stage	F	f_h	f_v	F_d	u_s	$Cycles_h$	$Cycles_v$
		(kN)	(Hz)	(Hz)	(kN)	(mm)	(-)	(-)
CNDL_7	1	90	0.25	0.25	±45	5	10	10
	2	90	0.5	0.5	±45	5	10	10
	3	90	1.0	1.0	±45	5	10	10
	4	90	2.0	2.0	±45	5	10	10
	5	90	3.0	3.0	±45	5	10	10
	6	90	4.0	4.0	±45	5	10	10
CNDL_8	1	180	0.25	0.25	±90	5	10	10
	2	180	0.5	0.5	±90	5	10	10
	3	180	1.0	1.0	±90	5	10	10
	4	180	2.0	2.0	±90	5	10	10
	5	180	3.0	3.0	±90	5	10	10
	6	180	4.0	4.0	±90	5	10	10
CNDL_9	1	90	0.5	0.5	±10	5	10	10
	2	90	0.5	0.5	±20	5	10	10
	3	90	0.5	0.5	±30	5	10	10
	4	90	0.5	0.5	±45	5	10	10
	5	90	0.5	0.5	±60	5	10	10
	6	90	0.5	0.5	±90	5	10	10

5.2.2.2 Test results

Test results under different normal force conditions (CDNL_1)

Test results under different normal force conditions are shown in Figure 77, Figure 78, Figure 82, Figure 80, Figure 81 and Figure 82. Under the normal impact load and cyclic horizontal shear displacement, shear force and friction coefficient show cyclical behavior. With the increase of normal force and superimposed dynamic normal force, the peak values of shear forces increase, while the friction coefficients are more or less the same in the stable stage. The friction coefficient decreases with increasing normal force with superimposed dynamic normal load. The stable period of the friction coefficient becomes smaller with ongoing number of cycles. This is caused by progressive surface damage of the joint.

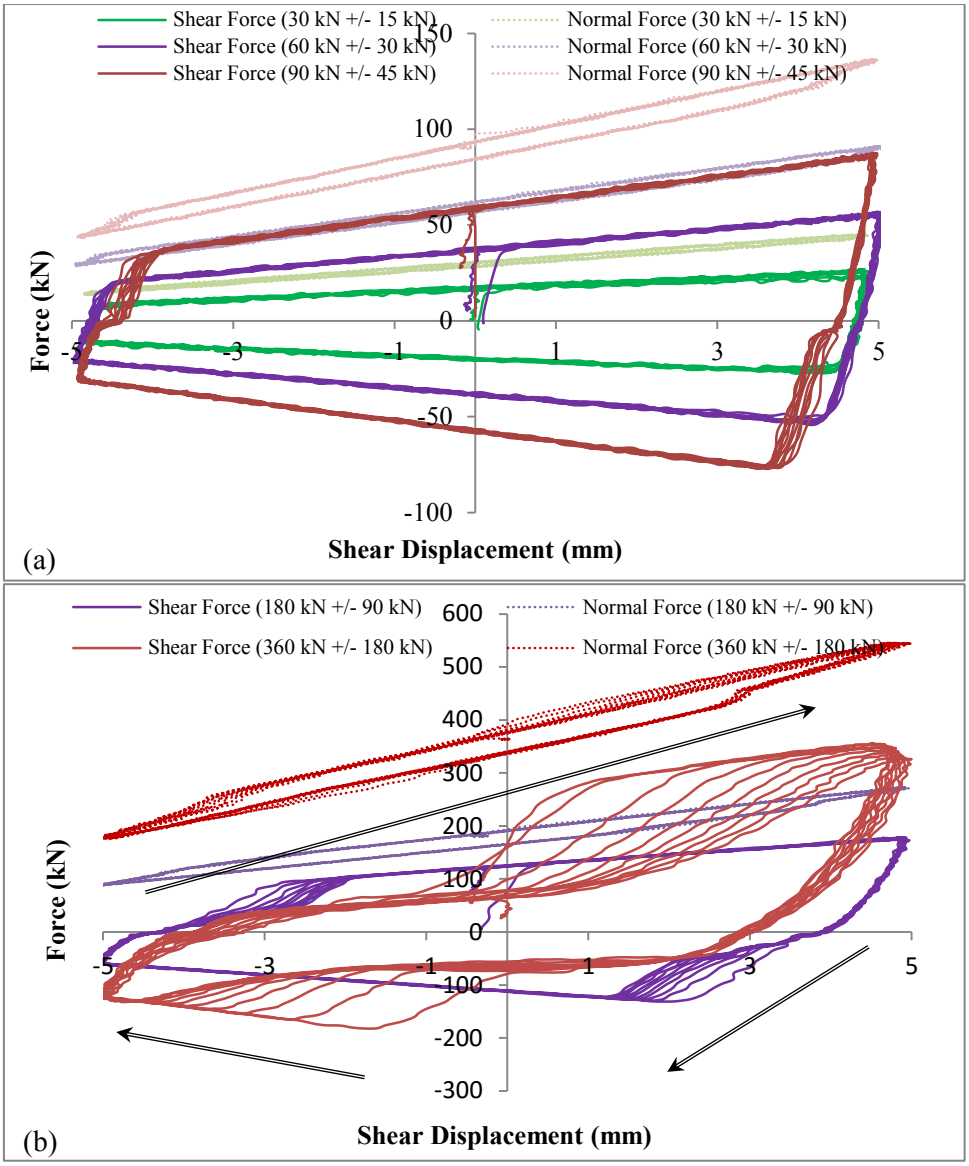

Figure 77. CDNL_1: Normal and shear force vs. shear displacement under different static normal force with superimposed dynamic normal force at horizontal frequency of 0.5 Hz, vertical frequency of 0.5 Hz, and horizontal shear displacement amplitude of 5.0 mm.

Maximum shear force is related linearly to the normal force. However, minimum shear force decreasing rate becomes smaller with increasing normal force. The amplitudes of normal displacement increase with increasing superimposed dynamic normal loads (Figure 82). The settlement increases with increasing number of cycles. During the shear reversal (backward shear stage), decrease of normal load enhances the decrease of shear force. Figure 77 also shows that under higher normal force (180 KN +/- 90 kN or 360 kN +/- 180 kN), damage of the joint surfaces is observed.

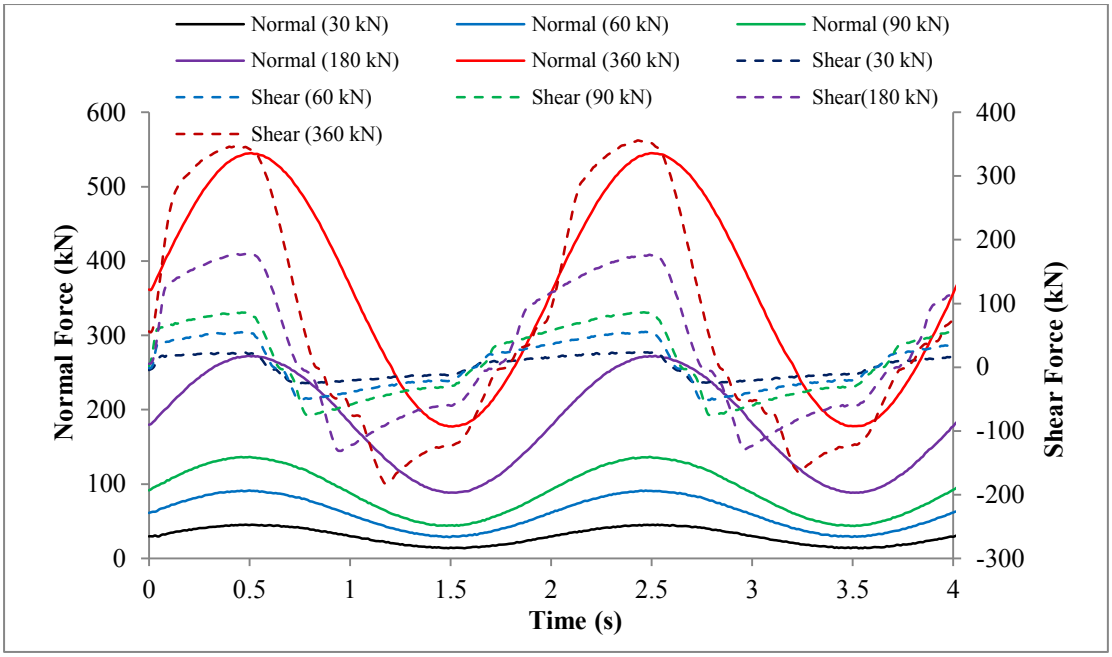

Figure 78. CDNL_1: Normal and shear force vs. time under different normal loads at horizontal cyclic frequency of 0.5 Hz, vertical impact frequency of 0.5 Hz and horizontal shear displacement amplitude of 5.0 mm.

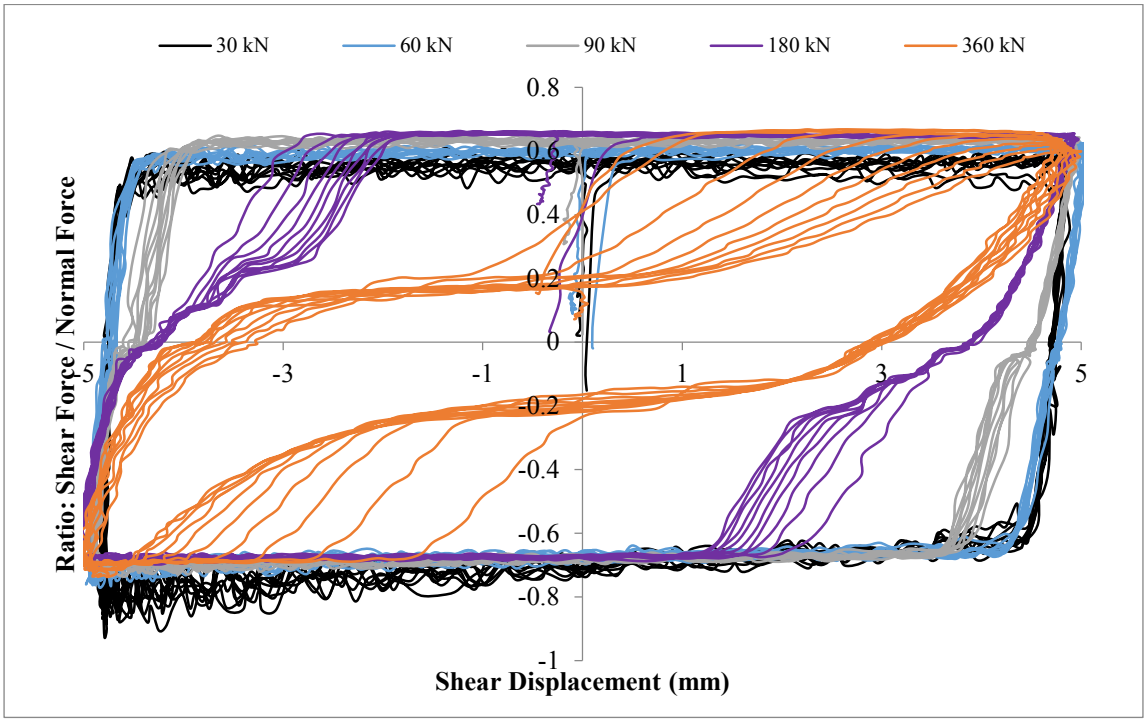

Figure 79. CDNL_1: Friction coefficient vs. shear displacement under different normal loads at horizontal frequency of 0.5 Hz, vertical frequency of 0.5 Hz and horizontal shear displacement amplitude of 5.0 mm.

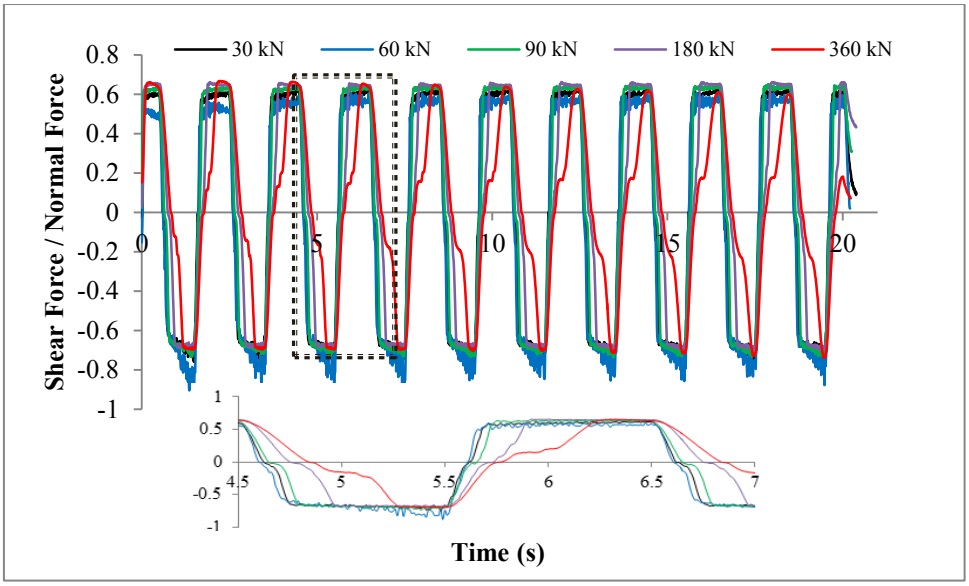

Figure 80. CDNL_1: Friction coefficient vs. time under different normal loads at horizontal frequency of 0.5 Hz, vertical frequency of 0.5 Hz and horizontal shear displacement amplitude of 5.0 mm.

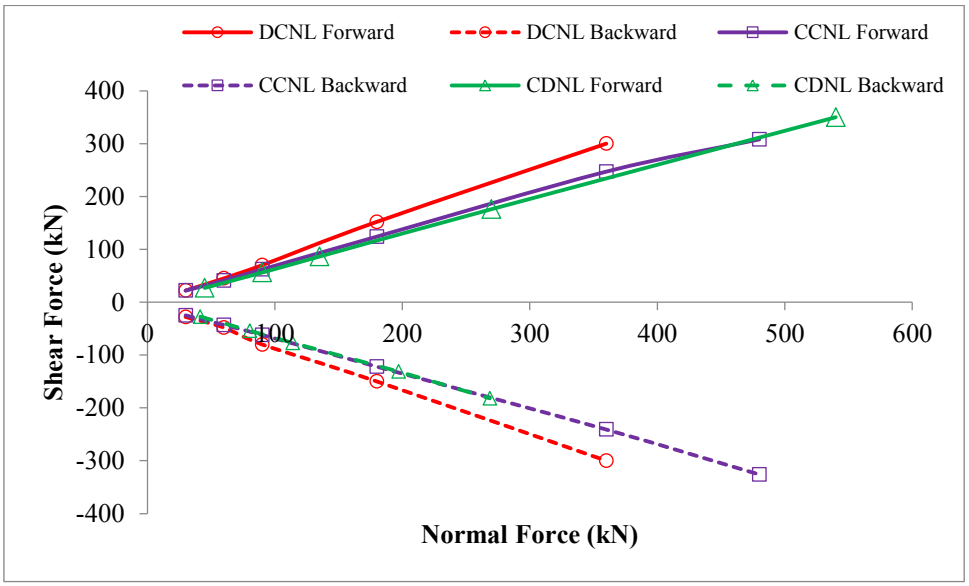

Figure 81. CDNL_1: Maximum and minimum shear force vs. normal force at horizontal frequency of 0.5 Hz, vertical frequency of 0.5 Hz and horizontal shear displacement amplitude of 5.0 mm.

Under smaller normal loads (below 180 kN), the peak shear force in the backward shear direction is located in the positive shear displacement phase. However, it is located in the negative shear displacement phase under higher normal loads (360 kN). This is caused by the damage of the joint surfaces and large shear displacement which

is needed to reach the peak shear forces. Shear direction reversal and normal force decrease leads to peak shear force in the backward shear direction smaller than in the forward direction.

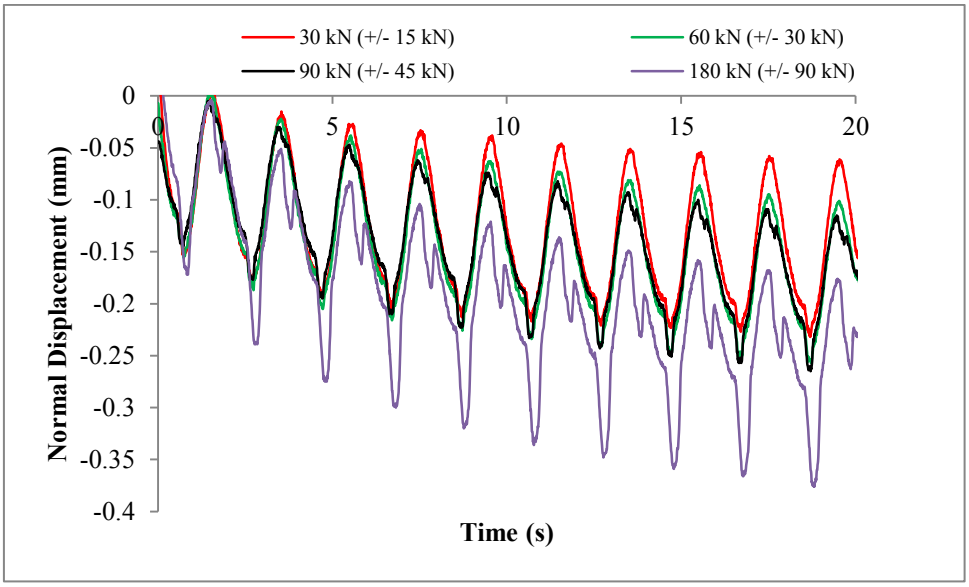

Figure 82. CDNL_1: Normal displacement vs. time under different normal loads at horizontal frequency of 0.5 Hz, vertical frequency of 0.5 Hz and horizontal shear displacement amplitude of 5.0 mm.

Test results under different horizontal shear displacement amplitudes (CDNL_2)

Test results under different horizontal shear displacement amplitudes are shown in Figure 83, Figure 84, Figure 85, Figure 86 and Figure 87. The test results show that shear force, normal force, friction coefficient and shear displacement are cyclically changing with ongoing time. With the increase in horizontal shear displacement amplitude, the peak shear force in the forward shear direction is nearly constant (only a minor increase with increasing shear displacement amplitude is observed), while the peak shear force in the backward shear direction increases with increasing shear displacement amplitude. During each shear cycle, peak shear force is nearly constant (slightly decreasing) in each test case. The evolution of the friction coefficient shows more or less the same trend (square wave like) in each cycle, but the peak friction coefficient is maintained longer in the stable stage in case of larger shear displacement amplitude. The peak shear force in the forward shear direction is reached at the point of peak normal force with maximum shear displacement.

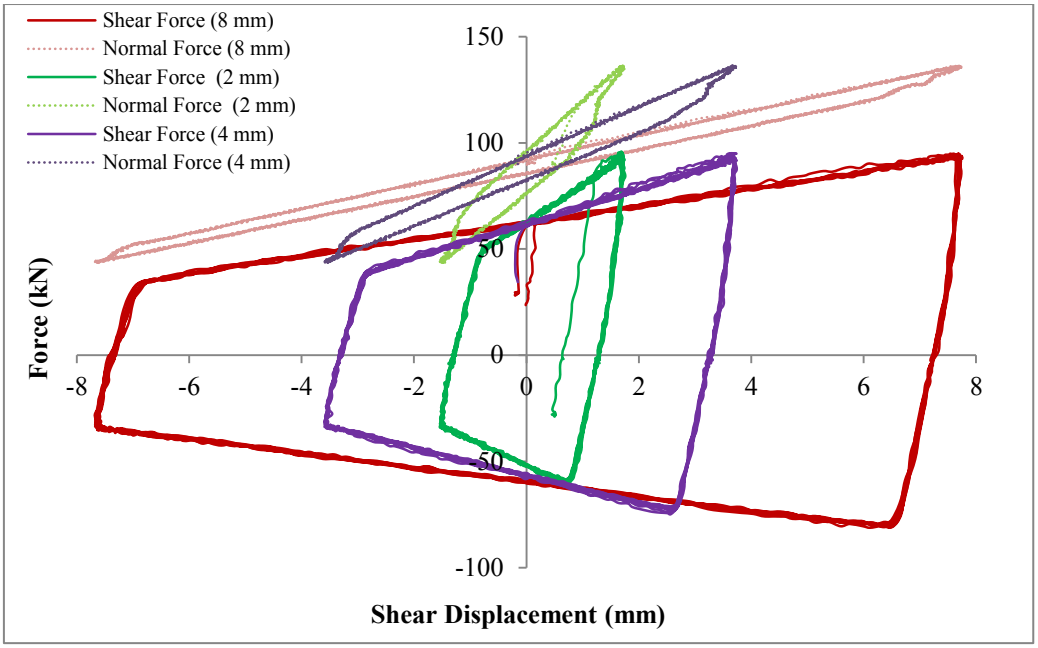

Figure 83. CDNL_2: Normal and shear force vs. shear displacement under normal load of 90 kN and superimposed dynamic load of ±45 kN at normal impact frequency of 0.5 Hz with different horizontal shear displacement amplitudes.

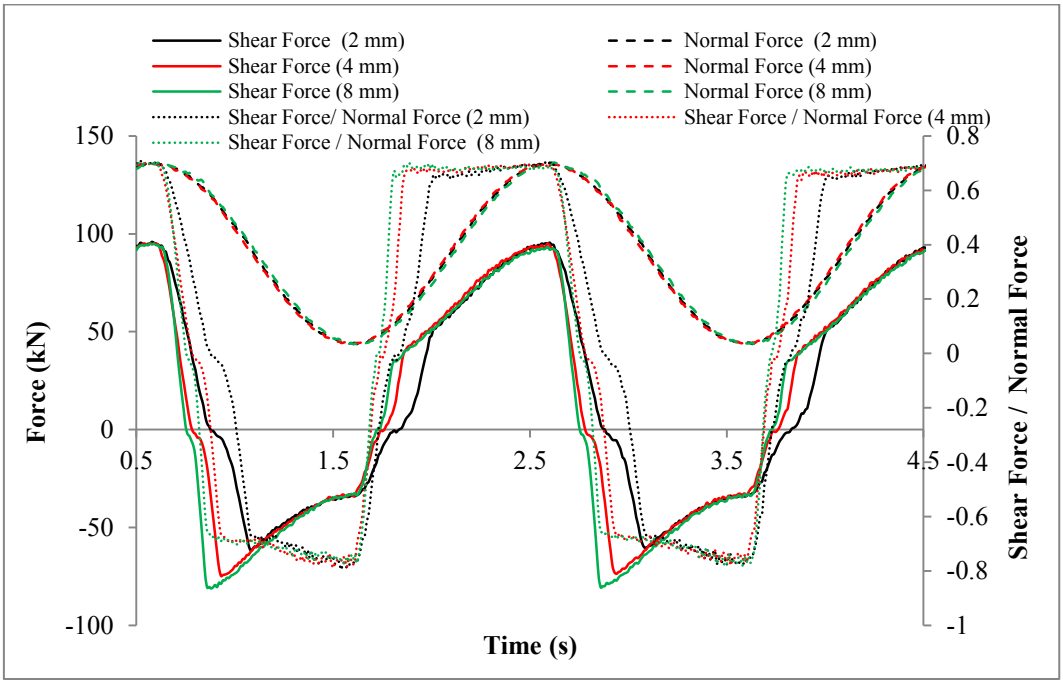

Figure 84. CDNL_2: Normal force, shear force and friction coefficient vs. time under normal load of 90 kN and superimposed dynamic load of ±45 kN at normal impact frequency of 0.5 Hz with different horizontal shear displacement amplitudes.

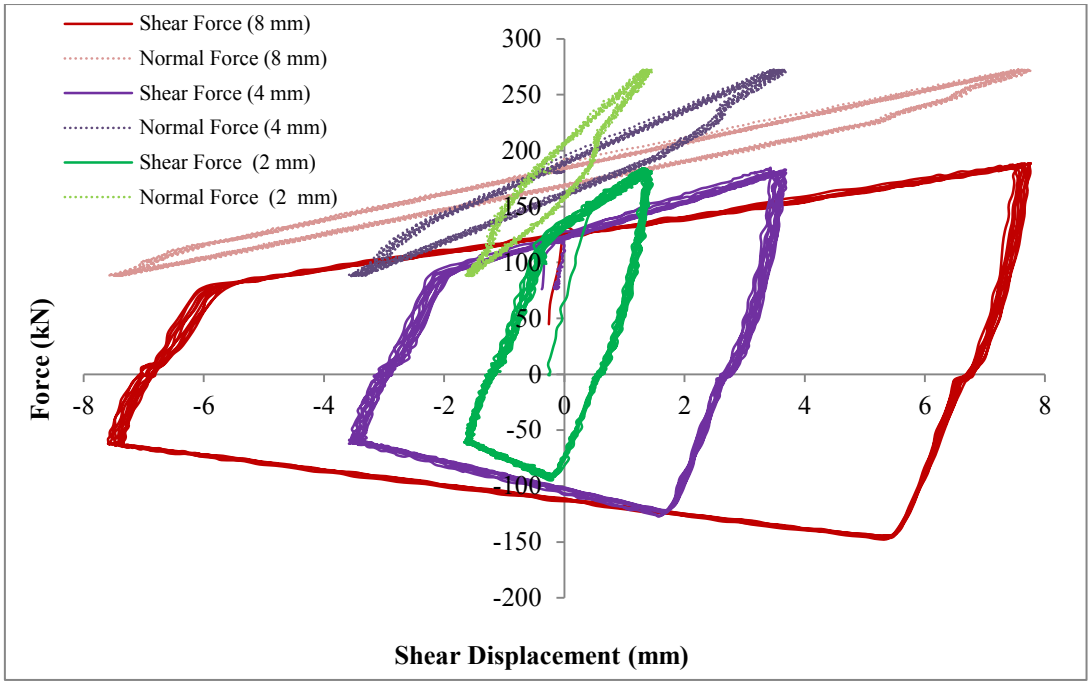

Figure 85. CDNL_2: Normal and shear force vs. shear displacement under normal load of 180 kN and superimposed dynamic load of ±90 kN at normal impact frequency of 0.5 Hz with different horizontal shear displacement amplitudes.

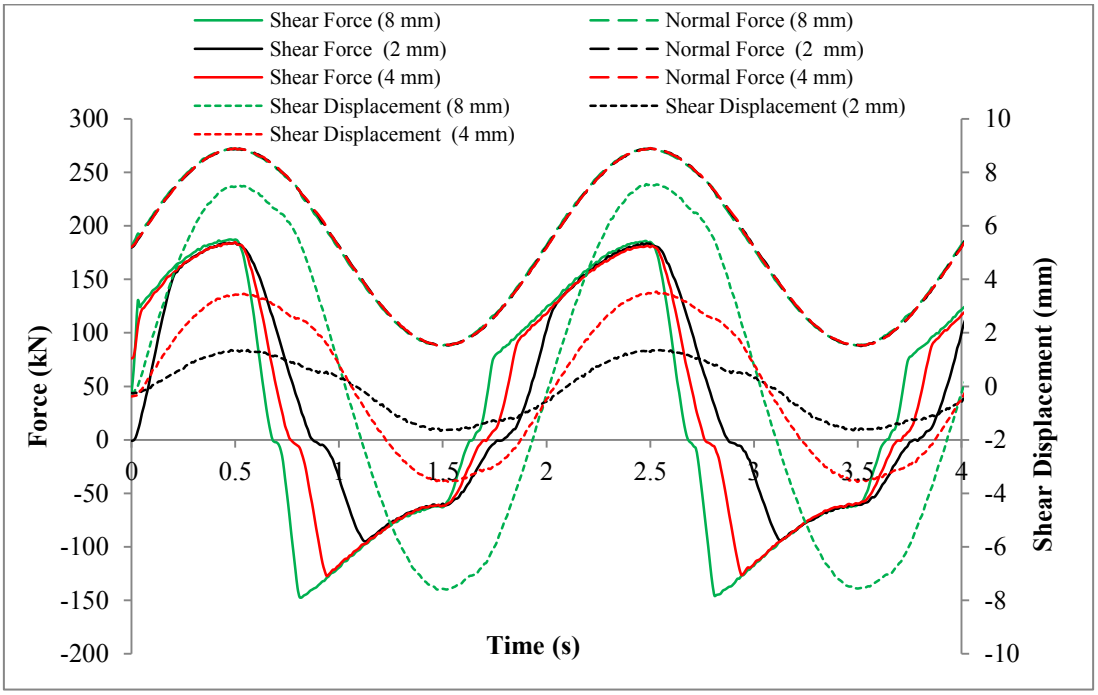

Figure 86. CDNL_2: Normal force, shear force and shear displacement vs. time under normal load of 180 kN and superimposed dynamic load of ±90 kN at normal impact frequency of 0.5 Hz with different horizontal shear displacement amplitudes.

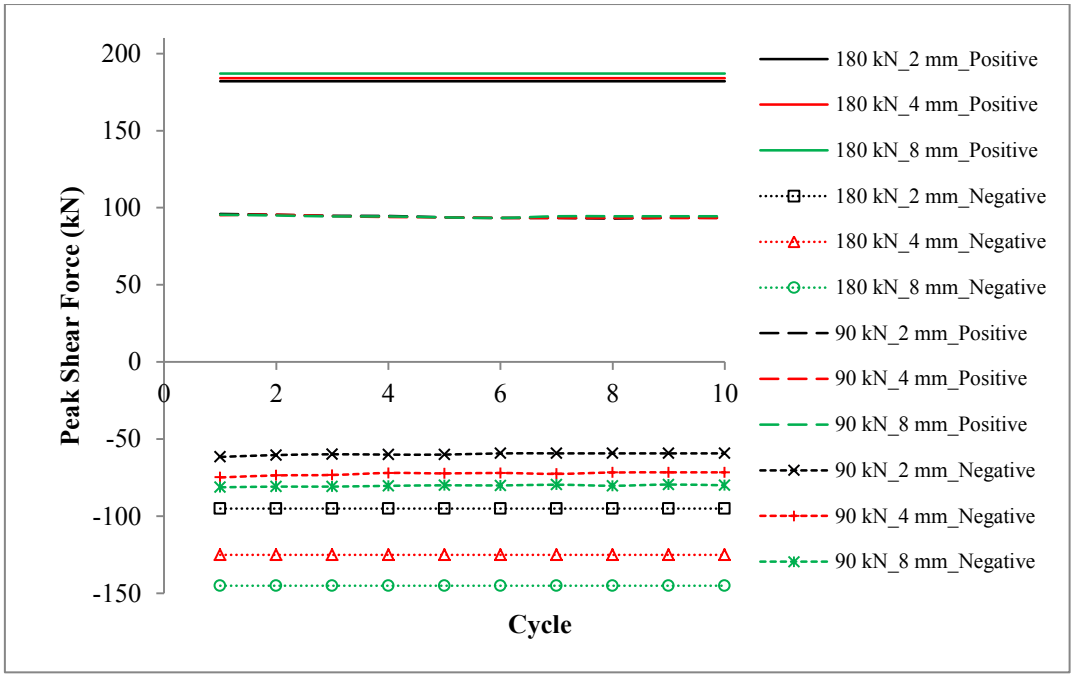

Figure 87. CDNL_2: Peak shear force vs. number of cycles at normal impact frequency of 0.5 Hz with different horizontal shear displacement amplitudes.

Test results under different vertical impact and horizontal cyclic shear frequencies (CDNL_3 to CDNL_8)

Evolution of shear force and friction coefficient under different normal impact frequencies and different horizontal cyclic shear frequencies are shown in Figure 88 and Figure 89. In the forward and backward shear directions, peak shear forces show different behavior. Peak shear forces in the forward shear direction have more or less the same value under different vertical normal impact frequencies and horizontal shear frequencies. Three situations can be distinguished:

$f_h > f_v$: Shear forces are cyclically changing along with the horizontal cyclic shear displacement. The peak of the shear force in the forward and backward shear directions is reached nearly at the same point when maximum normal force is reached. Peak shear force is almost the same in each cycle. Evolution of shear forces is square wave like with different amplitudes.

$f_h = f_v$: Shear forces are cyclically changing along with the horizontal cyclic shear displacement. The peak of the shear force in the forward and backward shear direction

is reached nearly at the same point when maximum normal force is reached. The peak shear force in the backward shear direction has more or less the same value, but it drops dramatically (about 70% of the peak values if vertical impact frequency is not equal to horizontal shear frequency). With the increase of normal impact frequency and horizontal shear frequency, the peak shear force in the forward shear direction drops slightly, while the peak shear force in the backward shear direction decreases dramatically.

$f_h < f_v$: Shear forces are cyclically changing along with the horizontal cyclic shear displacement. But the shear forces have more inflection in the forward and backward shear direction. The peak shear force in the forward and backward shear direction has almost the same value during each vertical impact cycle.

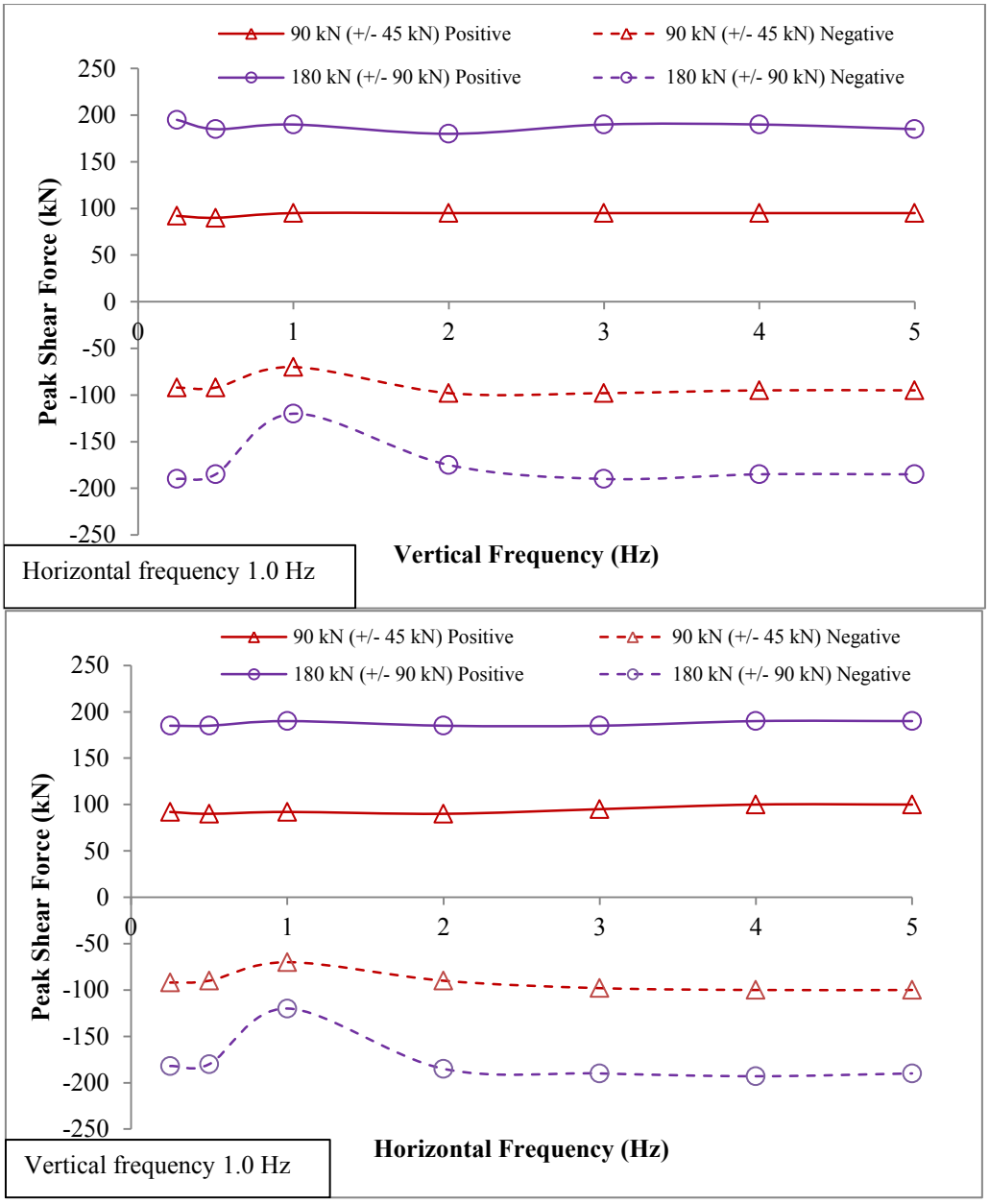

Figure 88. CDNL_3 to CDNL_6: Peak shear force under different vertical and horizontal impact frequencies at horizontal shear displacement of 5.0 mm.

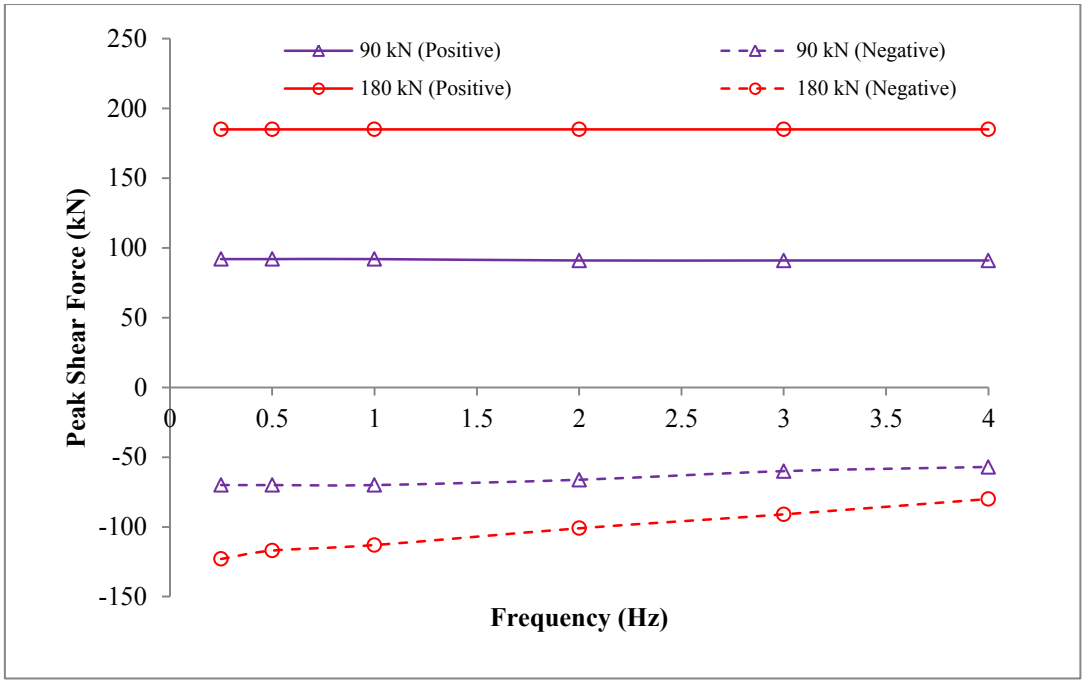

Figure 89. CDNL_7 and CDNL_8: Peak shear forces vs. frequencies ($f_h = f_v$).

Test results under different normal impact amplitudes (CDNL_9)

Evolution of shear forces, shear friction coefficient and normal displacement behavior under different normal impact amplitudes is shown in Figure 90, Figure 91 and Figure 92. Peak shear forces in the forward shear direction increase with increasing normal impact amplitudes. However, the peak shear force in the backward shear direction is constant, and the time of the stable stage decreases with increasing normal impact amplitudes. Evolution of friction coefficient is more or less the same (square wave like). Normal displacement is cyclically changing along with the cyclic normal impact. Larger normal impact amplitude leads to bigger normal displacement amplitude.

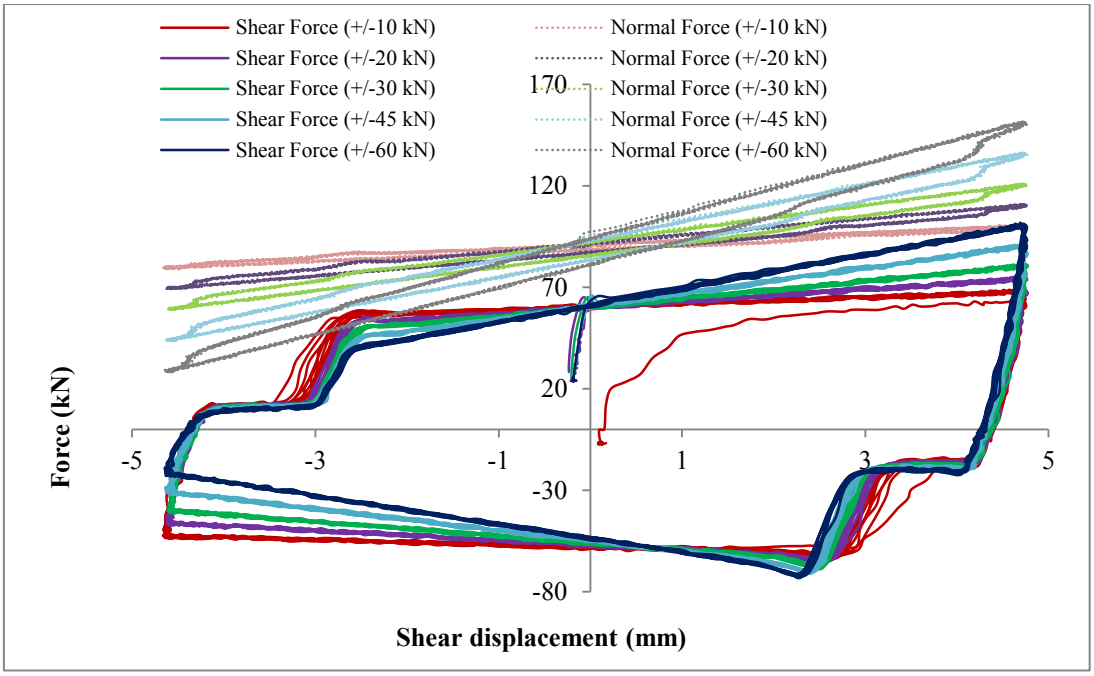

Figure 90. CDNL_9: Normal and shear force vs. shear displacement under different superimposed normal load at horizontal cyclic shear frequency of 0.5 Hz and vertical impact frequency of 0.5 Hz.

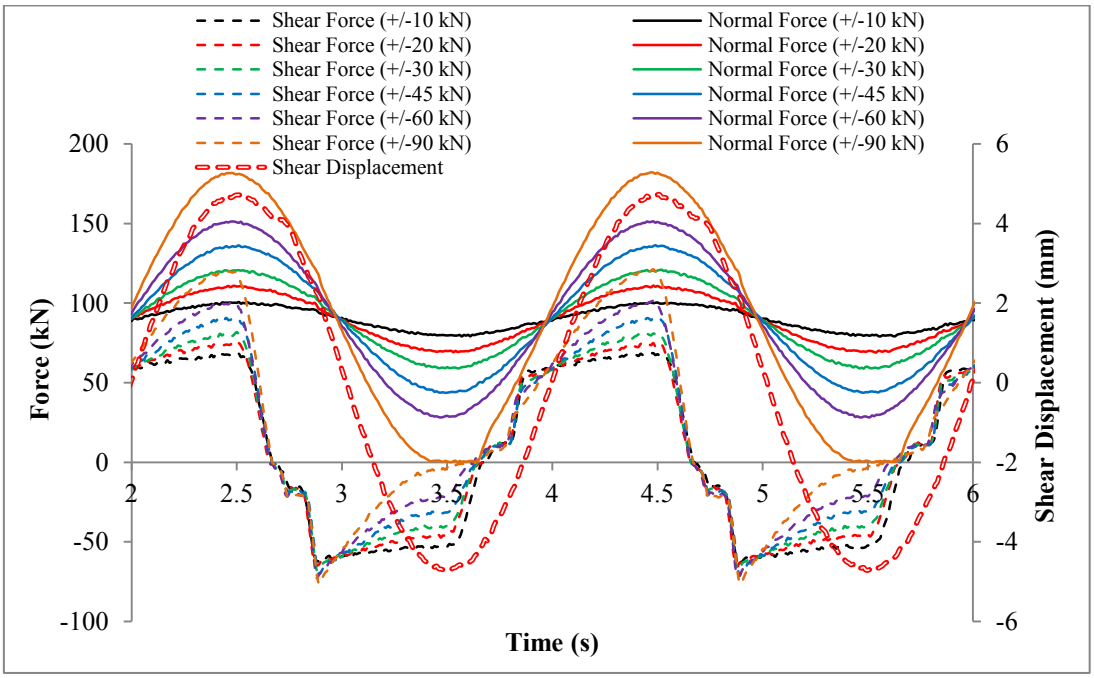

Figure 91. CDNL_9: Normal force, shear force and shear displacement vs. time under different superimposed normal load at horizontal frequency of 0.5 Hz, vertical frequency of 0.5 Hz and horizontal shear displacement of 5.0 mm.

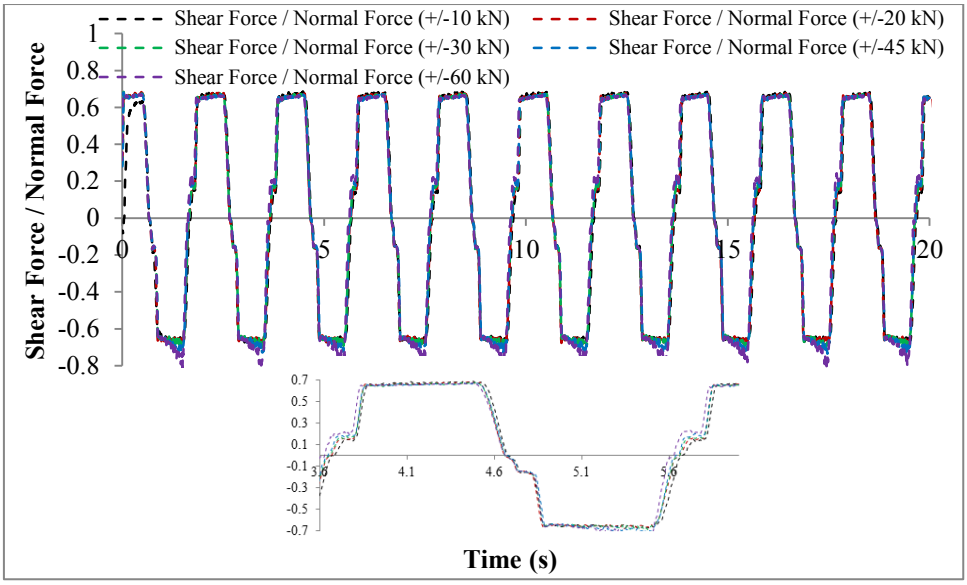

Figure 92. CDNL_9: Friction coefficient vs. time under different normal load and different superimposed dynamic load at horizontal frequency of 0.5 Hz, vertical frequency of 0.5 Hz and horizontal shear displacement of 5.0 mm.

Shear strength criterion

According to the above described test results, the evolution of the friction coefficients follows a square wave like form with nearly identical peak values. The period of the square wave is related to the horizontal shear frequency. Square waves can be synthesized by a number of sinusoidal waves using the Fourier transformation technology. Longer Fourier series lead to better approximation of the square waves (Figure 93). Therefore, the dynamic shear friction coefficient can be calculated from the following equation:

$$f(t) = ABS(k\sum_{n=0}^{n\max}(\frac{1}{2n+1}\sin((2n+1)t)))\text{.....}(n \in (0,1,2,3\ldots)) \quad (28)$$

where k is the maximum friction coefficient,

n is the number of Fourier series elements.

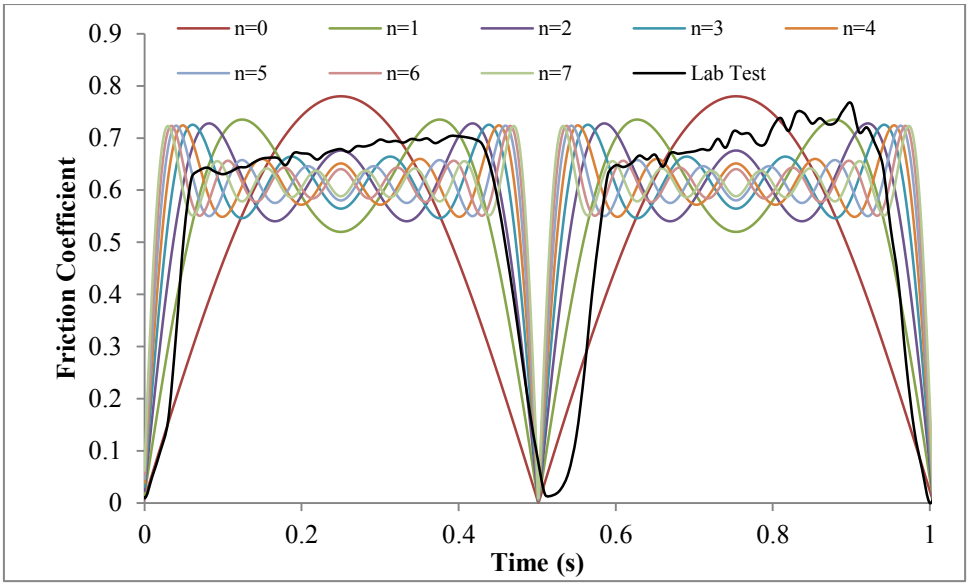

Figure 93. Synthesized friction coefficient compared with lab test results vs. time according to Eq. (28).

The normal stress can be calculated by Eq. (29):

$$\sigma_n = \frac{F_s + F_d \sin(2\pi f t)}{S} \tag{29}$$

Taking into account the above mentioned considerations and laboratory test results, the following expression for the shear strength is proposed for plane joints under sinusoidal DNL conditions:

$$\begin{aligned} \tau &= f(t)\sigma_n \\ &= ABS\left(k \sum_{n=0}^{n\max} \left(\frac{1}{2n+1}\sin((2n+1)t)\right)\right) \cdot \frac{F_s + F_d \sin(2\pi f t)}{S} \quad .....(n \in (0,1,2,3...)) \end{aligned} \tag{30}$$

where k is the maximum friction coefficient,

n is the number of the Fourier series elements.

Figure 94 shows a comparison between the derived shear strength criterion and the lab test results. The shear strength criterion is in close agreement with the measured values, which indicates that the novel shear strength criterion is able to predict the cyclic shear strength under DNL conditions.

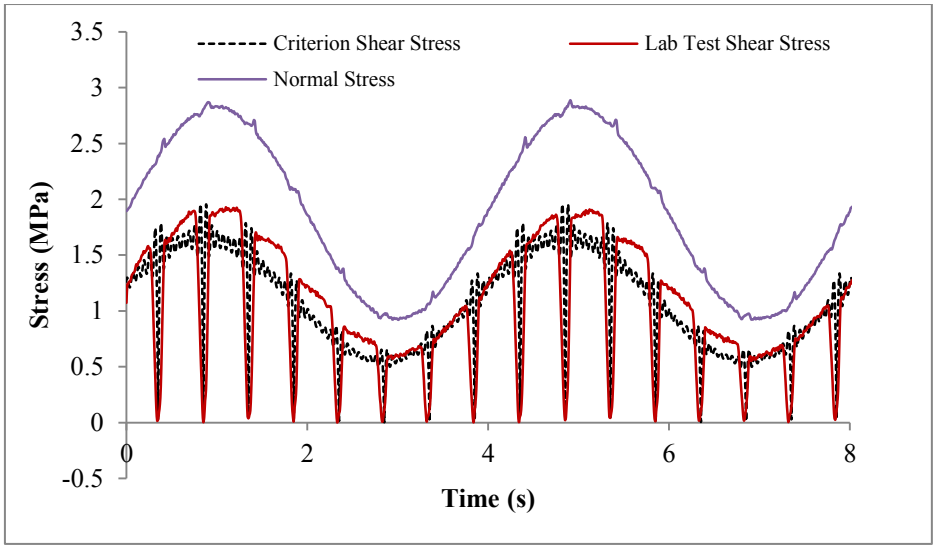

CNDL_5-1: f_h= *1.0 Hz* f_v=*0.25 Hz*

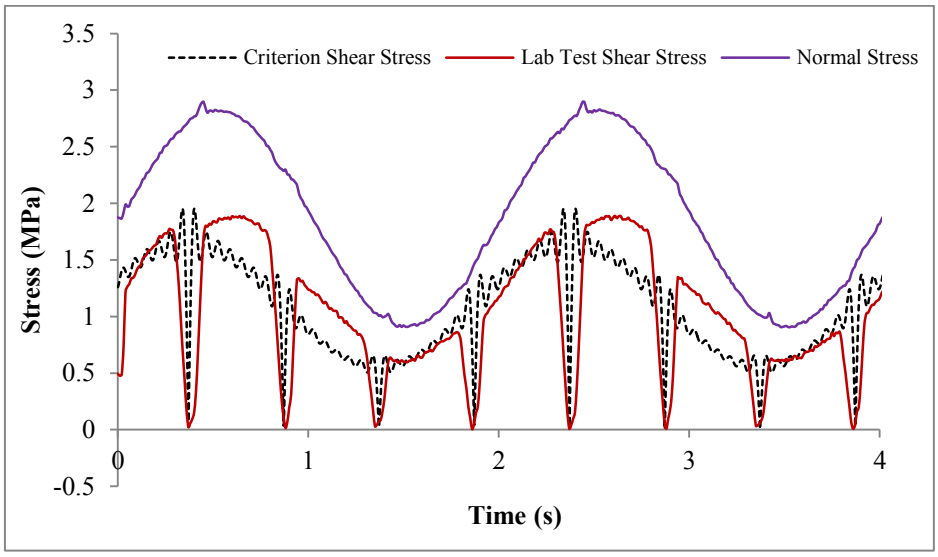

CNDL_5-2: f_h= *1.0 Hz* f_v=*0.5 Hz*

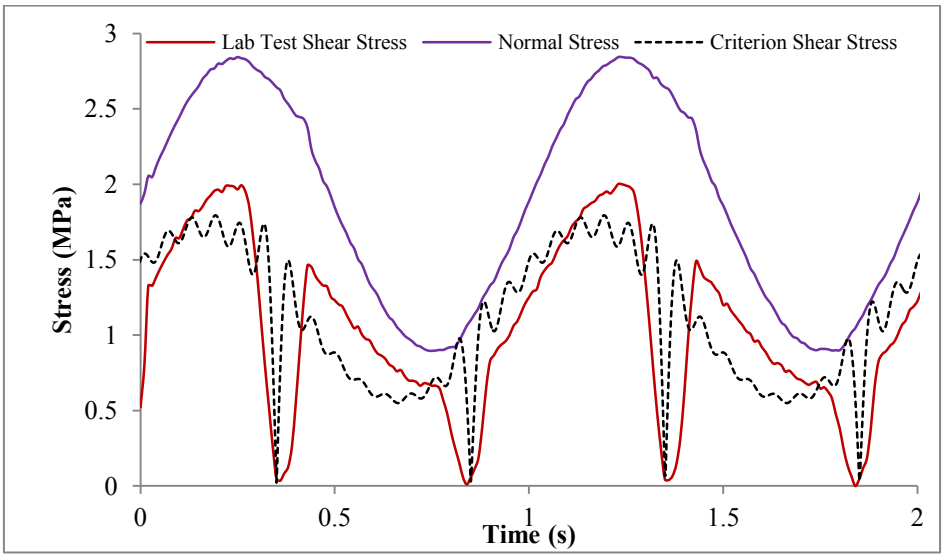

CNDL_5-3: f_h= *1.0 Hz* f_v=*1.0 Hz*

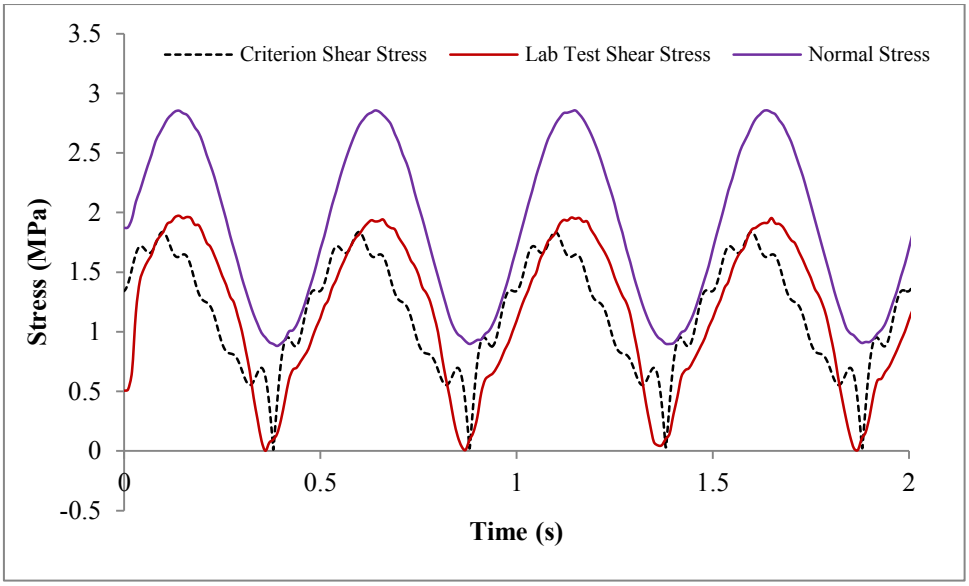

CNDL_5-4: f_h= *1.0 Hz* f_v=*2.0 Hz*

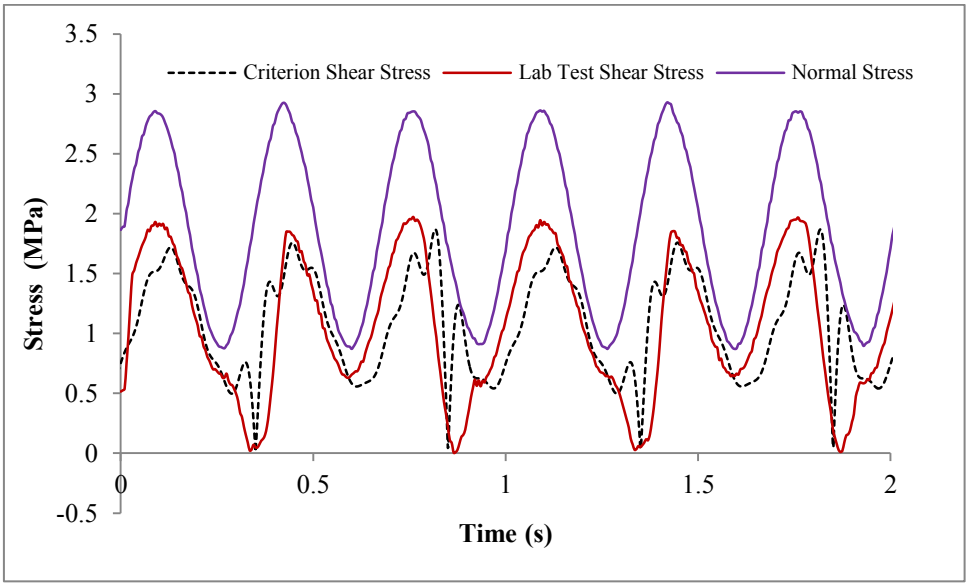

CNDL_5-5: f_h= *1.0 Hz* f_v=*3.0 Hz*

Figure 94. Normal stresses as well as predicted and measured shear stress vs. time (n=7).

6 Numerical simulations of the shear box device and lab shear tests

In this chapter, numerical modeling of the big shear box device GS-1000 itself and the joints under different boundary conditions are presented. Numerical simulation results obtained by using the numerical simulation tool FLAC^{3D} (Itasca, 2010) are compared with lab test data.

6.1 Numerical simulation of GS-1000 shear box device

Rock mechanical lab measurements do not only reflect the properties of rock, but contain, at least to some extent, the influence of the test equipment itself even if measurements are designed to minimize the influence of the test equipment. Therefore, a detailed numerical model of the test device itself including the specimen was built and evaluated.

As documented in Chapter 3 stresses and deformations of the sample itself are not measured directly. They can only be inferred from forces and displacements measured outside of the shear box. Exemplary, multistage direct shear tests of specimens with plane joint are used to demonstrate how numerical modeling of the whole test equipment can give significant additional information. A 3-dimensional numerical model of the shear box device including the sample was built and the laboratory tests were simulated. The numerical model comprises the loading frame, the hydraulic pistons, and the shear boxes along with the sample and considered also the measuring devices. The numerical model is able to reproduce the non-uniform stress distribution at the joint including sample rotation, which in turn produces unwanted frictional forces at the upper shear box. Consequently, only 91% ~ 94% of the applied and measured normal force really acts at the joint. Moreover, numerical simulations also show to what extend the different parts of the loading frame deform.

6.1.1 Model set-up and simulation procedure

The numerical model (Figure 95, Figure 96 and Figure 97) is restricted to those parts of the shear box device, which are essential to observe the interaction between machine and sample. Size and shape of the real device and the numerical model are identical. Figure 97 illustrates the numerical model, which consists of the following parts: horizontal and vertical frame, horizontal and vertical hydraulic cylinder, horizontal and vertical piston, loading plate, lower and upper shear boxes, lower and upper part of specimen.

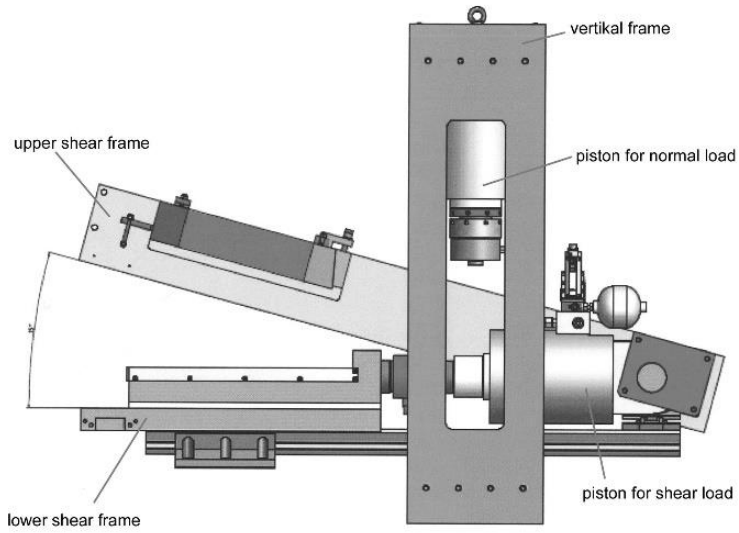

Figure 95. Main components of the shear box device.

Surface between upper and lower part of the specimen and the different components of the shear box device are modelled by interface elements. Interface elements are represented by a collection of triangular elements, each of which is defined by three nodes (interface nodes). Each interface element distributes its area to its nodes in a weighted fashion. Each interface node has an associated representative area. The entire interface was thus divided into active interface nodes representing the total area of the interface. The thickness of interfaces in FLAC^{3D} is zero. The constitutive behavior is given by Coulomb sliding and/or tensile and shear bonding. The properties associated with the interfaces are friction angle, cohesion, dilation angle, normal stiffness, shear stiffness, tensile and shear bond strength. The numerical model

consists of 162,117 grid points, 129,646 zones, 5,023 interface nodes and 9,520 interface elements.

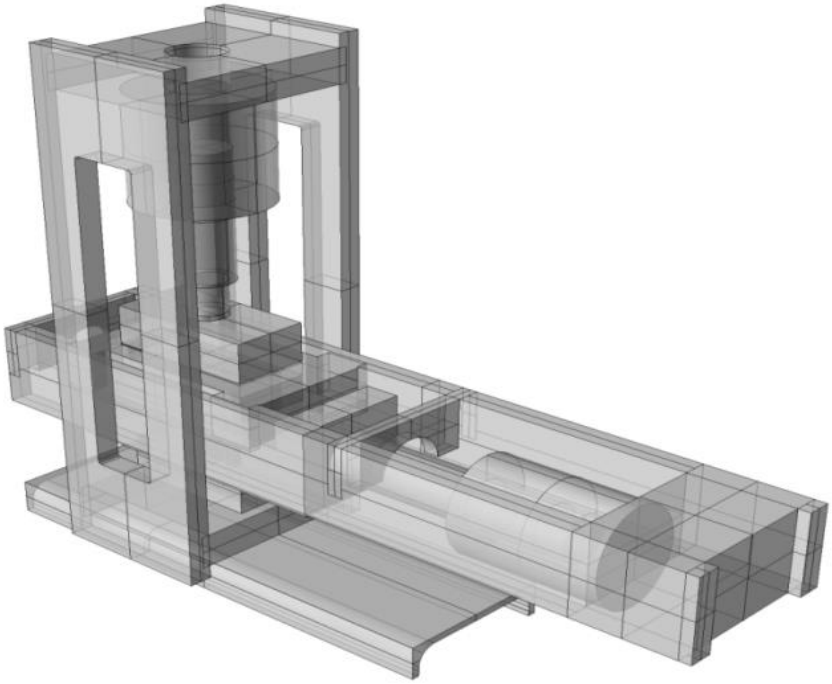

Figure 96. Simplified CAD model.

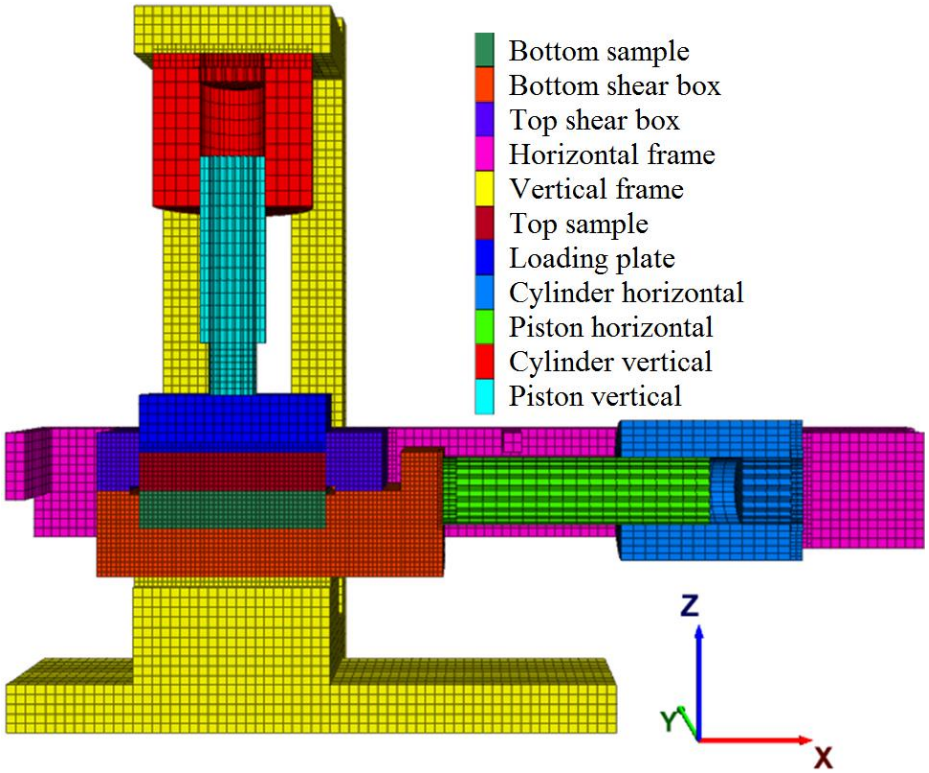

Figure 97. 3-dimensional model of GS-1000 shear box device.

Applied boundary conditions were chosen in such a way that they duplicate the conditions of the machine. Figure 99 shows the boundary conditions in the numerical model. The foundation is fixed in *X*, *Y* and *Z* directions; horizontal frame, horizontal cylinder and horizontal pistons are partly fixed in *Z* direction; a point fixation is set in the left central part of the horizontal frame (there is a pair of bolts to fix the horizontal frame inside the shear box device). Mohr-Coulomb matrix and joint constitutive models are chosen for the specimen and the interfaces, whereas an elastic constitutive model is chosen for the steel frame and the shear box elements. Several physical quantities (forces, stresses, displacements, deformations) including derived values were observed at selected observation points (histories). History locations and interfaces are shown in Figure 98. Also, the complete stress-deformation state is stored and analyzed at different points in time during the testing. Besides, the normal and shear stresses of different interfaces can be evaluated.

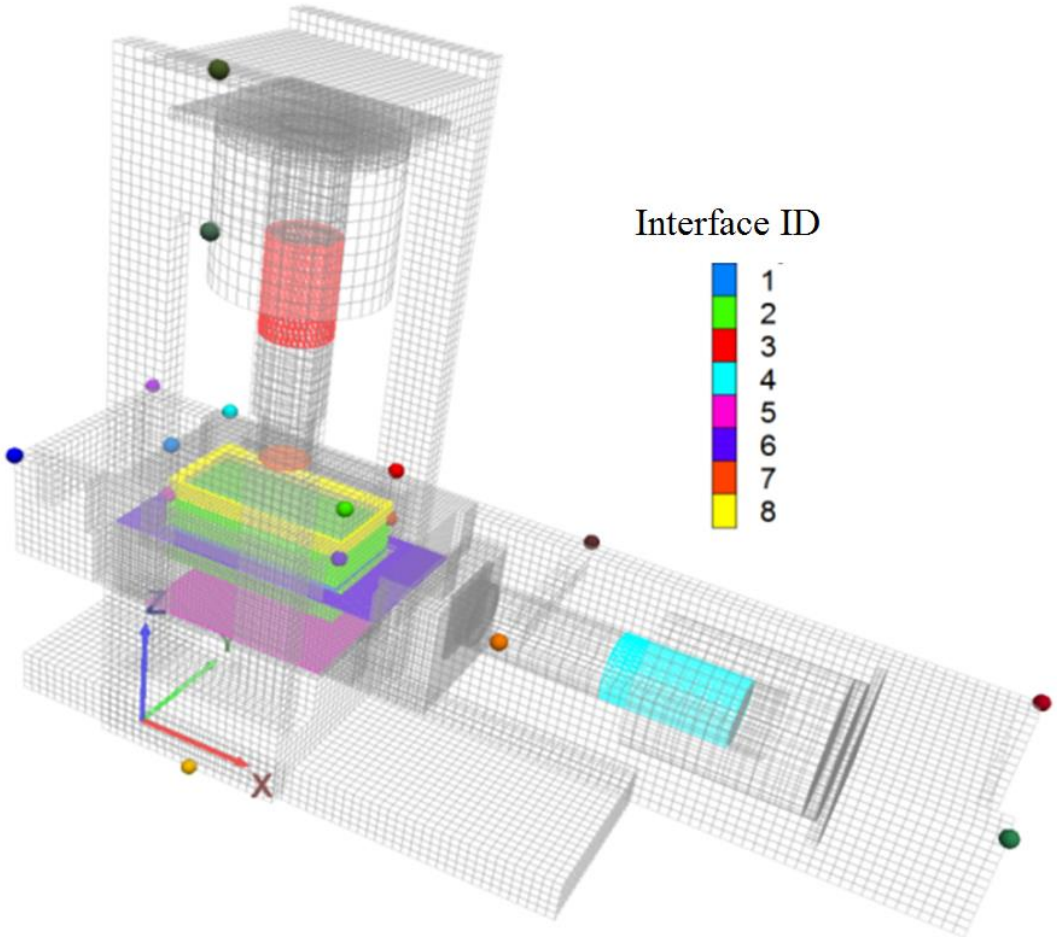

Figure 98. Interfaces and history locations.

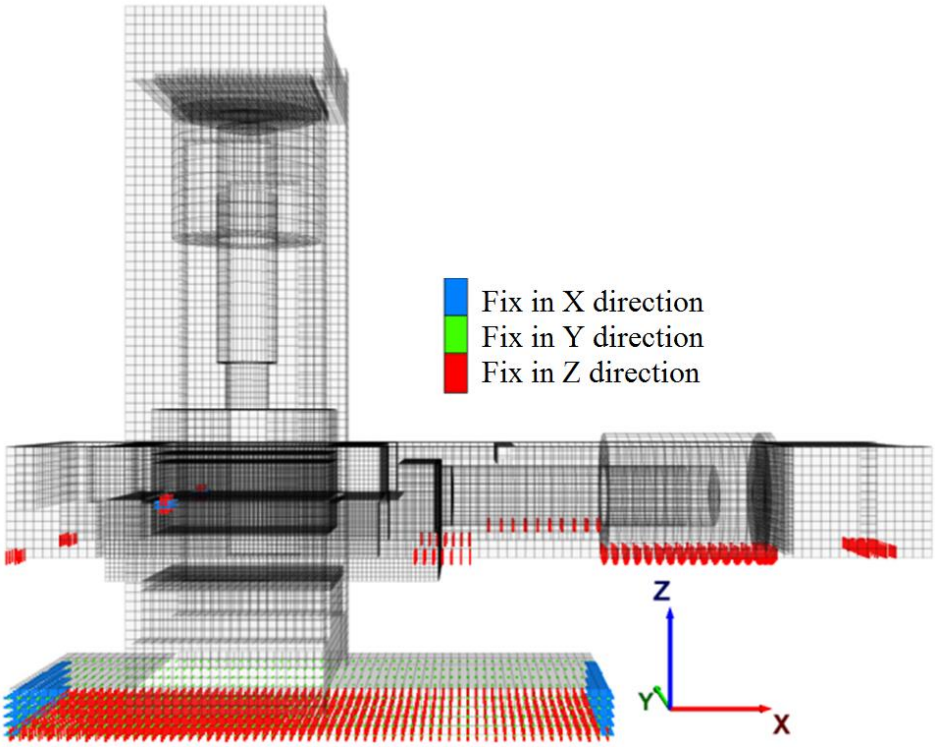

Figure 99. Boundary conditions.

Table 8. Parameters of interfaces.

ID	Kn (Pa/m)	Ks (Pa/m)	Friction (°)	Position
1	(0.4-6.2)e10	(0.4-6.2)e10	39.5	Between lower and upper part of specimens
2	2.1e12	2.1e12	2	Between specimen and shear box
3	3.15e14	3.15e14	0	Between piston and cylinder in the vertical direction
4	3.15e14	3.15e14	0	Between piston and cylinder in the horizontal direction
5	3.15e14	3.15e14	0	Between bottom shear box and vertical frame
6	2.1e14	2.1e14	0	Between upper shear box and bottom shear box
7	1.6e14	1.6e14	0	Between vertical piston and loading plate
8	2.1e14	2.1e14	2	Between loading plate and upper shear box

The simulation procedure duplicates the lab testing by the following steps:

- Running the model until equilibrium under gravity.
- Applying the constant normal forces in the vertical cylinder / piston.
- Applying a horizontal velocity to the horizontal piston. At the same time, the reacting force (force equilibrium via numerical servo-algorithm) is applied to the horizontal cylinder.

Table 9. Mechanical parameters.

Item	Tensile strength (MPa)	Compressive strength (MPa)	Young's modulus (GPa)	Poisson's ratio	Cohesion (MPa)	Friction angle (°)	Dilation angle (°)	Density (g/cm3)
Specimen	2.5	19.1	30	0.2	7.2	40	10	2.50
Shear box	-	-	200	0.33	-	-	-	7.85
Vertical frame	-	-	210	0.33	-	-	-	7.85
Horizontal frame	-	-	210	0.33	-	-	-	7.85
Loading plate	-	-	200	0.33	-	-	-	7.85
Piston	-	-	215	0.33	-	-	-	7.85
Cylinder	-	-	200	0.33	-	-	-	7.85

6.1.2 Simulation results

Numerical simulation results are shown in Figure 100, Figure 101, Figure 102, Figure 103, Figure 104, Figure 105, Figure 106, Figure 107 and Figure 108. Vertical and horizontal frames deform as shown in Figure 100 and Figure 101. Vertical frame, vertical piston and vertical cylinder incline and the inclination increases with increasing shear stress. However, even under large normal and shear forces (Figure 102 and Figure 103), the deformation of the shear box device is small (under normal load of 450 kN the maximum elongation of the device is only about 0.1 mm). This proves that the stiffness of the frame is sufficient to perform tests under large normal and shear forces. Largest strain increments are located at the inside top corner of the vertical frame and at the middle part of the horizontal frame (Figure 104).

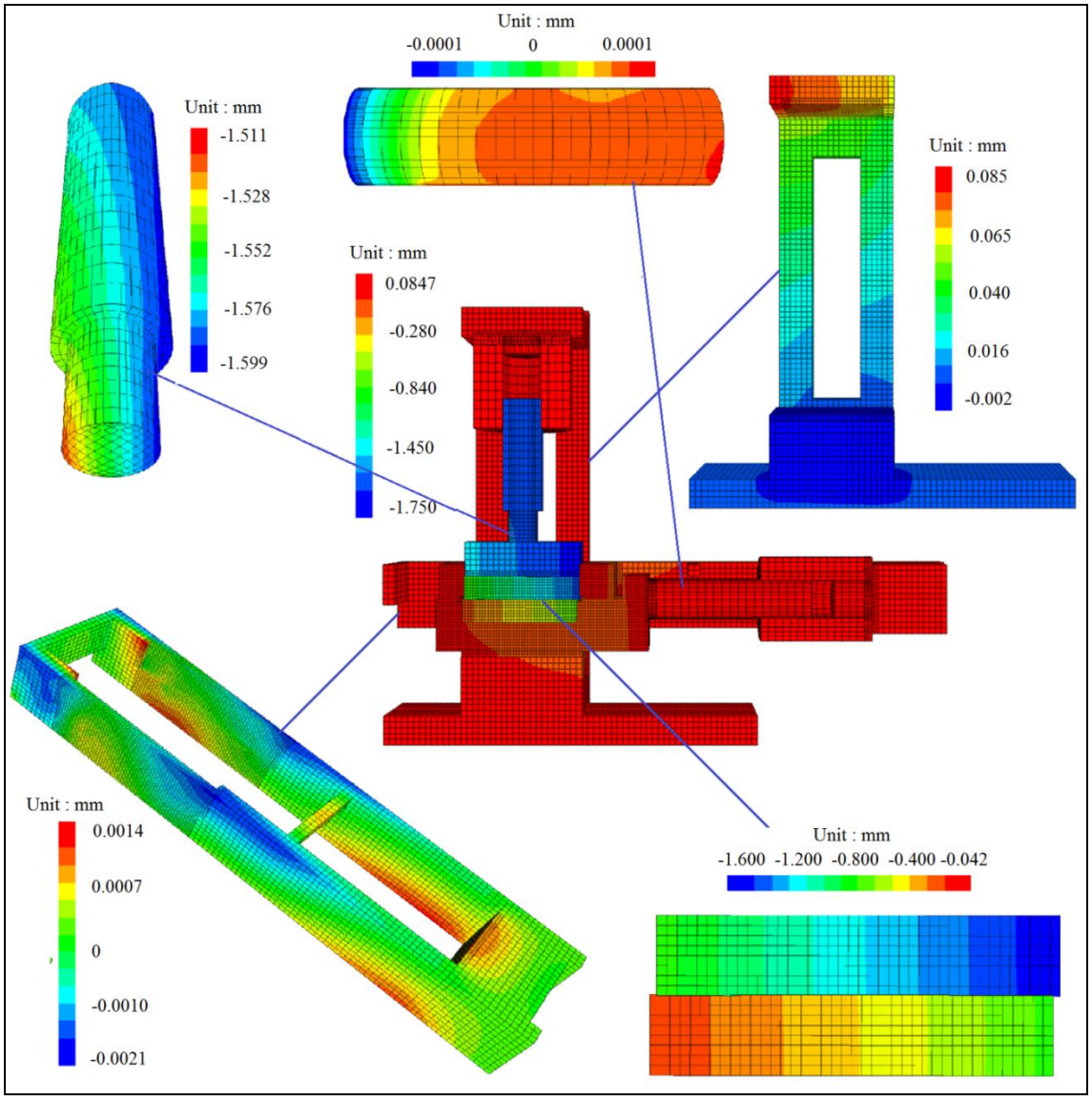

Figure 100. Contours of Z-Displacement under normal stress of 1.875 MPa and horizontal shear displacement of 1.0 cm.

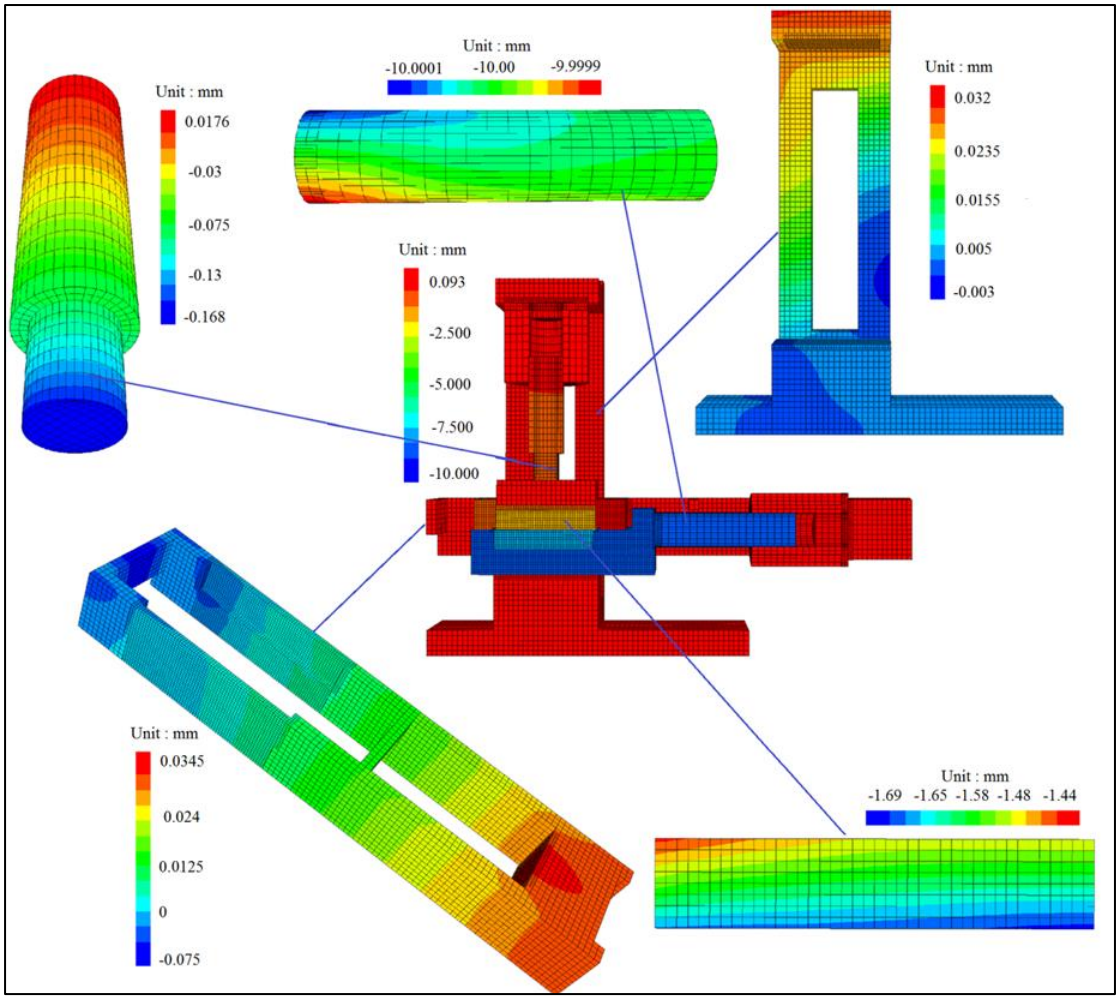

Figure 101. Contours of X-Displacement under normal stress of 1.875 MPa and shear displacement of 1.0 cm.

Like measured during the lab tests, the loading plate and the top specimen experience rotation during shearing connected with inhomogeneous stress pattern of the interface (Figure 104). A defined gradient develops along the interface with minimum shear stress of 0 MPa at one end and 2.09 MPa at the other end of the interface. Average normal stress defined as mean force divided by the total area of the shear plane is $\sigma_{N,AVG} = 1.875 \sim 2.009$ MPa, depending on the actual shear displacement. However, as expected the average normal stress considering the whole joint surface equals to the applied normal load. For example, Figure 105 illustrates the actual stress distribution at the joint. The high stress at the right side of the specimen leads to serious damage of the surface. Figure 106 and Figure 107 show that the numerical simulation results agree well with laboratory testing results. Peak angles of inclination of the specimen increase with increase of normal stresses.

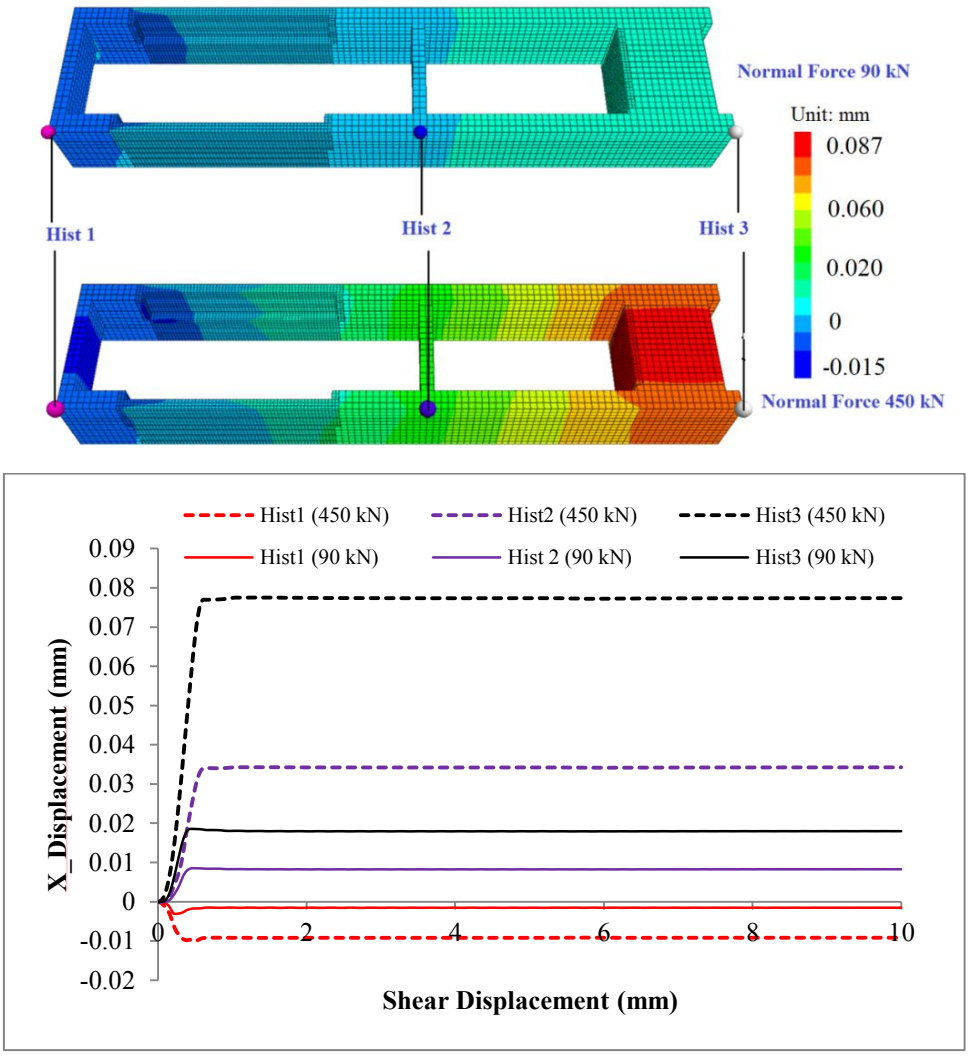

Figure 102. Contours of X-Displacement under different normal loads and X-Displacement vs. shear displacement of sample.

The rotation (tilting) of the loading plate causes additional friction. Unwanted high local friction force (Figure 108) appears in the contact area between loading plate and upper shear box frame. As a consequence, the complete applied normal force (applied force is measured by load cells) is not acting at the specimen (Figure 109 and Figure 110). With the increase of normal stress, the rotation increases as well as the corresponding normal force loss (Figure 109). This loss of force can reach nearly 10 % and should be for instance included in the calculation of the friction angle of the joint surface (Figure 110).

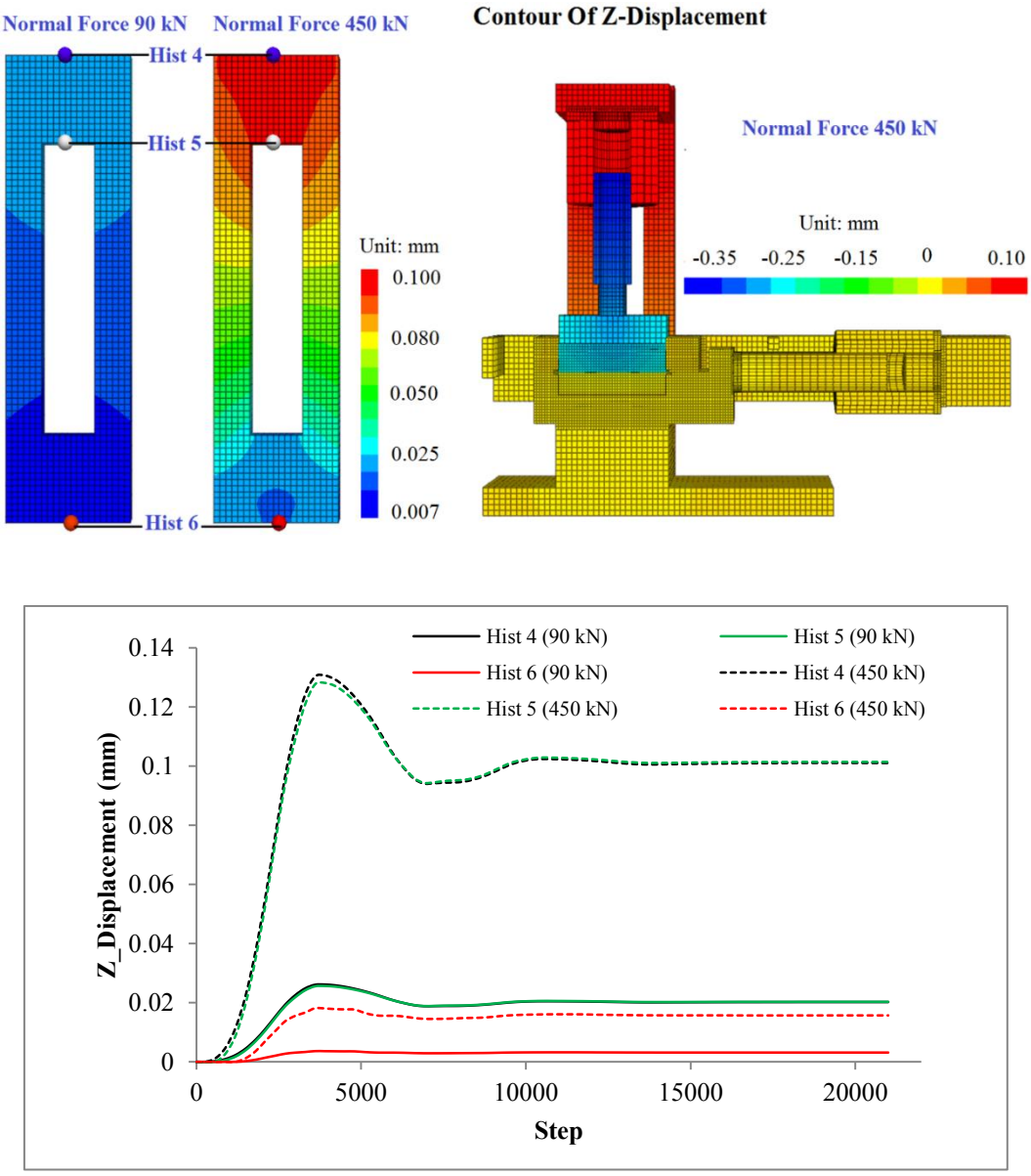

Figure 103. Contours of Z-Displacement under different normal loads and Z-Displacement vs. numerical calculation steps.

The combined evaluation of lab tests and in parallel conducted numerical simulations considering the complete test set-up and test-procedure can help to get missing information and will increase quality of parameters deduced from lab test results.

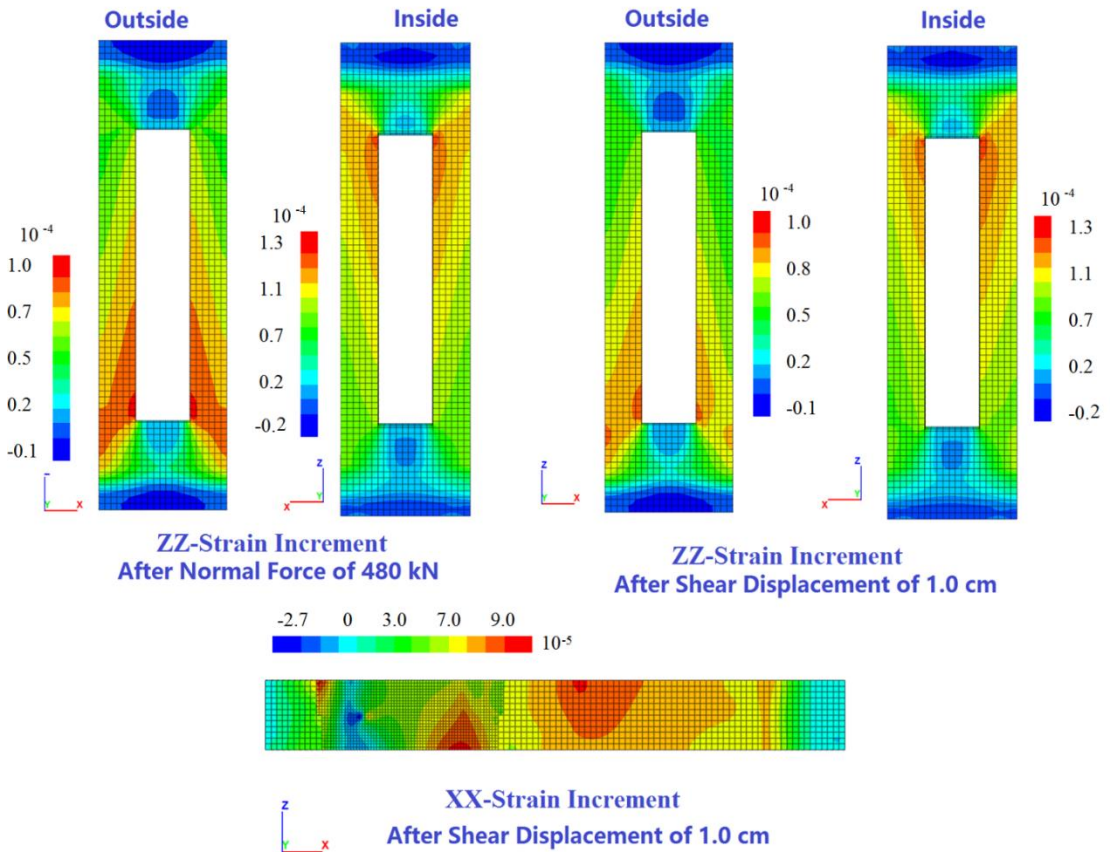

Figure 104. Contour of strain increment of the vertical and horizontal frames.

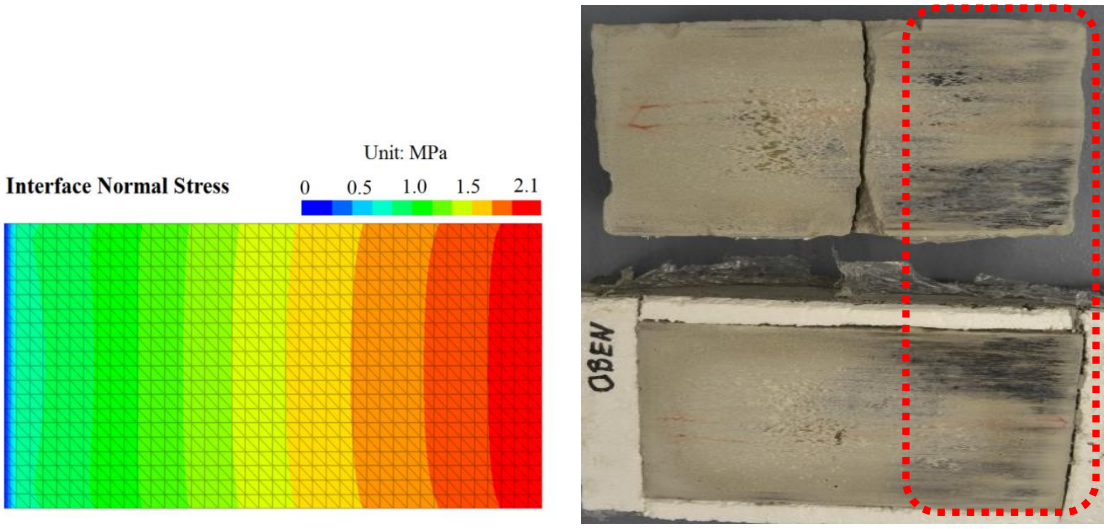

Figure 105. Interface (ID: 1) normal stress contour under normal stress of 1.875 MPa at shear displacement of 1.0 cm and corresponding lab photo.

The numerical model has delivered the following additional information: (i) Quantitative value for deformations including misalignment of loading frame and piston as function of applied forces, (ii) detailed inhomogeneous stress distribution

along the joint as function of loading and shear displacement, (iii) determination of sample rotation and inclination of vertical loading piston, and (iv) quantitative proof of sufficient system stiffness. In addition, the numerical model can be used to modify or enhance components of the device (developing tool).

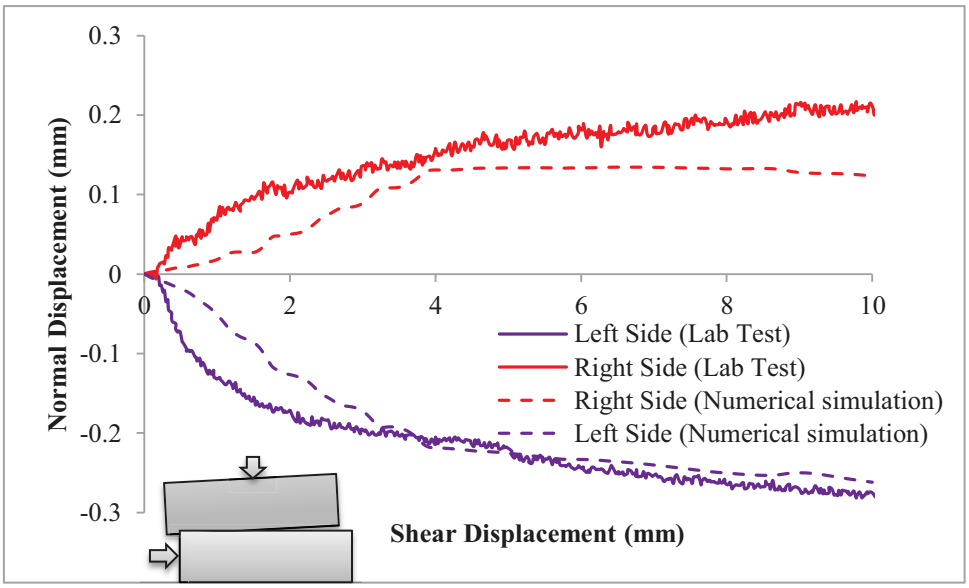

Figure 106. Normal displacement vs. shear displacement under normal stress of 1.875 MPa.

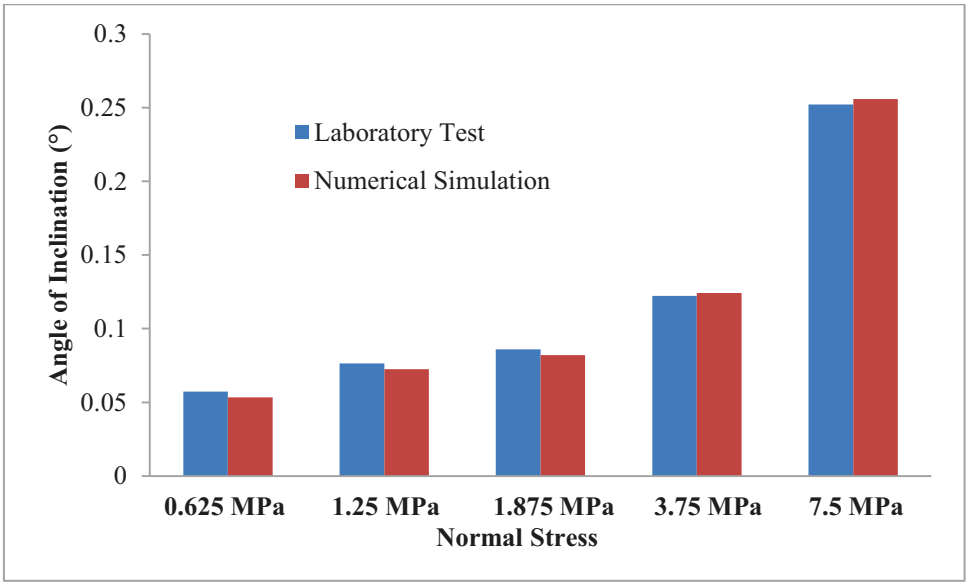

Figure 107. Angle of inclination under different normal stresses and the shear displacement of 1.0 cm.

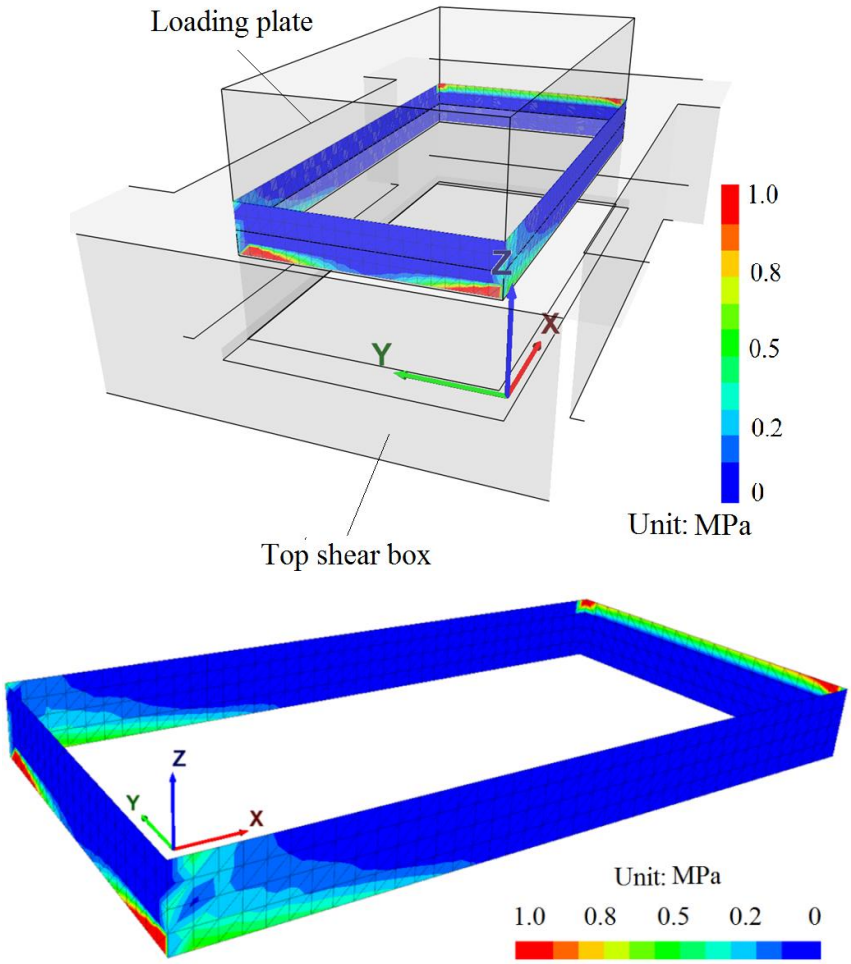

Figure 108. Interface (ID: 8) shear stress contour under normal stress of 1.875 MPa and shear displacement of 1.0 cm.

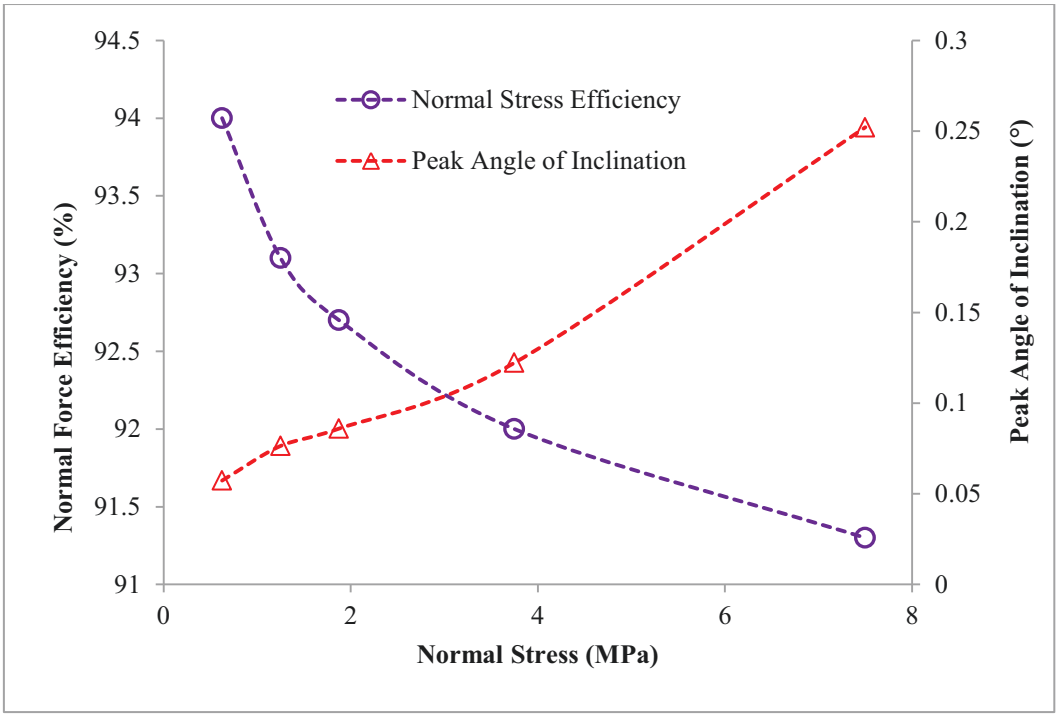

Figure 109. Normal force efficiency (percentage of measured normal stress actual acting on the joint) and peak angle of inclination under different normal stress.

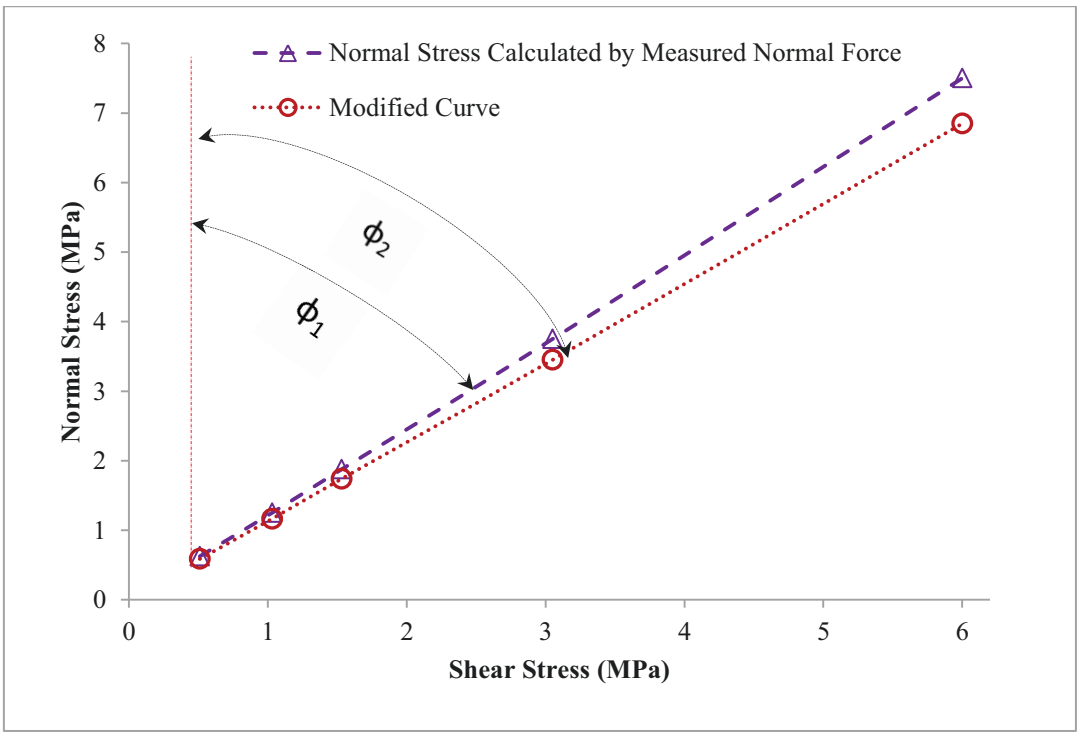

Figure 110. Peak shear stress vs. normal stress.

6.2 Numerical simulations of CNL shear tests

6.2.1 Direct shear test simulations

6.2.1.1 Model set-up

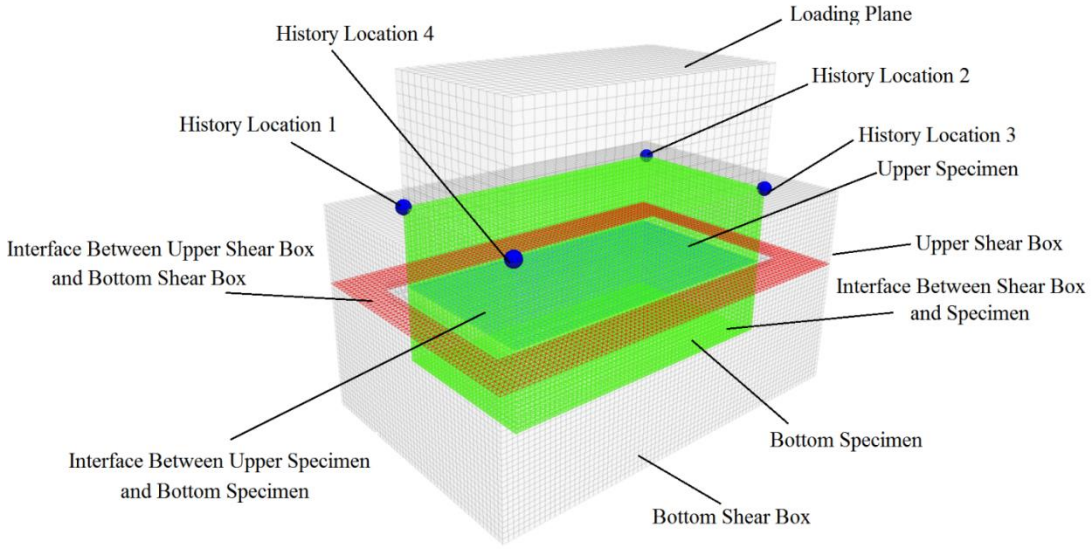

Figure 111. General model set-up used for simulating the direct shear test in FLAC^{3D}.

Table 10. Parameters of the interface.

ID	Kn (Pa/m)	Ks (Pa/m)	Friction (°)	Position
1	3.0e10	3.0e10	0-30	Between sample and shear box
2	6.0e10	6.0e10	0-30	Between bottom shear box and top shear box
3	(0.4-6.2)e10	(0.4-6.2)e10	39.5	Between bottom and top samples

The whole model consists of several parts (Figure 111): Loading plate, lower shear box, upper shear box, lower and upper part of specimen and corresponding interfaces. The size and shape as well as initial and boundary conditions are identical to that of the lab tests. The numerical model consists of 202,568 grid points, 179,184 zones, 16,222 interface nodes and 27,776 interface elements. Normal force is applied on top of the loading plate. The top shear box is fixed in *X* and *Y* direction. Shear velocity is applied to the lower shear box. A Mohr-Coulomb constitutive model is chosen for the specimen and interfaces. An elastic constitutive model is chosen for the shear box. Mechanical parameters are shown in Table 10. Normal displacements at the four corners of the upper part of the specimen and the normal and shear stresses at the joint (sample interface) are recorded. These simulations are called Model O.

6.2.1.2 Simulation results

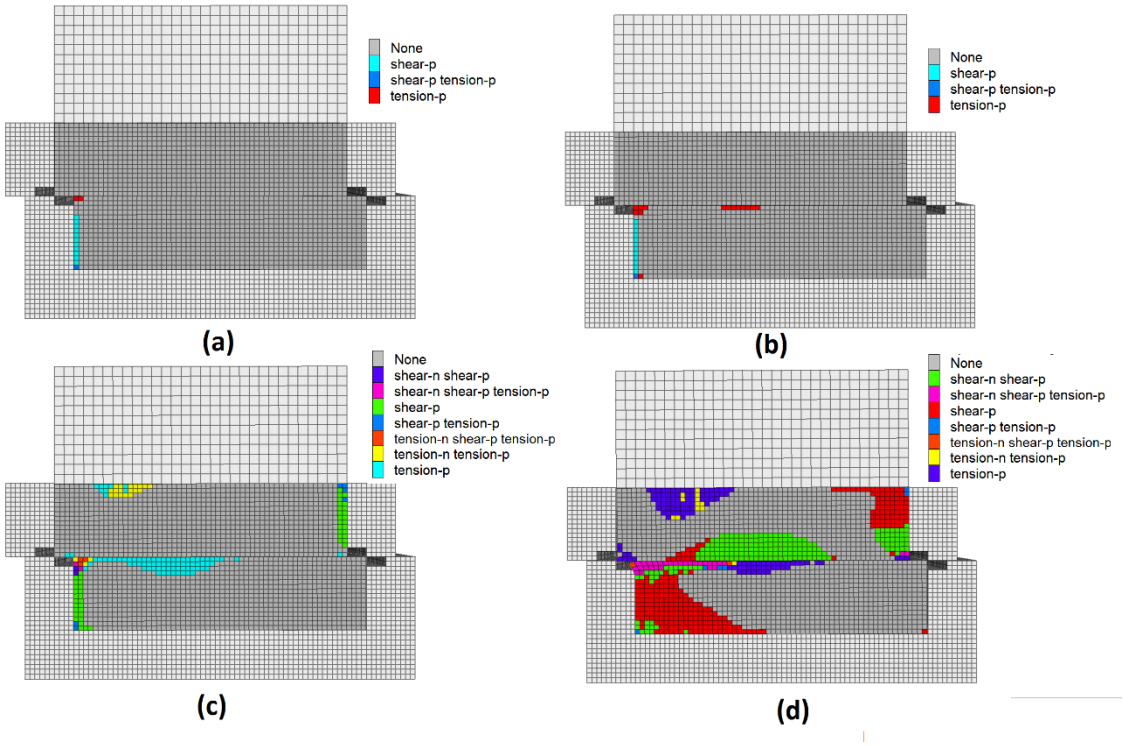

Figure 112. Plasticity state under different normal loads and shear displacement of 2.0 cm: (a) 30 kN, (b) 60 kN, (c) 180 kN and (d) 360 kN (n: actual at failure, p: failure in past).

Numerical simulation results are shown in Figure 112, Figure 113, Figure 114, Figure 115 and Figure 116. Figure 112 shows the plasticity state during shearing. The higher stresses at the left side of the specimen lead to partial failure of the rock matrix. At 2.0 cm of shear displacement and normal load of 30 kN (Figure 112 (a)), only a few zones show shear plasticity in the left edge of the bottom part and there are some zones which experience tension plasticity in the left edge at the contact surface of the bottom sample. When the normal force reaches to 60 kN (Figure 112 (b)), plasticity in tension appears in the middle part of the contact surface of the bottom part. Under the normal force of 180 kN (Figure 112 (c)), the top part of the sample starts to break, shear plasticity appears in the right side and tension plasticity occurs on the top surface in the right side. The area of the zones plastified in tension in the contact surface increases. When the normal force is 360 kN (Figure 112 (d)), the broken area increases profoundly and the contact surface of the top part experience failure in tension. In total, the numbers of plastified zones increase with increasing

normal load. The plastified zones are mainly located in the left edge of the bottom sample (shear failure), in the contact surface (tension failure) and in the right side of the top sample (shear failure).

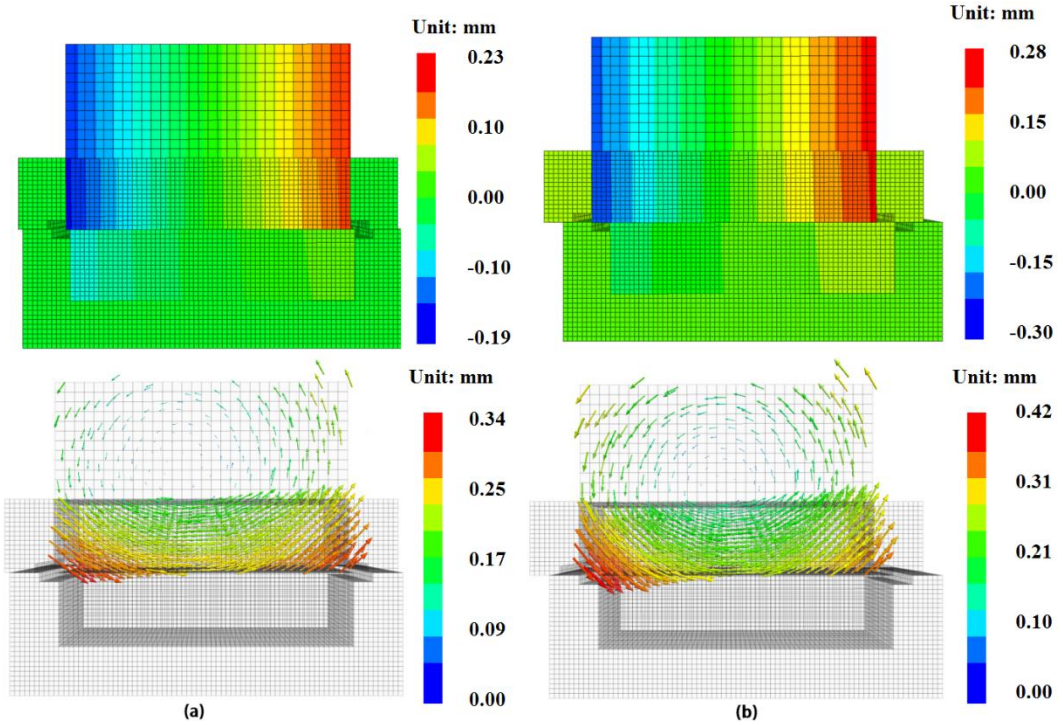

Figure 113. Contours of the vertical displacement and displacement vectors under normal force of 90kN and different shear displacements: (a) 0.5 cm and (b) 2.0cm.

The normal displacement contours (Figure 113) show that the left side of the simulation model goes down and the right side goes up. And the absolute value of the settlement (0.3 mm) in the left side is bigger than the heave (0.28 mm) in the right side Figure 113 (b). It reflects that the upper part of the model has the inclination behavior during shearing. The displacement vectors of the loading plate in the model have an intuitive feeling of the anti-clockwise rotation during shearing, and the rotation center was moving from the central part to the right bottom part (shear direction side). With the increase of shear displacement, the amount of movement gets bigger and bigger, i.e., the rotation became even more pronounced (when the shear displacement was 0.5 cm the maximum displacement is 0.34 mm, it reaches 0.42 mm when the shear displacement is 2.0 cm). The simulation results agree with the explanations of the laboratory tests results in Figure 114 and Figure 115.

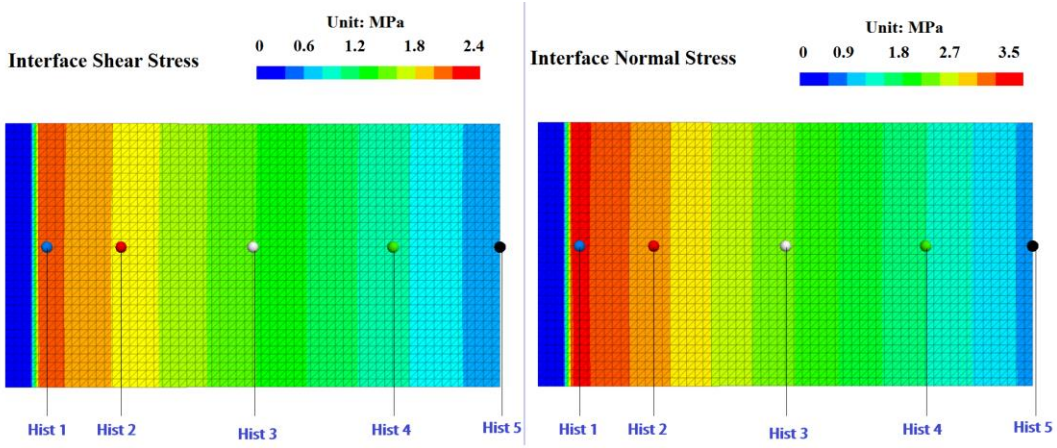

Figure 114. Model O: Contours of shear and normal stresses for shear test under normal load of 90 kN and shear displacement of 2.0 cm.

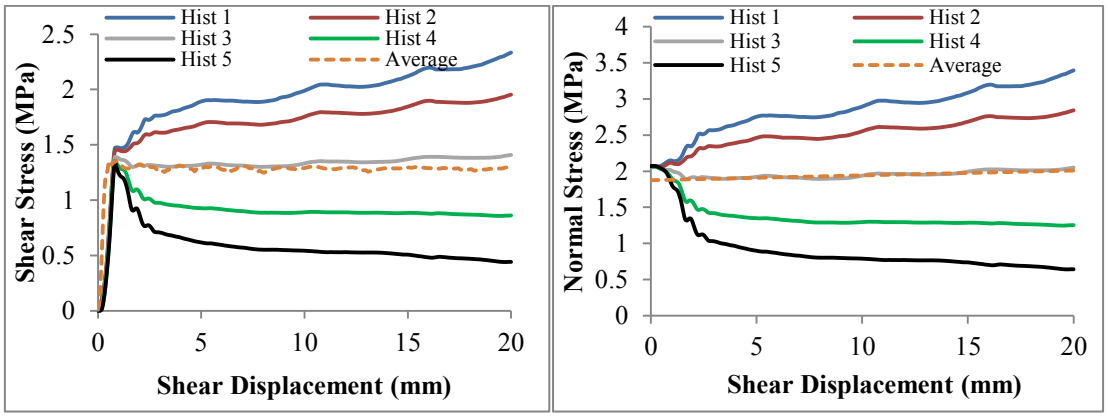

Figure 115. Shear and normal stresses at different observation points according to Fig.114 vs. shear displacement under normal load of 90 kN.

As Figure 114 shows, a very inhomogeneous stress pattern with a distinct gradient develops along the interface with minimum shear stress of 0.5 MPa at one end and over 2.4 MPa at the other end of the joint. The average normal stress defined as the mean normal force divided by the total area of the shear plane is $\sigma_{N,AVG} = 1.875 \sim 2.009\,MPa$ $\sigma_{N,AVG} = (1.875\text{-}2.009)\text{MPa}$. In the same manner as observed in the lab tests, shear stress increases with increasing shear displacement until a peak value is reached. Afterwards shear and normal stresses show non-linear increase or decrease depending on the location (Figure 115). Only the central part shows a more or less constant value. However, as expected the average normal stress considering the whole joint surface equals to the applied normal load.

As Figure 117 and Figure 118 show that, the assumption of constant normal stiffness will not lead to agreement with measured sample inclination for different normal stresses. Only an increase of normal stiffness with increasing normal loads leads to satisfying agreement. A corresponding fitting equation was deduced for the relation between normal load and normal stiffness:

$$K_n = 3E\text{-}06F^2 + 0.1754F - 1.5162 \ (R^2 = 0.9994) \quad (32)$$

where: K_n is normal stiffness,

F is normal force.

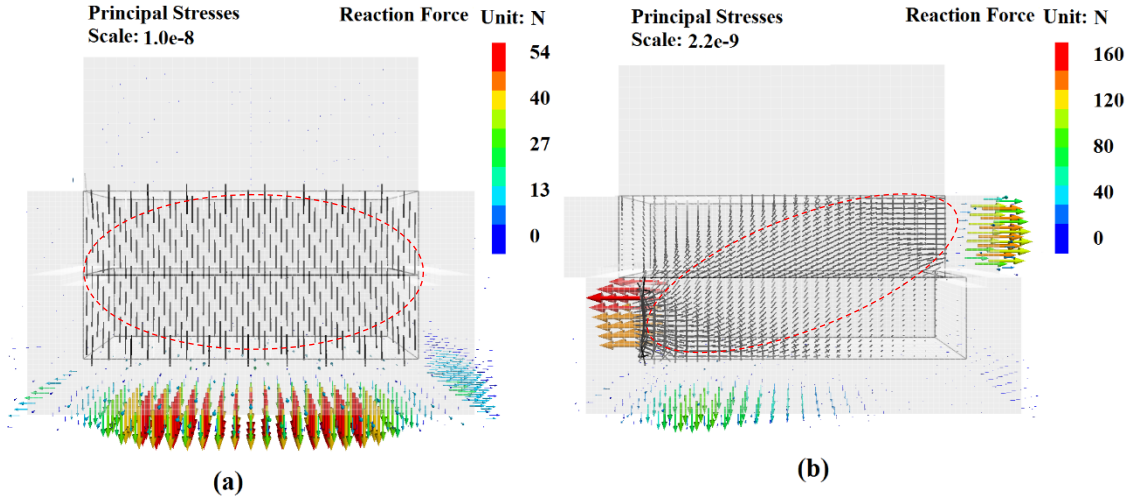

Figure 116. Reaction forces and principal stress: (a) at equilibrium under normal load but before shearing and (b) at shear displacement of 2.0 cm.

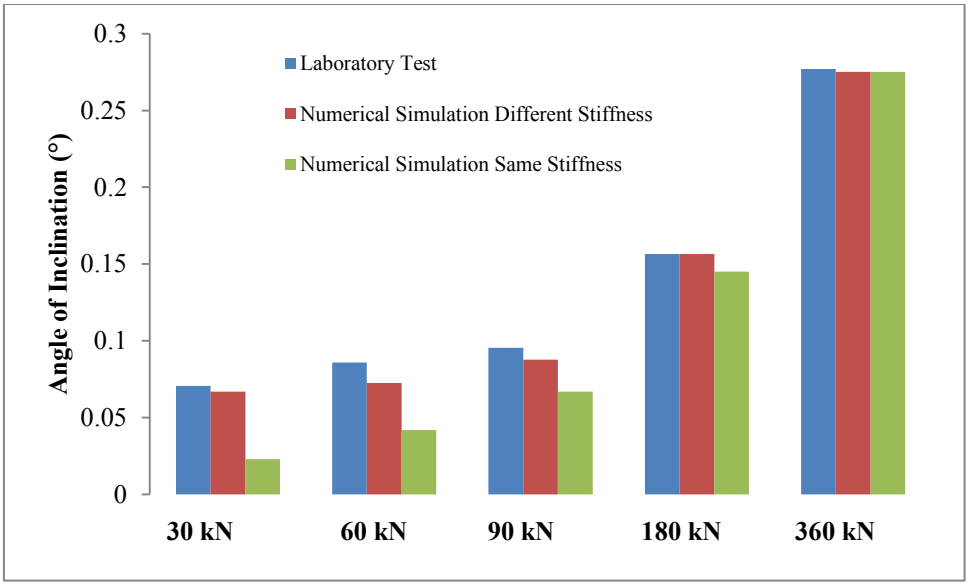

Figure 117 Angle of inclination under different normal loads at the shear displacement of 2.0 cm.

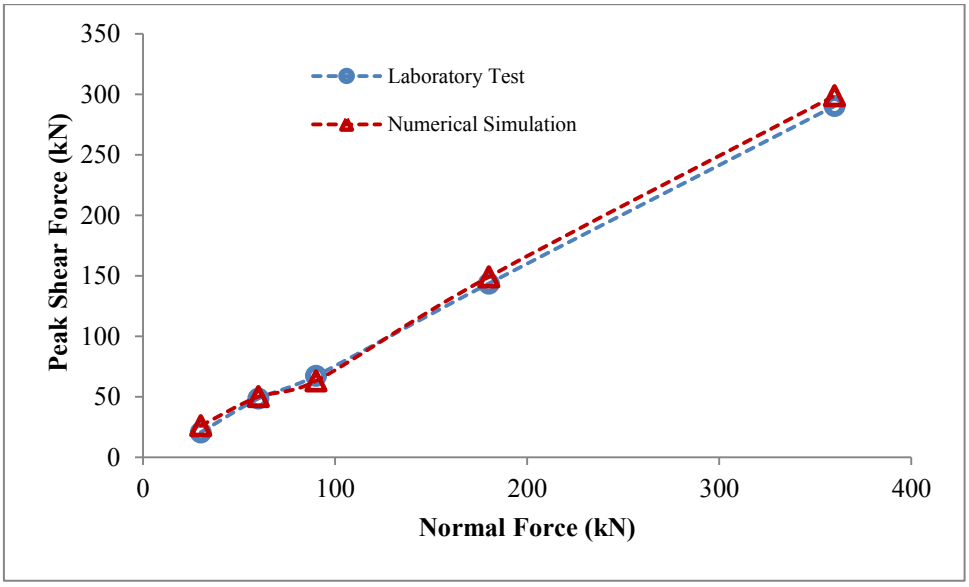

Figure 118. Peak shear forces versus normal forces.

The final calibrated numerical model shows satisfying agreement between peak shear forces for different normal loading (Figure 118).

6.2.2 Cyclic shear tests simulation

6.2.2.1 Model set-up

For the simulation of the cyclic shear tests, the dynamic module of FLAC^{3D} is activated. Therefore all quantities are related to real time. Damping is neglect. The mesh is optimized to save computational time (coarser mesh), but all model parts like loading plate, lower and upper shear box, lower and upper part of specimen and corresponding interfaces are included in the same way as for the simulations of the static tests. The numerical model consists of 34,403 grid points, 27,600 zones, 3,417 interface nodes and 6,312 interface elements. Normal force is applied on the loading plate, the top shear box is fixed in *X* and *Y* direction, and the cyclic shear velocity is applied to the lower shear box. A Mohr-Coulomb constitutive model is chosen for the specimen and interfaces and an elastic constitutive model is chosen for the shear box.

6.2.2.2 Simulation results

Numerical simulation results are shown in Figure 119, Figure 120, Figure 121, Figure 122, Figure 123 and Figure 124. Figure 119 shows the plasticity state of the samples under normal load of 90 kN, shear displacement amplitude of 5.0 mm and shear displacement frequency of 1.0 Hz for different points in time. The horizontal cyclic movement leads to progressive plastifications. After 0.25 seconds, only a few zones show failure in tension in the right side of the contact area. After 0.75 seconds however, plasticity occurs also on the left side of the contact area. This indicates progressive joint surface degradation with increasing numbers of cycles.

Normal displacement contours and displacement vectors (Figure 120**)** indicate that the upper part of the specimen and the loading plate move in a different manner. At 0.25 seconds, left side of the sample moves downwards and right side moves upwards (anti-clockwise rotation). However, at 0.75 seconds, left side of the sample moves upwards and right side moves downwards (clockwise rotation). During each cycle, rotations reverse. The simulation results agree well with the lab measurements presented in Chapter 5.

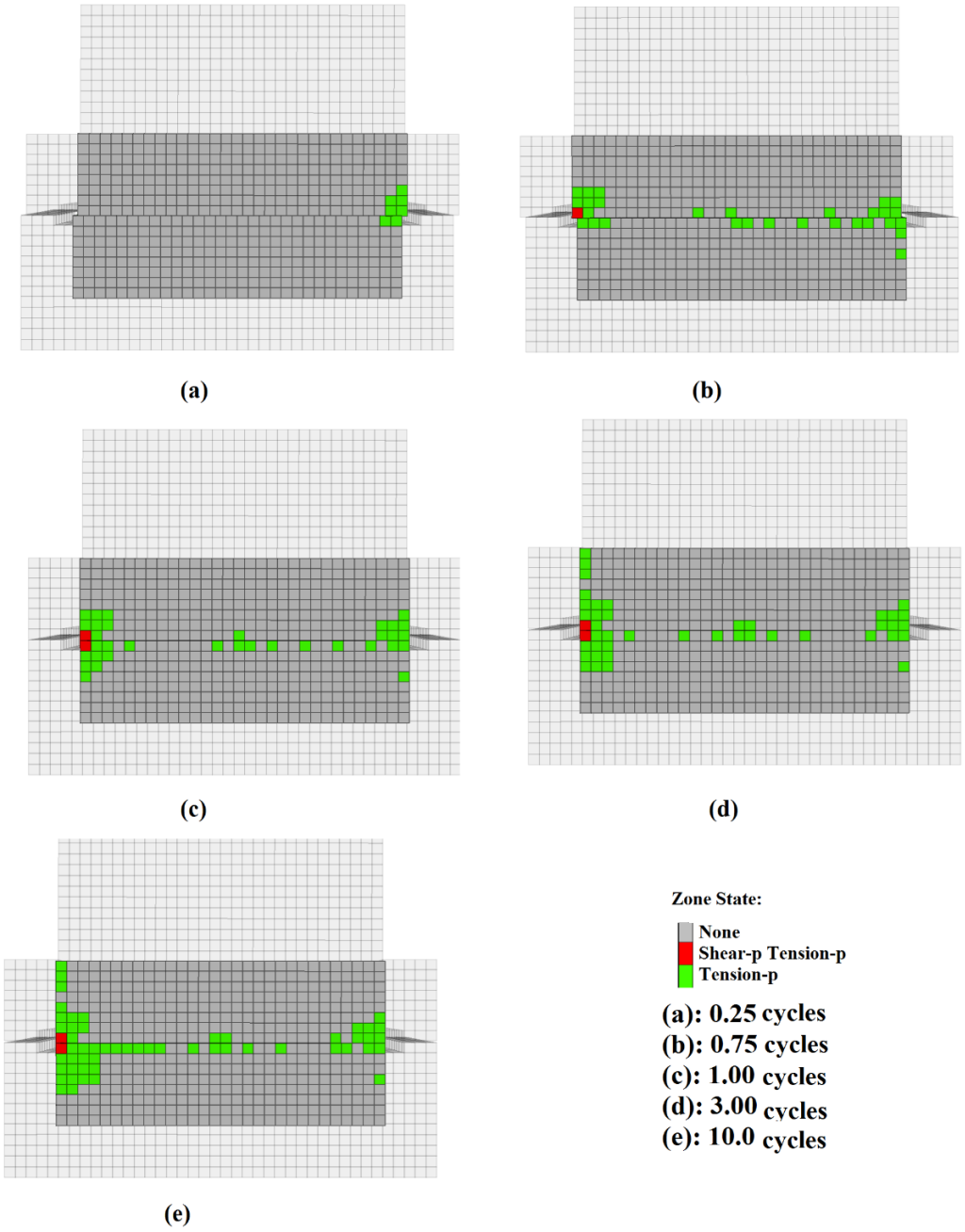

Figure 119. Plasticity state under normal load of 90 kN, shear displacement amplitude of 5.0 mm and frequency of 1.0 Hz.

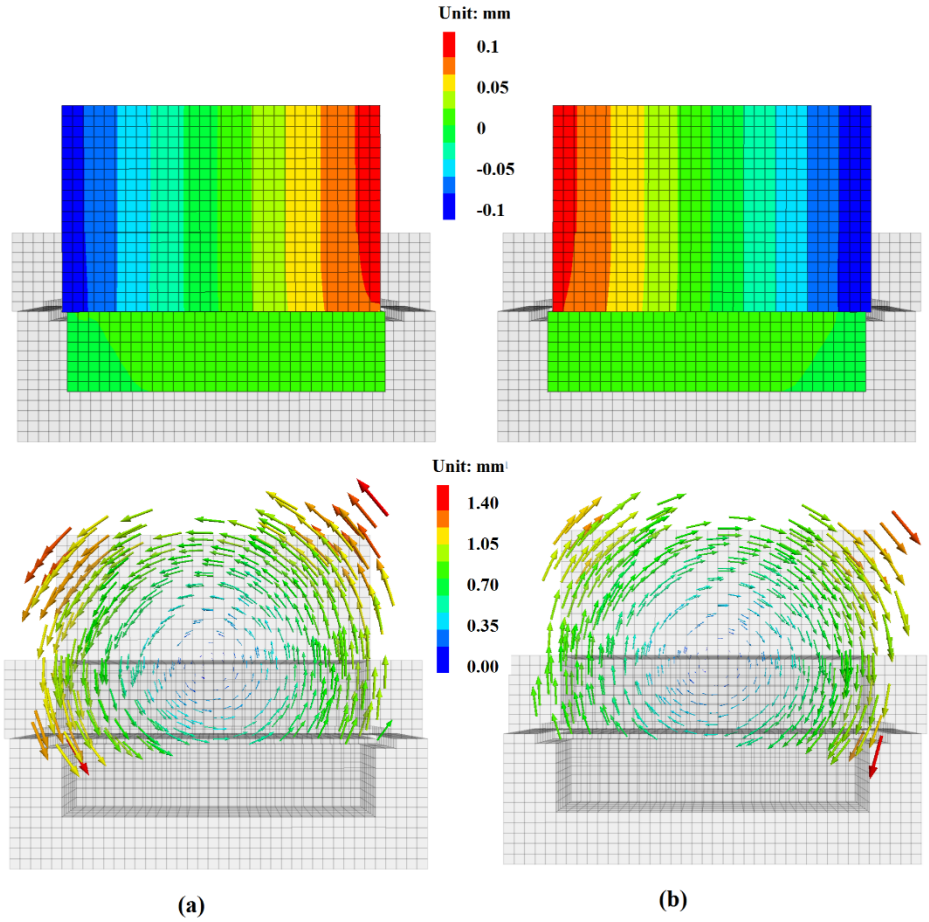

Figure 120. Normal displacement contours and displacement vectors at different positions and frequency of 1.0 Hz: (a) after 0.25 sec and (b) after 0.75 sec.

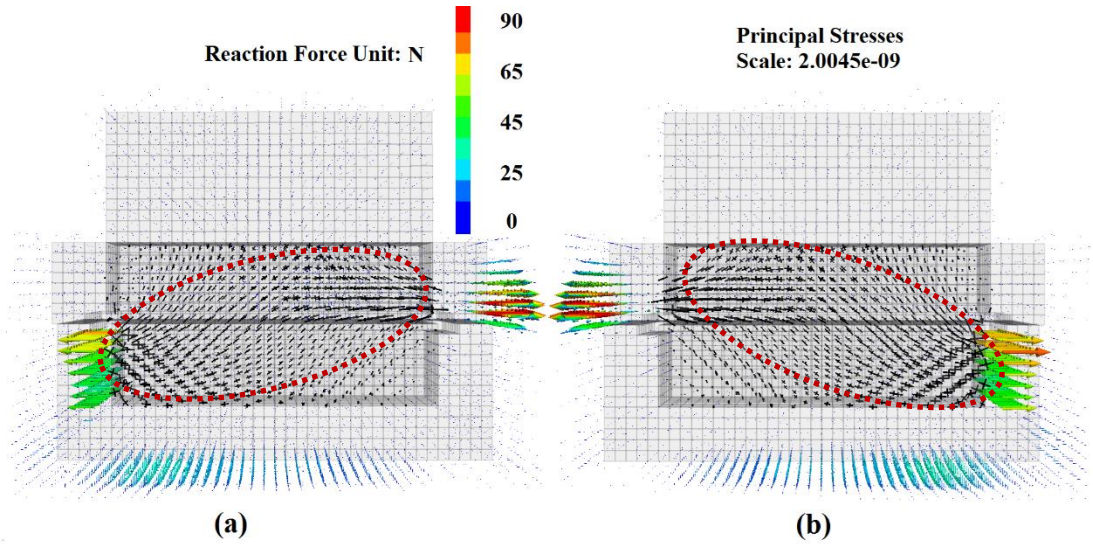

Figure 121. Reaction forces and principal stresses at different positions under normal load of 90 kN, horizontal frequency of 1.0 Hz, shear displacement amplitude of 5.0 mm: (a) after 0.25 sec and (b) after 0.75 sec.

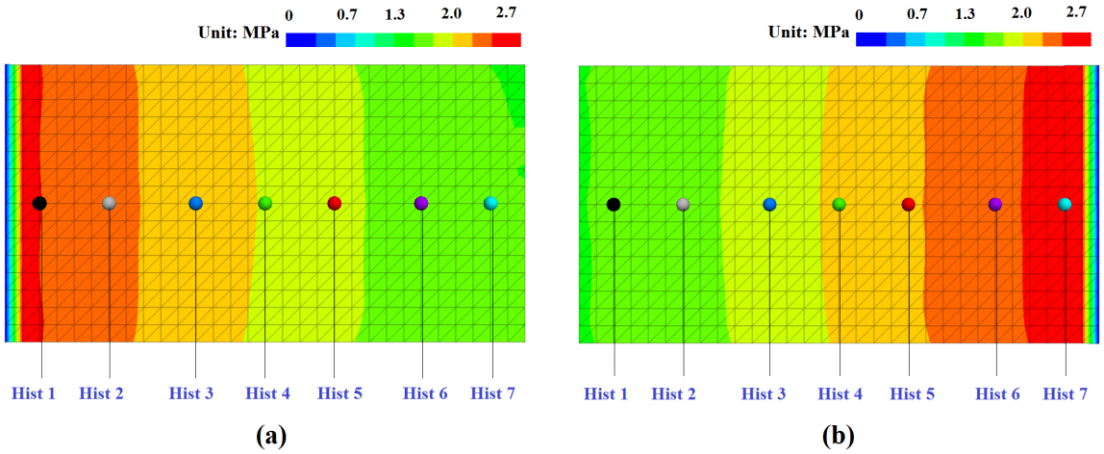

Figure 122. Normal stress contours under normal load of 90 kN, horizontal frequency of 1.0 Hz, shear displacement amplitude of 5.0 mm: (a) after 0.25 sec and (b) after 0.75 sec.

Numerical simulation results show satisfying agreement with lab test results in respect to peak shear forces for different normal loads, normal displacement and time (Figure 128, Figure 125, Figure 126 and Figure 127). Figure 128 illustrates the time shift between maximum shear force and maximum shear displacement.

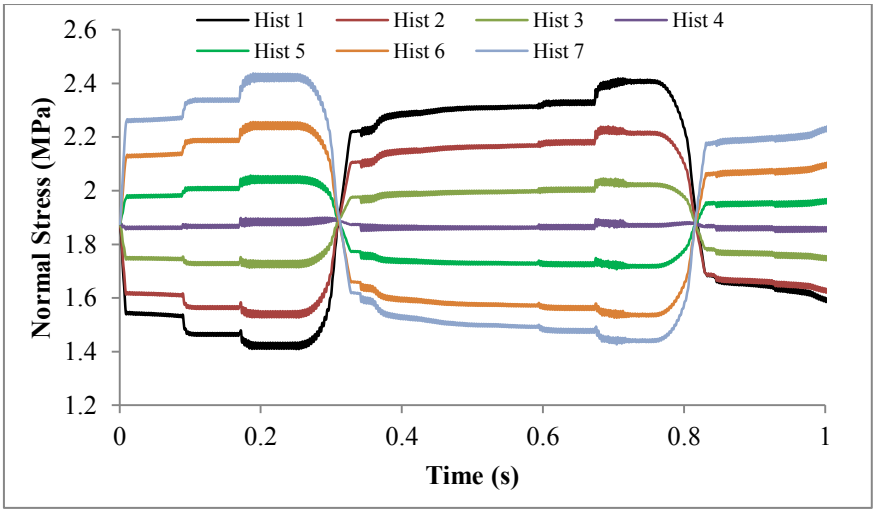

Figure 123. Normal stress vs. time, static normal load of 90 kN, normal impact frequency of 1.0 Hz and shear displacement amplitudes of 5.0 mm.

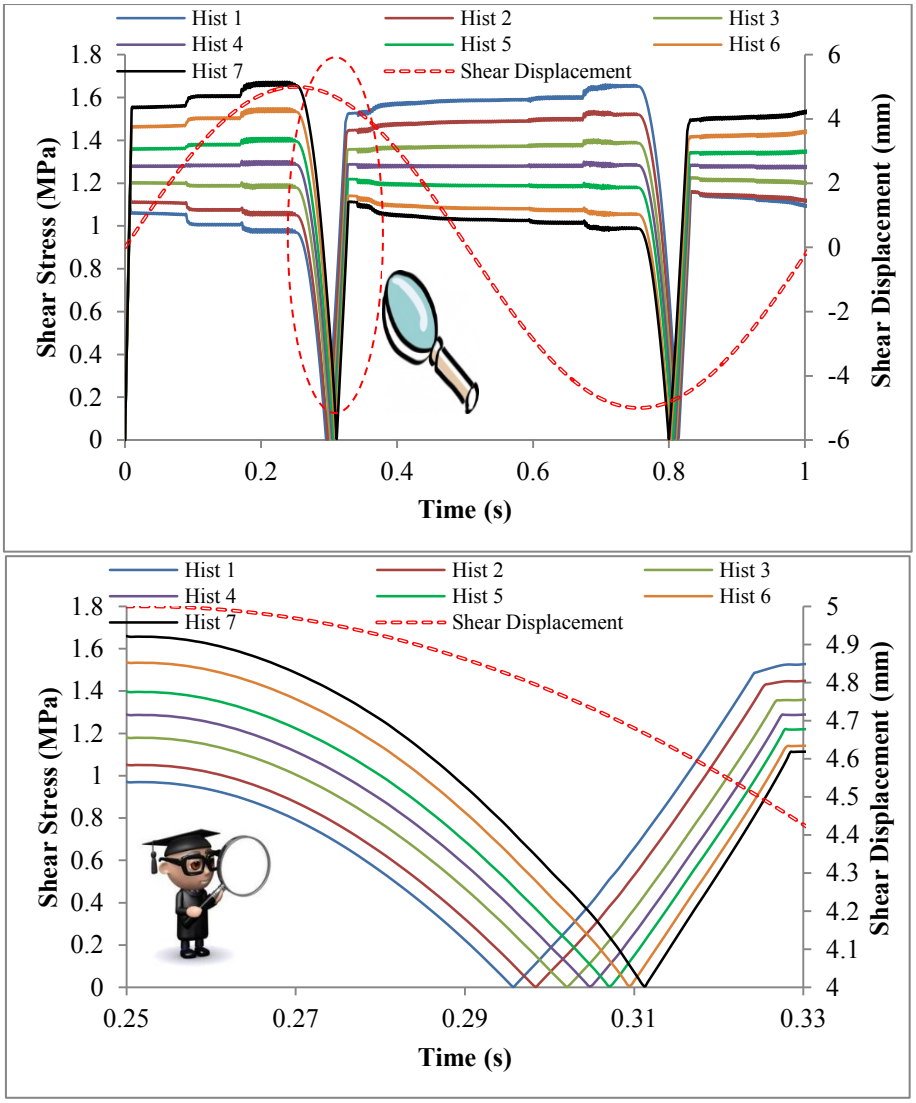

Figure 124. Shear stresses vs. time, static normal load of 90 kN, normal impact frequency of 1.0 Hz and shear displacement amplitudes of 5.0 mm (according to Figure 122).

Figure 121 shows the behavior of the reaction forces and the principal stresses at different points in time. After 0.25 seconds, force chains are developed from the lower left to upper right of the specimen. Reaction forces concentrate in the vertical direction in the left half side of the shear box and in the horizontal direction in the right side of the upper shear box and in the left side of the bottom shear box. However, after 0.75 seconds, force chains are developed from the upper left to lower right of the specimen. Reaction forces concentrate in the vertical direction in the right half side of the shear box and in the horizontal direction in the left side of the upper shear box and in the right side of the bottom shear box.

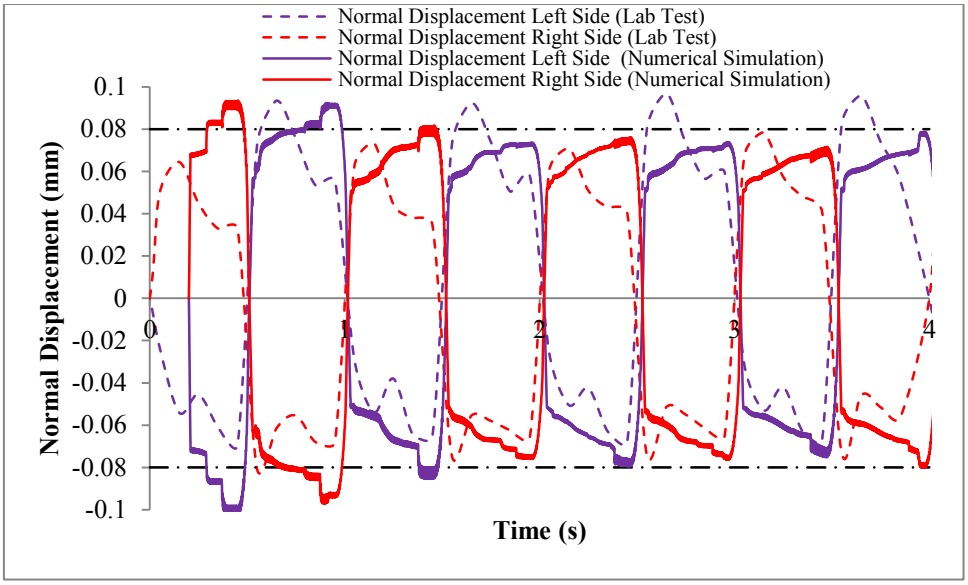

Figure 125. Normal displacement vs. time, normal static load of 90 kN, shear displacement amplitude of 5.0 mm and frequency of 1.0 Hz.

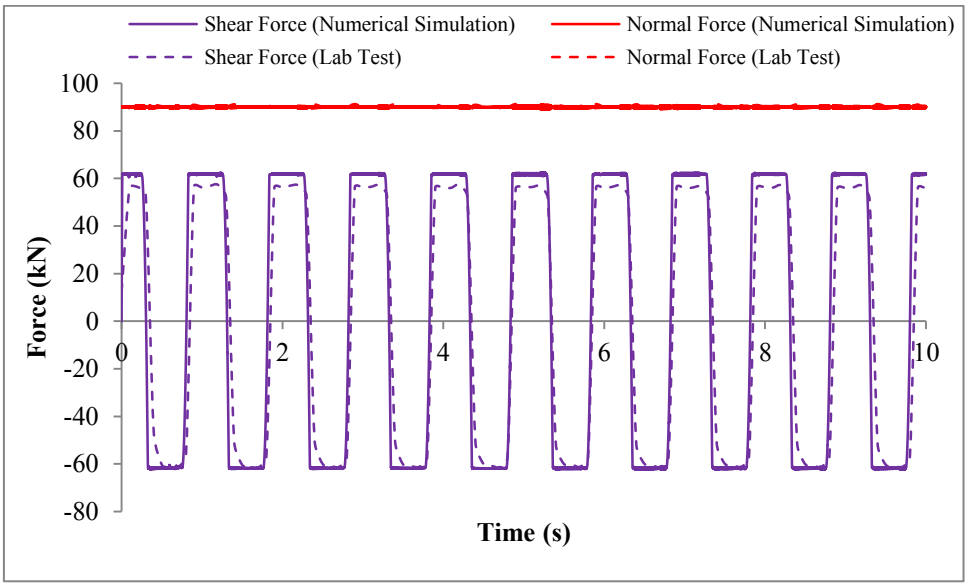

Figure 126. Normal and shear forces vs. time, static normal load of 90 kN, shear displacement amplitude of 5.0 mm and frequency of 1.0 Hz.

Figure 122, Figure 123 and Figure 124 reveal a very inhomogeneous stress pattern with a distinct gradient along the interface: Minimum normal stress of 1.4 MPa at one end and over 2.7 MPa at the other end of the joint. Similar as observed in the lab tests, within one cycle, shear stresses increase with increasing shear displacement until a peak value is reached. The inhomogeneous stress pattern shows cyclic change. Only at the central part of the interface a nearly constant value is observed which

corresponds to the average value of normal and shear stresses. 124(a) also shows that after 0.25 seconds (shear direction reversal point), shear stresses decrease with ongoing time until a minimum value is reached. Afterwards, shear stresses increase but with opposite stress gradient along the joint.

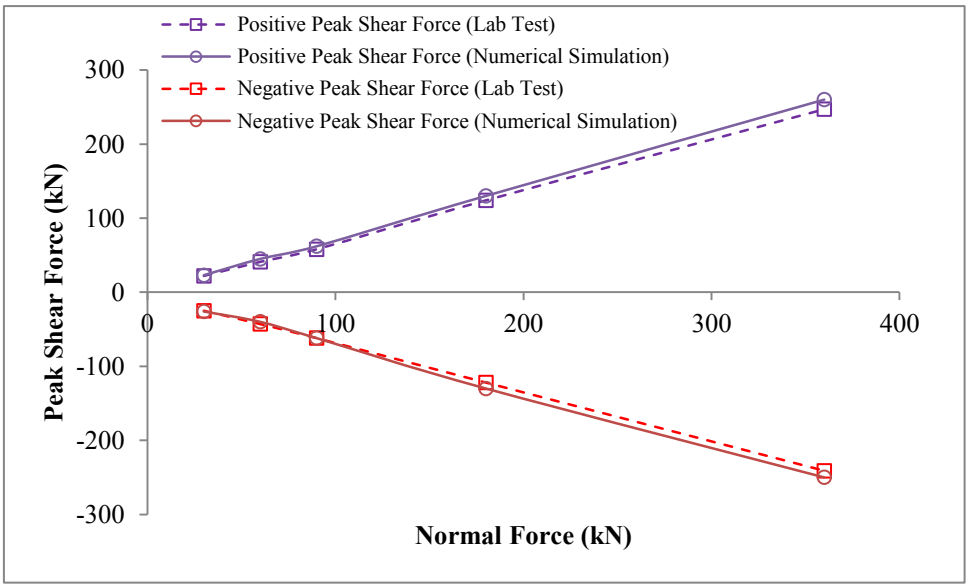

Figure 127. Peak shear forces vs. normal forces.

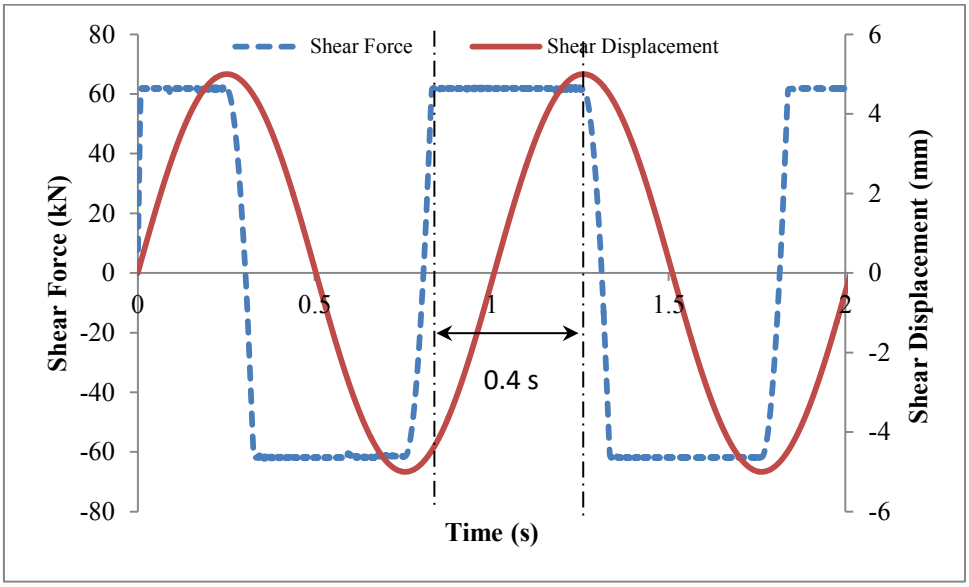

Figure 128. Time shift between maximum shear force and maximum shear displacement (numerical simulation results).

6.3 Numerical simulations of DNL shear tests

6.3.1 Direct shear tests simulation

6.3.1.1 Model set-up

The numerical model for the direct shear test under DNL conditions is same as the one which was used to model the cyclic shear tests under CNL conditions. Only the boundary conditions are different. In this model, a sinusoidal dynamic normal stress signal is applied at the loading plate in the vertical direction. At the same time, a constant shear velocity is applied at the bottom shear box.

6.3.1.2 Simulation results

Numerical simulation results are shown in Figure 129, Figure 130, Figure 131, Figure 132, Figure 133 and Figure 134.

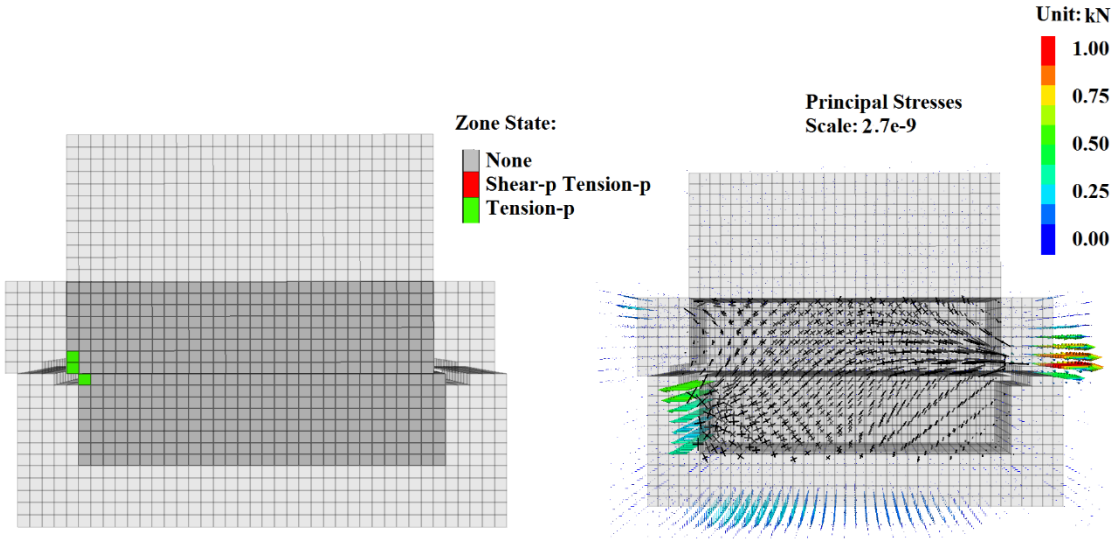

Figure 129. (a) Plasticity state and (b) principal stresses and reaction forces under static normal force of 90 kN with superimposed normal force of 45 kN at shear displacement of 1.0 cm and normal impact frequency of 1.0 Hz.

Figure 129 shows the plasticity state, reaction forces and principal stresses at a shear displacement of 1.0 cm. Like in the direct shear tests under CNL conditions, higher stresses at the left side of the specimen lead to local failure in the matrix. Displacement vectors of the loading plate and the top specimen are shown in Figure 130.

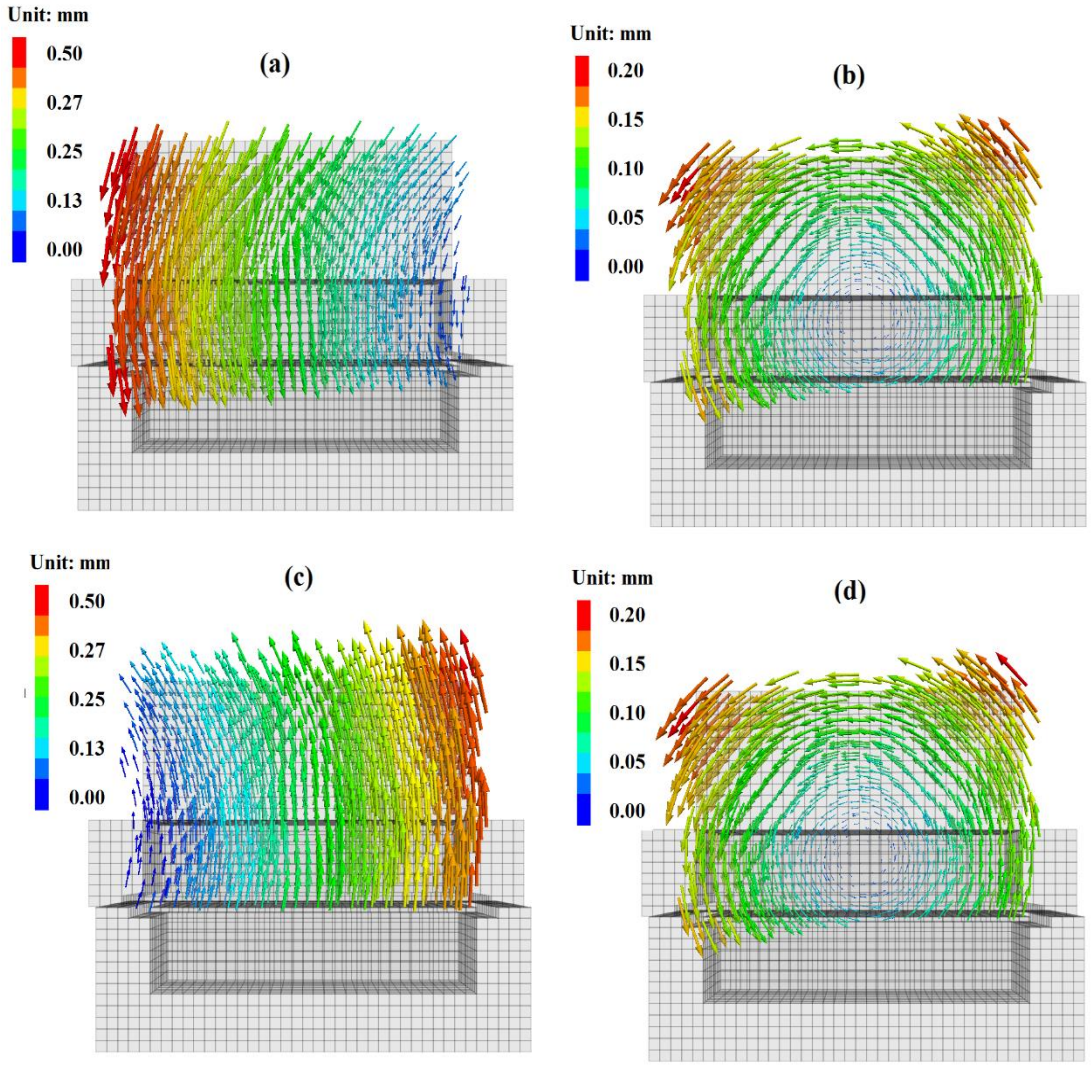

Figure 130. Displacement vectors for upper model part under static normal force of 90 kN, superimposed normal force of 45 kN and vertical normal impact frequency of 1.0 Hz: (a) 7.25 seconds (b) 7.5 seconds (c) 7.75 seconds and (d) 8.0 seconds.

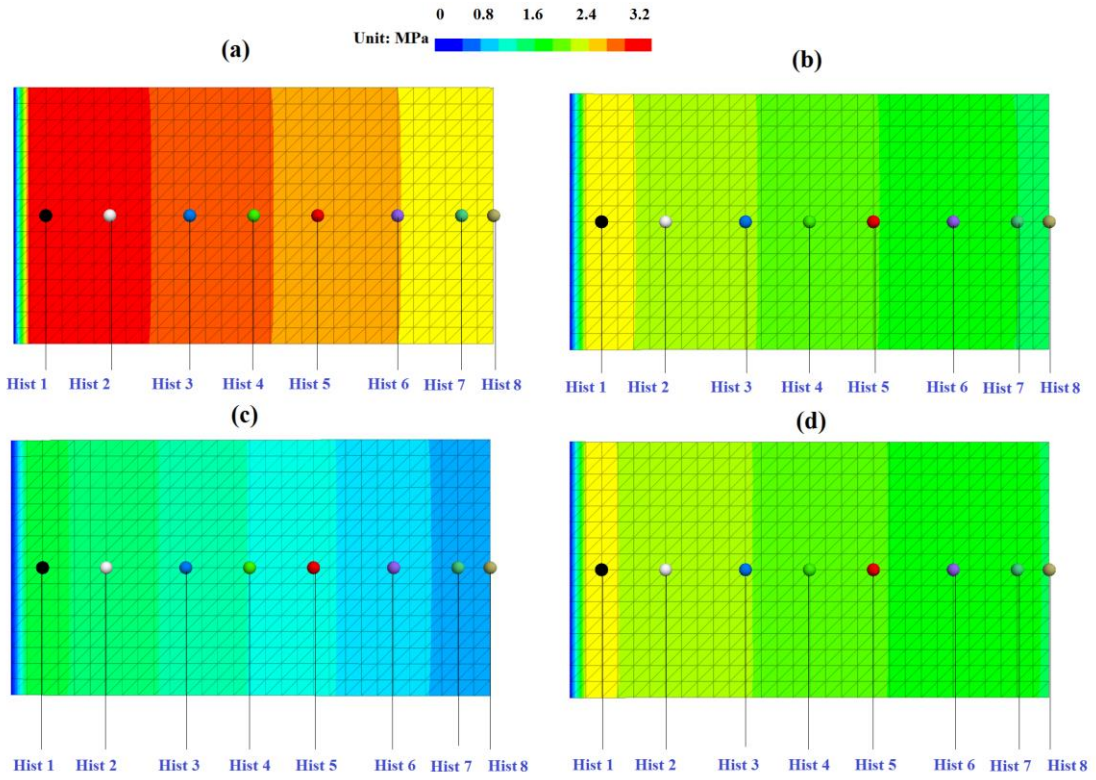

Normal stress at the interface

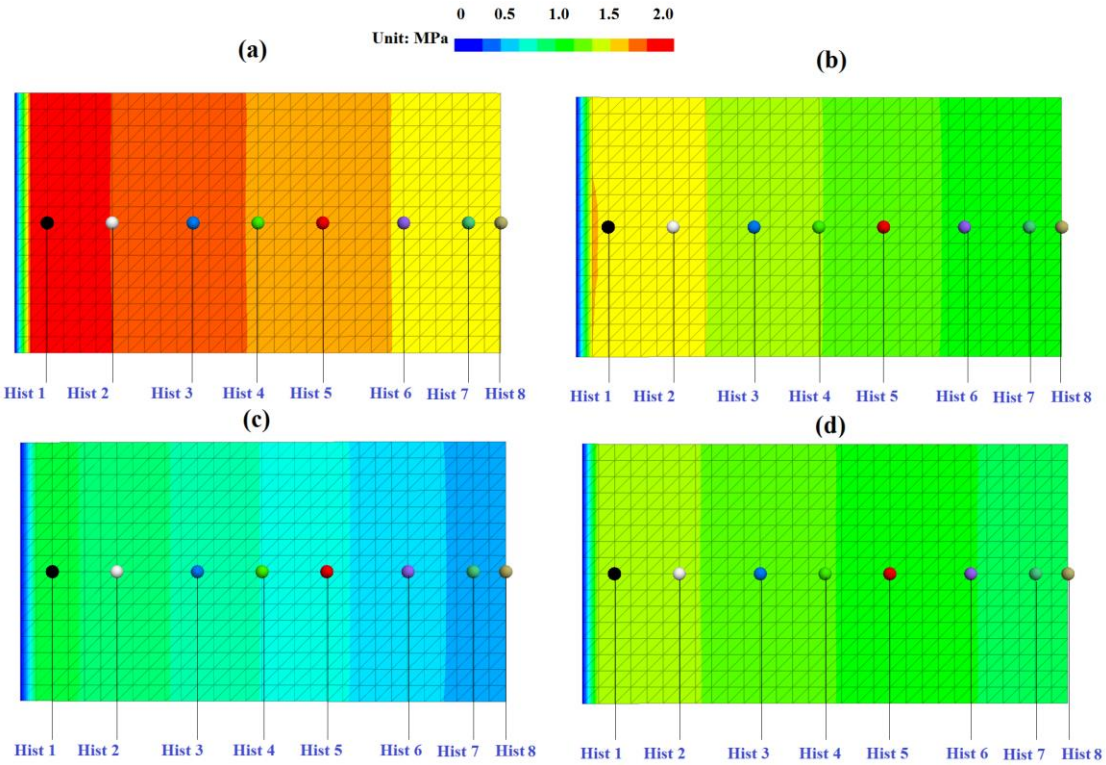

Shear stress at the interfaece

Figure 131. Interface stresses at different positions under static normal force of 90 kN, superimposed normal force of 45 kN and vertical normal impact frequency of 1.0 Hz: (a) 7.25 seconds, (b) 7.5 seconds, (c) 7.75 seconds and (d) 8.0 seconds.

Dynamic time: 7.0 to 7.25 seconds

The superimposed normal stress increases with ongoing time until a maximum value is reached. Settlement of top specimen and loading plate increase with increasing superimposed normal stress. The top specimen shows anti-clockwise rotation. Normal and shear stresses at the interface show a very inhomogeneous pattern with a distinct gradient along the interface (decreasing from left side to right side). Normal and shear stresses at the interface are increasing with time.

Dynamic time: 7.25 to 7.50 seconds

The superimposed normal stress decreases with ongoing time until the initial value is reached. Top specimen and loading plate move upwards. Top specimen shows anti-clockwise rotation. Normal and shear stresses at the interface show a very inhomogeneous pattern with distinct gradient along the interface (decreasing from left to right side). Normal and shear stresses at the interface are decreasing with time.

Dynamic time: 7.50 to 7.75 seconds

The superimposed normal stress still decreases with ongoing time until a minimum value is reached. Top specimen and loading plate move upwards. The amount of anti-clockwise rotation of the top specimen is reduced. Normal and shear stresses at the interface decrease with time.

Dynamic time: 7.75 to 8.0 seconds

The superimposed normal stress increases with ongoing time until the initial value is reached. Top specimen and loading plate move downwards with anti-clockwise rotation. Normal and shear stresses at the interface increase with ongoing time.

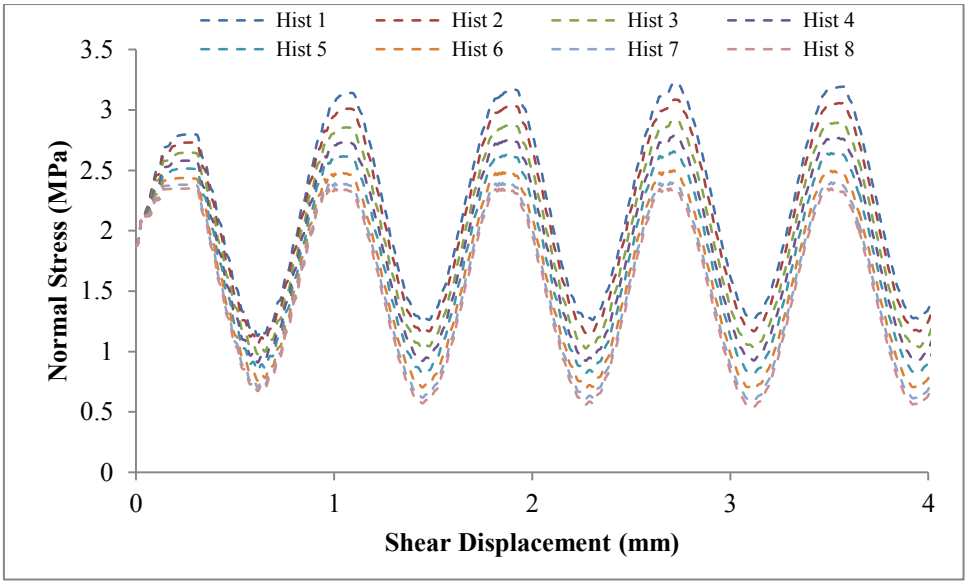

Figure 132. Interface normal stress vs. shear displacement under static normal force of 90 kN, superimposed normal force of 45 kN and vertical normal impact frequency of 1.0 Hz.

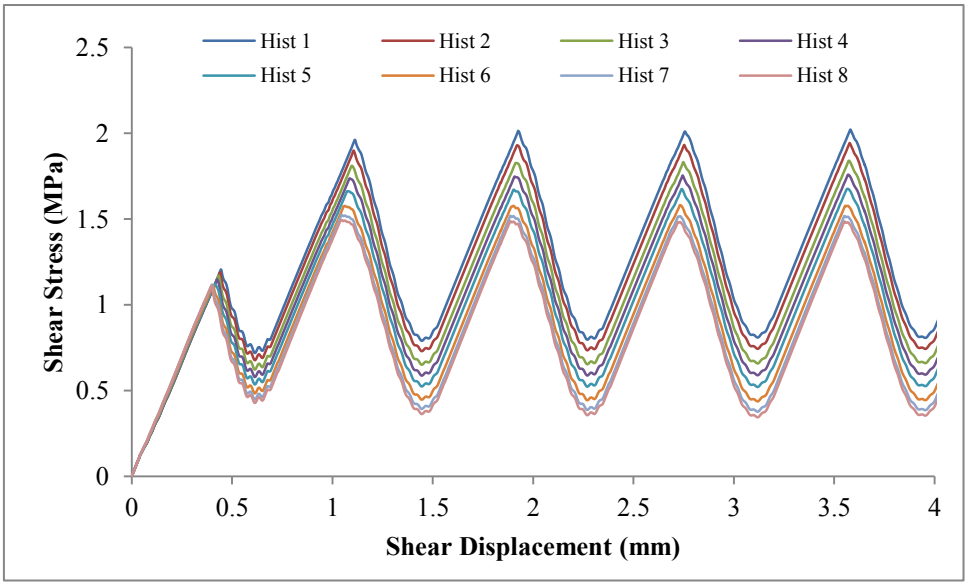

Figure 133. Interface shear stress vs. shear displacement under static normal force of 90 kN, superimposed normal force of 45 kN and vertical normal impact frequency of 1.0 Hz.

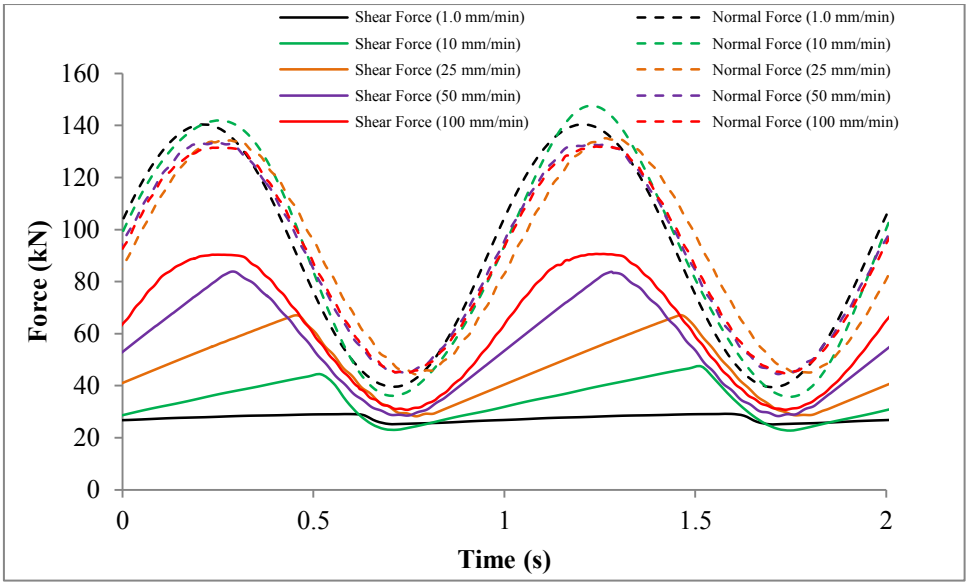

Figure 134. Shear and normal forces vs. time for different shear velocities (numerical simulation results), stable stages were taken and the starting time was shifted to zero.

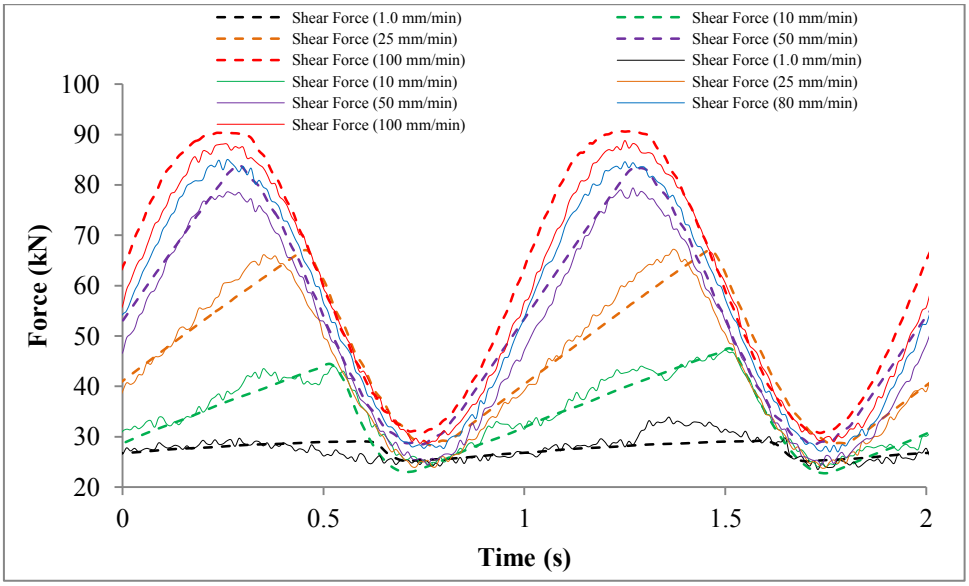

Figure 135. Shear force vs. time for different shear velocoties (solid lines: lab test results, dotted lines: numerical simulation results), stable stages were taken and the starting time was shifted to zero.

Numerical simulation results also show that there is a significant time shift between the peak normal force and peak shear force. As Figure 135 documents, lab test results and numerical simulation results are in close qualitative and quantitative agreement.

6.3.2 Cyclic shear test simulations

6.3.2.1 Model set-up

The numerical model used is same as the one which was used for the cyclic shear tests under CNL conditions. Only the boundary conditions are different. In this model, dynamic signals are applied in the vertical and horizontal direction at the same time. In the horizontal direction a sinusoidal displacement signal and in the vertical direction a sinusoidal force signal is applied.

6.3.2.2 Simulation results

Numerical simulation results are shown in Figure 136, Figure 137, Figure 138, Figure 139, Figure 140, Figure 141, Figure 142, Figure 143, Figure 144 and Figure 145.

Figure 136 shows the plasticity state of the samples under normal load of 90 kN and shear displacement amplitude of 5.0 mm with horizontal frequency of 1.0 Hz and vertical normal impact frequency of 1.0 Hz for one and ten cycles, respectively. The horizontal movement of the specimen is repeated several times. Consequently, more and more plasticity zones are formed and these zones are mainly located at the two edges of the contact surface. It is similar with the lab test results.

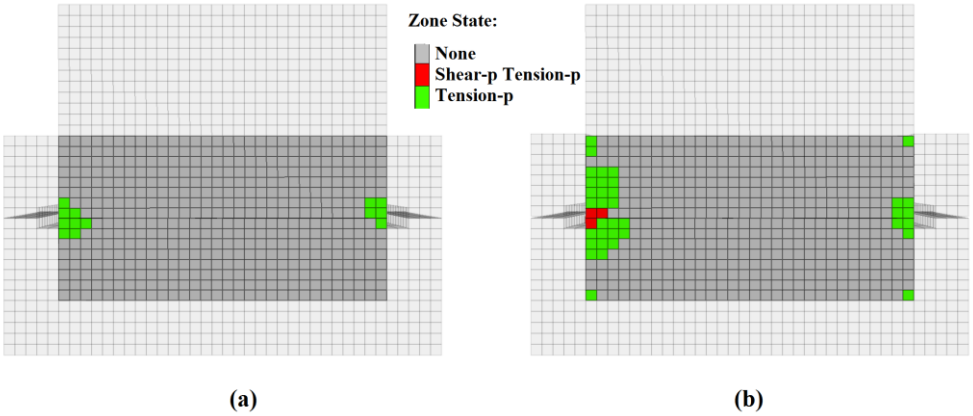

Figure 136. Plasticity state under normal load of 90 kN +/- 45 kN, shear displacement amplitude of 5.0 mm with horizontal frequency of 1.0 Hz and vertical normal impact frequency of 1.0 Hz: (a) after 1.0 cycle and (b) after 10.0 cycles.

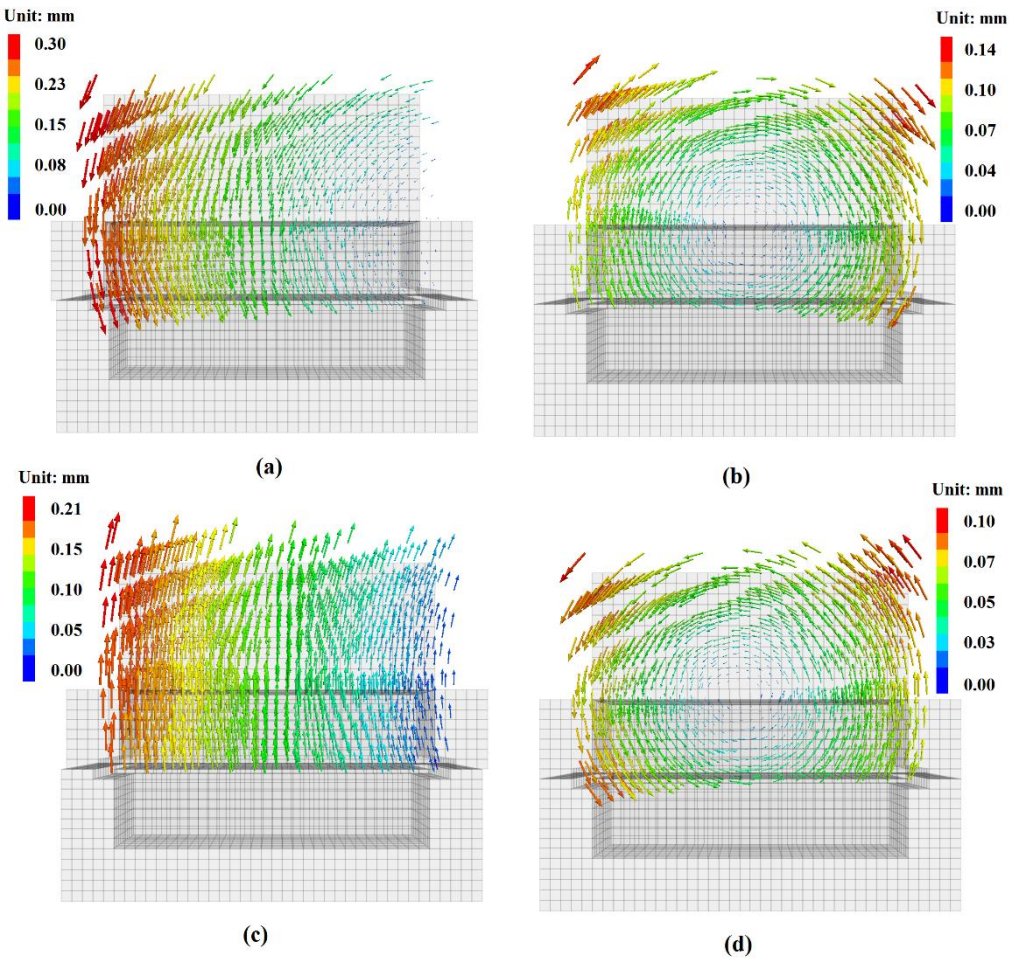

Figure 137. Displacement vectors of upper part of model under normal load of 90 kN +/-45 kN, shear displacement amplitude of 5.0 mm with horizontal frequency of 1.0 Hz and vertical normal impact frequency of 1.0 Hz: (a) after 0.25 cycles, (b) after 0.5 cycles, (c) after 0.75 cycles and (d) after 1 cycle.

Figure 137 and Figure 138 show the movement behavior of top specimen and loading plate, reaction forces and principal stresses during the cyclic shearing under DNL conditions. The behavior can be described as follows (taking one case for example: normal load of 90 kN with superimposed normal force of 45 kN, shear displacement amplitude of 5.0 mm with horizontal frequency of 1.0 Hz and vertical normal impact frequency of 1.0 Hz).

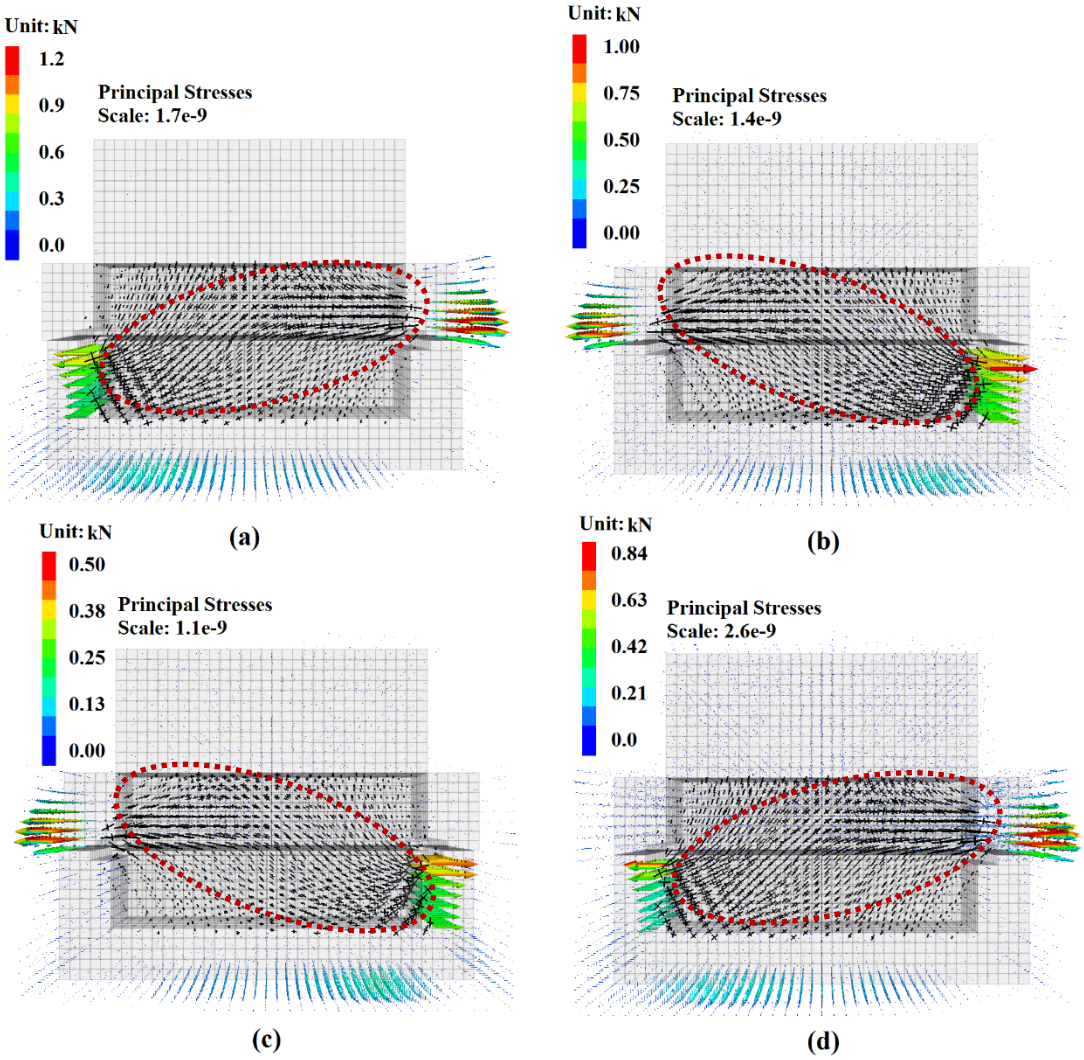

Figure 138. Reaction forces and principal stresses under normal load of 90 kN, superimposed normal force of 45 kN, shear displacement amplitude of 5.0 mm with horizontal frequency of 1.0 Hz and vertical normal impact frequency of 1.0 Hz: (a) after 0.25 cycles, (b) after 0.5 cycles, (c) after 0.75 cycles and (d) after 1 cycle.

Dynamic time: 0 to 0.25 seconds:

The lower part of the specimen moves horizontally from the initial position to a positive maximum value. At the same time, the superimposed normal stress reaches its maximum. Top specimen and loading plate show anti-clockwise rotation. Force chains develop from the lower left to the upper right part of the specimen. Normal and shear stresses at the interface show a very inhomogeneous pattern with a distinct gradient (decreasing from left side to right side). The normal and shear stresses at the interface are increasing with ongoing time.

Dynamic time: 0.25 to 0.5 seconds:

The shearing direction reverses and sample moves back into the initial position. The superimposed normal stress is decreasing up to zero. The anti-clockwise rotation of top specimen and loading plate are reversed into clockwise rotation. The stress gradient along the interface is also reversed. Normal and shear stresses at the interface are decreasing with ongoing time.

Dynamic time: 0.5 to 0.75 seconds:

The specimen is sheared from initial position until the negative maximum value is reached. The superimposed normal stress is still decreasing until the minimum value is reached. Top specimen and loading plate move upwards. Principal stresses, reaction forces, normal and shear stresses at the interface are decreasing because of the decreasing superimposed normal stress until the minimum value is reached.

Dynamic time: 0.75 to 1.0 seconds:

The shearing direction is reversed and sample moves back into the initial position. The superimposed normal stress is increasing until zero. The heave of top specimen and loading plate decreases and finally they show anti-clockwise rotation. Force chains develop first from the upper left to the lower right of the specimen and reverse later to upper right from the lower left of the specimen. Moreover, the reaction forces in the vertical direction are concentrated in the left half side of the shear box. The interface stress distribution pattern is changed (increasing from left side to right side reverses to decreasing from left side to right side). Normal and shear stresses at the interface are increasing with ongoing time.

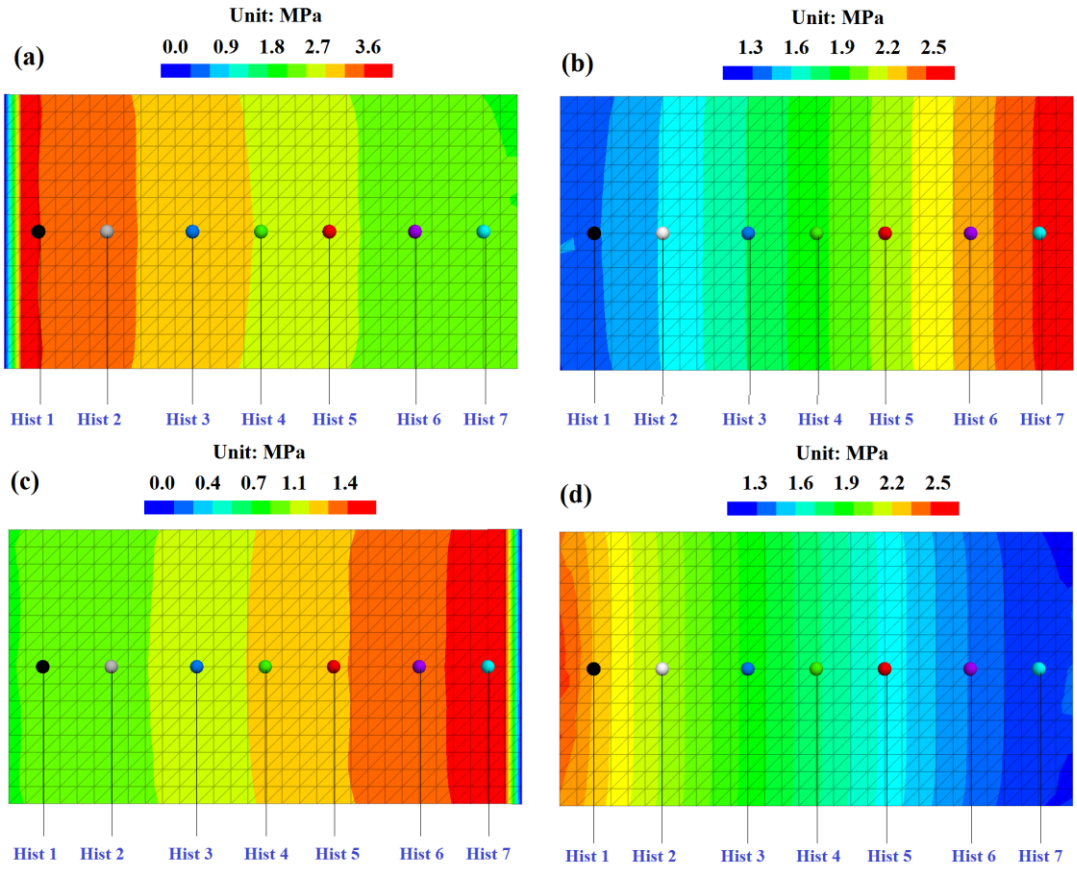

Figure 139. Interface normal stress under normal force of 90 kN, superimposed normal force of 45 kN, shear displacement amplitude of 5.0 mm with horizontal frequency of 1.0 Hz and vertical normal impact frequency of 1.0 Hz: (a) after 0.25 cycles (b) after 0.5 cycles (c) after 0.75 cyclesand (d) after 1 cycle.

At special points in time (e.g., after 0.25 or 0.75 seconds), shear direction and superimposed normal stress reverse. Due to the material characteristics stress and shear direction changes need a certain amount of time. Consequently, it creates a time shift (Figure 141) between peak shear displacement and peak normal stress (or peak shear stress).

Figure 142, Figure 143, Figure 144 and Figure 145 show numerical simulation results under different horizontal or vertical impact frequencies. These figures show the interface stress distribution pattern and illustrate the shear and normal stresses reversal associated with the reverse of shear direction and superimposed normal stress.

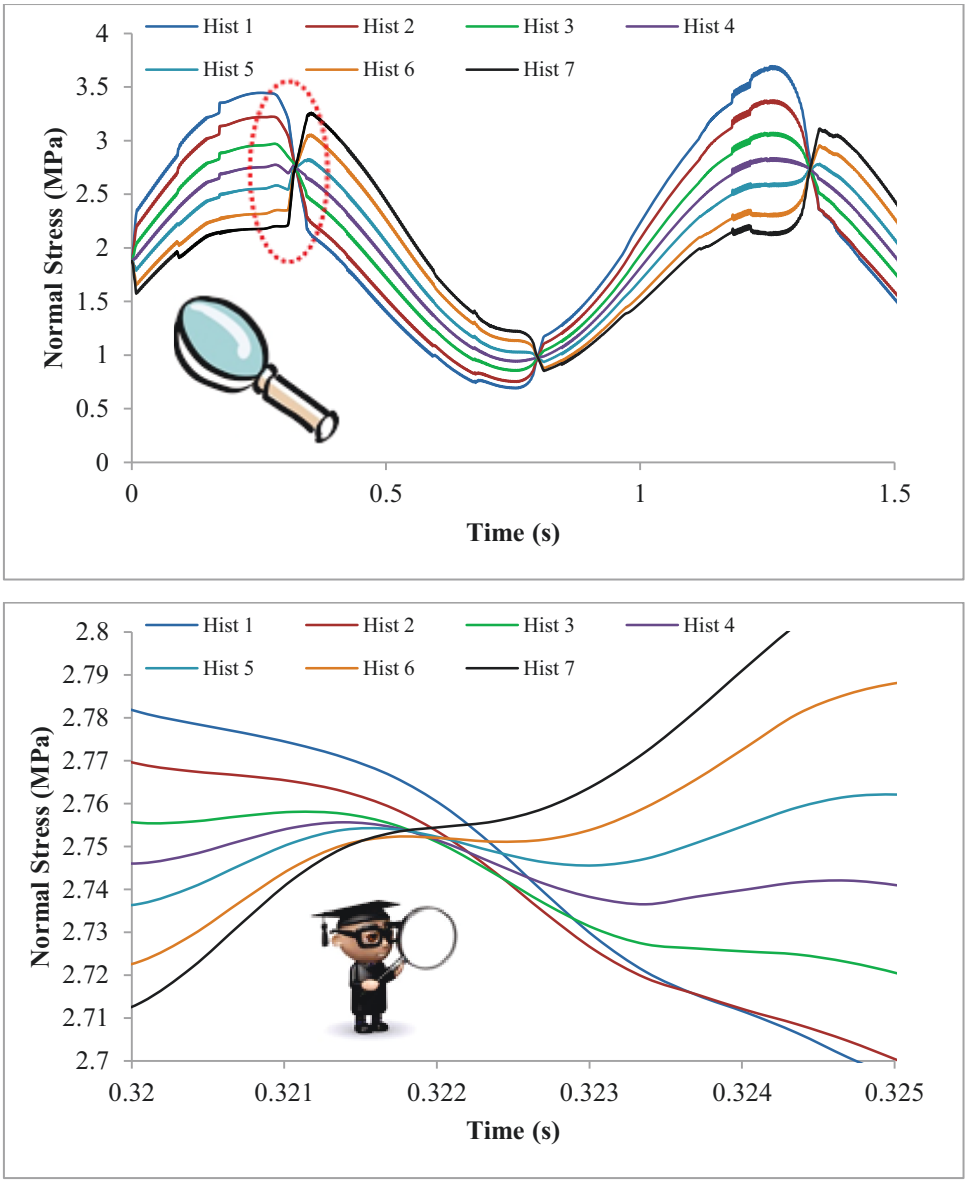

Figure 140. Normal stress at the interface vs. time under normal force of 90 kN, superimposed normal force of 45 kN, shear displacement amplitude of 5.0 mm with horizontal frequency of 1.0 Hz and vertical normal impact frequency of 1.0 Hz.

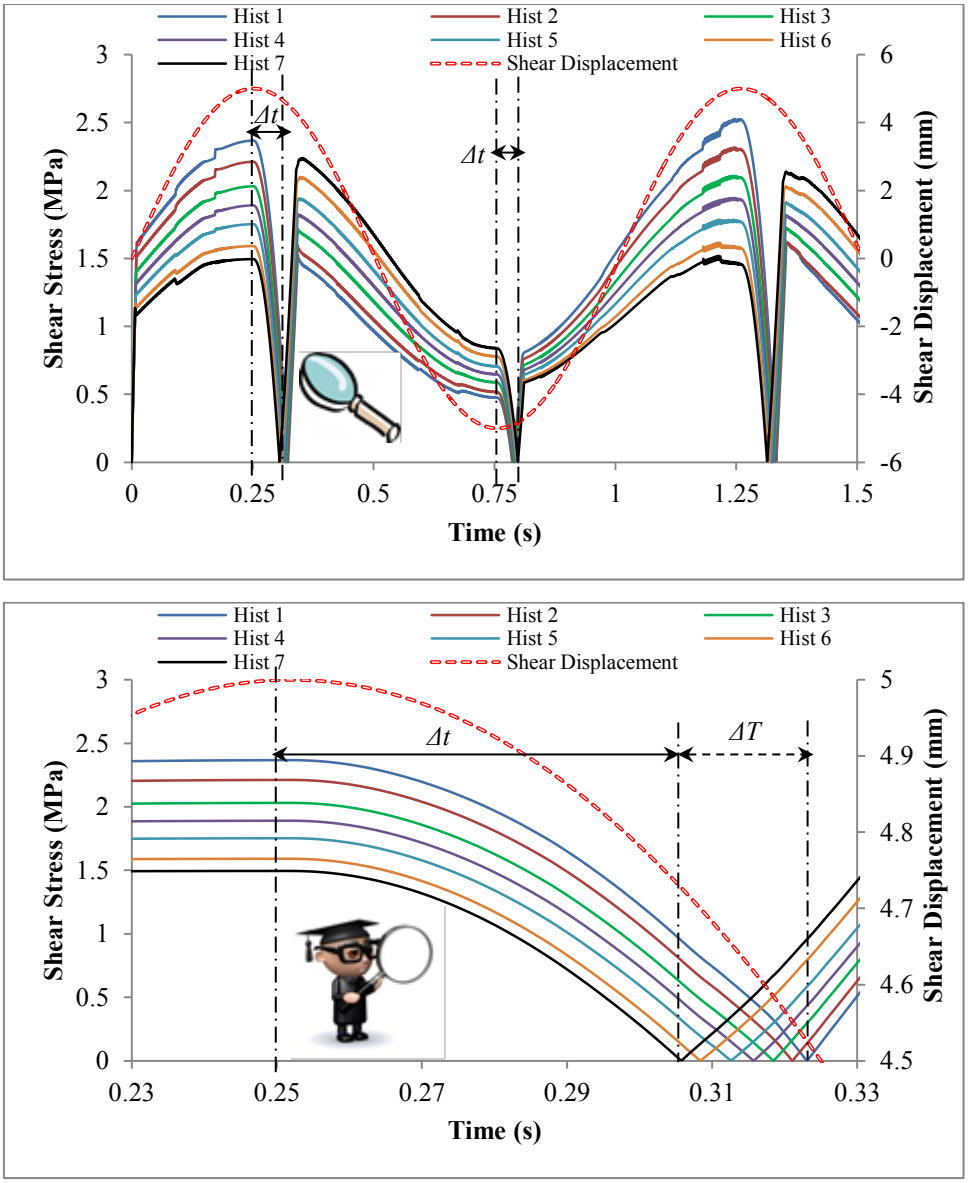

Figure 141. Shear stress at the interface vs. time under normal force of 90 kN, superimposed normal force of 45 kN, shear displacement amplitude of 5.0 mm with horizontal frequency of 1.0 Hz and vertical normal impact frequency of 1.0 Hz.

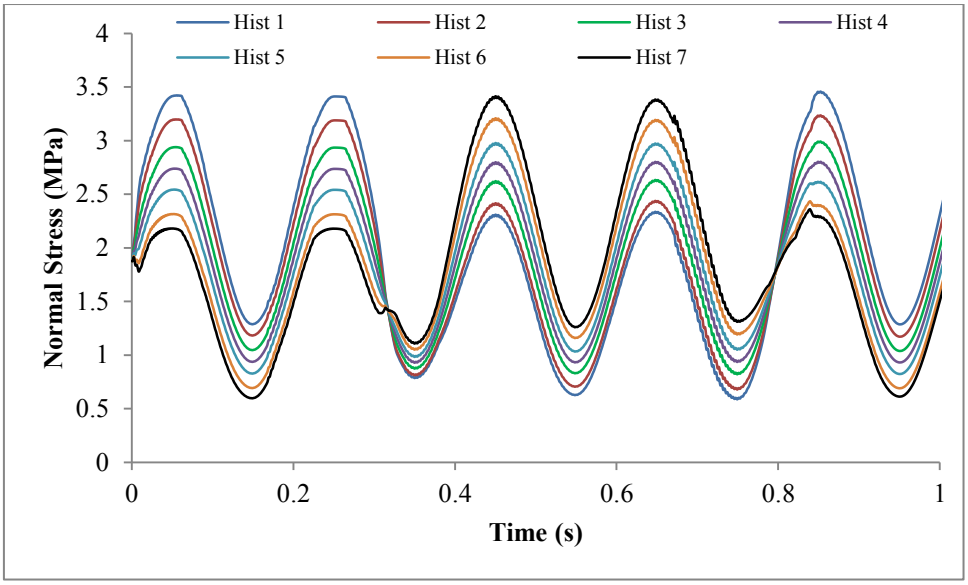

Figure 142. Normal stress at the interface vs. time under normal force of 90 kN, superimposed normal force of 45 kN, shear displacement amplitude of 5.0 mm with horizontal frequency of 1.0 Hz and vertical normal impact frequency of 5.0 Hz.

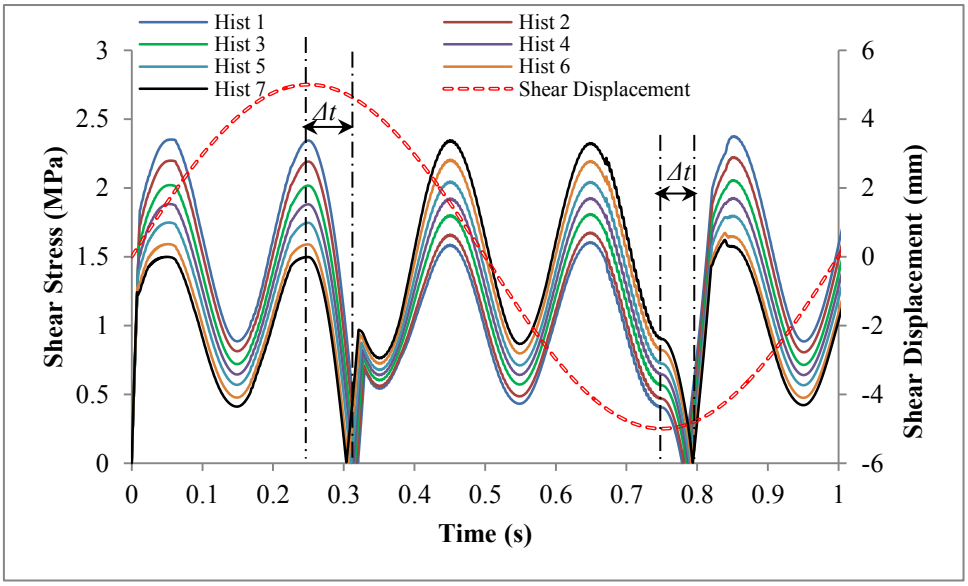

Figure 143. Shear stress at the interface vs. time under normal force of 90 kN, superimposed normal force of 45 kN, shear displacement amplitude of 5.0 mm with horizontal frequency of 1.0 Hz and vertical normal impact frequency of 5.0 Hz.

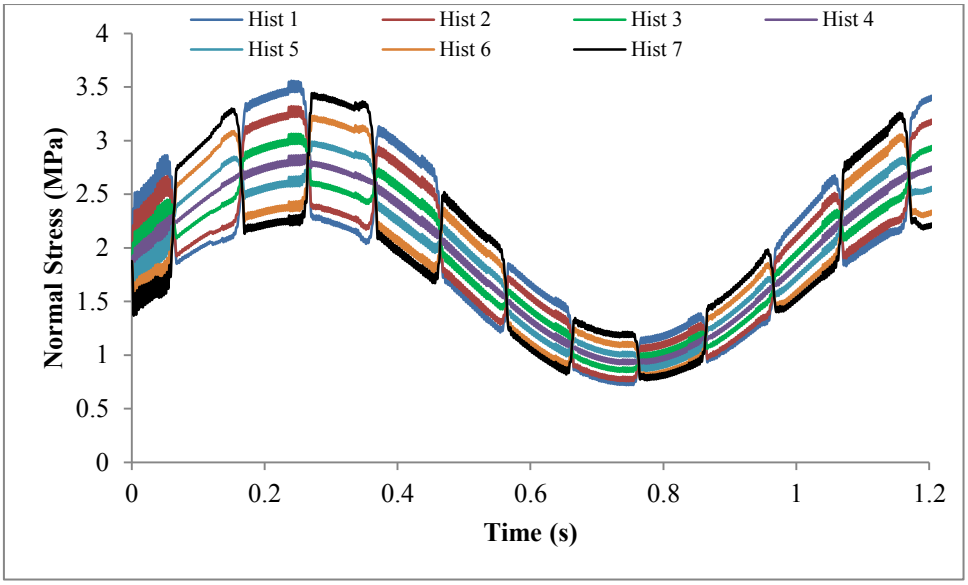

Figure 144. Normal stress at the interface vs. time under normal force of 90 kN, superimposed normal force of 45 kN, shear displacement amplitude of 5.0 mm with horizontal frequency of 5.0 Hz and vertical normal impact frequency of 1.0 Hz.

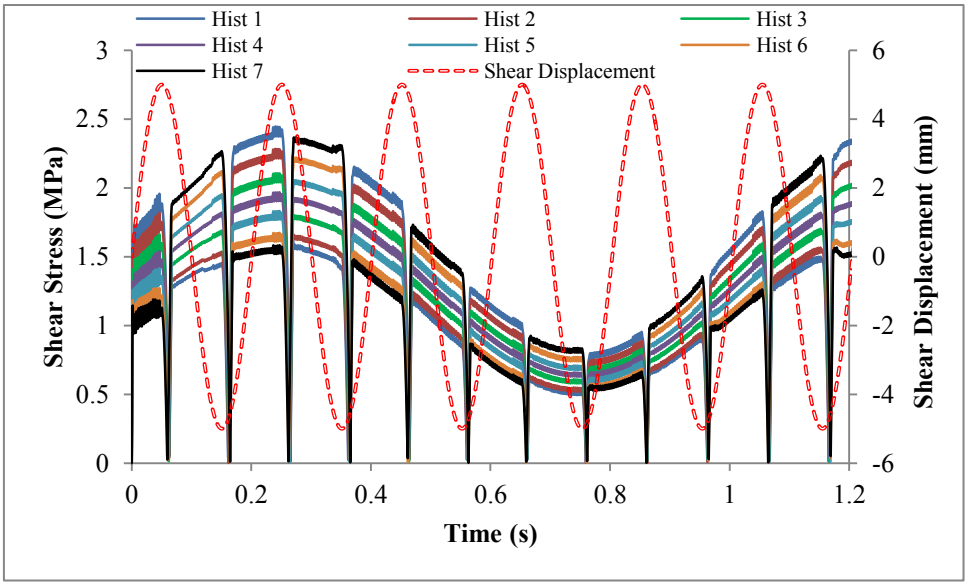

Figure 145. Shear stress of the interface vs. time under normal force of 90 kN, superimposed normal force of 45 kN, shear displacement amplitude of 5.0 mm with horizontal frequency of 5.0 Hz and vertical normal impact frequency of 1.0 Hz.

Figure 146 compares numerical simulation results with the lab test results under different dynamic excitations.

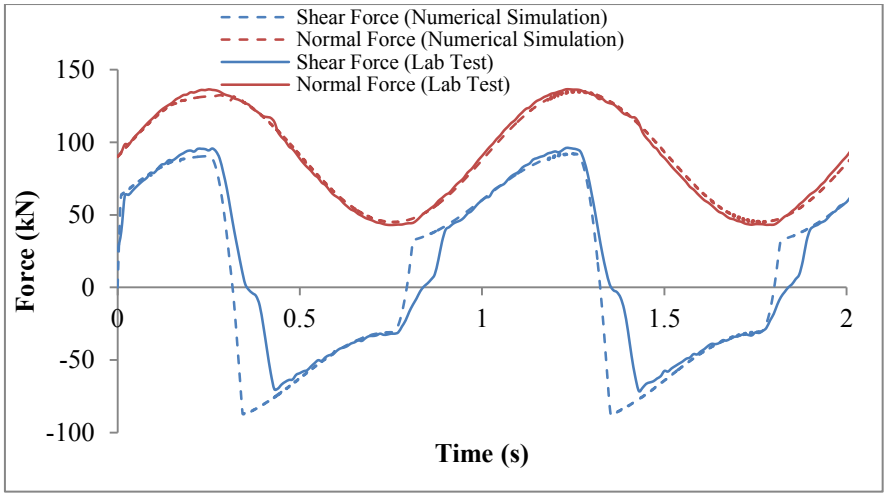

CNDL_5-3: f_h= *1.0 Hz* f_v=*1.0 Hz*

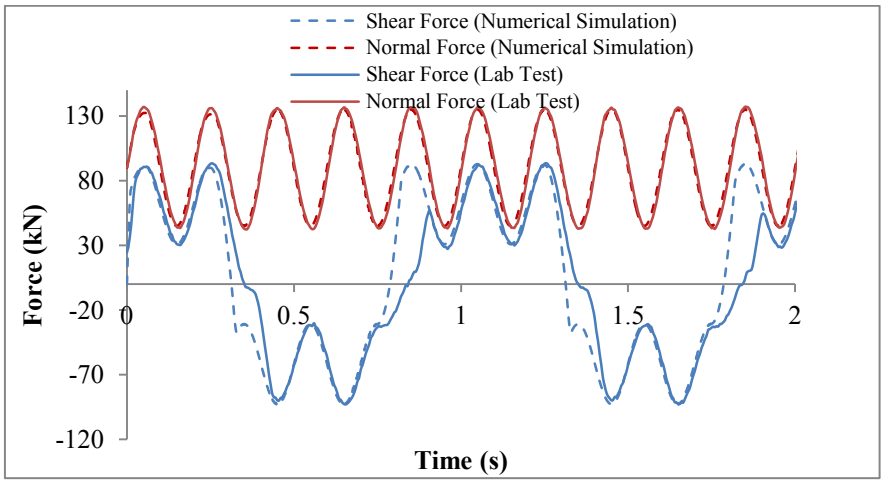

CNDL_5-7: f_h= *1.0 Hz* f_v=*5.0 Hz*

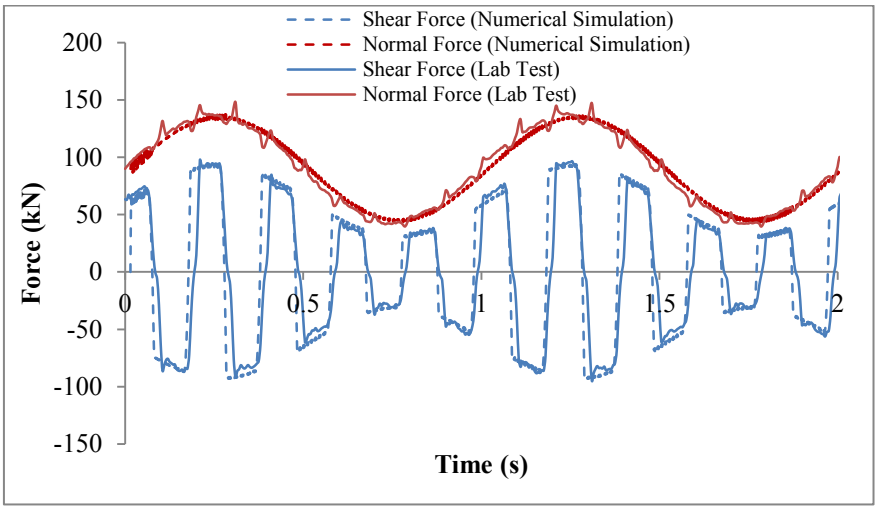

CNDL_3-7: f_h= *5.0 Hz* f_v=*1.0 Hz*

Figure 146. Shear and normal forces vs. time, comparison between numerical simulations and lab test results under normal load of 90 kN, shear displacement amplitude of 5.0 mm.

6.4 Investigations to reduce sample rotation

Sample rotation and non-uniform stress distributions along the interface make evaluation of lab tests complicated and reduce acceptance and validity. Some ideas to overcome this problem and the corresponding verification are the content of this chapter.

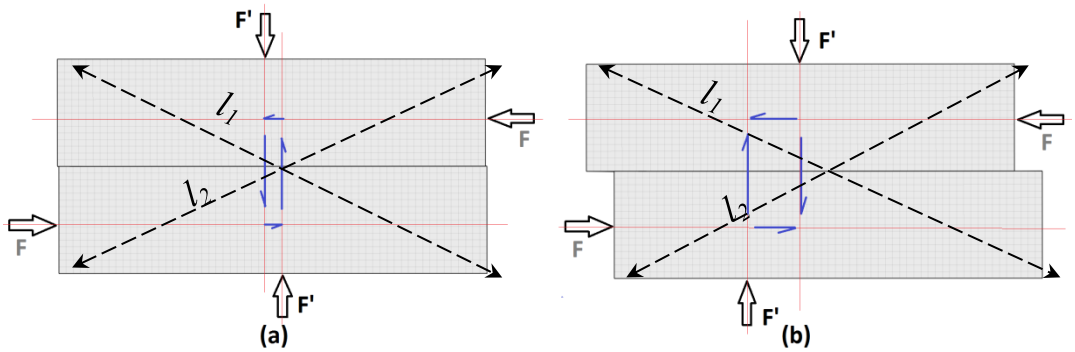

Figure 147. Principle of torque development during shear test: (a) small shear displacement and (b) larger shear displacement.

The undesired rotation is caused by uneven force distribution which leads to moments and consequently inclination (rotation) of the sample. As illustrated in Figure 116 the reaction forces and principal stresses are uniformly distributed after applying the normal load. However, with ongoing shear displacement, reaction forces become more and more non-uniform. The length of diagonal l_1 increases and l_2 decreases, which leads to sample rotation (Figure 147). Also, it is evident that the area in contact is decreasing as the shearing progresses and therefore the stresses at the joint interface increase. This change in area has to be considered in the test data evaluation and was performed for all lab tests and numerical simulations presented within this thesis.

It would improve the accuracy of the laboratory testing data, if the area of contact surface would remain constant. Also, any arrangement of the equipment, which would be helpful to reduce the sample rotation and inhomogeneous stress distribution along the interface.

In order to check the influence of joint contact area and shear velocities on rotation and stress distribution at the interface, several additional models were built

(Table 11). Simulation results in terms of the vertical displacement and distribution of shear stress at the joint are shown in Figure 148, Figure 149, Figure 150 and Figure 151 for 2.0 cm of shear displacement. In order to compare the shear stresses at the joint same history locations are used as for the modeling of the lab tests (Model O).

Table 11. Alternative shear box models.

Model	Bottom Model Size length*width*height (mm)	Shear Velocity and its Position
A	400*160*75	3 mm/min on bottom part
B	400*160*75	3 mm/min on top part
C	400*160*75	1.5 mm/min on top part 1.5 mm/min on bottom part
D	340*160*75	1.5 mm/min on top part 1.5 mm/min on bottom part

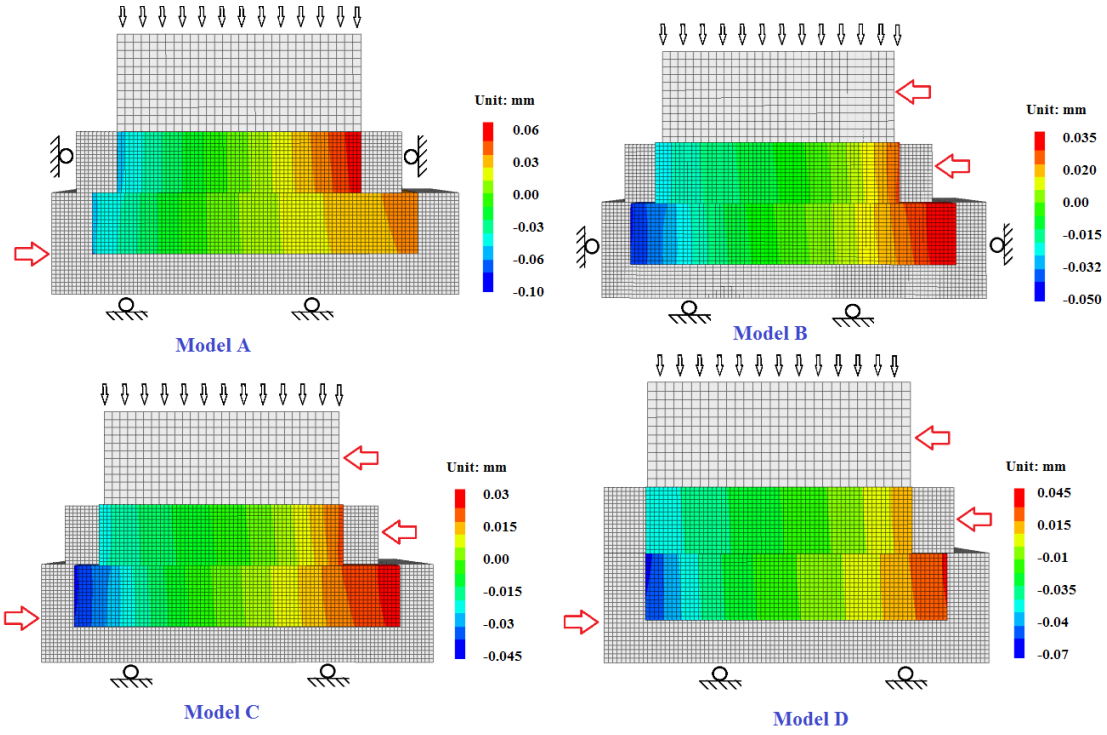

Figure 148. Vertical displacement contours after 2.0 cm of shear displacement.

Several tests according to Table 11 were investigated to find out which test arrangements would minimize sample rotation. Figure 148 illustrates corresponding

boundary conditions and shows vertical displacement contours of sample after 2.0 cm of shear displacement.

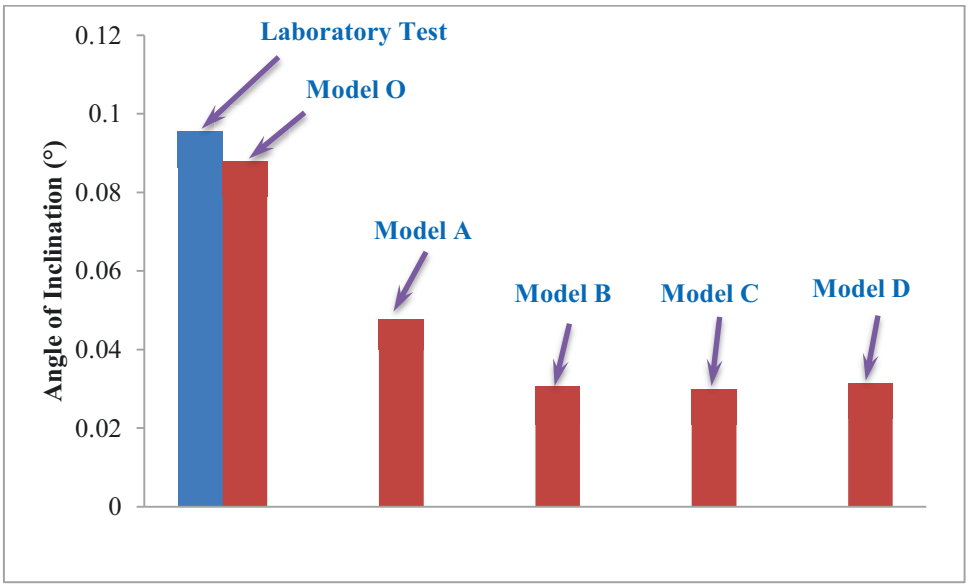

Figure 149. Peak angle of inclination.

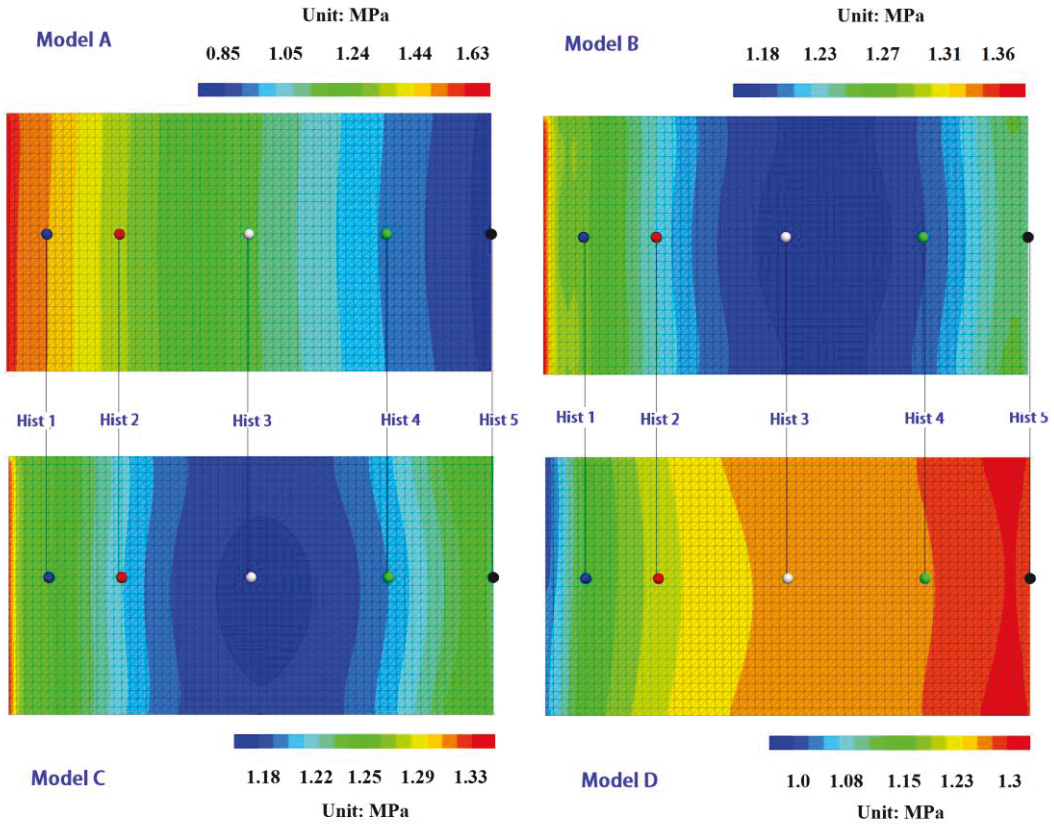

Figure 150. Shear stress distribution at the interface at shear displacement of 2.0 cm under normal load of 90 kN.

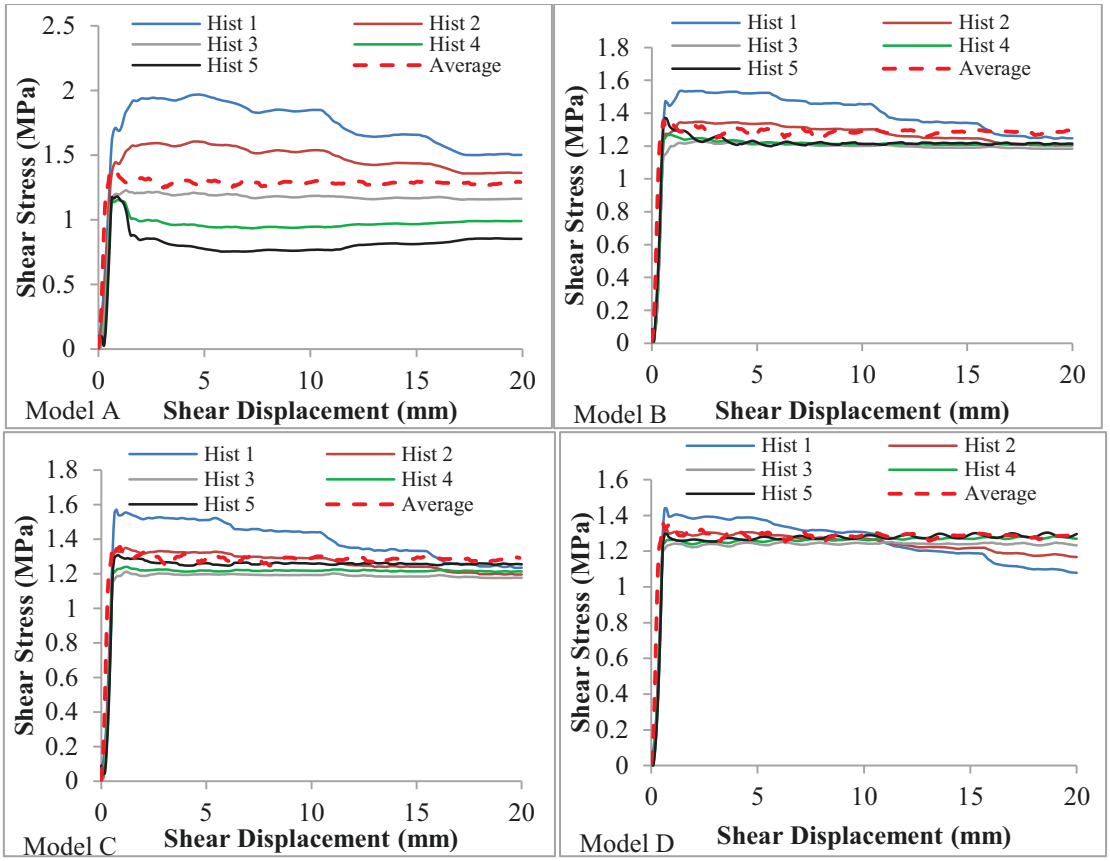

Figure 151. Shear stresses vs shear displacement for different observation points under normal load of 90 kN.

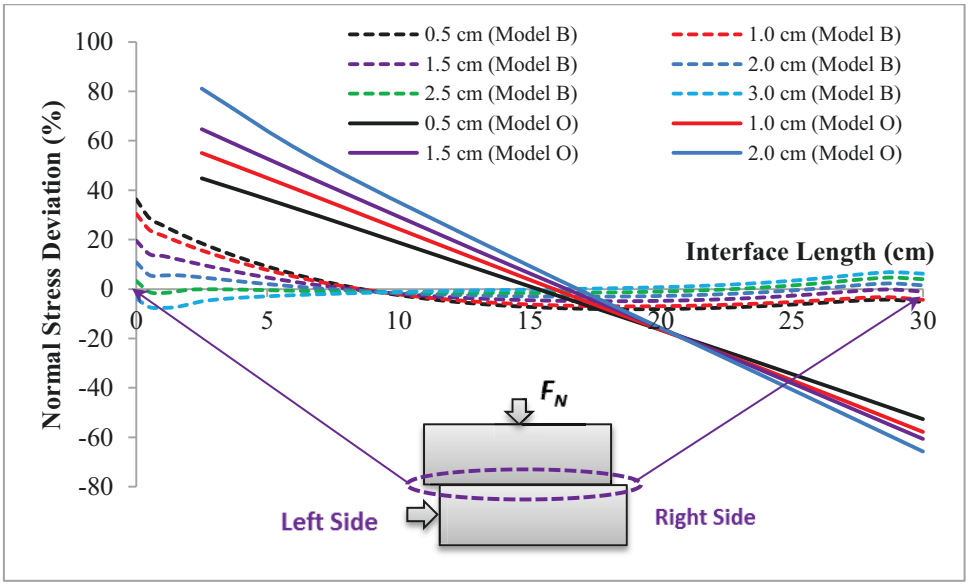

Figure 152. Normal stresses distribution from average value along joint for different values of shear displacement, normal load 90 kN (Note: in model O, there are 2.0 cm with no contact in the join plane when the shear displacement has reached 2.0 cm, therefore the start point for evaluation of model O was selected at 2.5 cm).

As Figure 149, Figure 150 and Figure 151 illustrate, models A to D show remarkable lower sample rotation in comparison to model O. This positive effect is caused by two factors, the increased sample length of the bottom part of the sample and the additional applied horizontal displacement of upper shear box and piston. Figure 152 shows in detail the rotational behavior for model B in comparison to model O. Along the joint the normal and corresponding shear stresses after 2.0 cm displacement vary from +82% to -65% for model O and only from +38% to -10% for model B. Moreover with ongoing shear displacement, the stress distribution becomes more and more non-uniform for model O and smaller and smaller for model B.

7 Conclusions and recommendations

7.1 Conclusions

Shear strength controls the failure in rock masses. Therefore, shear strength of jointed rock is one of the most important parameters in geotechnical engineering. The shear behavior of rock joint is a complex problem related to normal stress, direct shear rate, horizontal cyclic shear frequency, normal impact frequency, horizontal cyclic shear displacement amplitude and vertical impact force amplitude. Joint closure tests, direct shear tests and cyclic shear tests were performed on smooth joint surfaces under CNL and DNL boundary conditions in the laboratory. In parallel, numerical simulations were performed to understand the shear behavior of rock joints in detail. Based on the experimental and numerical simulation results, the following conclusions can be drawn:

1) Lab test results:

Joint closure test:

- Joint quasi-static stiffness increases with increasing normal force.
- Joint dynamic stiffness decreases with increasing superimposed normal force amplitudes.
- Normal impact frequencies have little influence on the joint stiffness.

Direct shear behavior under CNL conditions:

- Considering only average normal displacement and average stress evaluation method leads to a loss of information and prevents a deeper understanding of joint behavior under direct shearing.
- Shear forces and sample inclination (rotation) of the specimen increase with increase in normal load and decrease with increasing shear speed.
- For this concrete sample, shear speed has little influence on the shear force.

Cyclic shear behavior under CNL conditions:

- Peak shear forces increase with increasing normal loads and friction angle is smaller in a cyclic shearing process than in a quasi-static shearing test.
- During each cycle the normal displacements increase and decrease (rotational behavior in every cycle), peak angle of inclination increases with increase in the normal force and shear displacement amplitude.
- Peak shear forces are nearly independent on the cyclic shear displacement amplitude.
- There is a time shift between maximum shear displacement and maximum shear force. The corresponding time shift decreases with increasing normal load and increases with increasing shear displacement amplitude.

Direct shear behavior of jointed rock under DNL conditions:

- Shear force and friction coefficient show cyclic behavior, characterized by significant time shift between normal and shear force (shear force delay), between normal force and friction coefficient (friction coefficient delay).
- The relative time shift between peak normal force and peak shear force decreases with increasing impact amplitudes; the relative time shift between peak normal force and peak friction coefficient is nearly constant (about half cyclic).
- The peak value of friction coefficient has little influence by the impact amplitudes; the minimum value of friction coefficient decreases significantly with the increase in the impact amplitudes.
- Peak and minimum shear forces decrease with the increase of impact amplitudes.
- The ratio of dynamic peak-to-peak normal and shear force amplitudes decreases with increasing impact amplitudes.
- Dynamic shear strength cannot be estimated just by simple superposition of static and dynamic loading but needs the consideration of phase shift between normal and shear forces.

- A new shear strength criterion for joints under constant shear velocity and sinusoidal normal loading is proposed as follows:

$$\tau = \{c_1 + c_2 \cdot \sin[2\pi f(t + \frac{\pi}{f})]\} \cdot \frac{F_s + F_d \ \sin(2\pi f t)}{S}$$

  where c1 and c2 are modified factors, and c1 decreases and c2 increases with the increase of impact amplitudes.
- The shear forces, friction coefficients vs. shear displacement are nearly identical under the same SV-NIF.
- Peak shear force increases in the SV-NIF, minimum shear force is more or less constant.
- Minimum friction coefficient increases with increases in the SV-NIF, peak friction coefficient keeps more or less constant.
- The relative shift percentage between normal force and shear force decreases with the increase of SV-NIF; and increases with the increase of normal force.

Cyclic shear behavior of jointed rock under DNL conditions:

- The shear force is cyclically changing under the cyclic normal load and cyclic horizontal shear displacement. With the increase of normal force and superimposed dynamic normal load, the peak values of shear force in the forward and backward shear directions increase.
- The friction coefficient follows the same changing trend (as the square wave) and the same peak values during cyclic shearing under different conditions (except the surface is damaged under larger normal force).
- With the increase of horizontal shear displacement amplitude, the peak shear force in the forward shear direction is nearly constant, while the peak shear force in the backward shear direction decreases.
- Shear forces reverse behavior is mainly controlled by the horizontal shear direction.
- $f_h > f_v$: The peak shear force in the forward and backward shear direction is at the maximum normal force and maintains the same value during each vertical impact cyclic. Shear force looks like square wave with different amplitudes.

- $f_h = f_v$: The peak shear force in the forward and backward shear directions maintains the same value during each cyclic, but peak shear force is about 70% of the peak value under the condition that the vertical impact frequency is not equal to horizontal cyclic shear frequency in the backward shear direction. With the increase in normal impact frequency and horizontal cyclic shear frequency, the peak shear force in the forward shear direction drops slightly, while the peak shear force in the backward shear direction decreases dramatically.
- $f_h < f_v$: The higher vertical impact frequency, the shear forces inflection are more remarkable. The peak shear force in the forward and backward shear direction have the same value during each vertical impact cyclic.
- With the increase in normal impact amplitudes, the peak shear forces in the forward shear direction increase. However, the peak shear force in the backward shear direction is constant, but the time of the stable stage decreases.
- A novel shear strength criterion is developed:

$$\tau = ABS(k\sum_{n=0}^{n\max}(\frac{1}{2n+1}\sin((2n+1)t)))\cdot\frac{F_s + F_d \sin(2\pi ft)}{S} \quad .....(n \in (0,1,2,3...))$$

And it can reflect the cyclic shear strength under DNL conditions.

2) Numerical simulation results:

- Increasing normal loads lead to increasing joint stiffness.
- Due to the sample rotation, force distribution at the joint becomes very inhomogeneous. For a classical designed shear box device this effect becomes even more pronounced with increasing shear displacement. Locally, strong rotation can lead to extreme high stresses, which consequently may damage the sample.
- Because of the rotation of the loading plate, produces unwanted frictional forces at the upper shear box leading to only 91% ~ 94% of the applied and measured normal force are acting at the joint.
- Sample rotation can be significantly reduced, if lower part of the specimen is larger than the upper part in the shear displacement direction and also by controlled horizontal movement of upper shear box and piston reduces the rotations.

7.2 Recommendations

It is noted that the shear velocities attained in this study are considerably less than those associated with moderate earthquakes. There are many factors, such as surface roughness, waviness, infilling, mineralogy, water, temperature, normal stress and shear velocity which might be expected to influence the shear behavior of joints. To improve the understanding of the joints shear behavior, it is recommended that further research should be focused on:

- Specimen of the real rocks in nature with roughness should be investigated under DNL conditions and the corresponding shear strength criterion (considering the JRC) should be given.
- Dynamic signal in the normal direction and shear direction should be extended to real earthquake inputs.
- Numerical simulations for the dynamic tests should be performed with an even finer mesh resolution.
- Shear tests and numerical simulations with suggested approach (larger bottom shear specimen) should be performed.
- Different types of materials which can be used as a specimen should be tested (soft material: sand, clay, etc.; hard material: e.g. granite).
- In the current research no attention has been paid to investigate the influence of the scale on the shearing. The results have been validated only in the range of the samples tested in the laboratory. Further studies are needed to explore the applicability of the proposed model in actual field conditions.

References

Ahola, M. P., Hsiung, S. M., & Kana, D. D. (1996). Experimental study on dynamic behavior of rock joints. *Developments in Geotechnical Engineering, 79*(79), 467-494.

Allaby M, *A dictionary of Earth sciences - Third edition*. Vol. Third edition. 2008: Oxford University press.

Arulrajah, A., Rahman, M., Piratheepan, J., Bo, M., & Imteaz, M. (2013). Evaluation of interface shear strength properties of geogrid-reinforced construction and demolition materials using a modified large scale direct shear testing apparatus. *Journal of Materials in Civil Engineering, 26*(5), 1-9.

Asadzadeh, M., & Soroush, A. (2016). Fundamental investigation of constant stress simple shear test using dem. *Powder Technology, 292*, 129-139.

ASTM (2002). Performing laboratory direct shear strength tests of rock specimens under constant normal force. *D-5607*: 1-12.

Atapour, H., & Moosavi, M. (2013). The influence of shearing velocity on shear behavior of artificial joints. *Rock Mechanics & Rock Engineering,47*(5), 1745-1761.

Babanouri, N., Nasab, S. K., Baghbanan, A., & Mohamadi, H. R. (2011). Over-consolidation effect on shear behavior of rock joints. *International Journal of Rock Mechanics & Mining Sciences, 48*(8), 1283-1291.

Bagde, M. N., & Petroš, V. (2005). Waveform effect on fatigue properties of intact sandstone in uniaxial cyclical loading. *Rock Mechanics & Rock Engineering, 38*(3), 169-196.

Bahaaddini, M., 2014. Numerical Study of the Mechanical Behavior of Rock Joints and Non-persistent Jointed Rock Masses (PhD) UNSW Australia.

Bahaaddini, M., Hagan, P. C., Mitra, R., & Hebblewhite, B. K. (2014). Scale effect on the shear behavior of rock joints based on a numerical study. *Engineering Geology, 181*, 212–223.

Bahaaddini, M., Hagan, P. C., Mitra, R., & Hebblewhite, B. K. (2014). Parametric study of smooth joint parameters on the shear behavior of rock joints. *Rock Mechanics & Rock Engineering, 48*(3), 923-940.

Bahaaddini, M., Hagan, P. C., Mitra, R., & Khosravi, M. H. (2016). Experimental and numerical study of asperity degradation in the direct shear test. *Engineering Geology, 204*, 41-52.

Bahaaddini, M., Hagan, P., Mitra, R., & Hebblewhite, B. K. (2015). Numerical study of the mechanical behavior of nonpersistent jointed rock masses. *International Journal of Geomechanics, 16*(1).

Bahaaddini, M., Hebblewhite, B. K., & Sharrock, G. (2013). Numerical investigation of the effect of joint geometrical parameters on the mechanical properties of a non-persistent jointed rock mass under uniaxial compression. *Computers & Geotechnics, 49*(20), 2485-2488.

Bahaaddini, M., Sharrock, G., & Hebblewhite, B. K. (2013). Numerical direct shear tests to model the shear behavior of rock joints. *Computers & Geotechnics, 13*(51), 101–115.

Barton, N. (1974). Review of a new shear-strength criterion for rock joints.*Engineering Geology, 7*(4), 287-332.

Barton, N. (1976). The shear strength of rock and rock joints. *International Journal of Rock Mechanics & Mining Science & Geomechanics Abstracts, 13*(9), 255-279.

Barton, N., & Choubey, V. (1977). The shear strength of rock joints in theory and practice. *Rock Mechanics & Rock Engineering, 10*(10), 1-54.

Belem, T., Homand-Etienne, F. and Souley, M. (2000). Quantitative parameters for rock joint surface roughness. *Rock mechanics and Rock engineering* 33(4): 217-242.

Belem, T., Mountaka, S. and Homand, F. (2004). Generalized directional peak shear stress criterion for dilatant rock joints. *57th Canadian Geotechnical Conference*. Quebec**:** 1-8.

Belem, T., Souley, M. and Homand, F. (2007). Modeling surface roughness degradation of rock joint wall during monotonic and cyclic shearing. *Acta Geotechnica* 2(4): 227-248.

Cabalar, A. F., Dulundu, K., & Tuncay, K. (2013). Strength of various sands in triaxial and cyclic direct shear tests. *Engineering Geology,156*(2), 92-102.

Crawford, A. M., & Curran, J. H. (1981). The influence of shear velocity on the frictional resistance of rock discontinuities. *International Journal of Rock Mechanics & Mining Science & Geomechanics Abstracts, 18*(6), 505-515.

D'Andrea, A., & Tozzo, C. (2016). Interface stress state in the most common shear tests. *Construction & Building Materials, 107*, 341-355.

Dabeet, A. (2014). *Discrete element modeling of direct simple shear response of granular soils and model validation using laboratory tests*. (Doctoral dissertation). Civil Engineering, The University of British Columbia.

Dabeet, A., Wijewickreme, D., & Byrne, P. (2015). Evaluation of stress strain non-uniformities in the laboratory direct simple shear test specimens using 3d discrete element analysis. *Geomechanics & Geoengineering, 10*(4), 1-12.

Dang, W., Konietzky, H., & Frühwirt, T. (2016). Direct shear behavior of a plane joint under dynamic normal load (dnl) conditions. *Engineering Geology*, 213, 133-141.

Dang, W., Konietzky, H., & Frühwirt, T. (2016). Rotation and stress changes on a plane joint during direct shear tests. *International Journal of Rock Mechanics & Mining Sciences, 89*, 129-135.

Dindarloo, S. R., & Siami-Irdemoosa, E. (2016). A modified model of a single rock joint's shear behavior in limestone specimens. *International Journal of Mining Science & Technology, 26*(4), 577–580.

Dounias, G. T., & Potts, D. M. (1995). Numerical analysis of drained direct and simple shear tests. *Journal of Geotechnical Engineering,121*(2), 223-227.

Duriez, J., Darve, F., & Donze, F. V. (2011). A discrete modeling-based constitutive relation for infilled rock joints. *International Journal of Rock Mechanics & Mining Sciences, 48*(3), 458-468.

Fox, D.J., Kana, D. D. and Hsiung, S. M. (1998). Influence of interface roughness on dynamic shear behavior in jointed rock. *Int. J. Rock Mech. Min. Sci.* 35(7): 923-940.

Grasselli, G. (2001). Shear strength of rock joints based on quantified surface description. *Rock Mechanics & Rock Engineering, 39*(4), 295-314.

Grasselli, G. (2001). Shear Strength of Rock Joints Based on Quantified Surface Description, Doctoral Thesis. Lausanne: EPFL.

Grasselli, G. (2006). Manuel rocha medal recipient shear strength of rock joints based on quantified surface description. *Rock Mechanics & Rock Engineering, 39*(4), 295-314.

Grasselli, G., & Egger, P. (2003). Constitutive law for the shear strength of rock joints based on three-dimensional surface parameters.*International Journal of Rock Mechanics & Mining Sciences, 40*(1), 25-40.

Grasselli, G., Wirth, J., & Egger, P. (2002). Quantitative three-dimensional description of a rough surface and parameter evolution with shearing. *International Journal of Rock Mechanics & Mining Sciences,39*(6), 789-800.

Guo, Y. T., Zhao, K. L., Sun, G. H., Yang, C. H., Hong-Ling, M. A., & Zhang, G. M. (2011). Experimental study of fatigue deformation and damage characteristics of salt rock under cyclic loading. *Yantu Lixue/rock & Soil Mechanics, 32*(5), 1353-1359.

Haibo, L. I., Feng, H., & Bo, L. (2006). Study on strength behaviors of rock joints under different shearing deformation velocities. *Chinese Journal of Rock Mechanics & Engineering, 25*(12), 2435-2440.

Hazeghian, M., & Soroush, A. (2015). Dem simulation of reverse faulting through sands with the aid of gpu computing. *Computers & Geotechnics,66*(52), 253-263.

Hoek, E., & Bray, J. (1977). *Rock Slope Engineering*. *Rock slope engineering /*. Institution of Mining and Metallurgy.

Hoek, E., Bray, J., 1981. Rock Slope Engineering. *Taylor & Francis*, London.

Hoek, E., Brown, E.T. (1980). Underground Excavations in Rock. *The Institution of Mining and Metallurgy*, London.

Hossaini, K. A., Babanouri, N., & Nasab, S. K. (2014). The influence of asperity deformability on the mechanical behavior of rock joints.*International Journal of Rock Mechanics & Mining Sciences, 70*(9), 154-161.

Huang, X., Haimson, B.C., Plesha, M.E., et al. (1993). An investigation of the mechanics of rock joints - part 1. laboratory investagation. *Int. J. Rock Mech. Min. Sci.* 30(3): 257-269.

Indraratna, B., & Haque, A. (1997). Experimental study of shear behavior of rock joints under constant normal stiffness conditions. *International Journal of Rock Mechanics & Mining Sciences, 34*(3–4), 141.e1–141.e14.

ISRM. (1974). Suggested methods for determining shear strength. *Committee on standardisation of Laboratory and Field tests*: 1-23.

ISRM. (1978). Suggested methods for the quantitative description of discontinuities in rock masses. *International Journal of Rock Mechanics & Mining Sciences*. 15(6): 319-368.

Itasca. FLAC3D - Fast Lagrangian Analysis of Continua in 3 Dimensions - *Theory and Background. Itasca Consulting Group Inc*. Minnesota 55401 USA. 2012

Jacobson, D. E., Valdes, J. R., & Evans, T. M. (2007). A numerical view into direct shear specimen size effects. *Geotechnical Testing Journal,30*(6), 512-516.

Jafari, M. K., Hosseini, K. A., Pellet, F., Boulon, M., & Buzzi, O. (2003). Evaluation of shear strength of rock joints subjected to cyclic loading.*Soil Dynamics & Earthquake Engineering, 23*(7), 619-630.

Jiang, Y., Li, B., & Tanabashi, Y. (2006). Estimating the relation between surface roughness and mechanical properties of rock joints. *International Journal of Rock Mechanics & Mining Sciences, 43*(6), 837-846.

Johansson, F. (2016). Influence of scale and matedness on the peak shear strength of fresh, unweathered rock joints. *International Journal of Rock Mechanics & Mining Sciences, 82*(1), 36-47.

Kana, D. D., Fox, D. J., & Hsiung, S. M. (1996). Interlock/friction model for dynamic shear response in natural jointed rock. *International Journal of Rock Mechanics & Mining Sciences & Geomechanics Abstracts,33*(4), 371-386.

Kang, X., Cheng, Y., Ge, L., & Cheng, Y. (2015). Radial strain behaviors and stress state interpretation of soil under direct simple shear. *Journal of Testing & Evaluation, 43*(6).

Konietzky, H., Frühwirt, T., & Luge, H. (2012). A new large dynamic rockmechanical direct shear box device. *Rock Mechanics & Rock Engineering, 45*(3), 427-432.

Lee, H. S., Park, Y. J., Cho, T. F., & You, K. H. (2001). Influence of asperity degradation on the mechanical behavior of rough rock joints under cyclic shear loading. *International Journal of Rock Mechanics & Mining Sciences, 38*(7), 967-980.

Lee, Y. K., Park, J. W., & Song, J. J. (2014). Model for the shear behavior of rock joints under cnl and cns conditions. *International Journal of Rock Mechanics & Mining Sciences, 70*(9), 252–263.

Li, L., Hagan, P. C., Saydam, S., & Hebblewhite, B. (2016). Shear resistance contribution of support systems in double shear test.*Tunnelling & Underground Space Technology, 56*, 168-175.

Li, Y., & Zhu, Z. (2012). Study on the velocity of p waves across a single joint based on fractal and damage theory. *Engineering Geology, 151*(4), 82-88.

Lin, H., Liu, B. and Li, J. (2012). Numerical study of a direct shear test on fluctuated rock joint. *The Electronic Journal of Geotechnical Engineering* **17**: 1577-1591.

Lin, H., Liu, T., Xiong, Z., Cao, R., & Cao, P. (2014). Numerical simulations of the effect of bolt inclination on the shear strength of rock joints. *International Journal of Rock Mechanics & Mining Sciences,66*(1), 49–56.

Ling, X. Z., Zhang, F., Li, Q. L., An, L. S., & Wang, J. H. (2015). Dynamic shear modulus and damping ratio of frozen compacted sand subjected to freeze–thaw cycle under multi-stage cyclic loading. *Soil Dynamics & Earthquake Engineering, 76*, 111-121.

Liu, E., & He, S. (2012). Effects of cyclic dynamic loading on the mechanical properties of intact rock samples under confining pressure conditions. *Engineering Geology, 125*(1), 81–91.

Liu, E., Huang, R., & He, S. (2011). Effects of frequency on the dynamic properties of intact rock samples subjected to cyclic loading under confining pressure conditions. *Rock Mechanics & Rock Engineering,44*(5), 1-6.

Liu, J., Lv, P., Cui, Y., & Liu, J. (2014). Experimental study on direct shear behavior of frozen soil–concrete interface. *Cold Regions Science & Technology, 104*(3), 1-6.

Liu, S. H. (2011). Simulating a direct shear box test by DEM. *Canadian Geotechnical Journal, 43*(2), 155-168.

Luge, H. (2011). Entwicklung, Aufbau und Versuchssteuerung für ein neuartiges dynamisches hydro-mechanisches Felsschergerät für extrem hohe Kräfte. *Published by Geotechnical Institute*, TU Bergakademie Freiberg.

Mandal, N., Samanta, S. K., Bhattacharyya, G., & Chakraborty, C. (2005). Rotation behavior of rigid inclusions in multiple association: insights from experimental and theoretical models. *Journal of Structural Geology, 27*(4), 679-692.

Mirzaghorbanali, A., Nemcik, J., & Aziz, N. (2013). Effects of shear rate on cyclic loading shear behavior of rock joints under constant normal stiffness conditions. *Rock Mechanics & Rock Engineering, 47*(5), 1931-1938.

Mohapatra, S. R., Rajagopal, K., & Sharma, J. (2016). Direct shear tests on geosynthetic-encased granular columns. *Geotextiles & Geomembranes, 44*(3), 396-405.

Moradian, Z. A., Ballivy, G., Rivard, P., Gravel, C., & Rousseau, B. (2010). Evaluating damage during shear tests of rock joints using acoustic emissions. *International Journal of Rock Mechanics & Mining Sciences, 47*(4), 590-598.

Muralha, J., Grasselli, G., Tatone, B., Blümel, M., Chryssanthakis, P., & Jiang, Y. (2014). Isrm suggested method for laboratory determination of the shear strength of rock joints: revised version. *Rock Mechanics & Rock Engineering, 47*(1), 291-302.

Nabassé J.F. Koupouli, Tikou Belem, Patrice Rivard, & Hervé Effenguet. (2016). Direct shear tests on cemented paste backfill–rock wall and cemented paste backfill–backfill interfaces. *Journal of Rock Mechanics\s&\sgeotechnical Engineering*.

Nemcik, J., Mirzaghorbanali, A., & Aziz, N. (2014). An elasto-plastic constitutive model for rock joints under cyclic loading and constant normal stiffness conditions. *Geotechnical & Geological Engineering,32*(2), 321-335.

Nguyen VH (2013) Static and Dynamic behavior of joints in schistose rock: Lab testing and Numerical simulation. PhD Dissertation, Geotechnical Institute, TU Bergakademie Freiberg

Nguyen, V. M., Konietzky, H., & Frühwirt, T. (2014). New methodology to characterize shear behavior of joints by combination of direct shear box testing and numerical simulations. *Geotechnical & Geological Engineering, 32*(4), 829-846.

Oda, M., & Iwashita, K. (2000). Study on couple stress and shear band development in granular media based on numerical simulation analyses. *International Journal of Engineering Science, 38*(15), 1713-1740.

Oda, M., & Konishi, J. (1974). Rotation of principle stresses in granular material in simple shear. *, 14*(4), 39-53.

Oh, J., Cording, E. J., & Moon, T. (2015). A joint shear model incorporating small-scale and large-scale irregularities. *International Journal of Rock Mechanics & Mining Sciences, 76*, 78-87.

Patton, F. D. (1966). Multiple modes of shear failure in rock. *Proceeding of the Congress of International Society of Rock Mechanics* (Vol.1, pp.509-513).

Potts, D. M. (1987). Finite element analysis of the direct shear box test. géotechnique. *Géotechnique, 37*(1), 11-23.

Qiu, X., Plesha, M.E., Huang, X., et al. (1993). An investigation of the mechancis of rock joints - Part II. Analytical investigation. *Int. J. Rock Mech. Min. Sci.* 30(3): 271-287.

Sneed, L. H., D'Antino, T., Carloni, C., & Pellegrino, C. (2015). A comparison of the bond behavior of pbo-frcm composites determined by double-lap and single-lap shear tests. *Cement & Concrete Composites,64*, 37-48.

Stein, R. S., & Stein, R. S. (1999). Stein, r. s. the role of stress transfer in earthquake occurrence. nature 402, 605-609. *Nature, 402*(6762), 605-609.

Suhr, B., & Six, K. (2016). On the effect of stress dependent interparticle friction in direct shear tests. *Powder Technology, 294*, 211-220.

Tatone, B. S. A., & Grasselli, G. (2013). An investigation of discontinuity roughness scale dependency using high-resolution surface measurements. *Rock Mechanics & Rock Engineering, 46*(4), 657-681.

Tejchman, J., & Bauer, E. (2005). Fe-simulations of a direct and a true simple shear test within a polar hypoplasticity. *Computers & Geotechnics, 32*(1), 1-16.

Wang, G., Zhang, X., Jiang, Y., Wu, X., & Wang, S. (2016). Rate-dependent mechanical behavior of rough rock joints. *International Journal of Rock Mechanics & Mining Sciences, 83*, 231-240.

Wang, Z., Jing, G., Yu, Q., & Yin, H. (2015). Analysis of ballast direct shear tests by discrete element method under different normal stress. *Measurement, 63*, 17-24.

Wijewickreme, D., Dabeet, A., & Byrne, P. (2013). Some observations on the state of stress in the direct simple shear test using 3d discrete element analysis. *Geotechnical Testing Journal, 36*(2), 1-1.

Wilson, G. M. (2013). Underground excavations in rock: hoek, e; brown, e t London: institution of mining and metallurgy, 1980, 527p. *, 18*(2), 27.

Yan, Y., & Ji, S. (2010). Discrete element modeling of direct shear tests for a granular material. *International Journal for Numerical & Analytical Methods in Geomechanics, 34*(9), 978–990.

Zhao, J. (1997). Joint surface matching and shear strength part a: joint matching coefficient (jmc). *International Journal of Rock Mechanics & Mining Sciences, 34*(2), 173-178.

Zhao, J. (1997). Joint surface matching and shear strength part b: jrc-jmc shear strength criterion. *International Journal of Rock Mechanics & Mining Sciences, 34*(2), 179-185.

Zhou, Z. L., Zhi-Bo, W. U., Xi-Bing, L. I., Xiang, L. I., & Chun-De, M. A. (2015). Mechanical behavior of red sandstone under cyclic point loading.*Transactions of Nonferrous Metals Society of China, 25*(8), 2708–2717.

Zou, L., Jing, L., & Cvetkovic, V. (2015). Roughness decomposition and nonlinear fluid flow in a single rock fracture. *International Journal of Rock Mechanics & Mining Sciences, 75*, 102-118.